The University of Nottingham

Pattern recognition of micro and macro grinding phenomenon

with a generic strategy

to machine process monitoring

By

James Griffin

BEng and BSc(hons)

School of Mechanical, Materials and Manufacturing Engineering

Thesis submitted to the University of Nottingham for the degree

of Doctor of Philosophy

December 2007

Abstract

In modern manufacturing environments waste is an issue of great importance. Specifically the research in this thesis looks at issues in establishing the initial steps to gain a generic process monitoring system that ensures that grinding is both optimised but not the determent where costly malfunctions mean the scrapping and re-melting of expensive quality intensive materials.

The research conducted in this thesis investigates the process of cutting, ploughing and rubbing during single grit scratch tests. These investigations meant the correlation between physical material removal phenomenon and the emitted material dislocations gained from acoustic emission extraction. The initial work looked at different aerospace materials and the distinction of cutting, ploughing and rubbing during single grit radial scratch tests. This initial work provided novel results not seen in this area before and paved the way for more robust results in investigating the same phenomena during horizontal single grit scratch tests. This work provided more robust classification of cutting, ploughing and rubbing and transferred directly to grinding pass cuts from 1μm and 0.1mm depth cuts respectively. In using robust classifiers such as the Neural Network and novel classifiers such as non-linear data paradigms, Fuzzy-c clustering with Genetic Algorithm optimisation, cutting, ploughing and rubbing phenomenon was investigated. These investigations showed that more cutting occurs when there is more interaction between grit and workpiece based on the increase depth of cut. Other thesis results investigated a generic classifier using Genetic Programming to classify multiple

anomaly phenomena. This work can be bridged together with the unit event grit classification work.

Publications

Conference Papers:

Griffin J, Chen X, **Investigation of Grinding Burn through Various Extracted Sensory Information**, Proceedings of the 11th Chinese Automation & Computing Society Conference in the UK, Sheffield University, 2005, pages 263 – 267.

Griffin J, Chen X, **Classification of varying levels of ploughing, rubbing and cutting during Single Grit tests using Evolutionary Inspired Computer Techniques,** ICMR, Liverpool John Moore University, September 2006, pages 217 -222

Griffin J, Limchimchol T and Chen X, **Multivariable classification of Grinding Burn and Chatter, using evolutionary inspired classification techniques,** Proceedings of the 12th Chinese Automation & Computing Society Conference in the UK, Loughborough University, 2006, pages 211-216.

Limchimchol T, Griffin J and Chen X, **Multi-class classification of grinding chatter using support vector machines,** Proceedings of the 12th Chinese Automation & Computing Society Conference in the UK, Loughborough University, 2006, pages 217-222.

Griffin J and Chen X., **The classification of rubbing, ploughing and cutting during grinding and the comparison of different evolutionary inspired classification techniques,** *40th CIRP International Manufacturing Systems Seminar, Liverpool University, 2007.*

Airbus UK Studentship winner for the 4th International Conference on Manufacturing Research (ICMR 2006), Liverpool John Moore University, 5th September 2006.

Journal Papers:

Griffin J, Chen X, (2006), **Classification of the Acoustic Emission Signals of Rubbing, Ploughing and Cutting during Single Grit Scratch Tests,** International Journal of Nanomanufacturing, Vol. 1, No. 2, pp. 189 - 209.

Chen, X., Griffin, J. (2007), **Grinding Acoustic Emission Classification in Terms of Mechanical Behaviours,** Key Engineering Materials, Vol. 329, pp. 15-20

Chen, X., Griffin, J., Liu, Q., (2007) **Mechanical and Thermal Behaviours of Grinding Acoustic Emission, International Journal of Manufacturing Technology and Management (IJMTM),** Vol. 12, No. 1~3, pp. 184-199.

Griffin J, Chen X, (2007), **Characteristics of the Acoustic Emission during Horizontal Single Grit Scratch Tests – Part 1 Characteristics and Identification,** International Journal Abrasive Technologies, Special Issue on: "Micro/Meso Mechanical Manufacturing (M4 Process)." Accepted and in Press.

Griffin J, Chen X, (2007), **Characteristics of the Acoustic Emission during Horizontal Single Grit Scratch Tests – Part 2 Classification and Grinding Tests,** International Journal Abrasive Technologies- Special Issue on: "Micro/Meso Mechanical Manufacturing (M4 Process)." Accepted and in Press.

Two more journal papers are in draft form for work carried out in Chapter 8.

Acknowledgements

I wish to thank my supervisor Dr Xun Chen for his proffesionalism and friendly manner which always inspired me to carry out this work. His indepth thought process always seemed to provide good discussion and keep me thinking much longer round the vast subjects regarding process monitoring.

I wish to thank Mark Daine for his expert support, John Lemon and his `health and safety rules` no doubt he managed to keep me safe throughout the studdies and continued research with my current research job. Of course I wish to say thanks to all the other technicians who are so valued within the Manufacturing Department at the University of Nottingham.

I wish to thank Dr Dragos Axinte for allowing me to have time off in putting the finishing touches to my thesis and offering continued help. Thanks to all the other academic staff I may have missed out with thier kind interactions that have also allowed me to get this far and triggerd great levels of inspiration.

I wish to thank all my friends at the University of Nottingham both past and present, thier support and inspiration is second to none which makes it a pleasure to work with them. I wish to thank Isabela Scarioli for her kind support all the way through this PhD and now sadly, all the way from Brazil (I still wait for the day England can beat Brazil in the World Cup Final!). I wish to thank my young lawyer friend, Laura Pritchard-Jones

Abbreviations

Subject	Full form	Chapter
AE	Acoustic Emission	4
Al_3O_2	Aluminium Oxide	4
BUE	Built Up Edge	2
CWT	Continous Wavelet Transform	5
DAC	Data Aquisition Card	4
DFT	Discrete Fourier Transform	5
DMA	Direct Memory Access	4
DSP	Digital Signal Processing	5
FFT	Fast Fourier Transform	5
FIR	Finite Impulse Response	5
fuzzy-c	Fuzzy-c Clustering Algorithm	6
GA	Genetic Algorithms	6
GP	Genetic Programming	6
ICA	Independent Component Analysis	6
IIR	Infinite Impulse Response	5
NDA	Non Destructive Evaluation	4
NN	Neural Network	6
MLP	Multi-Layer Perceptron	6
PAC	Physical Acoustic Corportation	4
PM	Process Monitoring	3
RMS	Root Mean Squared	2
SNR	Signal to noise ratio	5
SG	Single Grit	7
STFT	Short Time Fourier Transforms	5
SVM	Support Vector Machines	6
TCM	Tool Condition Monitoring	3
VIPER	Vitreous Improved Performance Extreme Removal Grinding	3
WPT	Wavelet Packet Transforms	5

Nonmenclature

Symbol	Quantity	Units
α	Learning rate	Integer
a_x	NN output x	Integer
A_p	Depth of cut	Mm
$AE_{V/\mu bar}$	AE pressure wave	V/μbar
$AE_{V\ m/s}$	AE transient wave	V m/s
$AE_{Threshold}$	AE dB Threshold	dB
$A_{surface}$	Left built up edge	μm^2
A_x	Accelerations in the x direction	m/s^2
b	Bias input to NN	Integer
$B_{surface}$	Right built up edge	μm^2
Δb	Bias change	Integer
$C_{surface}$	Groove area	μm^2
C	Heat capacity	J/K
D	Diameter	Mm
E	elastic modulus	Mpa
Σ	NN summation nodal point	Integer
F_x	Force in x direction	N
f	frequency	Hz
f_c	Cut-off frequency	Hz
Δf	Transition width of requency cut-off	Hz
fl	Flow rate	litre/minute
K	Thermal conductivity	W/m K
ME_j	Mean Error for j-layer	Integer
MRR	Material Removal Rate	cm^3/min
ρ	Mass density	Kg/mm^3
P_x	Input P_x to NN	Integer
R_a	Surface Roughness	μm
T	Temperature, temperature rise	K
T_x	Target x correlated with P_x input	Integer
ΔT	Temperature rise	K
t	time	seconds (s)
V_{DC}	DC Voltage level	V
V_o	Peak Voltage	V
V_g	Grain Cut Through Speed	mm/s
Vs	Cutting speed	m/s
Vw	Feed rate	mm/min
ω_n	Natural frequency	Hz
w_x	Weight w_x connected to P_x	Integer
Δw	Change of weight	Integer
λ	wavelength	seconds

CONTENTS

The University of Nottingham

The University of
Nottingham

The University of
Nottingham

The University of Nottingham

The University of
Nottingham

Chapter 1 Introduction

This chapter first describes the philosophy, motivation and aim behind the research undertaken, and then introduces the subjects of Tool Condition Monitoring and Tool Condition Monitoring for Grinding Technologies to the non-specialist reader. The original contributions made by this thesis are then listed summarising the addressed gaps and finally, a brief outline of the document structure.

1.1　Motivation and Aim

This thesis is concerned with technological advances in Process Monitoring (PM) and specifically, Abrasive Grinding PM. The research for the thesis has been carried out with the backing of The Engineering and Physical Sciences Research Council (EPSRC) and industrial collaboration with the Aerospace turbine company; Rolls-Royce. Not just aerospace companies are interested in process monitoring but also other manufacturing companies especially large ones like Honeywell and Motorola who use the manufacturing quality standard of Six Sigma[1](Linderman, Schroeder et al. 2003).

This research is primarily interested in PM however within that umbrella are sub PM disciplines such as Tool Condition Monitoring (TCM) which are concerned with the tool wear in machining. This thesis will be concentrating on TCM albeit other areas of PM will be discussed throughout the thesis.

---

[1] Six Sigma is where the tolerance minimum level of defects is three in every one million

The University of Nottingham

Manufacturing companies are interested in this research as it is key to more efficient manufacturing processes and specially grinding manufacture. For example; Rolls-Royce produces a lot of waste during its machining processes and is continually concerned with the reduction of waste which ultimately saves money.

The type of grinding technology employed at Rolls Royce is "VIPER Grinding" which is Rolls-Royce's acronym for "Vitreous Improved Performance Extreme Removal Grinding." The process was developed during the 1990s as a higher performance alternative to Cubic Boron Nitride (CBN) superabrasive and conventional creep feed grinding techniques for machining nickel based alloys. The process has been applied to a number of Rolls-Royce factories, but a turbine blade machining facility in the city of Derby is the most extensive, with ten VIPER-adapted machining centres. Using this process, the facility has reduced the lead time on production for a set of high pressure turbine blades from around 100 to 15 days (Henderson, 2004).

1.1.1 Research Aim

The aim of the proposed research is to investigate the methodology of extracting the features of acoustic emission signals in relation to different material removal mechanisms during grinding of aerospace alloys.

1.1.2 Research Objectives

The objectives of the research are:

The University of Nottingham

- To identify characteristics of acoustic emission in relation to material properties for different material removal processes.

- To characterise acoustic emission signals in terms of energy distribution and its feature in both the time and frequency domain.

- To classify grinding mechanics in terms of cutting, ploughing and rubbing through acoustic emission signal extraction.

- To investigate the relationship(s) between acoustic emission signals and wheel surface topography.

- To develop adaptive strategies for controlling grinding burn and workpiece chatter.

- To identify the varying effects of rubbing, cutting and ploughing during grinding via the extraction of AE, force, accelerations and temperature as well as the machining parameters verified by accurate measurements.

- To investigate different grinding phenomena identification with a generic monitoring approach to identify all researched grinding phenomena.

1.2   VIPER Grinding Overview

VIPER grinding is where an Aluminium Oxide (Al_3O_2) vitrified bonded wheel is used at high speed (v_s) as an abrasive grinding tool to remove hard to cut aerospace alloys. In addition to the high wheel speed there is now high feedrate (V_w) demanded by industrial pressures. See Figure 1.1 for a VIPER grinding schematic displaying the configuration of creep feed grinding which is the method of grinding behind VIPER grinding. High feedrate and depth of cut parameters to gain maximum efficiency albeit with no material

The University of Nottingham

defects. These two main parameters alone are the essential parameters to both control and monitor during grinding. With industrial demands on both high feedrates and wheel speeds there is a need for high pressure coolant flow (fl) to be present. This is to ensure material cooling, material removal and the non material welding effect where hot chip material to workpiece and grinding wheel surface occurs. By ensuring less abusive grinding conditions the residual stresses tend from tensile (heat induced) to compressive which is required for material strengthening characteristics and avoidance of material defects.
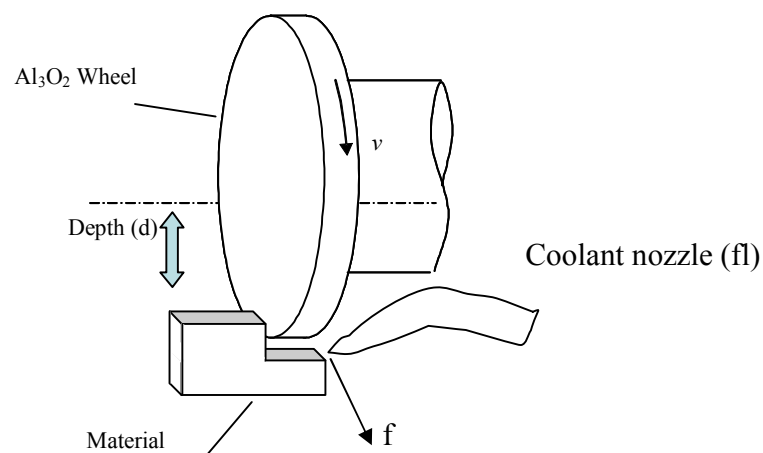
Figure 1.1 Schematic of the VIPER Grinding Process

The University of Nottingham

Grinding is used for both high rate material removals as well as being a material finishing process. The machine used for experimentation was a Machino A55 Machine Centre but for VIPER grinding any machine can be used. The technology and acronym is based on the type of wheel used. The wheels used ranged from a high dense bond and randomly moulded grits to less dense bond and randomly moulded grits. These wheels range from giving a good material finish to high material removal rates respectively.

There have been investigations (Liu 2004) on the cost implications of using super abrasives such as Diamond or Cubic Boron Nitride (CBN) wheels against Al_3O_2 abrasive wheels. The investigations would look at the overall machining costs as well as the dressing, machine and workpiece cleaning and, the wheel costs for sustained mass material removal manufacturing. These investigations showed that for mass material removal VIPER grinding wheels proved the most cost effective over time. This research motivation aims to make VIPER grinding high efficiency without surface defects and ensure maximum efficiency of wheel is utilised in terms of dressing ratio or replacement of used wheel for a new wheel.

1.3 Macro and Micro Grinding Overview

For a successful grinding PM system it was thought that current condition monitoring research was focussing its research on the macro aspects of grinding when if a system looked at the macro aspects through a micro view then grinding PM would be more robust, accurate and more efficient. To facilitate the description of details of

The University of Nottingham

experiments, two concepts are introduced: macro and micro grinding. The description of micro grinding effects is where Single Grit (SG) experiments are carried out to look at SG scratches and monitor the sensory outputs (primarily AE sensors to pick up material elastic and plastic deformation characteristics) for the different levels of cutting, ploughing and rubbing. Cutting, ploughing and rubbing are the mechanics experienced during grinding. In the macro grinding aspects this is considered as real grinding. For the perfect SG cut case there is firstly rubbing then ploughing of the material followed by cutting in the middle. Towards the end of the cut (conical needle scratch) there is ploughing and lastly rubbing phenomenon or in most cases after ploughing rubbing with slight plastic deformation. To confirm rubbing, ploughing and cutting, material measurements both longitude and latitude are carried out. These cut profiles provide the material removal in terms of built-up remaining edge as well as the cut depth. For macro grinding, there should be more of a continuous cutting action however, with wheel loading there is more rubbing and ploughing present during the cut causing heat affects from the build up of temperature. See figure 1.2 below for schematic set-up for both SG and macro grinding set-up.

Stroke

Al₃O₂ Wheel

Grit tip

Scratch

Stroke

Material

v
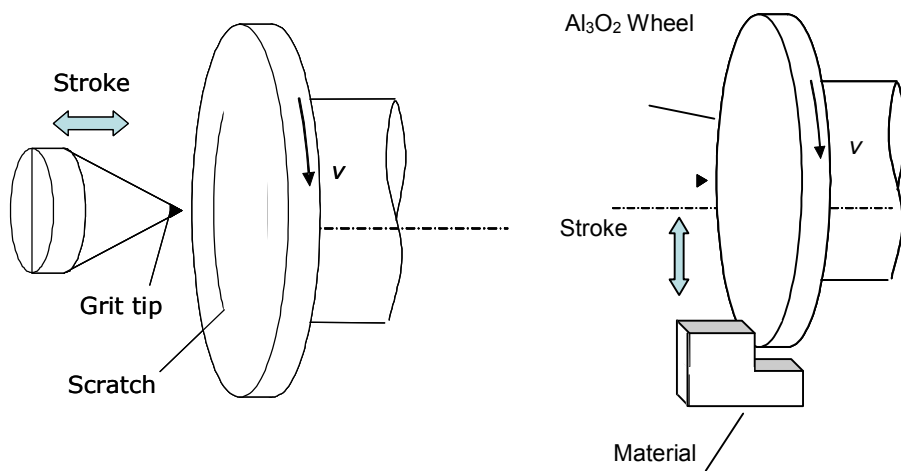
Figure 1.2 Left schematic displays SG setup, right schematic displays Macro Grinding setup

From looking at the fundamental mechanics of grinding and identifying the overall mechanics of grinding a more robust PM system is achieved. This thesis will investigate and provide results for the grinding philosophy.

1.4 Multiple Classification System

The fundamental view of grinding provides a useful strategy to look at different phenomenon experienced through grinding. At the same time of investigating a generic multiple classification system from a fundamental look, there is also a need to investigate a straight macro multiple classification system. Ultimately the two technologies can merge together to provide both an accurate and hierarchical grinding PM system. A multiple grinding classification system is very important to grinding process monitoring as most research classification investigations look at identifying single phenomenon and not a range of multiple phenomena. During the micro grinding tests, there was some shallow depth of cut macro grinding tests which were tested for

The University of Nottingham

against the micro grinding signal data and the previous classified and trained ratios of cutting, ploughing and rubbing. From continued research more tests of micro grinding and more tests between micro and macro grinding would bridge the gap between the two grinding technologies which make it possible to provide the ratios of cutting, ploughing and rubbing for unwanted anomalies such as grinding burn and chattering.

1.5 Contributions

This thesis has provided a number of findings which have materialised into a list of publications adding primarily to knowledge, the dynamic research frontier of grinding technologies. This research can be applied in other disciplines such as nano-manufacturing which is currently a new and emerging field within manufacturing.

Single grit analysis has been carried out for a range of different hard to cut aerospace alloys. This analysis looks at both the micro aspects with SG cut interactions as well the macro interactions from a micro cut perspective. This finding is significant to this thesis within process monitoring and presents away for future research to look from a bottom-up approach as opposed to the mass presented view; the top-down approach. This initial work can be taken further to look at different grit sizes, many different types of material as well as different wheel speeds and more accurate depth cuts (½ micron instead of a micron used in all of the exhaustive SG tests). This thesis has looked at both cylindrical mounted workpiece SG tests as well as horizontal mounted workpiece SG tests.

Investigations of purely macro grinding process monitoring have been looked at with a comparison to the micro/macro hybrid generic classifier. The purely macro grinding

process monitoring paradigm uses Genetic Programming as one classification technique which has not been used in process monitoring before and offers an advanced alternative to Neural Networks and the like. The micro/macro hybrid generic classifier uses a Fuzzy Cluster/Genetic Algorithm regime to provide the different levels of cutting, ploughing and rubbing mechanisms for both SG and grinding analysis. This is the first time such a cluster algorithm has used as a biologically inspired technique to search for the best parameters and accurately map the three grinding phenomena. The generic classifier for both micro/macro and just macro classification was used to distinguish the multiple phenomena from grinding chattering to grinding burn. Much presented research looks at the single classification of one material defect and not more which is in short; is more interest to industry. To gain a rich summary of the time extracted signal, statistical windowing techniques are used with some of the classifiers. In summary, the list of contributions for the thesis is presented below:

(1)   Micro and Macro grinding analysis through dual Acoustic Emission signals verified with force, power, moment and accelerations of force.

(2)   Looking at both cylindrical and horizontal SG analysis with novel SG holder fixture.

(3)   Classifying burn with coolant through Acoustic Emission signal signatures.

(4)   Multiple classifier for distinguishing chattering and burn using the Genetic Programming (GP) technique.

(5)   GA-Fuzzy Cluster algorithm for quantifying levels of rubbing, ploughing and cutting for both micro and macro grinding analysis.

The University of Nottingham

(6)   Independent Component Analysis (ICA) to reduce signal data and GP to provide a hybrid multiple grinding phenomena classification system.

(7)   Statistical windowing technique used to provide a rich summary of information for both micro and macro grinding extracted signals.

1.6   Thesis Structure

The thesis layout displays a progression of research with the introduction and background information providing the material for Chapter 1. Chapter 2 is the research literature review broken up into three sections; Advances in Tool Condition Monitoring, Classification Techniques and Material Surface technology and Single Grit Analysis both Micro and Macro view. Chapters 3 and Chapters 4 look at both Material surface and grinding experimental setup analysis and, sensor technology respectively. Chapter 5 looks at the signal processing techniques used to extract the sensor information. Chapter 6 looks at the classification techniques used in the research work carried out in this thesis. Chapter 7 discusses the results for both single grit radial and horizontal scratch tests. Chapter 8 discusses the macro multiple classification grinding anomalies such as workpiece burn and chattering using a generic classifier technology. The burn results established for workpiece burn are under both coolant and no coolant conditions (for multiple classifications dry conditions were used). The Last chapter; Chapter 9, concludes the thesis with the thesis conclusions and future work discussion. Figure 1.3 displays the thesis structure.
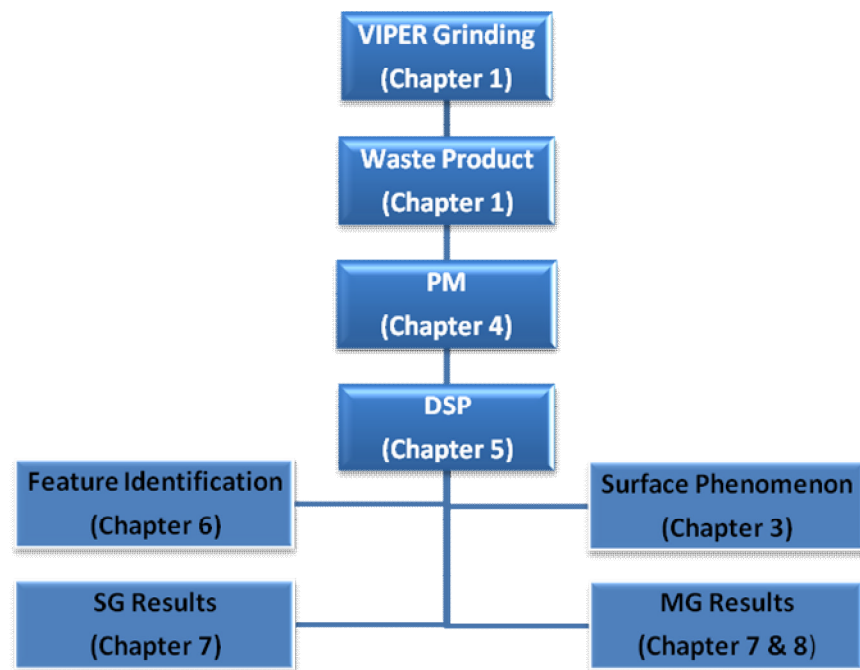
Figure 1.3 Schematic of thesis structure

Chapter 2 Literature Review

2.1 Introduction

This chapter is separated into three parts; the first part looks at an introduction into condition monitoring and specifically grinding condition monitoring, the second part investigates multiple classification techniques and finally, the third part looks at more fundamental issues within grinding in terms of single grit scratch technology and its application to grinding condition monitoring. Within both grinding condition monitoring and single grit technology, material and surface analysis will be discussed as well as current classification systems.

Process monitoring generally entails the following:

- Signal extraction and interpretation techniques

- Key feature extraction from signals

- Identification of machining conditions through classification techniques

2.2 Grinding Behaviour

Grinding is considered as a machining cutting process that has undefined cutting edges unlike other machining processes such as milling, turning or drilling. Instead, the grits are randomly placed in a bonded material and often considered to have high negative rake angles when compared with milling and other like machining processes. Grinding behaviour involves; grinding wheel behaviour, the effects of force from both wheel and

The University of Nottingham

coolant and, the thermal damage are discussed. Grinding is often considered as a mechanical-thermo process (Griffiths 2001) meaning; the stresses range from compressive to tensile when tending to more abusive grinding conditions. In addition, the quality of the workpiece and wheel life is considered the most important issues during grinding operations.

2.2.1 Abrasive Wheels

The grinding wheel is used for both roughing and finishing material removal operations and applied to various materials (extensive research displaying grinding for brittle, hard and ductile materials). The grinding wheel has thousands of cutting points which are held in a matrix bond and separated by pores. The pores provide a dedicated space for coolant to penetrate the wheel and flush away fractured material from both workpiece and wheel. In addition, the temperature at the grinding zone is reduced. Different chip sizes can give different grinding behaviour such as smaller chips are used for better surface roughness requirements and larger chips are used for coarse grinding and greater material removal rates (MRR). Material removal rates, wheel speed and the distribution of the cutting edge can all be determined by the shape of the chip (Shaw 1996).

There are four major grinding wheels used in production today, the first two are considered as Superabrasive grinding wheels; Cubic Boron Nitride (CBN) and Diamond. These superabrasives offer a competitive solution over conventional abrasive grinding wheels in that they have greater wear resistance and higher thermal conductivity. In

The University of Nottingham

providing these useful characteristics superabrasives ensure high material removal rates without the thermal damage and high tensile residual stresses which are critical in aerospace manufacture. Precision grinding with CBN however due to the high hardness and the inability to self-sharpen the grits meant special dressing techniques were required for such superabrasive grinding wheels (Chen, Rowe et al. 2002). The force required for this dressing technique is very high and the dressing technique is usually less than 5μm just touching the wheel to ensure the grits are sharpened and ready for further grinding passes. The challenge here is the initial contact between wheel and dressing tool and to complicate matters, coolant is also used to ensure no material deposits and wheel geometry roundness is maintained. Conventional abrasive grinding wheels are as follows; Aluminium Oxide (Al_3O_2) and Silicon Carbide (S_iC). Conventional abrasive grinding wheels however cost a lot less than superabrasive grinding wheels this is in terms of the initial cost and continual maintenance ensuring the wheel is maintained sharp for a cleaner cut rather than a smudged dragging cut when the wheel is in fact blunt. Such dressing techniques are used in some of the grinding pass work discussed in chapter 8; such dressing ratios and frequency of use are always conveyed to the reader. There are other novel dressing techniques that use a fixed copper brush to remove the material wheel loadings (Tawakoli 2002; Tawakoli, Westkaemper et al. 2007a; Tawakoli, Westkaemper et al. 2007b). Such technology can be applied in a continuous manner during machining where the copper wire also provides a heat sink for removing unwanted increase in grinding temperatures. This type of technology is used with dry grinding conditions and at a dressing depth of cut of 3μm and grinding depth of cut of 25 μm. This dry grinding machining process is better for the environment, cutting

down costs, reduced coolant forces and at the same time, providing a cheaper solution. This research (Tawakoli 2002; Tawakoli, Westkaemper et al. 2007a) has only been applied to super abrasive grinding wheels. The wheels used throughout the research only had a 25% grit surface area where the rest is space, these wheels provide a competitive grinding finish and roughing solutions when compared with 100% grit surface area. In addition (Tawakoli, Westkaemper et al. 2007b) discusses using a continuous diamond blade dresser with ultrasonic assistance to give better rates of dressing in terms of D-ratio[2], less forces (both normal and tangential) present meaning, less temperature and therefore suitable for dry grinding conditions and lastly, more uniform dressing application across the surface area of the wheel. Such research has application for single grit analysis and acoustic emission (AE) monitoring this is due to the following; no coolant noise present which ensures a most suitable environment for AE, such precision needs to be controlled with a sensitive measurement device such as AE, the 25% grit surface area and other grit percentage topologies can be further experimented in terms of efficient grinding (cutting, ploughing and rubbing ratios). A note is made here that the research in this thesis will concentrate on using Aluminium Oxide (Al_3O_2) grinding wheels as these are used in vast quantities to produce aerospace turbine engines and the turbine blades which is the primary focus of the research discussed in this thesis. In addition, some of the single grit analysis work discussed later in this chapter and chapter 7 can be applied to automated efficient dressing wheel strategies.

---

[2] D-ratio is the dressing ratio similar to the G-ratio (grinding ratio)

The University of Nottingham

2.2.2 Thermal and mechanical effects

Aerospace manufacture often uses creep-feed grinding for its roughing and finishing operations in cutting difficult to cut alloys. Other machining operations however are used for more intricate shapes. With reference to the last sentence this thesis is solely concentrating on grinding and specifically that of creep-feed grinding which requires large amounts of fluid to ensure the grinding zone does not experience burst like high temperatures which can be detrimental to the workpiece surface quality with inclusions or increased residual stresses which are inspected for when applied to aerospace applications. Increasing the depth cut, wheel speed, lowering the feed rate and decreasing coolant flow all result in rising the temperature at the grinding zone and inherently; causing catastrophic malfunctions. A thermal model which considers the coolant temperatures and transient workpiece/wheel temperatures during a grinding pass (Guo and Malkin 1994) has been investigated. Other research (Kim and Guo 1997) investigated the heat radiating effects in terms of energy dissipation from the grinding zone through the use of fixed thermocouples. This again would give the transient heat measurements achieved in the grinding zone. Kim's findings concluded that creep-feed down grounding is more in favour than creep-feed up grinding when considering the thermal effects. Griffiths (Griffiths, Middleton et al. 1996; Griffiths 2001) discusses the process of grinding as a thermo-mechanical process where most machining processes are mechanical-thermo processes such as that seen in milling, turning and reaming for example. It is a thermo-mechanical process as 70% of the heat dissipates into the workpiece and the remainder 30% heat, is lost to the broken away chip. With turning however, only 5% of the heat generated passes into the workpiece. That said there are

more possibilities for sub-surface cracking, white layer and brittle surface regions and material inclusions when grinding with conditions tending towards abusive. The mean rake angle for grits during grinding tends to be more negative than positive. As the grit interacts with the workpiece the positive to negative shallow rake angles (positive to -10°) tend to provide cutting. Ploughing or prow creation material actions occur at larger rake angles (-10° to -70°) and lastly, when the rake angles tend towards large negative rake angles rubbing and smearing rather than cutting and ploughing occurs (-70° to -90°) (Doyle E.D. and Samuels L.E. 1974) see Figure 2.1 for more details (Griffiths 2001). When these properties are identified there is a need for dressing the wheel or even truing the wheel to ensure the grits are sharp and roundness is in full integrity.
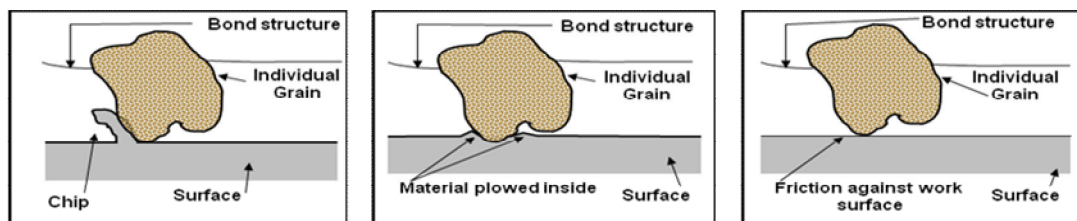
Figure 2.1 Displays the grinding mechanics of cutting, ploughing and rubbing (Griffiths 2001)

Plastic deformation, phase transformations, thermal expansion and contraction are all different grinding phenomenon that can cause residual stresses in a ground surface. Out of these different grinding phenomenon, thermal expansion and contraction offer the most undesirable effects during grinding this is due to the residual stresses tend towards tensile rather than compressive. Chen (Chen, Rowe et al. 2000) investigated the relationship between the onset of residual stress and grinding temperature which in short

means; the control of stress controls the grinding temperature. Chen also described three different types of residual stress in the surface layer of the ground workpiece.

- Outmost surface layer becomes untempered martensite (compressive residual stress) and sub-layer tempered (tensile residual stress).

- Workpiece cooled – phase transformation and re-hardening occur.

- Severe Grinding Burn.

Specified heat flux of the grinding zone which is the power per unit area of grinding zone and the convection coefficient at the workpiece surface has been investigated (Demetriou and Lavine 2000). Demetriou illustrated his findings by producing a completely coupled thermal model which consisted of wheel grains, workpiece chip material, coolant and workpiece surface analysis. This model looked at the thermal effects where the heat is generated at the grains' wear flat; then into the grain, the workpiece and shear planes. Finally, the heat is transferred to the chips and workpiece. Demetriou found that up-grinding measured higher temperatures at the grinding zone compared with down-grinding, this is due the chips getting cooled more directly in down-grinding than with up-grinding (i.e. the heat flux cools the maximum temperature at the grinding zone in down-grinding when compared with up-grinding which is not cooled at the maximum rate of the grinding zone).

Workpiece melting cannot occur on the surface as the grinding temperature is only significant for 1 ms pulse and therefore not enough for the material transformation seen in material melting. The cooling effectiveness of creep-feed grinding was investigated

The University of Nottingham

and beyond the burn-out limit in which coolant film boiling occurs (Guo and Malkin 1994; Guo and Malkin 1995; Guo and Malkin 1996). Here the temperature rises to catastrophic levels although the boiling point is understood and can be predicted. Experiments were carried out on an aerospace nickel based alloy Inconnel 100 (HRC 37) and with an aluminium oxide wheel. It was understood if the depth of cut was reduced then burn-out was less likely to occur.

Burn experienced from grinding performs permanent change in the microstructure of the surface layer which in short deteriorates the surface performance of the workpiece (Kwak and Song 2001; Kwak and Ha 2004). Continuous high temperature in the grinding zone is the main cause of workpiece burn. In addition, the temper colours observed from burn relate to the thin oxide layer of the workpiece surface and correlate the severity of workpiece burn. As soon as workpiece burn occurs the forces exerted during the grinding process are increased, along with rates of wheel wear which directly impact the surface roughness of the workpiece in a diminishing manner. When grinding wheel characteristics are as follows; hardened grit materials, smaller abrasives and higher grades of grinding wheel the more likely burn is to occur.

Investigations such as the one carried out by Brinksmeier (Brinksmeier and Heinzel 1999) looked at the relationship between workpiece/grit friction, cooling and lubrication in grinding. The combination of lubrication and cooling ensures there is reduced wheel wear, surface quality is improved and unwanted chips are washed away during the grinding process. Different types of coolant such as emulsion, oils or near dry grinding

The University of Nottingham

solutions all affect the coolant and heat generation at the grinding zone. As the coolant changes from water to a more dense oil based solution the wheel wear, surface roughness and grinding forces all decrease. Film boiling is caused by the evaporation of coolant where the rapid heat transfer is taken from the workpiece (burn) into the flowing coolant. An increase in coolant pressure ensures the chips are washed away, the workpiece is sufficiently cooled and the boiling film effect is delayed or even eliminated. This increase in coolant pressure multiples the forces already present in the grinding zone and the rapid cooling effect can give rise to mist which is unwanted in any manufacturing environment. With the mist and environmental concerns there has been significant research to provide a water-based fluid which can act similar to oil based coolant solutions in prolonging wheel wear and decreasing surface roughness. Not only is it the type of coolant that is used but as mentioned before, the direction of coolant application is important as is the wheel loading effects experienced by inferior coolant types. The investigations concluded that wheel loading occurs with both water and oil based coolant types when applied to a CBN wheel when grinding nickel based super alloys. Both Emulsion and synthetic fluid all exhibited significant amounts of loading. Wheel failure is mainly attributed to the build-up of material during wheel loading which can be minimized from techniques such as scrubber jet removal or pulsed laser surface cleaner (Chen, Feng et al. 2004; Chen, Feng et al. 2004).

The University of Nottingham

2.2.3 Chatter and vibration effects in Grinding

Both tool and workpiece vibrations are concerns within the manufacturing environment. A vibration that multiplies on itself is that of chattering. It is the dynamic instability of the machining process in which high unacceptable noise is attributed to high feed speeds, incorrectly tightened fixed fixtures and finally, from considerable grinding wheel loading phenomenon (experiments carried out in this thesis concentrated on the former and latter of these tribulations). The regenerative chatter condition is a common problem in grinding. The tool holder, workpiece and spindle will vibrate at some natural frequency giving rise to the chattering condition. The Chattering of both the workpiece and wheel produce waviness chattering marks along the workpiece. This waviness can then cause a variable load on the next grinding pass which multiples as the next grinding pass is made and so on. This effect of chatter has to be recognised and minimised (Chiou, Chung et al. 1995; Hashimoto, Marui et al. 1996; Chiou and Liang 2000b).

The result of chatter impacts the miss-shape of workpiece geometry and undulations (roughness) of grits bonded within the grinding wheel structure. This is highly undesirable for cutting efficiency as dull grits and flexible bonded material give rise to a ploughing phenomenon which is not efficient grinding and should therefore be more in the way of cutting phenomenon. There are two types of grinding chatter experienced in the manufacturing environment; self excited chatter or vibration and, forced chatter or vibration. To that end, before grinding chattering problems exist it is worth measuring the natural frequency of the machine and eliminating operations that occur near to those measurements. In addition, abusive grinding conditions should be discouraged which

give rise to the forced chattering phenomenon (Inasaki, Karpuschewski et al. 2001; Kwak and Ha 2004):

- Decrease feed rate if chattering is present.

- Increase wheel (not to the point of wheel bounce phenomenon) speed.

- Ensure the flood coolant nozzle is correctly positioned to cool the chip area and ensure material removed particles are washed away and not adhesive to either the wheel or workpiece.

- Ensure the fixture clamping the workpiece is correctly tightened.

- Ensure the redressing interval is optimised or continuous to eliminate significant material wheel loading.

- Trade-off depth of cut levels to ensure good material removal rates (MRR) although not to the detriment of workpiece quality.

There are several material surface patterns associated with grinding chatter these are; straight, spiral or mottled. The chatter (wheel generative chatter) associated with the development of lobes within the surface of the grinding wheel is self exited in nature and caused at low wheel speeds. If however the converse is true and high wheel speeds are exerted with lobe material build up then this is referred to a workpiece generative chatter. Chatter can be reduced by both wheel and feed rate speed reductions, in addition to these provisions; either a larger or softer grinding wheel can be used to minimise chatter. Further reductions can be made with chatter where the chatter amplitudes are reduced from the variation of grinding wheel speed (Sri Namachchivaya N. and Beddini

The University of Nottingham

R. 2004). The forces experienced during grinding which result in the specific energy give an accurate representation of the behaviour occurring in grinding (Marshall and Shaw 1952). Other researchers discuss using other signals to represent grinding behaviour such as; the machine vibration. Vibration has been used to determine the wheel wear and wheel redress life (Malkin and Cook 1971; Zeng and Forssberg 1994; Zeng and Forssberg 1994; Inasaki 1998; Hassui and Diniz 2003). The theory behind this research is based on two phenomenon occurring during vibration; the first is the self excited vibration where the chatter is caused by the random interaction between workpiece and wheel grain particles, the second is the forced vibration which can detect unbalanced set-up (such as unbalanced shafts or misshaped grinding wheels through loading) or other external sources of vibration (collision of particles occurring at the end of the grinding pass or movement).

2.2.4 Grinding Condition Monitoring

Condition Monitoring systems have been used to optimise manufacturing processes in terms of maintaining quality driven products, automating the process with less human interaction, optimising the machine process to ensure continuous manufacture (for instance; be able to monitor several different machining processes within a machine centre), reduce or eliminate costly machine down times through machine damage/repair (in terms of fixtures, machine parts and tools) and the cost of machine set-up time. All these points have been investigated by researchers however, researchers (Al-Habaibeh and Gindy 2000; Al-Habaibeh and Gindy 2001; Kwak and Ha 2004) previously

The University of Nottingham

investigated generic tool condition monitoring systems that can monitor several manufacturing processes contained within a single machine centre.

Root Mean Squared (RMS) amplitude detection levels to identify different grinding phenomena (Akbari, Saito et al. 1996) have been used in early grinding monitoring work. This method can be very useful for online monitoring; however the monitoring system would require more information to ensure an accurate and efficient classifier system. With RMS signals some of the high frequency components can be missed which provide richer data in terms of determining potential catastrophic tool failure or data significant to tool dressing/tool swap out.

Chiou and Liang (Chiou and Liang 2000a; Chiou and Liang 2000b) designed and implemented a Process Monitoring (PM) model based system on observations made from actual grinding outputs such as the measured chatter frequency and chatter AE emitted amplitude. Chiou and Liang made some assumptions that different AE signatures are made from different width of cut as well as the actual depth of cut. Vibration and cutting speed is also reflected within the AE signatures. This is a very important observation and therefore emphasises the need for the training and test data to encompass the general grinding parameters such as feed rate, wheel speed, down or up grinding and both, width and depth of cut. From this approach it can be seen that the AE_{RMS} signal is inversely proportional to the cutting speed. Different AE signatures for the start and end points when broaching were observed (Axinte and Gindy 2003) which are also inherent in grinding and should be taken into consideration. This suggests that

AE if verified through other sensory signals then it can be used to identify miniscule and quick burst phenomenon which is significant to current process monitoring paradigms.

In understanding the grinding process we know there is material removal from each individual grain (Chen and Rowe 1996; Chen and Rowe 1996; Chen, Rowe et al. 1996). Factors within the top layer of the grinding area are primary inputs to the grinding process. Also environmental factors were considered such as machine tool structure, work piece and coolant delivery. These factors are significant to a generic condition monitoring system for grinding technologies and will be addressed within this thesis.

Chen and Liu (Chen and Liu 2004; Chen, Liu et al. 2005) carried out similar research in using Wavelet Packet Transforms (WPTs) to transform extracted AE in terms of dynamic time-frequency represented signals taken from material that experienced either burn or no burn. This transformation is where the raw time signal is converted to both the time and frequency domain through a dynamic window which allows a rich and precise picture of what is occurring during the extracted signal. Chen and Liu used a Fuzzy-Neural Network (ANN) classifier to distinguish between burn and no burn phenomena.

The amplitude of grinding increases gradually throughout the wheel wear process, the predetermined vibration 'f' shifts towards the natural frequency (ω_n) and the time varying signal is monitored to evaluate when outside limits and therefore becomes unacceptable when the wheel needs to be redressed (Chen, Rowe et al. 1996). An

The University of Nottingham

Artificial Neural Network (ANN) was used to identify wheel life which consisted of a pre-processor of 8 band-pass filters supplying the ANN input neurons across the total range of chatter frequency. Vibration is one of the main determinants for diagnosing when wheel dressing or swap out is required. In addition, the wheel shape tends towards a polygon shape. The chatter frequency increases with radial force which is the force between wheel and work piece. AE amplitude which is a function of time could be used to measure wheel life (Mokbel and Maksoud 2000).

The surface condition of the wheels could have an influence on surface and sub-surface cracks of ground hard and brittle materials which reduce their final strength. The variations in both AE spectral (Mokbel and Maksoud 2000) amplitude and surface roughness were taken from different grinding wheel conditions albeit for the same wheel grit size and different bond types.

Tonshoff et al (Tonshoff, Jung et al. 2000; Tonshoff and Friemuth 2002) described the relationship between surface roughness and AE extracted signals, and, the contact detection of dressing superabrasive grinding wheels. The surface roughness is measured using a Talysurf measuring system. It was considered that high AE signals were achieved from worn tools as opposed to faulty sharpened tools. Tests were carried out to understand the relationship between AE signal characteristics and surface anomalies which is pertinent to the research conducted within this thesis.

Al-Habaibeh and Gindy (Al-Habaibeh and Gindy 2000; Al-Habaibeh and Gindy 2001; Al-Habaibeh, Zorriassatine et al. 2002) use a reduction matrix technique 'Taguchi' to

The University of Nottingham

ensure sensors with useful information are used instead of sensors with useless or 'don't care' data, this was applied to the milling process. By using Orthogonal Arrays (OAs) through Taguchi, each matching parameter from the level of signals was evaluated. This method could be adapted to the grinding process. In addition, the classification technique of a Fuzzy-ANN non-linear classifier provides a robust control system for carrying out PM.

Kwak and Ha (Kwak and Ha 2004) use a ANN and Digital Signal Processing (DSP) techniques to gain the identification of the onset of burn and chatter vibrations. To gain these phenomena both AE and power signals were extracted. Static power and dynamic power were determined as the power parameters; the peak of the RMS and the peak of the FFT were applied as AE input parameters to the ANN for classification. It was noticed that at the onset of grinding burn, grinding force wheel wear rates, increase sharply and the surface roughness deteriorates. This particular research takes into consideration the grinding conditions, grinding wheel, dressing conditions and coolant application. To predict the fault phenomena such as the burning and the chatter vibration, this needs to be diagnosed at the early stages and avoided as much as possible. When burn occurs, the static power changes from a constant, to a varying rate. Chatter vibration has significant magnitude which changes both in regard to static and dynamic power.

A useful piece of research that can be applied to on-line monitoring or near on-line monitoring is provided by Wang (Wang, Willett et al. 2001). Wang uses the band power,

kurtosis, skew and autoregressive (AR) coefficients (Wiener coefficients) of the raw extracted time AE signal. This is a very useful technique to identify burn and no burn; however this technique has not been applied to both the time and frequency domain using STFT or other time-frequency representations providing richer summary data to the classifier. In addition, there are other statistical functions that can be used to distinguish interesting phenomenon from the copious amounts data presented by a raw AE signal. Quick reduction techniques are very useful for ensuring near instantaneous classification and are imperative for an online monitoring system.

As well as using a range of DSP techniques and extracting several signals (all providing machine rich information in parallel) there is a need for a generic classification system that can identify a range of different phenomenon such as that seen in multi-classification recognition systems. That said, the system has to be able to deal with large data systems and make accurate decisions, even ignore outliers spoiling the generalising capability of the classifier system. There are the already mentioned ANN classification systems which have been used to classify burn and no burn during a grinding pass. The real 'break-through' in classification systems is based on the online classification system where most current systems are either off-line or semi-online (i.e. make a decision based on a finite time to distinguish the phenomenon from extracted signal).

Other classification systems such as fuzzy clustering, Support Vector Machines (SVMs) and Evolutionary Algorithms (Genetic Algorithms and Genetic Programming) can all be used; either as a single classification system or, a combination of classification systems

The University of Nottingham

(hybrid system). A combination of two ensures a more robust and accurate classification system that can provide multiple classifications for large amounts of n-dimensional information. For example; a ANN can provide fairly accurate classifications however if the boundaries are close and the vector inputs are very large, the ANN with conventional learning techniques such as the back-propagation training rule may have solution spaces ending up in a local minima (even if the learning momentum is optimised). If the learning rule is combined with back-propagation and the solution strategy of survival of the fittest through Genetic Algorithms then the solution space maybe less likely to fall into local minima and arrive at a near/global minima.

Semanta (Samanta 2004), compared the performance of ANN and SVM in bearing fault detection (fault or no fault recognition). This work discussed genetic algorithms and its optimisation in the configuration of the number of nodes within the hidden layer of an ANN and the radial basis function kernel parameters (width) in the case of SVM. The data is split in terms of training and test data with the majority being used for training the classifier. The results signify the effectiveness of features selection optimisation within a classifier and its ability to detect machine conditions. That said; the SVM optimised by feature selection outperformed the optimised ANN based on the SVM ability to work in n-planes and n-dimensional spaces with no great increase in complexity as is the case with ANN.

Cus and Baltic (Cus and Balic 2003) used a combination of GA and ANN to optimise the machine operating cutting parameters. The ANN would learn the best cutting conditions based on applied data however the GA would enable better previous cutting

data to be used in place of the recently applied data. This GA acted as a feedback tuning device for the ANN and results proved both efficient and accurate.

Tsukimoto and Hatano (Tsukimoto and Hatano 2003) used a GA to optimise the local back propagation error within a feed-forward ANN. The GA here works in the way where the ANN gets to a certain point within its training (end of a finite batch) and then compares the weights to input-output relation with others within the batch and recognises which one gave the best results. The best result in the batch is chosen for insertion and reproduction (encouraging fittest speciality) within the next generated populated set and in an iterative fashion the learning batch takes place again. The GA also determines the initial weight values thus giving some prior knowledge to the network before commence of training.

There are other classification techniques used for huge data sets and ones that are continually being presented with extra data. Such classification systems need to be unsupervised in deterministic characteristics, thus the data classification becomes more robust as the amount of applied data increases. With the ANN however, there needs to be a reasonable level of information (though not too much where over fitting of the network occurs) to make the generalisation for applied data (this is known as a supervised classifier). With supervised classifiers they are more constraints in terms of continual data when compared to unsupervised classifiers. Chen and Liu (Chen and Liu 2004; Chen, Liu et al. 2005) used WPTs to transform extracted AE signals taken from grinding passes of aerospace alloys that either experienced burn or no burn. WPT

The University of Nottingham

converted the raw time extracted signal into both time-frequency domains thus giving a richer summary of information to classifier. Chen and Liu used a Fuzzy-ANN classifier to distinguish between both burn and no burn phenomena. This is where a Fuzzy clustering algorithm was used to identify the significant non-linear features and reduce data dimensionality; the ANN however would perform classifications from a compressed-salient data set (using n-dimensional reduction techniques).

Researchers such as Yao (Yao, Li et al. 1999) have applied fuzzy clustering classification to defined cutting edge machining utilising both the AE and power signals to identify the different levels of cutting tool wear within milling. This is a very useful technique to apply to a generic classification paradigm as it can handle increased amounts of data, be that training data or test data.

Howard et al (Howard, Roberts et al. 1999a) uses Genetic Programming (GP) to identify targets (vehicle and ship detection). A number of experiments mixed in with statistical measures provided GP with some very useful results. It was found that a 1st detector would be used to scan over the image and then a 2nd detector would be used as a more accurate spot detector. If both detectors resulted in a hit then the overall result would be a hit. If the first detector identified a hit and the second detector provided a result that it was unsure of, GP would more than likely output a hit, only when both detectors provided a miss would the GP program output a miss.

The University of Nottingham

There has been a number of different papers produced on this subject for instance, Poli (Poli and Langdon 2006) looked at similar approaches however the metric fitness measure was not based on a Fuzzy Rule set such as that used by Howard et al. The Fuzzy Rule set fitness measure was required due to the GP method not identifying some obvious grade 1 target (targets measured from 1 – 5, with 1 being the most obvious image). For vehicle detection, concentric rings were used to identify the salient features based on the statistical properties (size and characteristic features of a vehicle).

The modified metric fitness measure is as follows:

Fitness = (((sum of hits * (5 - ship grade)) / ((sum of targets * (5 – ship grade)) + FP))

Where FP: False positives

Poli (Poli, Langdon et al. 2005) also looks at how GP can improve on random search algorithms such as particle swarm which merges the richness of two strategy algorithms to give a hierarchical classification system. The research discussed by Howard et al (Howard and Dangelo 1995; Howard, Roberts et al. 1999a; Howard, Roberts et al. 1999b; Howard, Roberts et al. 1999c; Howard and Roberts 2002; Howard, Roberts et al. 2006) is of particular importance to this research as it displays a method where every target is pre-processed and trained against a GP Paradigm. The Fitness measure is based on the amount of correct classifications found. These pre-processed targets are converted into an understandable computer format such as a bit map image and then categorised through statistical measures (variance, Fourier Mellon Moments and statistical means). For the research presented in this thesis a powerful classifier such as GP could be used

The University of Nottingham

to look for significant features in a range of anomaly data. GP suffers from n-dimensional data problems however it provides a hierarchical tree rule based system, which can provide different levels of multiple classifications. This suggests that a technique to reduce the data before being applied to the GP would be extremely advantageous thus a hybrid system such as Fuzzy clustering or n-dimensional data reduction technique merged with GP could provide a powerful generic classifier.

2.2.5 Condition Monitoring in the Grinding Process

One of the largest obstacles to overcome in providing a successful monitoring system for grinding technologies is to understand the complexity of the grinding process. This is why force models and unit event models (single grit scratch tests) give the grinding community more understanding of the grinding process and from this understanding an attempt to control parameters based on varying extracted output products can exist. To gain a successful monitoring system, systematic investigations with clear logical aims in mind must be carried out to build a successful paradigm although constraint to certain machining parameters varying, and some parameters, remaining constant. This constraint is more in order to build a manageable system that does not look at every changing aspect as this would require an exhaustive data set; instead, models cater for the extremities through the extrapolation of finite, pre-determined and verified information. In short, within the grinding process there are some 'don't care' states and some states that need to be focused on and identified when considered a problem. There are three main considerations to be made when introducing a grinding monitoring

system into the workshop. Firstly; design and implement a reliable although non influencing sensory system(s), secondly, use suitable digital signal processing techniques in terms of filtering the real world extracted signal then format into a rich summary data set for the last consideration, a developed model capable of distinguishing patterns describing the on-going process. The condition monitoring system must be able to demonstrate its added value as well as reliability from the repeatability of results. For example, to demonstrate such added value would mean the process identifies when a grinding wheel is required to be dressed or even exchanged. To ensure the sensory technologies are reliable and consistent, the sensors are tested and calibrated. From the testing and calibration the operator can be confident one signal from one day can be compared to another extracted signal another day.

To ensure a system is suitable for reliable monitoring the system under scrutiny must be able to operate as a stable platform under normal parameter cutting values. The monitoring system itself must be accurate, continuous, manageable in terms of data handling constraints, automatic or manual and finally, be fitted in a manner that does not affect the machining process although close enough to get as accurate a picture as possible. Once these normal operating conditions have been modelled and set up, then extreme or more towards abusive machining (less stable parameters) can be recorded. These different parameters should display trends from the normal operating conditions and from this controlled environment repeatability should be applied each time.

The aims of grinding monitoring systems:

- Extract data and perform knowledge representation – such actions allow the advancement of force and power models to represent a given process and are used to control the grinding process.

- To be able to identify grinding defects such as burn, chatter, burrs or even wheel loading that may lead to one of the former phenomenon.

- To act on this information and carry out actions to ensure the identified defects are observed and managed such as redressing the wheel, swap out, lower feed rate or spindle speed for example.

- The optimisation of the grinding process in terms of workpiece quality, machine time and machine costs.

Grinding monitoring systems provide a sound perspective in aiding and supporting existing manufacturing processes however such systems could be used to automate facilities especially as the expected labour skill shortage becomes more apparent. In addition, a machine is far better and more efficient at shutting down a process based on a sensor(s) identifying there is a problem with the coolant for example; blockage and falling nozzle pressure which is detrimental to the grinding of hard to cut aerospace alloys (burn and wheel wear can exist very quickly under these conditions). There are different sensor technologies available for extracting products of the grinding process. Such technologies are the use of temperature sensors to monitor for the initiation of burn (Deiva and Vijayaraghavan 1999), accelerators for the occurrence of chatter vibration (Inasaki, Karpuschewski et al. 2001) and ultrasonic sound sensors for the deterioration in surface roughness (Mokbel and Maksoud 2000) and (Tonshoff, Jung et al. 2000).

Table 2.1 displays the feasibility for measuring grinding phenomenon verses the sensor technology used to identify that phenomenon and how useful that technology is for a specific application. The sensor technologies presented in Table 2.1 have all been used for machine monitoring for instance; Tonshoff's earlier work used a range of sensor technologies such as AE, force and vibration sensors (Tonshoff, Fremuth et al. 1994). For temperature, load and eddy sensors; (Guo and Wu 1999) .

Table 2.1 Relevance of senor to grinding phenomenon

Grinding Phenomenon	AE sensor	Temp Sensor	Vibration sensor	Force sensor	Load sensor	LVDT sensor	Eddy Sensor
Workpiece Burn/white layer	√√	√√		√√	√√		√√
Workpiece Temperature		√√					
Workpiece Hardness	√	√		√√			√
Workpiece/ Wheel Chattering	√√		√√				
Workpiece Runout	√√			√√		√√	
Workpiece Size						√√	
Workpiece Stress	√	√√		√√			√√
Contact detection	√√		√√	√√	√√		
Unbalanced Wheel			√√				
Wheel form wear	√√			√√		√	
Wheel profile	√√					√√	
Wheel sharpness	√√			√√	√√		
Wheel run-out	√√		√√	√√			
System stiffness				√√	√√	√√	
Gap elimination	√√				√√		
SG scratch tests	√√			√√	√√		

Key: √√: highly relevant √: relevant

For each sensor technology there is high relevance (√√) with a lot of research supporting these findings and relevance (√) with only minor supporting research.

The University of Nottingham

2.2.6 Acoustic Emission

This thesis is primarily concerned with the extraction of acoustic emission (AE) signals and other supplementary signals (discussed further in Chapter 4) are used to verify the AE signal technology. The pioneers of AE came from Germany in the early 1950s (Kaiser 1950) and later Schofield and Tatro (Schofield, Bareiss et al. 1958) introduced Kasier's work to the United States. AE has been used for materials research in monitoring stresses from AE events emitted from crack initiation, structural defects, measurements, and other material anomalies. From this work it was found that most materials emit sounds or stress waves as they are deformed, these sounds provide the very nature of plastic deformation under different intensities which inherently give warning signals for impending failure of a specific material. A lot of work in the area of AE has been made on many different materials from homogenous/non homogenous metals/alloys to rocks and earth quake monitoring. The sensitivity of such sensors is of paramount importance, for instance; this thesis investigates micro-cracking and single grit action where the AE phenomenon is so miniscule and localized it is difficult to detect. For Earth quake seismic activity the sensitivity needs to be much less localized and with a focus of a much larger surface area. AE generated from material under stress refers to the generation of transient elastic waves during the rapid release of energy from the localized sources within a material. The difference between the AE technique and other nondestructive evaluation (NDE) methods is that AE detects the activities inside the materials, while other NDE methods attempt to examine the internal structures of the materials. Furthermore, AE only needs the input of one or more relatively small sensors fixed on the surface of the structure or specimen under examination. This allows the

The University of Nottingham

structure or specimen to be subjected to stresses whilst under in-service or laboratory operations and the AE system continuously monitors the progressive damage. Other NDE methods, such as ultrasound and x-ray, have to access the whole structure or specimen, and therefore, the structure or specimen often needs to be disassembled and taken to the laboratory to be examined.

The disadvantage of AE is that commercial AE systems can only estimate qualitatively how much damage is in the material and approximately how long the components will last. So, other NDE methods are still needed to do more thorough examinations and provide quantitative results. Moreover, service environments are generally very noisy, and the AE signals are usually very weak. Thus, signal discrimination and noise reduction are very difficult yet extremely important for successful AE applications.

As early as the advent of AE signal extraction to the work carried out by Tonshoff (Tonshoff 1992; Tonshoff, Fremuth et al. 1994) there has been the investigation of quantitative and non-destructive measuring of the surface residual stresses in metals. For example; surface residual stresses in aircraft propeller blades were investigated soon after the early applications emerged within the field of AE material analysis. Kaiser's initial work indicated a correlation between the occurrence of AE and certain physical and metallurgical characteristics of metals. The achieved quantitative state of stress in the material could be matched against physical and metallurgical condition. Such conditions can be identified as grain size and yield strength of the material which in short influences the acoustic emission response and suggests that the relationship of the AE response is peculiar to varying intensities of surface residual stresses in metals. Due

to the lack of explanation for identification of variables changing within the AE emitted from materials and correlated to surface residual stress this work stopped. Such a non destructive tool for the use of measuring residual stresses is an invaluable asset to any manufacturing quality assurance department. Kaiser continued to look at AE relating to material grain boundary distortion and shear from applied stress; it become clear from experiments that grain size was an influential parameter affecting emitted AE however it was not the primary contributor of AE. Further work was carried out and the difference in material heat treatment as well as other metallurgical variations can be detected by AE. Early AE work looked at voltage level detection in the form of count rates based on a count occurring every time the emitted AE passed a defined voltage level threshold. It was noticed from tests of many materials that the count rate steadily decreases with strain and increases rapidly prior to failure (Fisher and Lally 1967). Some of the largest intensities of AE are at the beginning of plastic deformation where shear has to pass the energy level for the material grain boundaries and dislocations to occur, once occurred, the plastic deformation will propagate in the applied direction until the energy causing the plastic deformation is lower than the energy required to cause the material plastic deformation (Tetelman and Chow 1972). Tetelman and Chow also looked further in microcrack propagation and noticed that brittle materials give off bigger AE signatures when compared with ductile materials, instead, ductile materials make steady rises of AE in a linear increasing fashion where brittle materials give step increases. This is due to brittle materials having less elastic material property and more plastic material property characteristics. The area under the envelope of the AE event is the energy, the envelope can be described from the initial rise in magnitude to the time the level drops

below the noise (voltage) threshold of interest (for these tests, 35db was the set pickup noise level). Tonshoff (Tonshoff and Friemuth 2002) also discussed that the root mean square value (RMS) increases with higher specific material removal rate. Additionally, thermal damage increases the amplitude damping rate of the acoustic signal (Klumpen 1994). The correlation between the emitted AE signal amplitude and the tensile residual stresses can be interpreted as a superposition of these effects. From tests carried out within this thesis there are noticeable oscillations and reflections of surface/material phenomenon apparent within the returned AE signal. Such oscillations are due to the size and thickness of the material, the level of energy emitted from the elastic/plastic deformation machining process, the distance between sensor, material anomalies and the material damping coefficient. Due to materials having different dimensions and characteristics there needs to be more work concerning the stability and reliability and this is why other sensors are used to verify the signal analysis. These other signal extraction techniques will be discussed in Chapter 3. With current understandings and calibration techniques, AE is becoming more widely accepted although there still remains more work to gain the confidence of other signal extraction techniques. These factors will be discussed in Chapter 4 along with the first principles behind the operation of AE technology.

2.3   Single Grit Technology

This Section discusses the primary research carried out in this thesis and is considered a significant area in understanding the fundamentals of grinding mechanics with a view to

acquire efficient grinding. This fundamental view of grinding is in regard to single grit (SG) scratch tests to mimic the microscopic interaction between grit and workpiece material. Already there is research within this field as several researchers try to bridge the gap between the microscopic and macroscopic mechanics of grinding and workpiece interaction.

Hamid (Hamid 1977) investigated grinding mechanics through a SG approach. From conducting experiments with a protruding Al_3O_2 grit glued to a metal disk attached to the machine centres spindle, SG analysis was carried out. It was found the more negative the rake angle the more cutting takes place and the less negative, the more ploughing takes place. Changing rake angles during the SG intersection express rubbing, ploughing and cutting phenomenon which are referred to as the grinding mechanics and is of particular interest to this thesis.

It was noticed when the grit was observed to be more dull and flat in terms of wear, more ploughing phenomena occurred. The converse is true of cutting where the grit is sharp and wear has hardly been experienced. The grit action was observed to be similar to a plunge feed device in that the sheer force at the tip acts similar to a snow plough. This is where several cuts from the different geometries are experienced from a single piece of grit. In addition, there is less material removal with soft materials when compared with hard materials.

The University of Nottingham

A computer simulation (Baul R.H. and Shilton R. 1967) of random grits based on rods with measured heights in terms of rectangles and squares (squares remove more material thus faster at removing material). To feed the information to the simulation, a scratch in the form of a length of hits would be measured. This type of simulation is very useful to the understanding of grit and workpiece interaction; ultimately it can provide more efficient grinding solutions. During these tests it was also noticed that the outmost grains have an impact on the quality of the ground surface. If these outmost grains are removed they would ensure a better surface quality of the ground surface this is indicative of fine dressing used to remove grains and give greater cutting ability to a previously worn grinding wheel. For the simulation it was noticed that the height distribution of a wheel surface profile is Gaussian.

From Hamid's SG work (Hamid 1977) two types of chips were identified; continuous with built up edges and random flake material. Another important observation was ploughing is considered a function of wheel speed and material hardness. For varying hardness of a material, the measured tangential and normal forces had negligible effects and therefore SG and grinding have different mechanics. This is maybe true however from SG to grinding passes there needs to be work that bridge the gaps and build on the understanding in a bottom-up approach which is what is proposed in the research discussed within this thesis.

It was noticed that tangential to normal force is approximately 1:2 ratio respectively this holds true for the coefficient of grinding which is based on the friction coefficient of

The University of Nottingham

grinding. Grinding compared to single point cutting however is measured as 20 times greater which would suffice considering the random bombardment of grits compared to one single protruding grit set-up for analysis purposes.

For both SG and grinding tests carried out within this thesis, the following was considered (Griffin and Chen 2006; Chen, Griffin et al. 2007):

- Original rigidity should be maintained

- The dynamic characteristics maintained

- Frequency response as high as possible for acquisition from load cells

- The cross interactions between measurements of force components should be minimal

Graham and Baul (Graham and Baul 1972) discussed that the response time must not be more than a third of pulse duration for extracted force signals obtained during the SG scratch tests. Crisp et al (Crisp, Seidel et al. 1968) discussed the dynometer response time should be the reciprocal of the natural frequency of the scratch and should not exceed a third of the event occurrence time. In other words, the resonant frequency of the dynometer should be at least three times that of the measured event.

Hamid (Hamid 1977) used different specimens with different hardness levels. All specimens were ground and polished to 0.015 μm surface roughness (Ra). For any SG analysis work it is important the initial surface is both flat and polished to a small surface roughness measurement. This is to assist the material analysis in terms of

The University of Nottingham

miniscule measurements. In regard to the different hardness measurements it was found best practice to keep the same scratch width throughout the tests. The scratch width of 0.18 mm was maintained during the tests under speeds of 11, 19, 28, 37m/sec through motor drive and slow speed (rotating the disc by hand). The experiment was tracked under the cutter with a speed of 17.7 m/min, these speeds are much slower than commercial production spindle speeds and although good for analysis work they are not transferable to current manufacturing practices as seen in VIPER grinding. The research in this thesis looks at much higher speeds which are the same as that used in aerospace turbine manufacture. In addition, the Machino A55 machine centre can achieve 1μm incremental movements which is far more accurate than what was used in Hamid's (Hamid 1977) work.

It was noticed that the depth of cut varies due to the elastic effects of the bond in the system set-up and the added effects of pile-up at the edge of the groove also contribute to the varying depth of cut. This is an important observation and explains certain phenomenon regarding to the research carried out in this thesis see Figure 2.2 for more information.
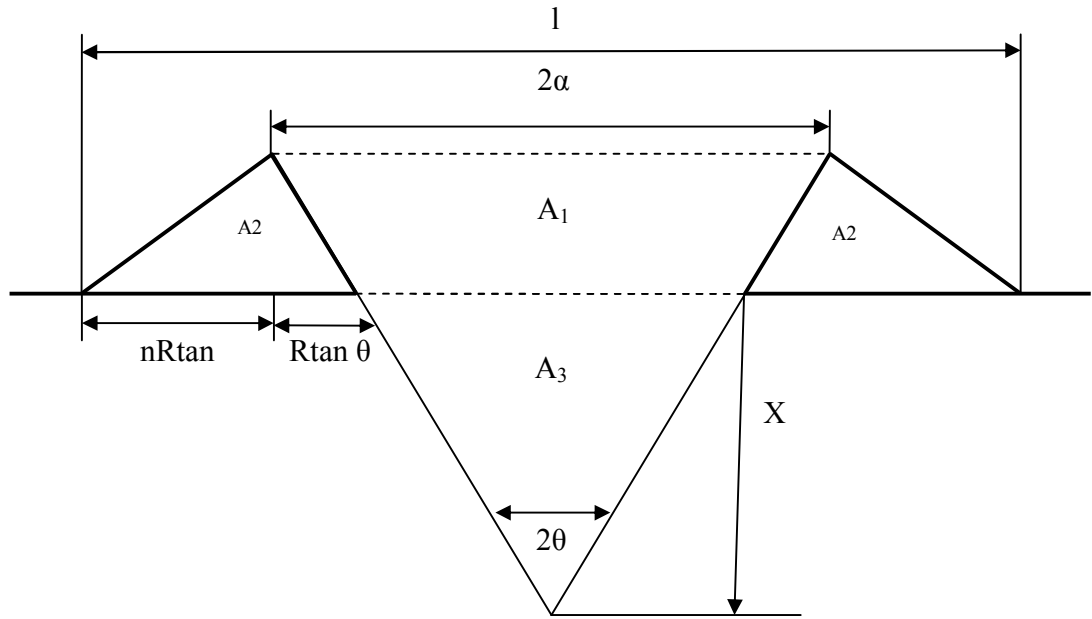
Figure 2.2 Single scratch parameters

Cutting efficiency $B = (A3-A2)/(A1+A3)$ (2.1)

Where: $A3 - A2$ = material removed

$A3 + A1$ = total groove volume

Figure 2.2 and the cutting efficiency equation of 2.1 displays a similar mechanism for calculating the different mechanics observed in a single grit scratch of the cutting, ploughing and rubbing. Here the cutting efficiency is calculated where >1 would be the best efficiency, thus material removed is more efficient than the actual groove cut. With cutting, ploughing and rubbing the more efficient emphasis of cutting is placed on the material removed however more emphasis is placed on the volume of the depth of cut signifying cutting rather than ploughing. Rubbing however is more consistent with

The University of
Nottingham

elastic deformation and found with thick wheel widths when grinding, this produces temperature and in extreme cases; burn.

Buttery and Archard (Buttery and Archard 1971) discuss grinding efficiency increases as the hardness increases and at the same time, speed also increases the cutting efficiency. Due to elasticity, it was found the tangential and normal force was proportional to load with soft materials however deviations with the hardest of materials occurred. So in short for this work of Hamid's (Hamid 1977), force predictions are good for softer materials and not so good for harder materials. In addition, force measurements not good at high speed but good at low speed as they correlate with SG model equations. Other findings of the work were as follows:

(1) The grinding coefficient dropped as the hardness of workpiece increased
(2) Grinding coefficient at higher speeds gave the same value

Prins (Prins 1971a; Prins 1971b) supports Hamid's work in using pyramidal cutters, where the grinding efficiency increases with the increase of material hardness and increasing speed. Similar results were also true in higher cutting speeds giving smaller forces and this confirms results obtained from single cutters. Also the grinding coefficient is the same with a single cutter as that of a grinding wheel pass. This is an important consideration for the work carried out in this thesis in bridging the gap between single grit scratch tests to actual grinding pass cuts.

It was noticed when using single cutters, and failure to specify and measure the groove or scratch correctly can lead to difficulties in interpretation. For example, if the scratch length is used to derive scratch depth thus assuming a circular path, the total depth will not be found as:

1)   Pile up will be neglected

2)   The cutter does not describe the grinding pass because of elastic effects.

Elastic deformation varies with the magnitude of grinding force. The harder the material the more of the ratio varies with regard to grinding force.

Assumptions from this work for sharp grit analysis (Prins 1971a; Prins 1971b):

1)   Majority of the grits in grinding have negative rake angles.

2)   Normal force in grinding is carried out by the frontal facets of such grits.

3)   The grit does not change its shape during the course of use, or, in other words; the attritions wear or grit fracture was neglected.

For dull grit analysis point (3) is changed to consider the wear flat measurement of the grit which is proportional to scratch width.

Hamid (Hamid 1977) noted errors in the measurement of cot θ were due to elastic recovery after the scratch had been made, this will have no effect on force predictions

but will effect wear predictions. Both non-symmetric and symmetric pile-up was considered and it was more effective to express efficiency in terms of pile up rather than the conventional β term. For better surface finish it is when the process is more efficient i.e. less pile-up. Also from the results it was noticed the force needed to produce a scratch with a specified width is always increased as the material becomes harder, this is an important observation to the work carried out in this thesis.

So in summary to this work, to predict the normal cutting force if the material pile-up is known and the material hardness then a 0.99 confidence is obtained from calculations. Farmer et al (Farmer 1967) discussed material surface finish is independent to hardness. From Hamid's work there is no doubt material hardness plays a large part in surface finish. In addition, more friction through thermal effects and vibration from blunt grit affects work piece quality then more fine dressing is needed to ovoid this.

Wang and Subhash (Wang, Subhash et al. 2001; Wang and Subhash 2002; Wang and Subhash 2002) discuss an approximate upper bound approach (UBA) for predicting Material Removal Rates (MRR), force (normal and tangential) and overall frictional coefficient (OFC). This approximate model investigates scratches caused from various feeds and speeds to understand the material removal process during a rotating scratch on annealed pure titanium. From investigations built-up edge (BUE) governs the material removal process of the rotating scratch. Specifically the features of side-ridge, front-ridge, BUE and the sub-layer plastic zone evolve in different ways during the rotating scratch. Three material removal mechanisms were observed during the rotating scratch

The University of Nottingham

process these being; plastic (shear) deformation, contact friction and ductile fracture. The scratch groove was broken up into two halves; the first and second part of the scratch interaction. It was noticed that the both plastic (shear) deformation and contact friction played a dominant role in the first half of the scratch process whilst in the second half of the scratch interaction the ductile fracture plays more of a prominent role. These three mechanisms were observed from optical microscopes which displayed material pile up of the scratch sides in the first part of the scratch, and, extensive tearing in the second half of the scratch profile. This research used a novel set-up in that either the pendulum creating the rotating scratch was executed from either motor or manually (pneumatic piston) hand driven. The UBA technique would use experimental results to model the scratch process taking into consideration the changing rotation angle (defining cutting and ploughing mechanisms) and the measured material scratch groove depth and width. These findings would be summarised into both a local coordinate and global coordinate system to be used in matrix vector equations and be able to predict MRR, force and OFC. Input parameters such as flow stress (k), contact pressure (p) based on hardness (H) and Coulomb's frictional coefficient μ for a given combination of depth of cut h, orientation θ and scratch velocity v, play a vital role for UBA predictions. The set-up used two high frequency load cells (Kistler, 200kHz) for normal and tangential force signal acquisition.

Liang et al and Wang et al (Liang, Li et al. 1996; Wang and Subhash 2002) investigated the correlations between the specific energy and indentation hardness, scratch hardness and tangential hardness. The research discussed here looks at the rotating scratch process

The University of Nottingham

in terms of the ratio of energy dissipation to the scratch groove volume. In short, the hardness was considered as function of plastic removal during the rotating scratch process.

In earlier work to the UBA technique, Wang et al (Wang, Subhash et al. 2001) observed adiabatic shear band (ASB) formation followed by cracking during a rotating SG scratch with pure titanium material. This was the pre-curser work to the UBA work in that observations from the OFC were found to oscillate strongly at the beginning and the end of the scratch but, increased steadily in the middle of the scratch. This work also bolstered Liang et al and Wang et al work (Liang, Li et al. 1996; Wang and Subhash 2002; Wang and Subhash 2002) in that the size dependence of the overall specific energy and instantaneous scratch hardness were introduced to characterise the process. These parameters were also found to be proportional to the instantaneous depth of cut. Adhesion and BUE are factors observed from the contact zone between the diamond conical tool tip (inscribing the groove) and workpiece. At this point there is a dead zone between the tool tip and workpiece and this is where material adhesion has occurred on the tip and moves along in the direction of the scratch. To reduce this adhesion effect the scratch velocity must be increased which provides lubrication between the tool tip and workpiece. There were four regions observed during a rotating SG scratch namely; a stagnant region, a lamella zone with shear bands, a hardened sublayer, and a propagating plastic zone. The ASB is the result of large local deformation along the shear surface where the crack at the toe of the front-ridge are attributed to high surface compressive stresses met with at the beginning of the scratch. Specific energy is determined by

The University of Nottingham

hardening; when the groove depth becomes large, the competition between the hardening and softening dictates the specific energy. The effect of increased to decreased scratch velocities has negligible effects on the specific energy (this was based on the different velocities used during the tests). It was seen that as the tool tip becomes duller and wears flat this attributes to more rubbing occurring and more energy dissipated.

Subash et al (Subhash, Loukus et al. 2001) looked at pre-curser work to UBA approach in that the rotating scratch is executed on brittle materials; Homalite-100 and Pyrex glass. The set-up was the same as that used in UBA technique and the force in both tangential and normal directions was obtained. The formed scratch was investigated from the acquisition of force signals and microscope analysis. The recorded force and material analysis revealed intermittent removal patterns and oscillatory force profiles. For the Homalite material, the removal occurred in a periodic burst which is proportional in size to the depth of cut. A technique using data dependent systems (DDS) was used to evaluate the obtained force in terms of physical features obtained from the damage characteristics of the scratch formation. These features were represented in terms of energy roots captured with Green's functions. These complex and real roots can be used to look at energy interactions in terms corresponding crack occurrences and the driving frequency of the scratch formation respectively (the closer the real root is to unity, the more the groove physical characteristics are mathematically defined). This has been applied successfully to brittle materials however could not be applied to ductile and hard materials this could however, be used for an on-line

monitoring approach. This DDS approach has been used for on-line monitoring in previous research where on-line sensing was made for tool wear in turning and the monitoring, diagnosis of bearing defects (Pandit and Lin 1991) and tool breakage detection (Roth and Pandit 1999; Roth and Pandit 2000) in end milling.

When an object is subjected to an external force, it will generate elastic waves due to material particle displacements and these waves can propagate in material media (Royer and Dieulesaint 2000). Following on from this, the released energy is released as an Acoustic Emission (AE). Due to the material particle displacements under various stresses, an AE is released in the form of material elastic energy. These elastic AE waves mimic the mechanical vibration and are extracted by AE sensors. When different external forces act on the same material or the same external force acts on different materials, the elastic waves will have different characteristics. This is an important consideration as elastic waves can be used for monitoring many machining processes and/or material non-destruction tests (Webster, Marinescu et al. 1994; Chen and Xue 1999; Coman and Marinescu 1999; Holford 2000; Liu, Chen et al. 2005; Liu, Chen et al. 2006).

AE monitoring for grinding is a much more difficult task when compared with non destructive tests. The Single Grit (SG) scratching experiments are especially important to the grinding of materials and specifically, this research will concentrate on aerospace alloys which are characteristically hard and heat resistive materials. With these properties in mind, the machinability of such materials poses a challenge during the

manufacture of aircraft engine parts. In this research there is a focus on identifying the different levels of cutting phenomenon in grinding. It can be said that varying levels of SG interaction is an easier phenomenon to observe when compared with that of full grinding. This is in terms of the distinguishing features between cutting, ploughing and rubbing phenomenon and, the irregular distribution of grains when interacting with the material workpiece.

The AE wave is described as a non-stationary stochastic signal. Traditionally AE signals obtained from material tests were Root-Mean-Squared (RMS) level detection, event count, energy distributions, amplitude and the power utilisation of dominate frequency bands. These techniques were broadly used and applied to general non destructive condition monitoring tests based on events that were recorded in days instead of seconds. With the grinding AE phenomenon producing both short-high frequency and long-low frequency components, there is a need to have a continual wave-stream extraction facility. This is opposed to an event driven one based on a threshold which triggers the system into extract and record mode. The continual wave stream is required as short burst high frequencies can be missed with an event driven method. Fast Fourier Transforms (FFT) have been used for condition monitoring in the past which is used to estimate the frequency band components as well as their associated amplitudes based on the trigonometric family functions. FFTs however have a drawback; they do not have any time information of when the event occurred which is fundamental to the very nature of spontaneously released transient elastic energy when materials undergo deformation or fracture or, a combination of both. It is because of this no time

The University of Nottingham

component that they are hard to distinguish. FFT calculates the frequency average over the duration of the extracted signal and can be applied to a non-stationary AE signal, however, the results do not adequately describe the transient features in terms of frequency resolution (Li and Wu 2000).

Another technique that emerged from the family of FFT is that of STFT. This technique is similar to FFT however it addresses the issue of considering time as well as the frequencies and their associated amplitudes. The STFT gets round the problem of representing when a particular phenomenon occurred although it still does not get round the problem of resolution which is needed for accurately distinguishing SG features. That said, and with the extra dimension of time, the STFT still offers a good solution when required to characterise an AE signal.

Wavelet Transforms (WT), a family of orthogonal basis functions, can overcome some of the limitations posed by both FFT and STFT (Strang and Nguyen 1996). This is based on WT representing non-stationary signals through scaled time-frequency analysis. WT provides both an approximate and a detailed representation of scaled time-frequency analysis. The scaled localised time-frequency analysis characterises AE signals in terms of high frequency burst of short duration and components of low frequency, long duration (Staszewski and Holford 2001; Mardei and Piotrkowski 2002). For this research, both WPT and STFT are being investigated to translate the raw extracted burst type SG phenomenon into time-frequency components. In addition, force will also be observed based on previous already discussed SG research.

The University of Nottingham

To date little work has looked at the energy signatures experienced during SG scratch tests in grinding. However this has been looked at in other areas of research such the characteristics of AE during single diamond scratching of granite (Clausen, Wang et al. 1996), where the RMS AE is extracted for different materials and different processes of rock cutting where the major mechanisms are microchipping, crack propagation and sliding friction. It could be said that microchipping, crack propagation and sliding friction for brittle materials are analogous to ploughing, cutting and rubbing for ductile materials respectively. The scratching of granite has many similarities with the scratching of alloys and in general, the higher the depth of cut made, the more the peak AE magnitude increases. These observations are very similar to SG scratch tests with aerospace alloys and Clausen et al (Clausen, Wang et al. 1996), discusses that the AE signatures differentiate between different granite materials this is true about different aerospace materials with different properties (this research work will investigate different material scratch tests).

2.4   Multiple Classification

The detection of grinding phenomena is a very important consideration when carrying out process monitoring of grinding technologies. There are many different types of processing phenomena ranging from cracks, scratches, material deformation, burn, chattering, cutting, rubbing and ploughing. The research presented here looks at the both the identification of grinding burn and workpiece chattering. Grinding burn can be considered as key unwanted phenomenon when grinding aerospace materials such as

Inconnel 718. If burn or even slight burn occurs during the manufacture process of engine turbine parts then that unit would have to be either re-melted and scrapped or further machined. This action is due to the aerospace requirements being very stringent when manufacturing commercial engine parts. For instance, if they fail due to a hair line crack caused by slight burn this could cause catastrophic results and ultimately result in death. Currently, burn is identified by the careful inspection of an engineer. This can be both time consuming and subjective to the task at hand. Process monitoring using extracted sensory features can provide the manufacturing process with an accurate watchful eye that is less subjective and, more sensitive to changing grinding phenomena.

Burn with coolant results have often been classified with force and acceleration signals as these are less susceptible to noise which is a problem when using Acoustic Emission signal extraction techniques. In addition, there are many conditions that can arise during the monitoring of a manufacturing process, to that end the more conditions that are considered in terms of establishing boundary type rules, the more efficient a process monitoring system can behave. With more data, the classifier can provide regression type rules for unforeseen circumstances and is considered useful for this type of manufacturing monitoring. Such aerospace manufacturing systems are not just used for one machining process but instead, many different machining processes can be used to obtain special features of interest. A generic monitoring system therefore has to be able to identify many demes of information when presented with live online data.

Grinding Burn occurs from the increased temperature of the abrasive material coming into contact with workpiece material. This temperature however, cannot dissipate quickly due to too much material being removed or, there is not enough coolant present. There are other factors such as a worn grinding wheel due to loading or even fractured grits. This burn has to be monitored in such a manner as to enable the safe detection of burn or better, just before it occurs. This can be done by monitoring the rise of extracted sensory signals such as Acoustic Emissions (AE) as discussed by (Yan, Sasaki et al. 2004). Some of the early monitoring systems used AE root mean square (RMS) detection levels to determine the different types of phenomena (Akbari, Saito et al. 1996). This approach is considered useful for online monitoring, however it is not the approach to distinguish between different types of phenomena with varying machining and material characteristics. For instance, during trials there are high amplitudes for the start and end of the cutting process, this could be confused with a phenomenon of concern. The research discussed by Chen et al (Chen, Rowe et al. 1996; Chen and Liu 2004) looks at the extraction and identification of grinding burn through AE signals. The research presented here looks at the results gained from two trials namely investigating grinding chattering and burn (same machine feed rates were used along with the same aerospace materials). The utilisations of advanced artificial intelligent techniques are discussed such as independent component analysis (ICA) and Genetic Programming (GP) evolutionary rule classification techniques. Both signals obtained from the two separate trials provide signals that are difficult to distinguish in terms of grinding phenomena especially segregating both chatter and burn with one classifier system. This type of classifier system provides the roots for a generic classifier system that can be

used to monitor several grinding passes manufacturing different parts. This type of classifier can be extended to other machining processes such as drilling and milling which is part of the total machining solution when producing engine turbine disks/blades. A machine centre such as the Machino A55 Machine Centre can then be monitored for several machining processes ensuring all the features are manufactured to a high standard. This generic monitoring system can be used with different materials or a combination of composite materials if desired; this is based on the work discussed in Chapter 7. Research from Chen et al (Chen, Rowe et al. 1996; Chen and Liu 2004) used both WPT and STFT to convert the raw extracted AE signal into an amplitude-time-frequency domain signals and identify phenomena of interest. The generic monitoring system can be used to control feedback in terms of identifying a progressively rough surface finish or a progressively more rubbing/ploughing machining process from a deteriorating grinding wheel due to wear. The former and the latter of these characteristics are ultimately responsible for grinding chatter and burn respectively. This level of understanding of grinding phenomena is what is required for a successful monitoring system and without useful extraction techniques and observable results (in terms of actual anomaly phenomenon obtained) the data is useless for presentation to such a generic classifier system.

With reference to the research discussed by (Tonshoff, Fremuth et al. 1994), chattering phenomenon has also been investigated in terms of the effects to the surface finish due to natural or self actuated vibration. Chatter will be the second phenomenon of interest with the same parameters used in burn phenomenon tests (same feed speed and same

The University of Nottingham

depth of cut however different grinding wheel speeds). In addition, coolant was used for the chattering phenomenon investigation this was due to the requirement in segregating the burn and chatter and not to have both at the same time. It was thought that the results from this actual grinding pass work could be linked with the cutting, ploughing and rubbing work seen in Chapter 7. However more work between bridging the gap between micro cutting and actual industrial cutting (see future work in Chapter 9) needs to be addressed and investigated first. That said; if the burn and no burn extracted AE signals are sufficiently normalised to 1µm signals then such a facility could already exist. Once the signal has been normalised, the parameters for normalisation in terms of reduction could be used to show the different intensities for more aggressive-grit interaction (this research can lead to the better control of both actual and micro-machining grinding strategies). The proposed work also looks at several signals obtained from the grinding chattering and burn trials, these signals being the grinding force, accelerations, and Acoustic Emission signals. Lastly, there is the proposed classification of such phenomena which will be discussed further in Chapters 6, 7 and 8. For verification of the generic classifier, a proven classifier technology such as the Fuzzy-c/GA clustering algorithm displayed in Chapter 7 will be used to compare the advancement in classifier technology.

2.5 Research Gaps

2.5.1 Gaps in Process Monitoring

The gaps that were identified during the review of research in process monitoring are as follows:

- Pre-processing and classification techniques such as STFT and WPTs and Fuzzy/GA clustering have not been applied to the classification of varying grinding phenomena such as ploughing, cutting and rubbing during grinding passes.

- A hybrid classifier for non-linear n-dimensional data reduction techniques have not been investigated for process monitoring such as a Fuzzy-c clustering algorithm with GA optimisation.

- Monitoring of grinding phenomena through all the parameters; temperature, spindle power, force, force acceleration, spindle moment and AEs has not been heavily received by industry to date. This mutli-sensor picture could be very useful for accurate robust classification.

- Burn and chatter has not been classified by GP through AE/force, accelerations and power.

- Burn and chatter has not been classified by Fuzzy-c clustering with GA algorithm optimisation.

- N-dimensional or information reduction techniques can provide the same results as the original extracted AE/force signal with a view to being used on-line for real-time monitoring purposes (ICA n-dimensional techniques have not been used in machine monitoring before).

2.5.2 Gaps in Single Grit Analysis

- To date there has not been any research looking at energy AE signatures for SG scratches of hard to machine aerospace alloys especially the investigation of horizontal scratches which closely resembles grinding conditions.

- To date there has not been any research looking at energy AE signatures. Such research into SG scratches (rotating scratches) of aerospace alloys which allows a deeper analysis into the process of grit interaction.

- To date there has been no bridge between the AE process monitoring of grinding and SG scratch test characteristics.

- To date there has been no use of WPT and STFT to distinguish AE signatures relating to cutting, ploughing and rubbing phenomenon.

2.5.3 Gaps within sensor technologies

Acoustic Emission (AE) first saw its use in the 1980s for machine monitoring; however there is no standardisation for AE sensors. This therefore means there is a big future for AE technology however for such technologies to be used as a precise standardised measurement system for small unit event interactions (single grit scratch tests) there needs to be more work in ensuring the sensor is verified for the specific application in mind. This thesis addresses a number of issues to standardise the AE sensor technology for use with both grinding and the single grit unit event however it is based on the specific materials and type of grit used. With the detection of miniscule anomalies the AE sensor is certainly the most precise sensor to use whilst making grinding passes and

single scratch tests. In addition, due to its sensitivity it is possible to see small variations in the AE amplitude which can be indicative to wheel wear and surface burn for example. Other sensors are used to validate the AE signatures as this is still a maturing technology within grinding monitoring and still requires more work for accurate and reliable standardisation (thus standardisation is based on specific material characteristics and dimensions). The other sensors measure the following as verification and further confidence in finding grinding phenomena, namely; force, accelerations, grinding zone temperature and spindle power. All the other sensors have lower acquisition sampling rates than the AE sensor/acquisition system and were used for single grit scratch tests however the results displayed no distinguishing phenomenon unlike that of the AE acquisition system (with much higher acquisition sampling rates). The following are considered as gaps within this technology (see Section 4.1.3):

- There are currently no standardised calibration methods for AE sensors such as standards to suggest an RMS or absolute value for particular force exerted in a specific material.

- There has currently been no work into standardising AE in terms of surface integrity analysis and giving a NDT and fast monitoring solution.

Chapter 3 Grinding Material Analysis and Experimental Setup

3.1 Introduction to Materials Analysis

Material Analysis is an integral part to the manufacture of aerospace alloys. This one constraint demanded by both quality and safety determines the machining process of manufacture. The first part of this chapter will look at machining defects which can mean the difference between accepting and not accepting a machined part.

3.1.1 Introduction to grinding material defects

The material analysis was conducted for both macro and micro aspects of grinding. For the micro aspects the material removal mechanisms and miniscule measurements were carried out to show the distinction between the grinding mechanics of cutting, ploughing and rubbing phenomena. For grinding however the surface finish is critical to the manufacturing process of turbine parts and blades which is the focus of this thesis. The finish is considered to be within nominal limits if defects are considered to be small enough to be ignored or in a perfect scenario not exist at all. The materials that were used for both macro and micro aspects of grinding are; CMSX4, Inconnel 718 (nickel based alloys), EN8 (Steel) and Titanium6-4. All of these materials have differing hardness values and have different roles within their relative position of the turbine system. There are different parts to the turbine system which are categorised under normal parts, critical parts and sensitive parts. Normal parts are not usually designated a

The University of Nottingham

category and although stringent metallurgical study can be ignored there are a still guidelines in which they must pass to gain operational status and be fitted to an engine turbine. Critical parts are those parts whose failure are likely to have hazardous effects and require special controls to ensure low probability of individual failure or failure before service designated time. Sensitive parts are not quite critical parts however their failure could seriously affect the engine performance, reliability and cost of operation. The next section will look at the critical anomalies and defects associated with grinding difficult aerospace alloy materials namely; burn, burrs, chatter, cracks and tears. A lot of work has already been carried out in actual grinding wheel topography and workpiece surface (Badger and Torrance 2000), this work instead of looking from a top-down approach pursues a bottom-up approach.

3.1.1.1   Burn

Referring to Chapter 2 of the literature review, grinding is a thermo-mechanical process in that most of the energy (approximately 70%) (Griffiths, Middleton et al. 1996) is transferred as heat and the other (approximately 30%) is transferred as mechanical energy. These two processes provide both tensile and compressive material stress respectively. In most cases workpiece burn during the grinding processes is essentially a kind of irreversible change in the microstructure of the surface layer. With heat being the largest source of energy it is very important to ensure the grinding zone is constantly lubricated and cooled. The use of coolant here is very important in terms of the mixture, the position of the nozzle and pressure of the flood solution. At the onset of grinding

burn, the grinding force and rate of wheel wear increase sharply and in most cases, the surface roughness deteriorates. If burn occurs it can form a white layer on the surface of the material which cannot be acceptable, if however only slight white layer exists, it can be removed from a gentle finishing process. If however the burn is much greater then it is possible that the surface integrity is diminished from different levels of hardening with small micro cracks occurring from the temperature induced tensile stress of the grinding manufacturing process (Chen and Xue 1999). The surface roughness can sometimes be smoother than normally ground surfaces this is due to the smeared outrun of the onset of burn which in short, gives a better surface finish although the surface integrity is suspect. However with severe burn, the surface can be much rougher than a normally ground surface. Burn can occur from the incorrect wheel geometry, insufficient coolant, worn grinding wheel where undulations are apparent from material loading. The change to parent material that is still continuous with the surface are; amorphous layer, re-crystallisation, alloy depletion and distorted layers. These changes from normal to abusive operating grinding conditions can cause a change to the parent material which is not desired. Extra finish ground machining can be used to remove these characteristics and provide a better surface. Sometimes foreign or non parent material inclusions from burn can be found in form of grit and can be eliminated from further finish machining although if severe, this can have detrimental effects to surface integrity and may have to be scrapped completely. From burn there can be discolouration and contamination from different chemical process mixes; both of these can be problematic if they are considered to be outside acceptable manufacturing limits. The work hardening layer causes strain on the material and if significant can cause cracks or twins which could become much

The University of Nottingham

longer in an operational hot environment and unacceptable to the manufacturing process. Figures 3.1 and 3.2 display two images a high definition digital image along with a detailed microscope image of burn.
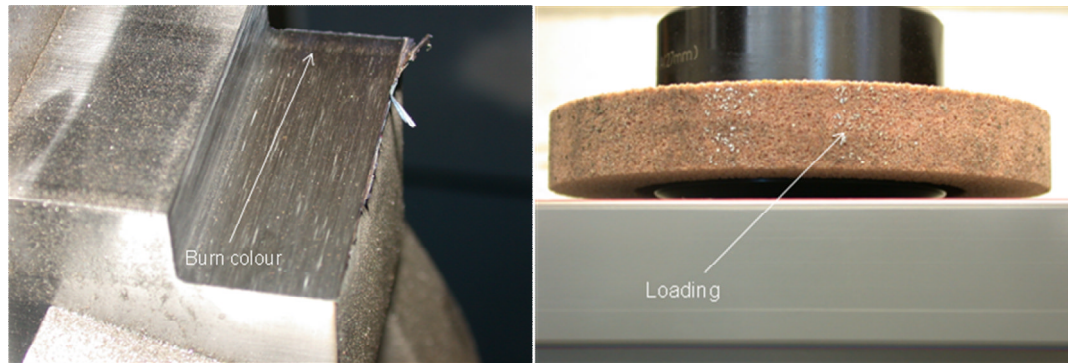
Figure 3.1 Left, Inconnel 718 burn of dry cut 1mm (a_p) and right, material Al_3O_2 wheel loading
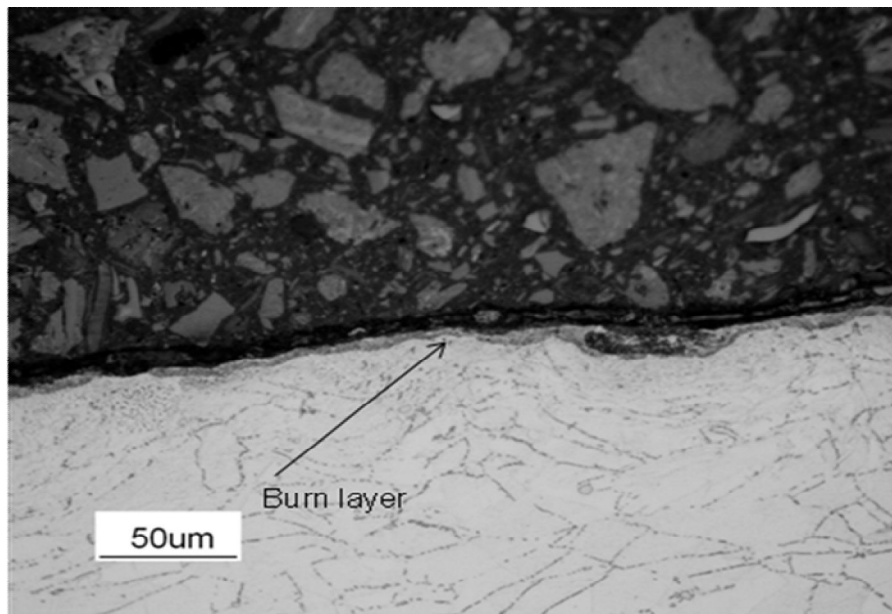
Figure 3.2 Material CMSX4 recrystallisation and white layer formed from burn
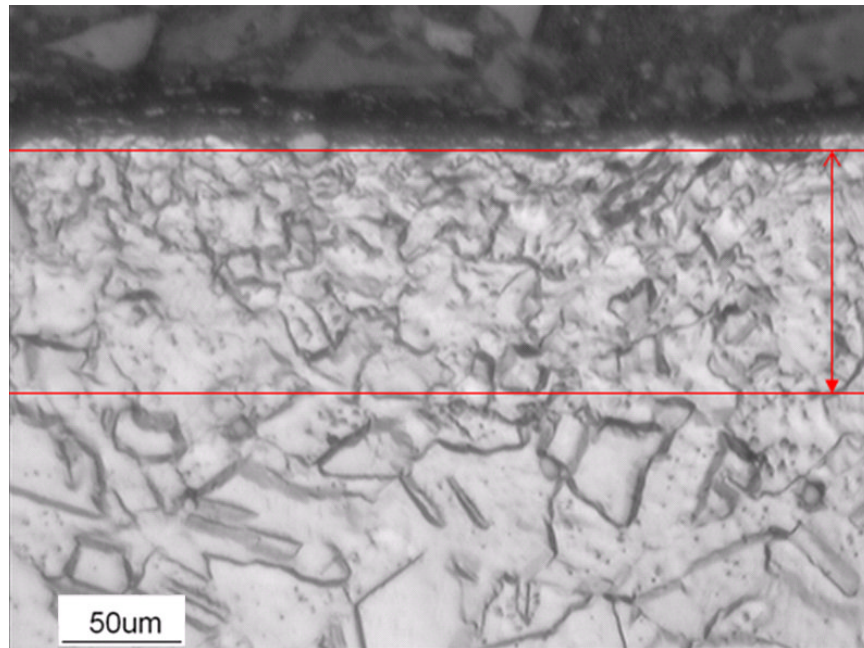
Figure 3.3 Material Inconnel 718 re-crystallisation and white layer formed from burn

Looking at both Figures 3.2 and 3.3 it is possible to see the white amorphous layer present along with re-crystallisation this is termed as burn although not severe burn and this could be machined away by performing a finishing machining process if acceptable to production. Reference Figure 3.3, just after the burn, the white layer can be seen where the crystal lattices of the material are broken and transformed into smaller sizes. Both Figures 3.2 and 3.3 images were taken in the direction of cut for complete analysis. A similar image is taken in the perpendicular direction to cut (as well).

3.1.1.2 Chatter

Similar to the burn defect, chatter has already been discussed in Chapter 2. This is an anomaly that is not required during machining as chatter decreases surface integrity by causing a number of secondary material defects such as plucking, burrs, cracks and the

The University of Nottingham

general decrease in surface roughness. Chattering is caused by the following; an increase in feed rate, machining with unacceptable wheel wear and workpiece not clamped sufficiently increasing stiffness for robust cutting setup. As already discussed, chatter is caused from either the induced machining vibration or prolonged natural frequency of the machine. Both these frequencies can transform themselves onto the form of the surface and affect the surface roughness/integrity.

3.1.2 Introduction to measurement systems and standards

This section looks at the measurement systems and methods used to identify the surface integrity of the workpiece. Surface integrity is especially useful when trying to understand the extracted signal phenomenon which is discussed in the next two chapters. Roughness, waviness and roundness are discussed in the following sections followed by an introduction into the stylus and interferometer measuring system.

3.1.2.1 Roughness

After machining the ground surface, many irregularities can exist; the roughness measure gives the operator a confidence in the level of irregularities. If the surface has a good roughness measure (i.e. low measurement of surface roughness) then it can be considered that there are minimal surface defects, however with a large measure of surface roughness the converse is true and more in-depth material analysis maybe required to note the depth of defect or anomaly. The surface roughness can be measured by a range of different devices. For the work carried out in this thesis the stylus method and laser interferometer were used. The stylus is perhaps the easiest measuring system to

describe. The stylus moves across a designated length of material and from the deflection of peaks and valleys experienced from the surface of the material reads back this deflected data in the form of varying voltage output. Over the length of measurement the peaks and troughs are plotted as a surface. To get an average roughness value (Ra) the length is segmented into finite lengths (typically five segmented lengths for a standard Ra value) across the overall specific stated length. The surface is read back and average height of depth of peaks and valleys calculates an average height to the surface norm. This value can be interpreted to how rough the surface is. Typically for grinding, the surface finish ranges from 0.8μm to 0.05μm and polishing 0.4μm to 0.01μm respectively (for the work carried out in this thesis the recorded Ra was at the lower end of the stated tolerances).

3.1.2.2 Waviness

The roughness value is very much an average value and does not take into consideration the waviness or the roundness of the material. Roundness will be discussed in the next section however equally important is the waviness; this measurement displays regular irregularities along the surface in the form of recurring waves. Such a surface phenomenon can be caused by the chattering of the grinding wheel or an incorrectly used fixture system. The waviness can be expressed as recurring frequency from a machine defect and to measure such a phenomenon the stylus or interferometer can be used. This should however be arranged in such a manner to take into consideration a much longer length than that taken for the Ra. Through filtration of the output measurement it should then be possible to see the machine waviness of the material

The University of Nottingham

surface. Form error is similar to waviness however this is due to a badly aligned or incorrect fixture of a tool and is measured in a similar fashion to that of waviness. Obviously, the longer the sample measurement length the more accurate roughness, waviness and form error measurements are made.

3.1.2.3   Roundness

The roundness of a surface is inherent from an unevenly machined surface; this can be caused from polishing a material where different forces are exerted on different areas of the workpiece material. This is certainly true for manual polishing systems but less so with automatic polishing systems. In addition, roundness can be attributed to the workpiece surface if the workpiece was incorrectly attached to the fixture system and not correctly checked for flatness. This roundness can cause a problem in microscopic measurements however with levelling software algorithms the problem is somewhat removed. Roundness can be seen from roughness or waviness measurements. Usually all three measurements are made from one measurement pass either by using a stylus or interferometer.

3.1.2.4   Stylus Instruments

Stylus instruments from Taylor Hobson (Hobson 2003) were used to measure the surface texture in terms or roughness, roundness, and waviness. These measurements were for standard grinding surface analysis and for more miniscule material analysis; an Interferometer was used. The stylus measurement would use a needle gauge which measures the difference in displacement between the reference datum and surface. Taylor Hobson Surtronic 3P® and Taylor Hobson Talysurf CLI 1000® systems were

The University of
Nottingham

used for making the surface integrity measurements. The schematic displayed in Figure 3.5 illustrates how the stylus instrument works.

Reference datum

Gauge measures difference in displacement
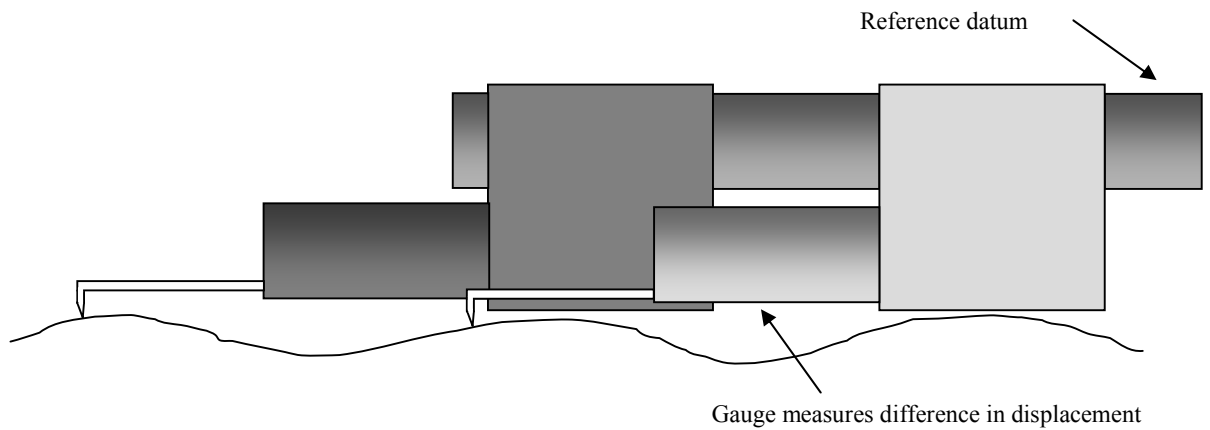
Figure 3.5 An independent datum provides a straight reference for the gauge traverse

To get an accurate measurement of the returned image, the step size in which the gauge takes is much smaller thus utilising high resolution (Sherrington and Smith 1988). However the measurement accuracy is based on testing a known slip gauge measurement this is to check the stylus reads back the same result as the standard marked roughness slip gauge. If the measurement is incorrect the reference datum and further calibration is attenuated to ensure the result is more accurate towards the known standard.

3.1.2.5   Scanning Interferometer

The scanning interferometer uses either a conventional white light or white light LED. A piezo drive system is used to scan the objective lens about a focal point. The workpiece is positioned on a precision X/Y plate and from using a camera view point the exact point of surface phenomenon is located. The imaging system is then traversed through

The University of
Nottingham

its defined height (Z) range by the focal point, each focal point is noted and stored in a CCD array (Schulz 2003; Danzl, Helmli et al. 2006). The lateral resolution of such system is approximately a 0.3µm by 0.3µm square; the vertical resolution is typically less than 0.1nm which is accurate enough to carry out miniscule surface integrity analysis. The scanning interferometer used was a Fogale Photomap 3D non-contact high resolution profiler, it should be noted much larger areas of interest could be measured using the Mountains® stitch image software which allows each still image to be accurately stitched together thus allowing an in-depth analysis of a 1mm scratch length for example. Figure 3.6 illustrates how the scanning interferometer works.
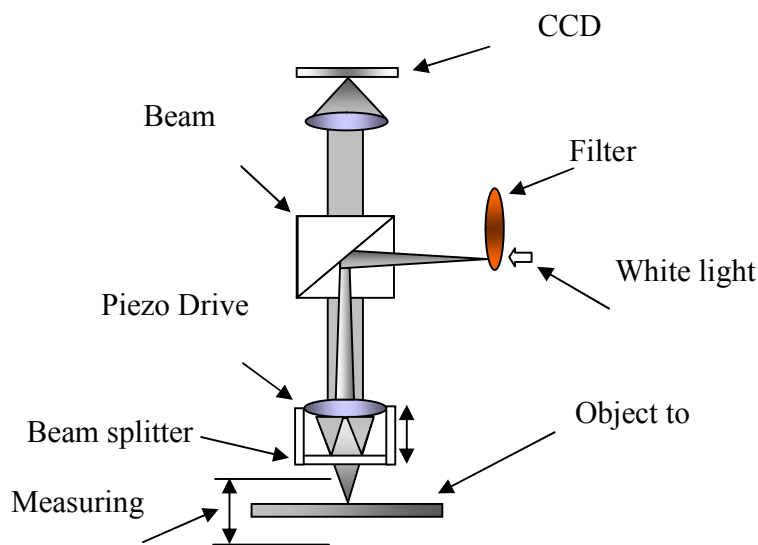
Figure 3.6 schematic of scanning interferometer

3.1.3 Scratch sample preparation

Polishing is required for accurate material analysis and even finish machining process. Materials are polished to a very high standard this is to be able to remove surface defects

The University of Nottingham

to prolong environmental defects and provide better aerodynamic characteristics. The harder the material the better the results are in terms of the finished polished surface. The next two sections will look at the standard method for polishing aerospace alloys for material analysis and a proposed semi automatic polishing rig which was found to be unsuitable for polishing requirements during the single grit scratch trials.

3.1.3.1   Polishing Regime

The polishing of material for surface measurement analysis is where abrasive paper is attached to a spinning motorised turntable. By increasing the speed bearing in mind the limits of the abrasive paper, the alloy is polished in incremental steps starting with coarse abrasive paper to fine abrasive paper. At each point of the polishing it is important to remove the scratches made by previous grit size before moving to a less coarse abrasive paper. The logic diagram Figure 3.7 displays the steps carried out for aerospace alloy polishing. At each step of the polishing method before going to the less coarse abrasive paper the workpiece is washed with warm water to ensure no larger grit or other material is taken to the next stage causing unwanted scratches or smearing. The workpiece is also sprayed with a degreaser as a further step to ensure no material contamination is taken onto the next stage. The last stage of the polishing process is carried out on specifically designed pads for 6μm and 1μm pastes respectively. This stage is where an alcohol solution accompanies the polishing process instead of an aqueous solution as used with the previous abrasive papers.
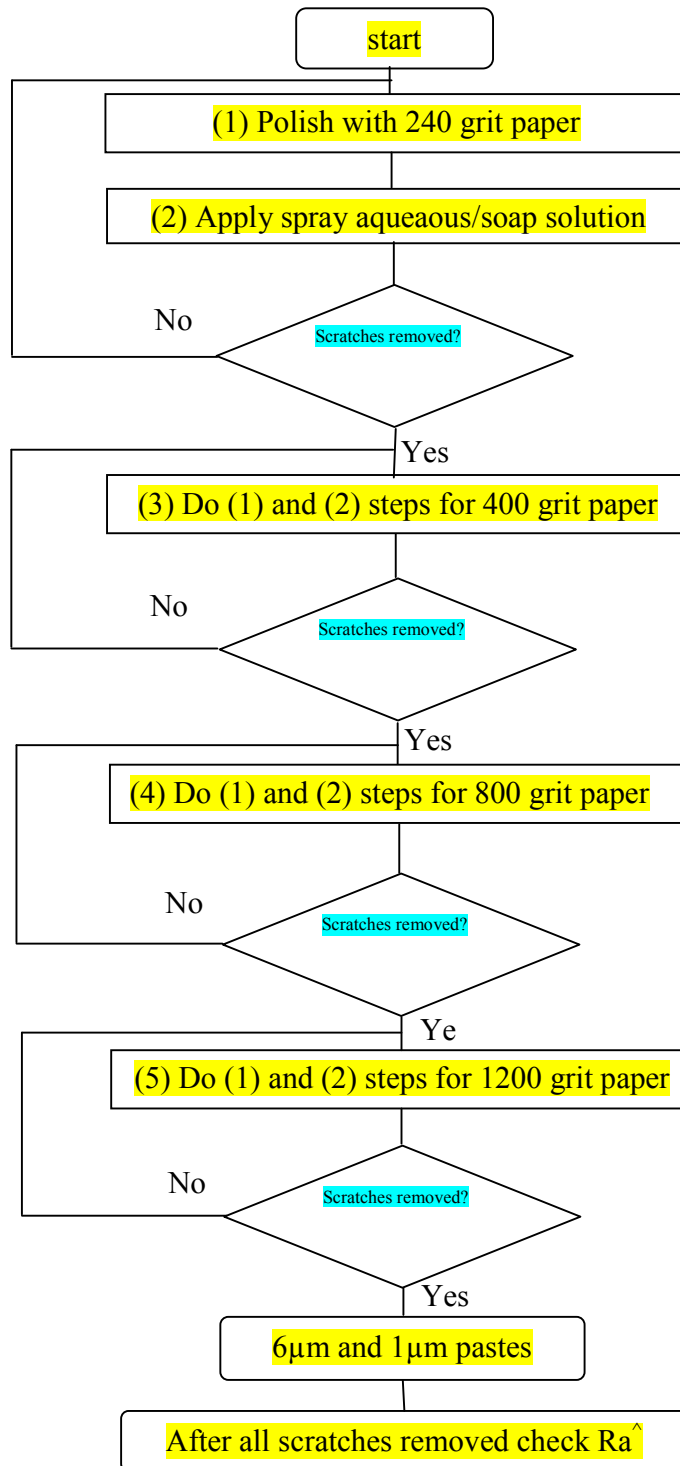
Figure 3.7 Logic diagram for polishing aerospace alloys (^if not removed and suitable Ra go back to level to ensure scratches are removed and acceptable Ra)

The same applies to the 6μm abrasive pastes, before going to the 1μm pastes, scratches and foreign debris are checked and if still remain, they are further polished before being washed in warm water and degreased in preparation for the final stage. Such process regarding the polishing and etching for Titanium can be found Axinte's work, this is where similar processes to etching and polishing strategies are carried out for other aerospace materials (Axinte, Kritmanorot et al. 2005).

3.1.3.2 Semi Automated Polishing

A semi automated polishing rig was set up for the first set of experiments where radial scratch tests were carried out however this test rig was considered unstable and not ergonomical in terms of its application. The rig was set up to require little force in a horizontal rolling fashion however instead, the rig was difficult to set up in an accurate flat format and caused severe roundness and even damage to the workpiece. With design modifications, such a polishing rig could be successful; such modifications are the use of smaller test piece samples and smaller attached chuck as well as stabilizers to ensure better sturdiness during the polishing process. Figure 3.8 displays the semi automated test rig.

Looking at Figure 3.8 the purpose built metal plate would have the workpieces attached to it by M5 bolts. A metal rod was screwed into the plate and fitted to the sliding rod holder seen on Figure 3.8 left, centre of the image.
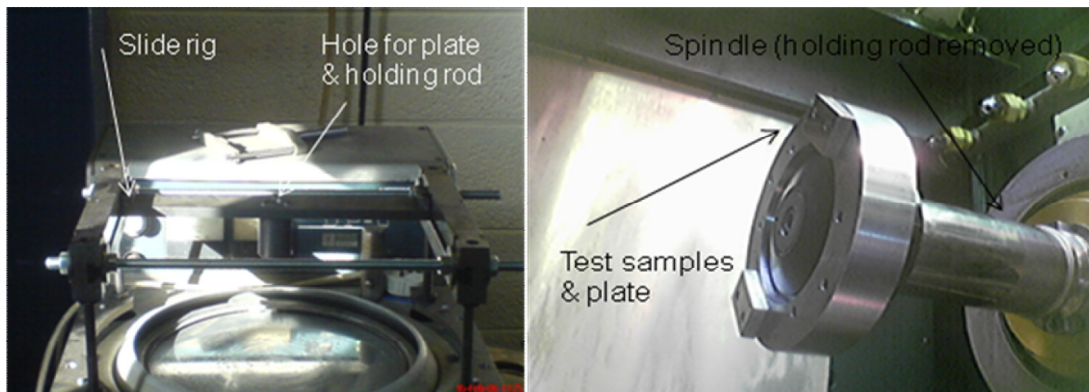
Figure 3.8 Left, displays the semi automated test rig, Right, metal plate with samples

3.2 Introduction to Single Grit Materials Analysis

A major part of this thesis is dedicated to Single Grit Scratch analysis with an aim to separate cutting, ploughing and rubbing signals experienced during grinding. It is extremely difficult to see these phenomena during a grinding wheel pass as the there is far too much material interaction to understand the mechanisms of grinding. This is why the single grit (SG) unit process is required to separate these mechanisms and then bridge the gap towards understanding a grinding wheel pass with the same signals. Figure 3.9 displays the experimental schematic set-up used for both radial and horizontal scratch tests respectively.
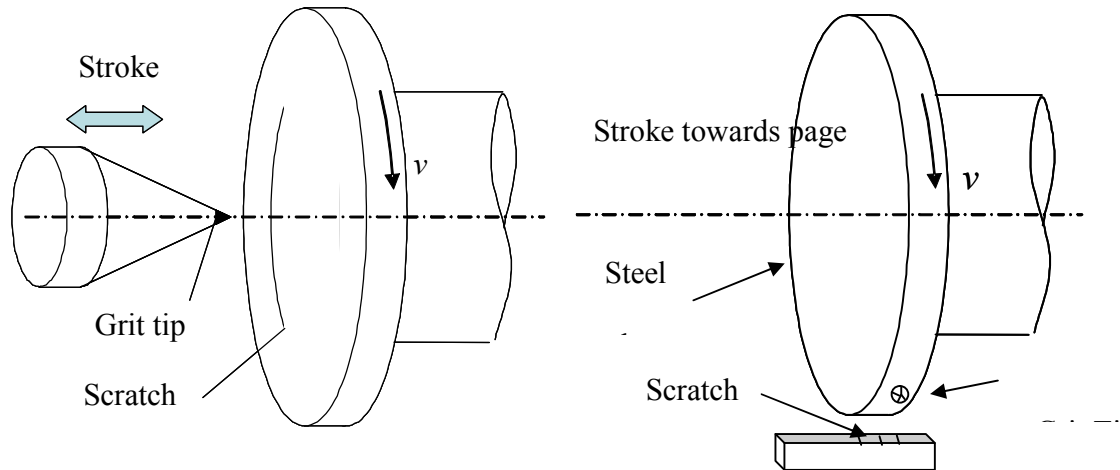
Figure 3.9 Left, SG radial scratch set-up Right, SG horizontal scratch

3.2.1 Radial SG Scratch

Looking at Figure 3.9 right and Figure 3.9 left the aerospace workpieces was set-up accordingly. The Grit was fixed in a specially designed clamping rig (Figure 3.10) that would house both the force load cell and the Acoustic Emission (AE) sensor placed appropriately next to the grit ready for signal extraction.
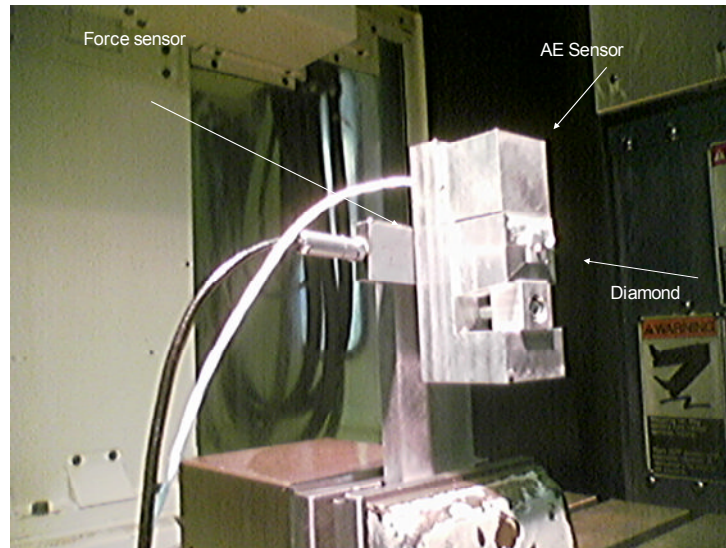
Figure 3.10 Radial scratch grit AE and force clamping rig

Next the SG horizontal scratch set-up will be discussed followed by the material analysis used to distinguish the cutting, ploughing and rubbing phenomenon displayed from interferometer measurements. From looking at literature this SG setup is the first time it has been used in experimental analysis and therefore considered novel.

3.2.2 Horizontal SG Scratch

The radial scratch tests were considered to be a good indication of the SG interaction process with a workpiece however with different flatness rates between the two workpieces meant the grit interaction would only occur on a single workpiece and not on both. In some cases the grit interacted on both workpiece surfaces and this was used for distinguishing the differing grinding mechanics. In addition, the rotating workpiece are not analogous to actual grinding wheel passes and it was considered that horizontal scratch mechanisms have a much closer resemblance to an actual grinding pass when compared with that of radial scratch tests. For horizontal SG scratch tests the grit would

be inserted in a drilled hole and glued in place (super glue was used for rigidity). The test piece and grit interact after the advancement of 1µm incremental wheel depth movements. The scratches are not continuous as this is the case with the radial scratch experiments, this allows material analysis to be carried out for each individual interaction, and thus signal and material interaction are easier to align. Both radial and horizontal SG scratch tests used for the material removal analysis are discussed in the next section.

3.2.3 Material Removal Mechanisms

When the process of grit to workpiece interaction occurs, the AE is emitted as a material stress release process. This emitted AE during the scratch may come from elastic or plastic shear stress due to material removal or material deformation. It should also be noted that the AE intensities start to rise as the grit slightly interacts with the surface albeit touching but not causing any plastic deformation. This is rubbing without plastic deformation where the grit is close enough to comb across the surface but not so close that it leaves a mark. As the interaction of grit increased, it results in both elastic and plastic deformation this is where all three phenomena exist. The previous no mark contact and current continuous cut length was used for analysis of the rubbing, ploughing and cutting phenomena respectively.

Different interactions were judged by measuring the material profile. A Fogale Photomap Profiler was used to provide an accurate 3D measurement of the SG groove. Figure 3.11 displays a photomap image of the 6th hit for horizontal scratch cut.
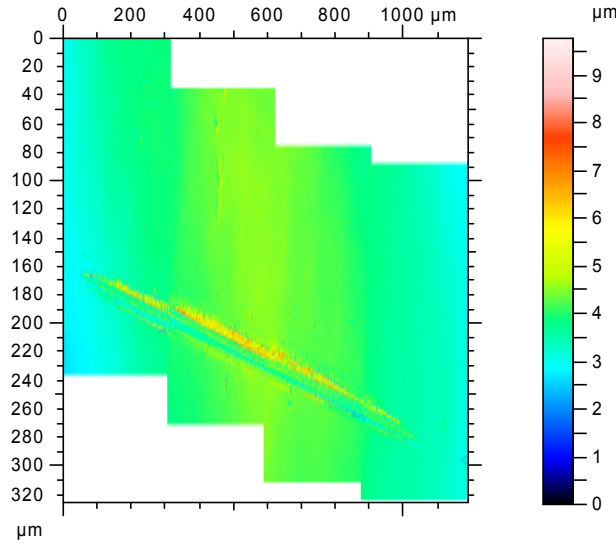
Figure 3.11 2D Photomap scratch image

The SG groove measurement analysis was obtained from 2D plan-view images and then an average cut over several stitched cuts would be used to make the phenomenon distinction. This profile cut was set against two observations (perpendicular to cut and cut direction profile measurements) to determine which phenomenon occurred out of rubbing, ploughing and cutting. The observation is based on the illustration of Figure 3.12. Equation 3.1 applies to Figure 3.12 to give a ratio for different phenomenon judgement:

$$M_{ratio} = \frac{A_{surface} + B_{surface} - (0.5R_a \cdot width(A_{surface} + B_{surface}))}{C_{surface} - (0.5R_a \cdot width(C_{surface}))}$$

(3.1)

Where the areas $A_{surface}$, $B_{surface}$ and $C_{surface}$ are all calculated from using the trapezoidal, area under a curve function (trapz, 2004). R_a is the surface roughness of the material at

that measurement point, the $width(A_{surface} + B_{surface})$ is the profile cross section cut widths for $A_{surface}$ and $B_{surface}$, the $width(C_{surface})$ is the width of the groove gap (distance in between $A_{surface}$ and $B_{surface}$). Where A and B are the material deposits left behind from the SG groove being cut (C). Considering the specific surface roughness, the results of cutting, ploughing and rubbing have more confidence than if the specific surface roughness was not considered. The material profile cross section calculations were backed up with observations of the profile length of the direction of cut. This method would ensure a good confidence of the found interaction.
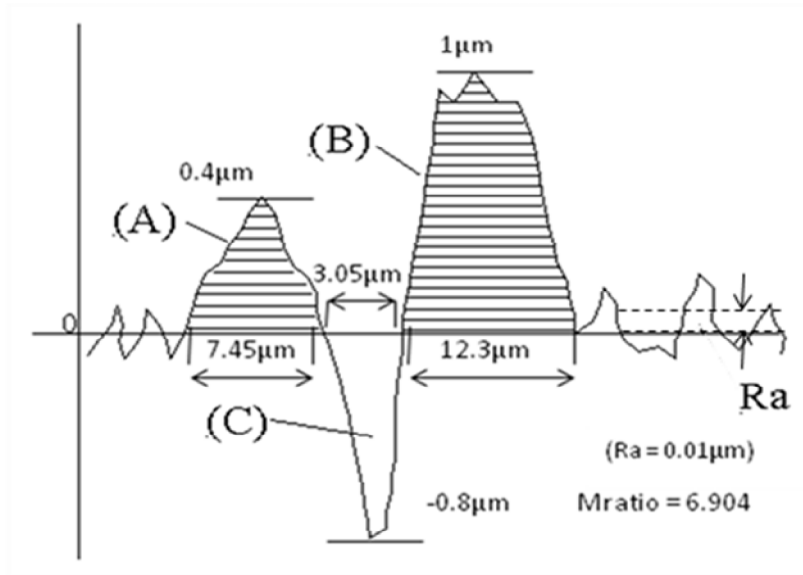
Figure 3.12 displays an illustration of single grit cut with ploughing phenomenon

Looking at the illustration in Figure 3.12 and equations 3.1 to 3.4:

Cutting phenomenon occurs, if

$$M_{ratio} < 0.9 \ \& \ \left(\frac{0.5 R_a \cdot width(A_{surface} + B_{surface} + C_{surface})}{A_{surface} + B_{surface} + C_{surface}} < 1 \right) \qquad (3.2)$$

PhD thesis by James Griffin   [88]

Ploughing phenomenon occurs, if

$$M_{\text{ratio}} > 1 \ \& \ \left(\frac{0.5R_a \cdot width(A_{surface} + B_{surface} + C_{surface})}{A_{surface} + B_{surface} + C_{surface}} < 1 \right) \qquad (3.3)$$

Rubbing phenomenon occurs, if

$$0.9 \leq M_{\text{ratio}} \leq 1 \ \& \ \left(\frac{0.5R_a \cdot width(A_{surface} + B_{surface} + C_{surface})}{A_{surface} + B_{surface} + C_{surface}} \geq 1 \right) \qquad (3.4)$$

Where the $width(A_{\text{surface}} + B_{\text{surface}} + C_{\text{surface}})$ is the profile cross section cut widths for A_{surface}, B_{surface} and C_{surface}. The example displayed in Figure 3.12 illustrates the ploughing phenomenon as the $M_{\text{ratio}} = 6.904$. For illustration purposes both sides of the ploughed A and B regions represents the mean Ra (this may be considered over exaggerated in the figure) which for the discussed SG tests is $0.01\,\mu m$. The M_{ratio} and Ra term are the extra parameters of equation providing the distinction between the three phenomena and is used to take the Ra into consideration when measuring the groove and ploughed BUE area, and the material measurements thus giving accurate material phenomenon results.

From looking at Equation 3.1 and the phenomenon boundary conditions it is possible to see that two factors will affect the value; the length of A, B and C; and the 0 line selection. In addition, extra ploughing materials might come from the ploughed material being pushed forward by the grains; also the remained surface roughness from sample preparation might distort the profile which is considered in Figure 3.13, Equations 3.1 to 3.4 and its associated boundary phenomenon conditions. The first set of single grit experiments of radial cuts (Griffin and Chen 2006) provided the first view of AE

The University of
Nottingham

behaviour of grit interaction with workpiece, but the interaction was not the same as in grinding. The new horizontal single grit scratch test was carried out to mimic the real grinding kinematical relations as shown in Figure 3.9 left.

The removal or none-removal of materials during a SG scratch pass depends on the cutting action of grit to workpiece interaction. The groove is ideally created from a starting rubbing grit action followed by a ploughing/cut combination, then actual cut followed by another ploughing/cut combination and then lastly, a rubbing action. Depending on the obtained cutting depth, the grit may experience rubbing, ploughing and cutting phenomenon that engages with the workpiece material. The proportion of rubbing, ploughing or cutting in a grit pass depends on the amount of grit engagement between grit and workpiece material (quantified in terms of the material and groove area). It is also noted that the stress under the grit depends on the undeformed chip thickness. The larger the undeformed chip thickness, the higher the force needed to remove the chip. Therefore higher stresses would be initiated. This material analysis was used to distinguish the three grinding mechanisms for both the radial and horizontal SG scratch cuts.

3.2   Material Properties

Table 3.1 displays the material properties reference all the aerospace material used in this thesis. These materials were used for both the Single Grit Scratch Tests and the unwanted anomalies multiple classification results. The material properties are very important to the work of AE signal extraction and machining as the ductility and

hardness in the material have a significant impact in terms of signal reflection and the intensities of noise emitted during material deformation or grain boundary fracture. Essentially, the AE emitted signal footprints, will be different from one material to the next however unless diversely different, the patterns for different phenomenon be that grinding mechanics or surface anomalies will have a generalised pattern. These patterns however can shift slightly on a day to day basis therefore it's imperative to reference the environment by carrying out essential calibration procedures before any machining takes place. Thus the calibration can be feedback and the data sets of signal analysis weighted with reference to the daily calibration measurements. This is essential for any accurate process monitoring system. Table 3.1 displays the material characteristics for the materials used during the SG scratch tests.

Table 3.1 displays the majority of the aerospace material properties used in this thesis [Steiner, 1990], [Kalpakjian, 2001]

Property	Inconel 718	CMSX4	Titanium-64
Composition (WT%)	Mo: 3, Cr: 18, Ti: 0.9 Nb: 5.1, Fe: 18.3, Ni: 53.7	Mo: 0.6, Cr: 7, Ti: 1, Al: 5.6, Co: 10 Ni: 67, Re: 3, W: 6	C: 0.08, Al: 5.5-6.75, Fe: 0.30, H: 0.010
Density (kg/m^3)	8193	8690	4650
Hardness	456HV	520HV	349HV
Tensile strength (MPa)	758-1407	1090	950
Yield Strength (Mpa=N/mm^2)	150	990	880
Elastic Modulus (GPa)	31	18.5	109.6
Elongation (%)	21-27	10-12	14
Melting point (°C)	1336	1395	847
Passion's Ratio	0.284	0.273	0.34
Thermal Conductivity (W/mk)	11.4~28.7	12~63	6.70
Special heat capacity (K/kgK)	430~700	381~544	450
Thermal diffusivity (x10^{-6}m^2/s)	2.01~8.24	2.54~21	16

3.3   Experimental Set-up

3.3.1 Radial Single Grit Scratch Experimental Set-up

The experiment of SG cutting interaction was carried out on a specially designed rig fixed within a Makino A55 Machine Centre as shown in Figure 3.14. All the sample materials were polished to a very high quality, which gave the tests further confidence with respect to material removal measurements. Roughness measurements (R_a) across

all workpieces were measured between 0.0278μm and 0.0477μm and were taken into consideration when calculating the groove cut area signifying whether ploughing, rubbing or cutting had taken place.

The single grit holding fixture was designed to ensure the SG would be firmly held in place as well as protruding to make sure the SG was the 1st object to touch the workpiece when controlled to within a micron of accuracy. The machine set-up consisted of both the AE and force sensor being attached in a manner to ensure maximum signal extraction (see Figure 3.13). To provide a sealed medium for the AE to vibrate from workpiece/SG to the sensor; grease was applied in between the AE sensor housing and SG holding fixture plate.

For monitoring the force and AE, two computers were synchronised by switch driven Digital Acquisition Cards (DAC). Signals were boosted through amplifiers connected between the sensor and computer.
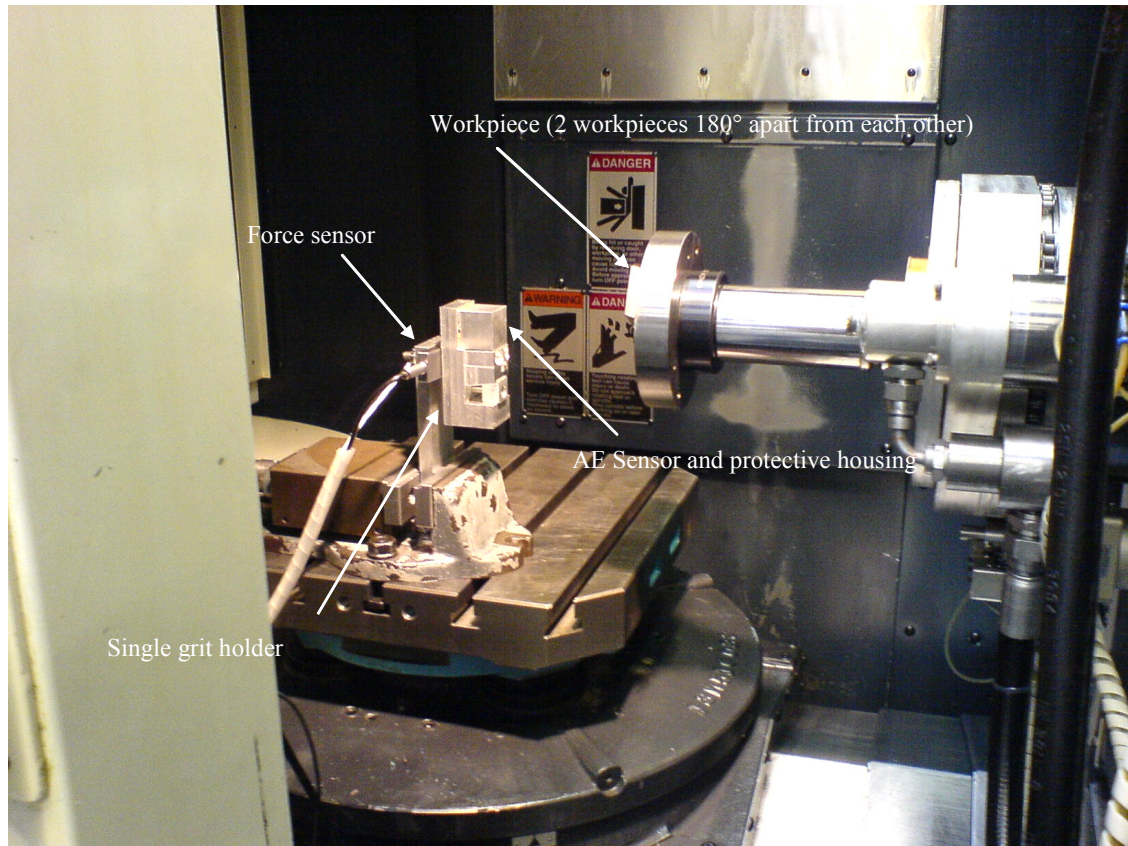
Figure 3.13 Makino A55 grinding centre machine set-up for SG test

By simulating the grinding chip formation with a scratch test, the acoustic emission of grinding chip formation may be investigated. The scratch test can be carried out by feeding an Al_2O_3 grit towards the rotational flat sample. With a grit in-and-out stroke, a scratch groove will be formed on the surface of the flat sample. The maximum scratch depth is about 1.5 μm, which is a typical value of grinding chip in high efficiency grinding. The scratching speed is 35 m/s. By using STFT, the features of AE at both time-frequency domains are obtained. The test set-up is illustrated in Figure 3.9 left. It can be noted that the AE feature frequencies are changing with respect to time during a single scratch action. This means the mechanical AE propagation should be considered

in both time and frequency domains. However, the prominent AE feature frequencies of the scratches are in the range 100 ~ 550 kHz, which are similar to the AE feature frequencies in grinding tests experienced in previous work (Chen, Griffin et al. 2007).

As discussed previously, AE is a stress released process. The AE in SG cutting may come from elastic and plastic shear stress due to material removal or material deformation caused by the process of grit-workpiece interaction. In order to examine the AE experienced in SG cuts, grinding tests were carried out on a Makino A55 machine centre. A PAC WD AE sensor was used to detect the AE signals. The sampling rate was 2 MHz to ensure no aliasing occurred when reconstructing the signal using the Matlab Digital Signal Toolbox (DSP). By using a Chebyshev Type II Infinite Impulse Response (IIR) bandpass filter with a cut-off frequency of 50 kHz to 1 MHz most of the noise generated by machine vibration and wheel rotation were eliminated at no great cost. Machine parameters for the SG experiments were as follows: Single grit material was Al_2O_3, SG dimensional depths and widths were approximately 1.5µm. The SG advanced towards workpiece with a one micron incremental step.

3.3.2 Horizontal Single Grit Scratch Experimental Set-up

The acoustic emission associated with grinding chip formation may be investigated by a scratch simulation of grinding. The experiment of single grit (SG) scratch test was carried out on a specially designed rig fixed within a Makino A55 Machine Centre as shown in Figure 3.14. The aerospace alloy CMSX-4 was chosen for the majority of SG tests and all samples were polished to a very high quality, which gave the tests further

The University of Nottingham

confidence with respect to measurements. Roughness (R_a) across all workpieces were measured between 0.01μm and 0.03μm and were taken into consideration when calculating the groove cut area signifying whether rubbing, ploughing or cutting had occurred. A single grit (SG) was glued into a microscopic drilled hole of the specially designed steel plate. The steel plate would then be fixed to the spindle and rotated at the same range of commercial grinding speeds. The SG was fixed to the plate in a protruding fashion which would ensure the SG was the 1st object to make contact with the workpiece when controlled within a micron of accuracy. The machine set-up consisted of both the AE and force sensor being attached in a manner to ensure maximum signal extraction.
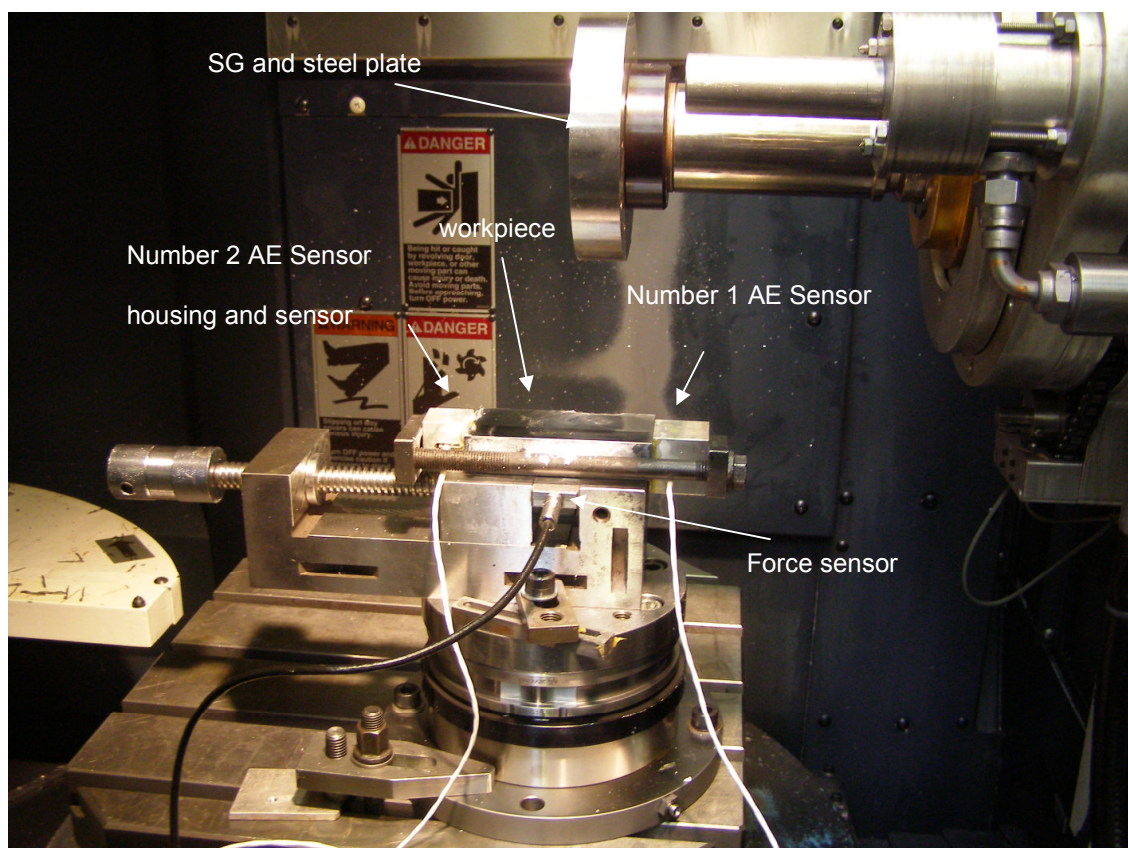
Figure 3.14 Makino A55 grinding centre machine set-up for horizontal SG scratch test

The University of Nottingham

The scratch test was carried out by feeding a rotating Al_2O_3 grit towards a flat horizontally placed workpiece as illustrated in Figure 3.9 Right. With a micron incremental grit stroke, a scratch groove will be formed on the surface of the flat sample. The average scratch depth is about 1 μm, which is a typical value of grinding chip in high efficiency grinding. The scratching wheel rotational speed is 4000 RPM with a feed rate of 4000 mm/min under the down grinding condition. During a single scratch action the AE feature frequency intensities change with respect to time. In short, the mechanical AE propagation should be considered in both time and frequency features. However, the prominent AE feature frequencies of the scratches are in the range 50 ~ 700 kHz, which are similar to the AE feature frequencies in grinding tests experienced in previous work (Chen, Griffin et al. 2007) and radial scratch tests (Griffin and Chen 2006).

As discussed previously, AE is a stress released process. The AE in SG cutting may come from elastic and plastic shear stress due to material removal or material deformation caused by the process of grit-workpiece interaction. In order to examine the AE experienced in SG cuts, grinding tests were carried out on a Makino A55 machine centre. An AE data acquisition system where two Physical Acoustics WD AE sensors were used which were both identical and with a frequency response range at 100 kHz to 1MHz. The two sensors were set-up equal distances apart this was to ensure the verification of the signal (see Figure 1 for set-up configuration). The sampling rate was set to 5 MHz to ensure no aliasing occurred when the signal was reconstructed using the

Matlab Digital Signal Toolbox (DSP) and all the short burst high frequency information was obtained. By using a Chebyshev Type II Infinite Impulse Response (IIR) bandpass filter with a cut-off frequency of 50 kHz to 1 MHz most of the noise generated by the Makino A55 machine centre was eliminated at no great cost. In fact, the natural frequency (ω_n) of the machine was measured at 11 kHz and was also eliminated from the extracted AE signals.

3.3.3 Grinding Experimental Set-up

By setting up the experiment and providing increasing depth of cuts it was possible to gain burn phenomenon with increasing intensities. The burn phenomenon would then be recorded by an AE sensor, force dynamometer, accelerometer, load cell (power) and the record of workpiece/grinding wheel image. The phenomenon would be measured in terms of where it occurred on the workpeice. The cut signal obtained by each sensor would then be stripped from the total recording stream and then measured to correlate the physical burn source with the digitised signal source. This is fundamental to the understanding of different grinding phenomena. It was considered to use the motor rotation poles of the A55 reluctance machine to achieve positional synchronisation however this was not pursued due to machine company regulations (this could however, be proved on a specially designed rig). Once all the signals correlated with one another (this is in terms of time) they would then be concatenated together ready for training and testing of the classifier system. The main characteristic used to link the other signal characteristics was that of the AE signal. Once the feature had been matched with the

physical property, this feature would be stripped out with a 2048 (2K) point wide block window. So in short, 2048 points were used to take out each phenomenon of interest.

Image data was extracted from a 25 times microscope recorded image reference to the material loaded wheel and obtained burn intensities. There was an increasing relationship between the greater the material loading and the greater the depth of cut. The image analysis used a grey scale edge detection threshold to determine the bright material against the dull, wheel grit and bond surface. This would give an indication of the level of wheel loading present.

With all these signals processed into an understandable format they can then be concatenated together to then be trained and tested against the classifier system. The method here would employ a test of several cases seen by the classifier and several cases not seen by the classifier. This technique would provide sufficient results to decide whether the classifier has generalised the difficult to distinguish phenomena. This would give the user an idea that the classifier can make generalised classifications as well as giving a higher confidence in terms of repeatability of results.

The University of Nottingham
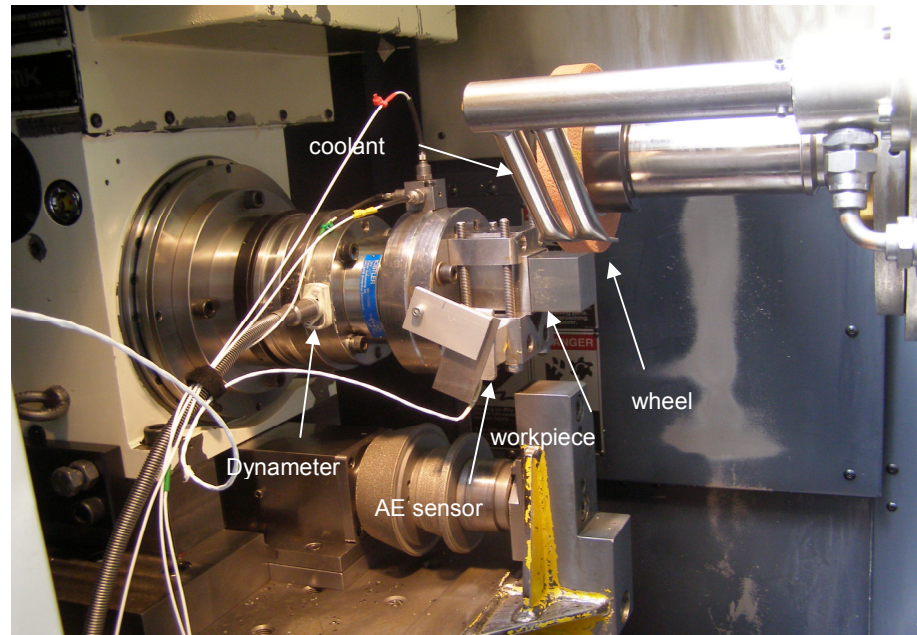
Figure 3.15 A55 Machine centre set-up for chatter trial

The set-up of the grinding process monitoring consisted of the following: A Makino A55 machine centre (see Figure 3.15), two Digital Acquisition Cards (DACs see Chapter 4) being housed on separate computers, a Kistler Dynamometer and force measurement system that would be situated next to the workpeice to take full advantage of material vibrations, Physical Acoustics Corporation (PAC) Wideband AE sensor and amplifier, along with appropriate software including; wave extractor and viewer would also be used to investigate and synthesise the AE extracted signals. The AE sensors were cased in purpose built sensor housing facilities to protect them from the harsh grinding environment with high pressure coolant. In addition, the Matlab Image Processing Toolbox was used to identify wheel loading features. The AE extracted signals consisted of both a continuous waveform and intermittent hit information which is based on a fixed threshold of 40 dB. The hit event triggered data is based upon a grinding event

occurring and achieving AE intensities over the 40 dB range which would then be extracted and stored as 1024 point block information segments. These 1024 blocks would be concatenated together in order of event with respect to time. This was only used for earlier experiments (AE extracted data based on surpassing a defined AE voltage level is analogous to reaching a defined AE dB threshold level). A lot of work however has been carried out in looking into the feasibility of distinguishing phenomena from the continuous wave format. This is due to the continuous waveform format providing all the required information and not losing anything due to the response times in acquisition.

Chapter 4 Grinding Signal Extraction Technologies

4.1 Introduction to signal extraction techniques

When grinding aerospace alloys, there are a number of signal extraction technologies that can be used to identify the onset of malfunction and these give rise to efficient grinding for the duration of manufacture. To ensure this process is carried out, information about the process is required to be recorded and interpreted and if a condition of concern is identified, this must be acted on (Byrne 1995). The more sensory extraction technologies used, the more confident the prediction can be, although with an increase in complexity. There are purpose built technologies looking at specific grinding phenomenon, such as Acoustic Emission (AE), which is very useful for the extraction of energy signals emitted from unit event single grit (SG) scratch phenomenon. Other sensors can be force sensors which are very useful for extracting workpiece deflection and even stiffness characteristics. Both AE and force sensors look at different or the same conditions within the grinding environment with importance being placed in the correct interpretation of the signal. This chapter will discuss all the sensory technologies carried out in the grinding experimentation documented in this thesis. Discussions will be made regarding certain limitation conditions that have to be taken into consideration when carrying out miniscule grit to workpiece interactions such as that seen in single grit scratch cut tests. In addition, sensory extraction for condition monitoring will also be looked at in terms of the macro grinding event with grinding wheel passes.

4.1.1 Principle of Acoustic Emission Operation

AE sensors use crystals or certain ceramic materials which generate a piezoelectric voltage when a mechanical stress is applied. Piezoelectricty was (Holford 2000) discovered by Piere Curie and the word is derived from the Greek *piezein*, which means to squeeze or press. The piezoelectric effect is reversible in that piezoelectric crystals when subjected to an externally applied voltage, change shape by a small amount which correlates to the stress readout. The deformation of the crystal is only small, approximately 0.1% of the original dimension. Such devices can be used to detect sound, the generation of high voltages, electronic frequency generation, microbalance, and ultra fine focusing of optical assemblies. In addition, bio-sensors and medical imaging (diagnostic ultrasound/medical ultrasonography) also use this technology which is very precise in terms of measurement and output. For good confidence levels in using AE technology, exhaustive tests are required to understand and define the boundaries of operation. This is same for any applied application.

The principle operation of the piezoelectric effect can be described by the following; when crystals are subjected to a change through being compressed, twisted or even distorted an electric charge is emitted and it is proportional to change in pressure/force. In short, when a load is applied to the sensing element, deformation of the crystal lattice exists (for example; SiO_2) which results in the generation of an electric charge. Figure 4.1 illustrates the phenomenon (Natarajan 2004).
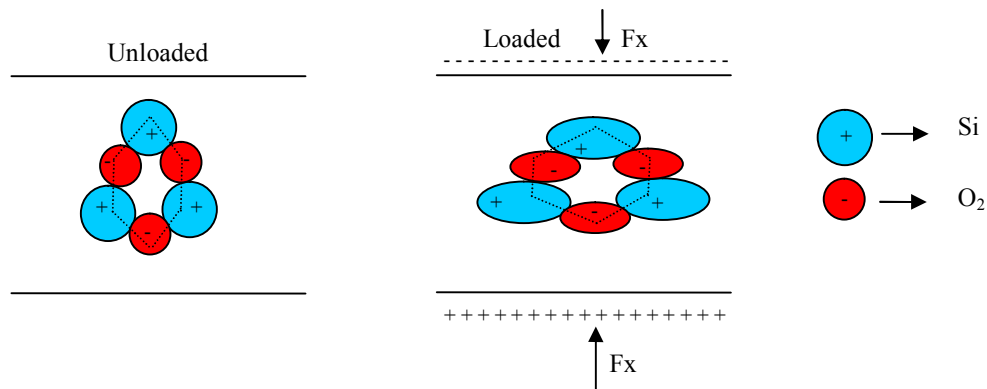
Figure 4.1 The Piezoelectric effect

In looking at the example of SiO_2 further (quartz crystal cell) there are three atoms of silicon (Si) and six atoms of Oxygen atoms (O_2). Each Si atom caries four positive charges while a pair of oxygen atoms carries four (2 times 2) negative charged atoms (reference Figure 4.1 one atom of O_2 atoms refers to an actual pair of O_2 atoms. The quartz crystal is said to be neutrally charged when in the unloaded state. When longitudinal, traversal or shear forces are loaded on to the sensor, the hexagonal lattice is deformed thus initiating negatively and positively charged particles each side of the crystal as shown in Figure 4.1. The quantity of force applied correlates with the resulting magnitude of the charge.

4.1.2 Acoustic Emission oscillation, damping and time of flight

Acoustic energy waves occur naturally when matter vibrates at a frequency usually between 0 Hz and 600 kHz (Fisher and Lally 1967). Acoustic energy can be described as sound which has a range between 20 Hz to 20 kHz and can be detected by the human

ear. Lower frequency acoustic energy has a long wavelength and takes a longer period of time to attenuate. The converse is true for higher frequency acoustic energy, where a shorter wavelength exists and therefore a shorter period of time to attenuate. For instance, a low note played from a piano lasts much longer than high note.

The AE experienced from the applied stress of either grinding or single grit scratch tests experiences damping which can be quantified in terms of a material damping constant for the emitted AE energy. It can be noted that if the material (Tetelman and Chow 1972) is brittle in nature, the damping coefficient is much less than if the material is more ductile in nature and thus experiences hardly any oscillations. It can be said the signal amplitude and damped oscillations decrease steadily relative to the material characteristics. Such oscillations add to the retrieved signal phenomenon thus suspending the propagation of dislocations in time. The oscillations contain important material information and should be noted when correlating the physical material characteristics with the extracted AE signal phenomenon. In addition to the material characteristics, the fixture and the grit material play an important part in the AE material damping coefficient as the stiffer the experimental set-up, the less oscillations will be allowed to be vibrate around the material medium (Chiou and Liang 2000a).

To see the differences in time of flight for the AE to return from the crack position of the pencil break, an experiment was set-up as displayed in the schematic Figure 4.2. This was to see the difference in rise of the signal over the norm (background noise with no AE emission). This would prove the subtle differences in returning AE to the AE

The University of Nottingham

receiver from the fracture of the pencil break. In addition, this experiment displays how sensitive the AE sensor was for the experiments carried out within this thesis.
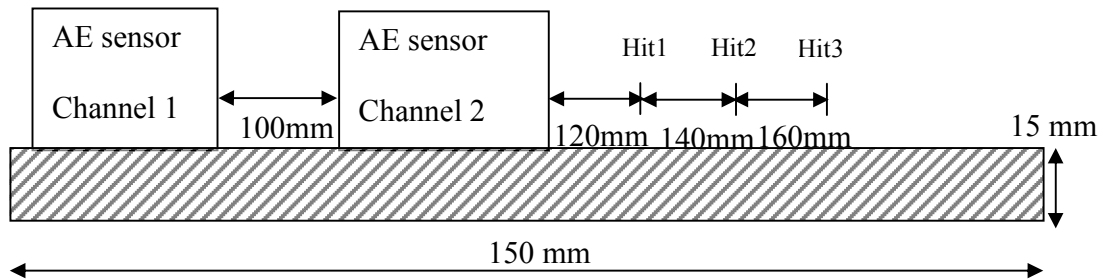
Figure 4.2 Pencil break time of flight experimental set-up

Figure 4.3 displays two AE sensors which were clamped to a metal plate 100 mm apart and pencil break hits with a 2H pencil (Barbezat, Brunner et al. 2004) were made after the channel 2 AE clamped sensor. The first hit was made 120 mm after the channel 2 sensor and then subsequent hits were made 20 mm from the first hit, with the last hit 40 mm from the 1st hit.
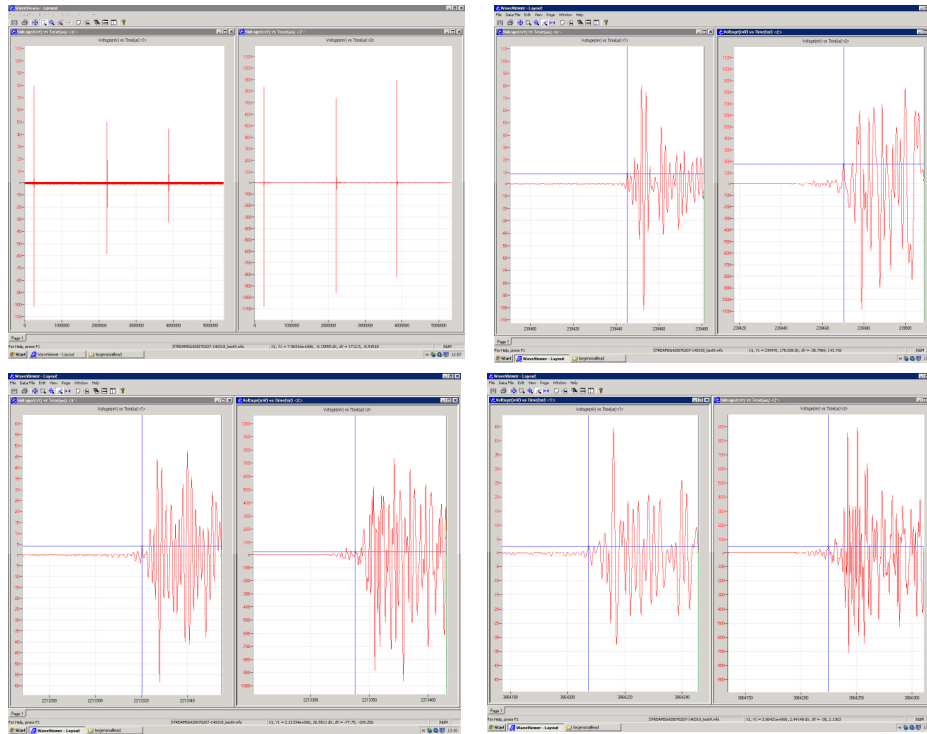
Figure 4.3 Pencil break tests from 1st to 3rd initiated breaks (hits)

Figure 4.3 displays the 3 hits taken directly from 'Waveviewer,' Physcial Acoustic Corporation (PAC ®) AE waveform software. The top left of Figure 4.4 displays the 3 consecutive hits with channel 1 AE sensor on the left and channel 2 AE sensor on the right. The top right of Figure 4.4 displays a more focused view of the 1st hit, bottom left, the 2nd hit and finally, bottom right, the 3rd hit. There was a delay between the two sensors picking up the first voltage rise which gives an indication of speed. For hit 1 the delay between channel 1 and channel 2 was 5μs, then for hit 2, 6μs and finally, 5μs for hit 3. This experiment concluded that 100 mm of distance gave approximately 5μs delay each hit. The magnitude decreased by a factor of 2 after each hit with increasing distance. With a 5μs delay for 0.1m (100mm) this gives an AE wave speed of 20000 m/s

in mild steel which is close to that discussed in literature (Pollock 1973; Pollock 1976; Pollock 1977; Pollock 1979; Pollock 2004).

Figure 4.4 displays the raw extracted time AE signal (Top) followed by its STFT representation (middle) and the Photomap measurement 3D image (bottom). Looking at the figure, the phenomena displayed from the STFT/time representations of AE hit correlates to a measured cut length of 401μm (Single grit scratch length for hit). The interaction between grit and workpiece takes 14μs which is calculated from the following equation:

$$v_g = \frac{\pi \cdot D \cdot RPM - v_w}{60} \qquad (4.1)$$

where v_g is the grain cut through speed, wheel rotational speed in *RPM* is 4000 RPM, the diameter *D* of the steel wheel on which the grit is glued upon is 138mm and the test piece feed speed v_w is 4000 mm/min. The calculation of v_g gives a very fast peripheral grain cut through speed of 28836 mm/s.

The University of Nottingham
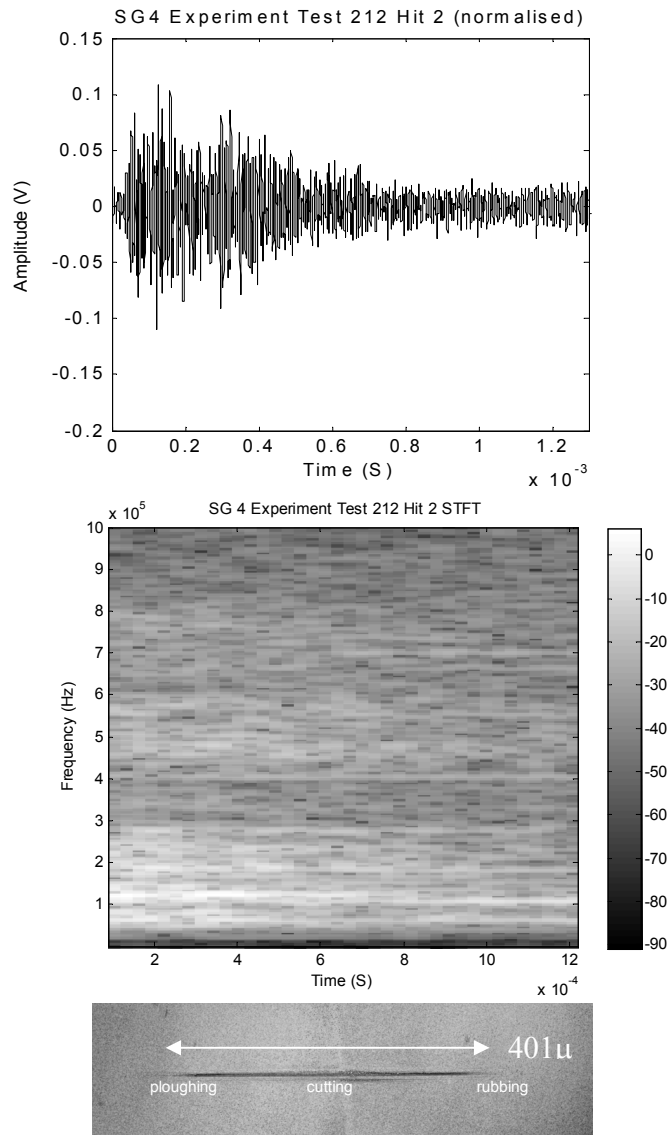
Figure 4.4 Top: Time extracted AE signal, Middle: STFT and Bottom: Photomap image

Looking at the Figure 4.4 again, the phenomena here took as long as 0.8 ms which is 50 times greater than the interaction time between grit and workpiece. The rubbing that is identified in the Figure 4.4 is rubbing with slight plastic deformation. This phenomenon might be explained in that the physical stress prolonged with a response time delay due to the transitional process of the propagating wave excited from the workpiece to the

pickup of the AE sensor(s). Therefore the AE behaviour representing cutting, ploughing and rubbing phenomena is expanded in time. Pencil break tests (Barbezat, Brunner et al. 2004) also displayed a large response time to what can only be described as a microsecond fracture. An experiment was carried out with a synchronised AE and force extraction using the pencil break method to also bolster this finding. The 50 times greater STFT/time signal is representative of oscillations and reflections reverberating along the material medium. Pendulum tests with a damped piece of material (shorter width aluminium test piece) and less damped piece of material (larger width aluminium test piece) displayed greater oscillation with the larger width which again concludes AE sensor extraction also provides material memory. Bearing this in mind, the cutting, ploughing and rubbing signals can still be matched from AE to physical material phenomenon based on signal/physical ratios of the AE energy envelope.

4.1.3 Acoustic Emission System and Calibration

Every time an experiment was carried out, a pencil calibration test would be made to ensure the sensor was set to the correct noise levels and operating normally based on previous tests. This calibration check ensures a fair and accurate comparison is made between the signals. The pencil tests can suggest if the sensitivity has been set too high or too low and may saturate during grinding acquisition.
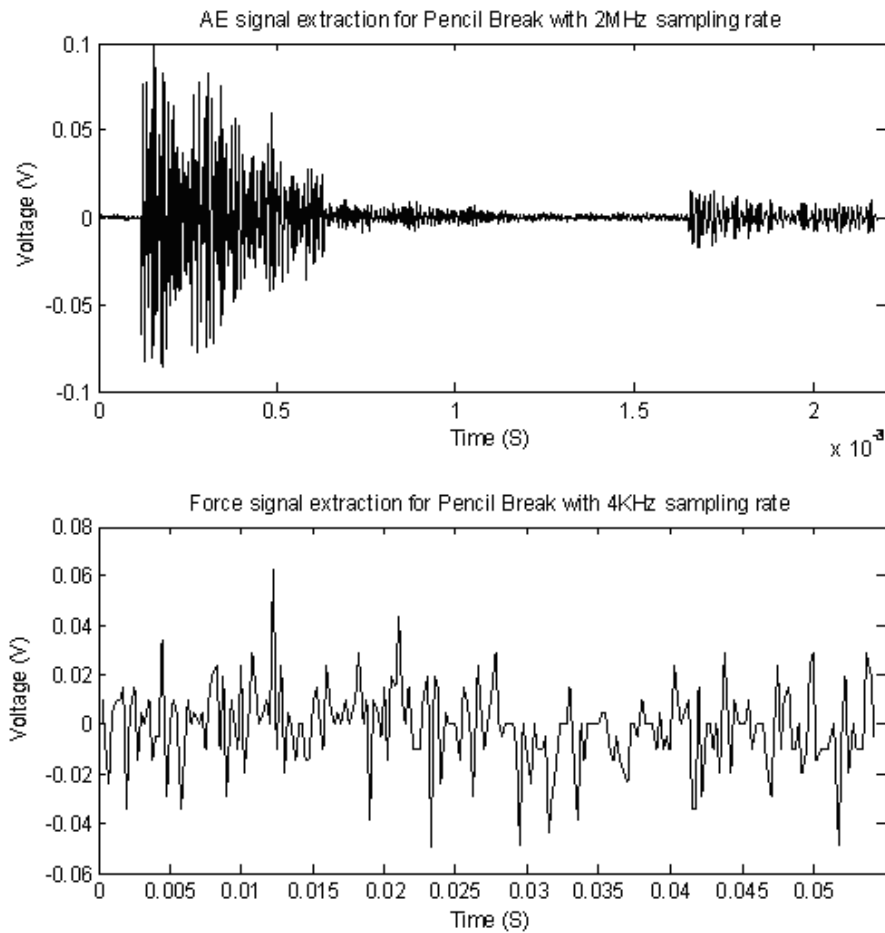
Figure 4.5 Displays, Top: AE pencil break hit and Bottom: Corresponding force signal

Figure 4.5 displays a pencil calibration and force experiment to display how sensitive the AE sensor is when compared to that of the force load cell. At the bottom of Figure 4.5 the peak rising to 0.06 V is representative of the pencil break fracture top of Figure 4.5. This displays a full signature of the specific pencil break phenomenon although a lot more information is present in the AE sensor extracted signal. The 2nd part of the AE signature is typical of bounce from the breaking lead phenomenon, giving a further AE emission which again displays the sensitivity of such sensing technology.

PhD thesis by James Griffin   [111]

The pencil break method is a manufacturing practice used for calibration checks of AE sensors across the world. The simulated AE source is known as the Hsu-Heilsen source (breaking of a high polymer graphite pencil lead to provide a localised AE burst (Barbezat, Brunner et al. 2004)) which provides a broadband step-release transient wave. Important factors to take into consideration are the length of the lead, lead diameter, lead hardness and angle of application between the lead and the surface of the workpiece, as these factors affect the frequency and amplitude of the extracted signal (Boczar and Lorenc 2006).

The sensor is required to be clamped or fixed as close as possible to the workpiece and grit interaction. The closer the sensor, the less time of flight, reverberations and signal reflections occur. Figure 4.7 schematic displays how the AE system is designed from the sensor/workpiece to the computer acquisition system. The current practices specify a 2H lead of 0.5 diameter, 3mm length should be used for the pencil calibration. Such a signal is displayed in Figure 4.5. Figure 4.6 shows a pencil break and force extracted signal displaying the calibration between force and AE emitted signal.
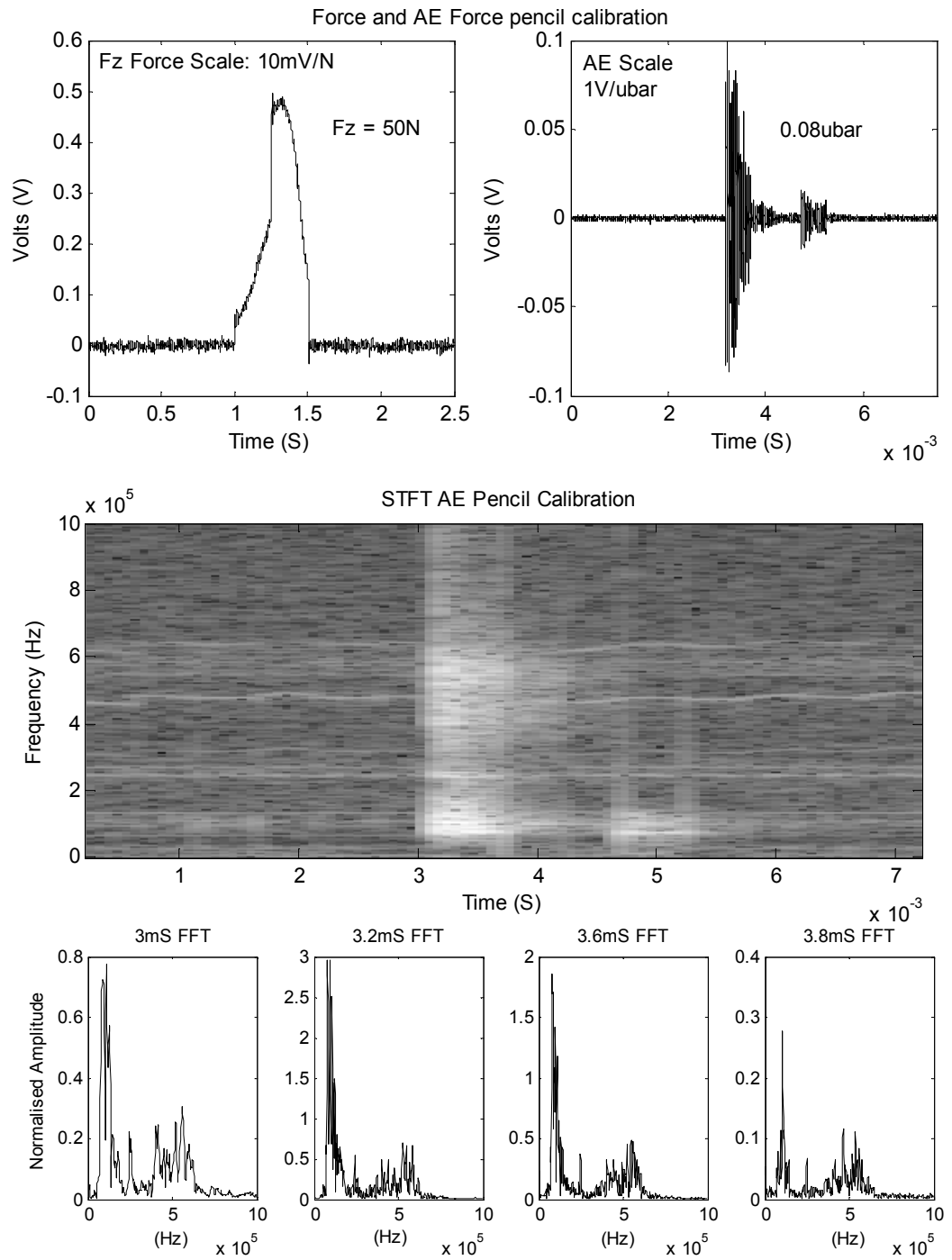
Figure 4.6 Top: force and AE pencil break, Middle: STFT, Bottom: FFT slices of STFT
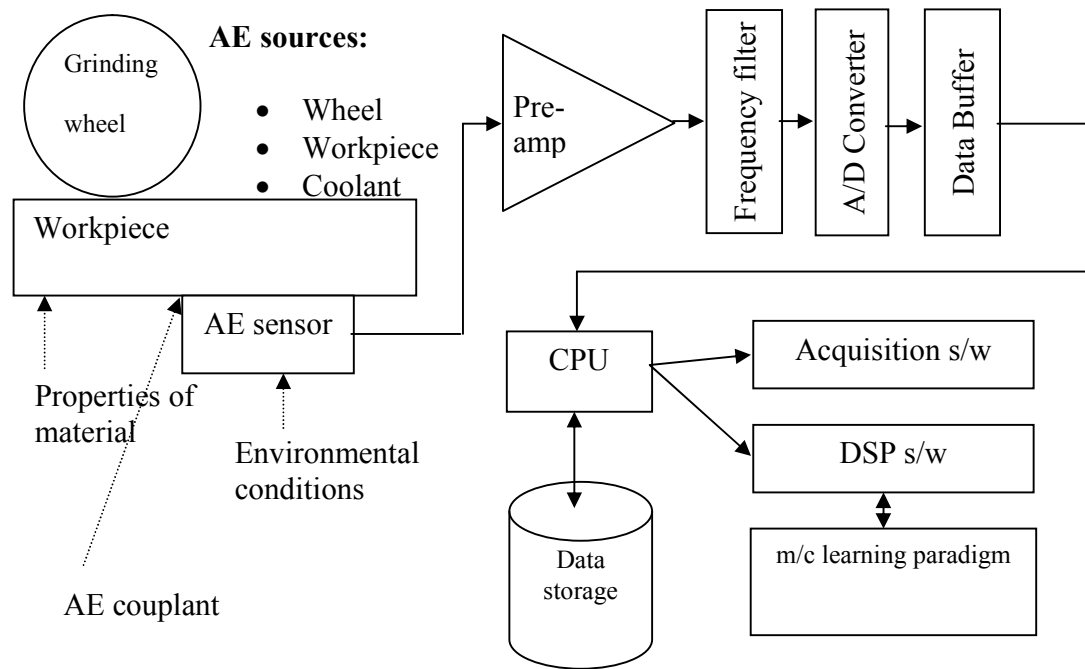
Figure 4.7 AE monitoring system for grinding process and SG scratch tests

Figure 4.7 schematic displays the stress in the form of elastic wave energy and is initiated from dislocations of grit and material fracture. This is caused by the high speed interaction for both the grinding and SG scratch tests. The mechanical stress is recorded in the form of AE time extracted signal where the effects are localised through the verberations of energy passing through the material workpiece medium. The couplant is either a dedicated AE wax or grease to ensure maximum transfer of acoustic energy to the sensor. The sensor then transfers the signal through the amplifier which boosts the magnitude and eliminates the noise caused by surrounding environmental factors. Filtration is the next step; this is where filters are used to remove any further unwanted noise. The signal coming from the amplifier is analogue in nature and representative of voltage per μbar of pressure. This signal is required to be converted to digital notation

(through an analogue to digital (A/D) converter) for post processing and analysis whilst inside the computer (CPU). Next step is where the data is stored as a permanent file in data storage. The data buffer, CPU and data storage all interact with one another in a handshaking manner to ensure the accurate and manageable storage of very large AE signals. Handshaking is where one device is halted (for example the external device – A/D converter) in terms of actions and another (for example the CPU) device communicates with that input buffer device. When this data has been transferred, new data (data sent in manageable blocks) is then transferred from the 1st device in the same manner. In short, once the buffer is full, the data transferred from the A/D converter and is halted. The buffer then communicates with CPU/data storage, once this has been done further information is transferred to the buffer once again. This is analogous to water being stored in a reservoir before consumer use. Once the data has been fully transferred to file through the acquisition software, it can then be processed by digital signal processing techniques. Next and final step, the processed and analysed data can be presented to machining learning techniques where significant features of interest can be identified and informed to the user.

4.1.4 PAC Acoustic Sensor Characteristics

AE sensors can be set-up either in single ended or differential (Raj and Jha 1994) where single ended design uses a single crystal to provide an omni-directional response, this is regardless of orientation to the AE excitation. Differential however, provides a common mode rejection of unwanted signals which is very useful in noisy environments. The

work carried out in this thesis always used differential AE sensor set-up. Jamielniak (Jemielniak 2001) discussed that AE frequencies of interaction between workpiece and grinding wheel normally vary between 50 kHz and 4000 kHz. The grinding interaction between workpiece and wheel acoustic emission may have a wide band of frequencies and to get this information, the corresponding sensors are required to have similar characteristics. There were two AE sensors used during the experimentation this provided a secondary verification check and in some cases identified the distance of the initiated phenomenon. The single grit (SG) scratch tests grit and workpiece interaction was so rapid the 2 AE sensors would verify the signals of the gained phenomena without spurious unwanted noise (such as coolant falling from previous trials or, power spikes often confused as a grit hit interaction). In addition, no other synchronised sensory interaction could pick up the SG phenomena as the NI integrated circuit board controller and sensor sampling rate/sensitivity was not high enough to extract the phenomenon of interest. The AE sensor used during the trials was a Physical Acoustic Corporation ® PAC WD (wide band) sensor. There were three AE sensors present, however only two would be used with one acting as backup (sensor (3) AL19). Table 4.1 lists each individual AE sensor characteristics.

AE sensor sensitivity is the ratio of pressure for each μbar from a given point of phenomenon and the open loop voltage caused by the sound pressure (piezoelectric effect). The sensors can be calibrated for either pressure waves (V/ μbar) or with transient waves (V m/s) but they can not be converted from each other once the calibration has been selected.

Table 4.1 Main specifications of AE sensors

	PAC WD Sensor (1)	PAC WD Sensor (2)	PAC WD Sensor (3)
Sensor number/date	AL04/(17/11/04)	AL05/(17/11/04)	AL19(11/12/02)
Construction	Differential	Differential	Differential
Sensor drive capability	Up to 100m with w/RG-58 AU cable	Up to 100m with w/RG-58 AU cable	Up to 100m with w/RG-58 AU cable
Dimensions (dia. * ht.)	17*16 mm	17*16 mm	17*16 mm
Peak sensitivity	-63.21 (dB ref 1V/μbar)	-63.30 (dB ref 1V/μbar)	-60.62 (dB ref 1V/μbar)
Operating freq range	50 kHz -1000 kHz	50 kHz -1000 kHz	50 kHz -1000 kHz

The sensor has a maximum displacement of approximately 200 pm which is extremely sensitive when compared with atomic radii (atomic force microscope) with a range displacement of 150 pm. With these characteristics, AE is very useful for monitoring material processing.

At high frequencies, the output of the AE sensor is very weak (i.e. low level and high impedance) and this kind of signal is very difficult read with the PAC acquisition board connected and configured to the monitoring computer. This is why a pre-amplifier needs to be connected in series and with minimal distance to ensure no unwanted pickup of electromagnetic interference. The pre-amplifier is required to increase the amplitude across the wide range of frequency pickup and match the low impedance of the cable whilst at the same time meet the high impedance of the piezoelectric crystal. These considerations ensure that lengthy coaxial cables can be used to connect the pre-amplifier to the acquisition card without attenuating the AE signal or at least attenuating the signal to negligible effects.

The University of Nottingham

The detected signals from the AE sensors were passed through pre-amplifiers with a gain of 100(40 dB). A threshold dB pick-up setting (software) of 35 dB was set-up in the AE PAC extraction software for SG tests, however, for burn and coolant grinding tests, the threshold was set much higher, between 40dB and 60 dB noise pickup threshold, with the pre-amplifiers set much lower at between 20dB – 40dB signal boost. If the gain is set too high then the amplified signal will saturate and the amplification will tend from linear to non-linear operation. From carrying out earlier test trials and checking the data, the AE acquisition system can be configured to the correct corresponding level to reference the phenomenon frequency response.

The pre-amplifier also minimises or even eliminates mechanical and acoustical background noise that exits at low frequency, which is up to and including 20KHz (Qiang 2004). With SG tests, the only noise causing any concern was that from the mechanical parts such as the motor/spindle of the A55 grinding centre machine. With the grinding trials testing for burn and chatter, both the spindle and coolant presented a problem that required careful filtration to ensure the signals of interest were identified appropriately. The background noise was measured at around the 50 kHz level and therefore only gave minimal influence upon the measuring system. The software methods used for signal processing filtered the signal with Chebyshev II bandpass filters with a cut-off frequency between 50 kHz and 1200 kHz where most of the background noise was eliminated from the extracted raw AE signals. The voltage supplying the

PAC preamplifiers was 28 V_{DC}, this is supplied internally via the coaxial cable from the acquisition board with no external power source present.

4.2   Force and Acceleration Measurements

The thesis is predominantly looking at grinding phenomenon through AE signal analysis however this technique requires verification from other sensory techniques. This section will look at the process behind the Kistler mini load cell for Single grit scratch tests and the dynamometer used for grinding, milling and hole making which is permanently housed within the A55 machine centre. This instrumentation is considered just as important as the AE sensor as it provides more reliable information in that there are fewer factors affecting the outcome of results when compared with that of AE sensory technology and thus needs to be set-up both accurately and reliably. The sensitivity of load and accelerometer devices is less than that of AE sensors, however, they are still sensitive and require calibration and test before being using in a trial situation. The Kistler dynamometer 9272A and 5017 amplifier were used for the main grinding trials as this gave a range between 5 and 20 KN which is more than adequate for grinding under extreme conditions. For the SG scratch tests, the dynamometer was not used as the sensitivity was too low and therefore a Kistler Type 9602 was used instead, providing only force displacement although the sensitivity was much higher than that of the dynamometer with a range between 0.5 KN to 5KN (two different sensitivities for different measurement ranges). Both systems have to be calibrated in terms of weights being applied to X, Y, and Z directions and note the corresponding output voltage. A linear interpolation of the weight to force relationship is used to convert the output

voltage to force in Newton's (N). The dynamometer and accelerometer has calibration constants to multiply by to give the correct output from voltage to Newton's and amplifier gain sensitivities to convert the extracted voltage into Newton's for force and gain and to convert into accelerations (meters per second squared) m/s^2; FX=1000, FY=1000, FZ=10000, Ax = 1, Ay = 1 and Az = 1.

This instrumentation has amplification, filtration, isolation and shielding all built into the design of 'plug and play' Kistler measurement devices. The data acquisition system is based on hardware and software connecting the real world to the binary computer world. For both Kistler devices and other sensory devices (excluding the AE sensors) LabVIEW engineering/scientific graphical programming suite was used to create applications for monitoring, data flow, sensitivity settings, interface between user and computer and simultaneous sensor(s) extraction. This powerful programming environment is based on graphical 'drag and drop' blocks that allow the user to tailor the application to the sensory needs. Such customisation may mean an alarm is raised if certain signals pass over a designated threshold voltage. The hardware for the grinding and SG scratch tests consisted of the following; LabVIEW SCB-100 shielded I/O connector and data logging card AT-MID-64E-3. The SCB-100 100 pin shielded connector block has 100 screw terminals that connect a total of 8 sensory input devices in differential reference mode or, 16 sensory input devices in single-ended mode. The difference between the two modes is that differential uses both the negative and positive sensory output and single ended, is between ground and the positive sensory output. The differential mode was used throughout the trials. For the SG scratch tests, the force and

power were recorded, however the results were inconclusive due to the SG scratch phenomenon occurring very quickly and unable to be recorded by the sensory technologies other than the two AE sensor channels. The NI 6061E DAQ (MIO-64E-3) data logging card is a high performance card with file data stream rates of 500 kS/s. This card was set-up with a 5V triggering input which was also connected to the input interface of the PAC AE system card (PCI-2 2 Channel AE system) thus synchronisation between the two sensory systems existed.

The MIO-64E-3 card has a maximum input voltage of 10V and a minimum quantised level of $10/2^{12}$ = 2.44 mV. With the use of an onboard multiplexer (switching device which allows many devices to communicate in a sequential manner) all the channels can acquire 500 kS/S for either differential or single ended mode. If however 10 channels are used simultaneously then the speed per channel is 10% of the maximum which equates to 50 kS/S for each of 10 channels simultaneously. There are three types of multiplexers available; time division, frequency division or a combination of both. The MIO-64E-3 card uses time division multiplexing. The multiplexer allows the sequential switching between each channel and an A/D converter is used to communicate the real world data to the binary computer world after multiplexing has taken place. It can be said the data card has to act very quickly carrying out a number of calculations and actions at any one time. The card, connection box and LabVIEW software is used to communicate with all sensory devices except the AE sensory device. In short, the force, accelerations, temperature, spindle moment and spindle power all communicate with the MIO-64E-3 card and SCB-100 Box.

4.3 Hardware and Software Setup

The LabVIEW software package is setup as an acquisition system for the user to define recording parameters. Such recording parameters are; the length of time for recording or trigger start and stop acquisition setup, the sampling rate for all channels, differential or single-ended mode selection and which channels are selected for monitoring. The sampling rate is limited to certain levels, the more channels in use the less the sampling rate should be, this is due to the limitations of the computer specification and input/output integrated circuit card. For gaining material information however, it is said the sampling rate should be at least four times the signal pickup frequency. This is due to the high resolution required for material analysis and therefore there is a trade-off between the amount of channels used and correct resolution to obtain the desired phenomenon signal. The signal processing functions of the software need to continually talk to the hardware, for instance, the read action has to extract for each channel with multiplexing, then, sample these signals according to the sampling parameters input by the user and then finally, the data needs to be streamed and saved to a file format. During acquisition, the channels can be set to different colours and viewed on a graphical window pane within the software environment. In addition, play back should be possible with the selection of the saved file. The display range can be adjusted to anywhere between -10V and 10V depending on the strength of the extracted signal. The sampling rate has a maximum limit of 500 kHz and max number of samples of 20,000 for one channel only. A signal processing panel for play back of the signals is also available, where the raw extracted signals can be converted to RMS values and output directly to the user. In addition, all of the extracted signals can be seen at any one time.

The University of Nottingham

As most of the signal processing was done in the Matlab ® Engineering/Science programming suite, the viewing was also done in Matlab, however, the LabVIEW tool set-up window panel would give a good 'heads-up' to the user during experimentation.

The AE system uses a Physical Acoustics PCI-2 AE system which is a 2 channel AE data acquisition and digital signal processing system on a single full-size PCI card. It has superior low noise and low threshold performance with an 18 bit A/D conversion, 40 MSample/second acquisitions with sampling averaging and automatic offset control. This performance has been possible from utilising pipelined, real time architecture, without any sacrifice in AE performance. Through the high performance PCI (Peripheral Component Interconnect) bus and separate Direct Memory Access (DMA) architecture for each channel, significant AE data transfer speeds can be attained , assuring wide bandwidth bus for multi-channel AE data acquisition and waveform transfer. The card is built on surface mount technology and high density ASIC (high density Programmable Gate Arrays) devices; this ensures that this single AE system with onboard 2 channels has a very fast acquisition capability for storing signals of interest.

4.3.1 Power Sensor

The Load Control sensors are another important consideration when considering the monitoring of grinding technologies. The sensor could just measure the current however at light loads there is no change and no linear straight line characteristics, whereas with power sensors this is far more sensitive and operates within linear straight line characteristics. A power sensor is configured in the following way, a voltage is

measured across a very high resistance (open circuit) and this is carried out across the first two phases of the three-phase machine (for example; in the case of A55 machine centre an induction motor is used to provide the spindle power). A Hall-effect sensor is used to measure the current within the last remaining phase, this works from sensing the magnetic field. Following on, when a current carrying conductor passes through a magnetic flux concentrator (donut) and the Hall Effect sensor is placed within a gap in the concentrator, the signal is proportional to current. This power signal is then filtered and verified through secondary voltage and current checks and is representative of the power used by the spindle of A55 machine centre. With a lot of noise present during grinding in terms of both mechanical noise and coolant, the signal requires significant filtering to make use of possible material surface anomalies. Or a more improved system is required to use the voltage readout in open loop configuration taken directly from the motor windings. The power is merely a check signal for force and AE extracted data. For the Load Control Sensor the response time is 35mS which is acceptable for monitoring most machining processes (including grinding) however just outside the range required for monitoring single grit scratch tests. Load Control sensors can be used for grinding gap elimination (contact detection between workpiece and tool) and used to detect dull wheels (worn grinding wheels) from an decrease in power, this is due to the sharper recently dressed wheel requiring less spindle power. This is due to sharper grits providing a cutting action as opposed to a rubbing and ploughing action which inherently gives off more energy into the workpiece as opposed to chip.

4.3.2 Temperature Measurement

The temperature measurement was only gained for certain experiments in the grinding pass trials. The predominant work carried out in this thesis is the analysis of SG scratch tests and for initial work there was no requirement to measure temperature as the grit-workpiece interaction was so quick the burst temperature hardly increased at all and would require a much more sensitive temperature measurement system than was used for these grinding trials.

The temperature caused in the grinding zone is dependent of the energy distribution from the interaction of increasing grinding parameters from nominal to abusive machining conditions (Rowe 2001a; Rowe and Jin 2001b; Rowe 2001c). When Fourier Law is applied to a sliding plane heat source condition, this allows most analysis to be carried out in terms of the conduction of heat occurring within the workpiece. The relationship between specific energy and temperature interpolation is based on the specific energy levels e_c (energy/power per unit volume removed) being determined from grinding parameters/characteristics such as the workpiece, the grinding wheel and grinding conditions which corresponds to the heat flux distributed over the grinding zone (contact area). As discussed in Chapter 2 with reference to grinding, most of the energy (in the form of heat) is transferred to the workpiece, chips and wheel and therefore much smaller amounts are used to actually cut. The focus of energy is therefore based on temperature measurements experienced in the wheel, chips and cutting fluid.

Lui (Lui 2004) discusses specific energy in terms of grinding elements and thermal conductivity. Practical temperature monitoring is very difficult to apply to a production environment and used more in laboratory test work to understand the machining process in terms of thermal activity and to model thermal conditions from different machining cutting parameters. All techniques for temperature measurement are based on heat conduction or heat radiation. For grinding however, as mentioned in Chapter 2, the heat experienced within the grinding zone is extremely hot (approximately >700 C°) although due to the quick wheel and feed speeds, these temperatures are only experienced for a short burst amount of time. To read such temperatures is very difficult and the measuring system requires an adequate time constant to be able to acquire such phenomenon. Grinding zone temperature is very important to measure during a grinding pass as it provides information of possible metallurgical burn anomalies which have an effect on tensile strength as well as causing white layer hardening, possible micro cracks, twinnings and unwanted burrs. There are eight common types of temperature measuring devices; thermocouples, thermistors, resistance temperature devices (RTDs), bimetallic strip devices, infrared radiation sensors, liquid expansion devices, thermal imaging camera, digital thermometer and change of state devices. With the nature of grinding and fixture of the workpiece, only thermocouples, thermal imaging camera and infrared radiation sensors are appropriate for application. Out of these technologies the thermocouple is the better technology for application. This is due to the fact that the thermocouple type material can be fixed between two test pieces at the centre of the grinding zone, near the ground surface which correlates with thermal damage (Guo and Wu 1999) at the grinding zone. The use of fibre optics with high sampling rate and a fast

acquisition system provides an accurate measurement of the grinding zone (Bezombes, Burton et al. 2006). To ensure good thermal conductivity a PVD thin film was fixed onto the grinding surface this acts as a thermal sensor during the grinding pass (Kato and Fujii 1997; Kato and Fujii 1999). With coolant present in the grinding process, this rules out other sensors such as thermal imaging due to the harsh environment and thermal blankets around the workpiece/grinding wheel zone of interest. Some of these technologies are only suitable for dry grinding application.

4.3.2.1   Sandwich Thermocouple

The thermocouple is the choice that was used to measure grinding temperature this is due to economical and fast response characteristics. The time constant is very important with such a device as it needs to be sensitive enough to read the burst temperature experienced during a grinding pass. The time constant is worked out from the grinding contact length (l_c) divided by the wheel velocity (V_w). For most grinding passes the time constant is between 0.16S to 3S and largest time constant for a thermocouple is 5 mS. In short, the thermocouple is well within the range to acquire the grinding zone temperatures. That said, for SG scratch test interaction this is much faster, with some 15 µS interaction time and therefore cannot utilise thermocouple technology.

The sandwich thermocouple (see Figure 4.8) works by using two specifically ground workpiece materials machined to dimensional tolerances and fixed within a purpose built test rig which is on top of the dynamometer. The first element used in the sandwich thermocouple is a single wire that provides the heat conduction to the thermocouple K-

Type configuration. The second metal is the workpiece material itself. The wire is sandwiched in-between the two identical machined workpieces with the clamping rig giving a tight fit between wire and workpieces. When grinding occurs, the active grits make contact with the two materials and a thermocouple is made. Operation of thermocouple carries on until the wire no longer conducts heat or is either worn or damaged.
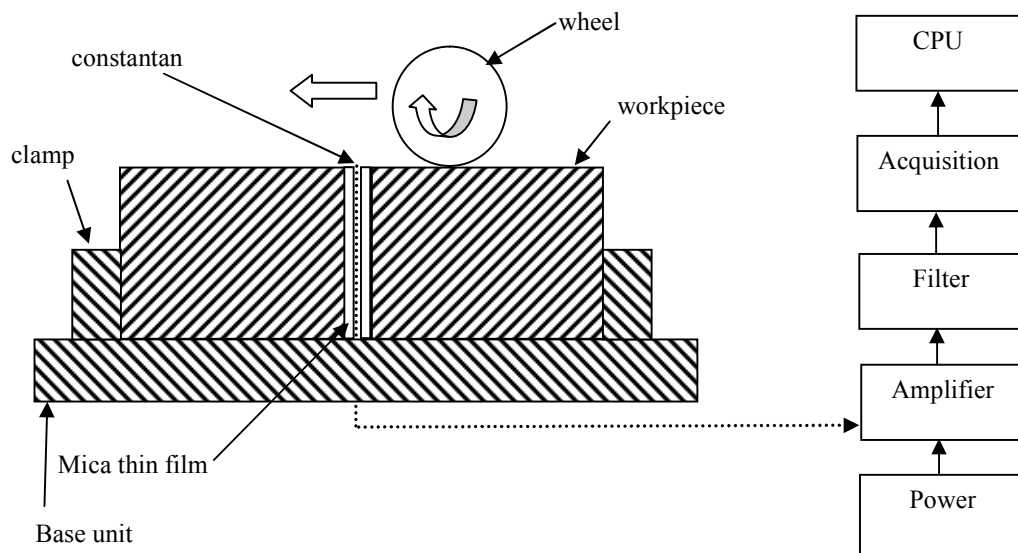
Figure 4.8 Sandwich thermocouple for measurement of grinding temperature

A K-Type thermocouple/amplifier was constructed with a monolithic thermocouple Integrated Circuit (IC); AD594. The AD594 IC (see left hand side of Figure 4.9) compares the ice point reference with a pre-calibrated amplifier to produce a (10mV/°C) corresponding output directly from a thermocouple signal. To achieve a temperature proportional output of 10mV/°C and accurately compensate for the reference junction

The University of
Nottingham

over the rated operating range of the circuit, the AD594 is gain trimmed to match the transfer characteristic of a J type thermocouple at $25^{\circ}C$. Resistors are used to provide gain control and transducer voltages, this is based on the circuit diagram illustrated in Figure 4.8. The recommended measuring range for AD594 for a power supply of 15V is approximately $1250^{\circ}C$. The basic circuit diagram of AD594 is shown to the left of Figure 4.9, on the right side connecting to the AD594 IC are two unity gain follower circuits which invert the signal and invert again to give a positive readout. This follower circuit is only used if the thermocouple voltage continually saturates above 10V, which the acquisition board AT-MID-64E-3 does not support (constrained to -10V to 10V input). The following acts as a divider circuit giving twice as much range and therefore accommodating the high end grinding temperatures. The thermocouple is calibrated from known temperature sources such as ice water (approx $0^{\circ}C$) to increments of different heat settings such as the application of a soldering iron placed above the two thermocouple materials. A linear curve will exist from ice water to the max soldering iron temperature of $400^{\circ}C$ ensuring a voltage to temperature conversion for the grinding trials. Temperature calibration data is presented in Figure 4.10.
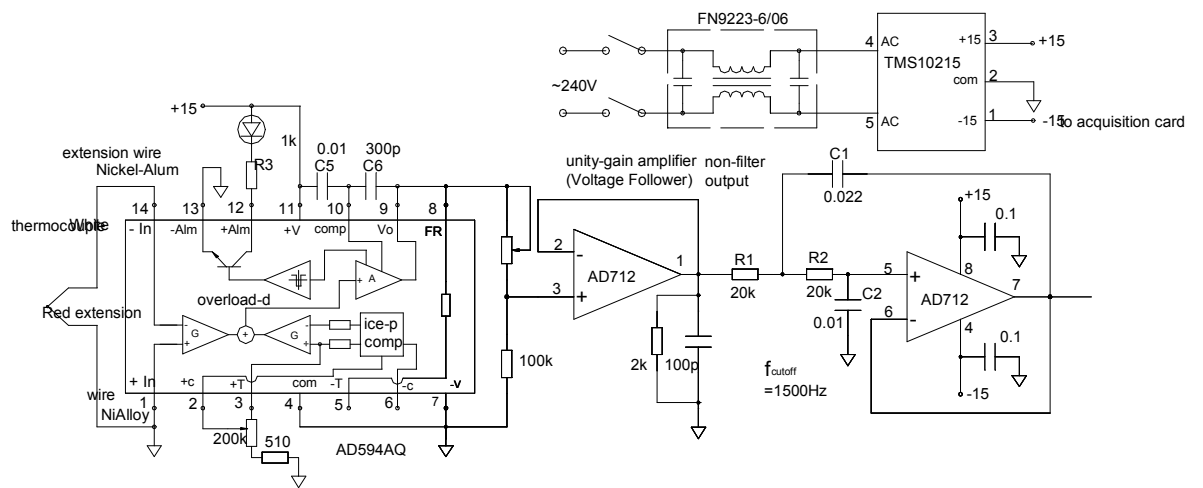
Figure 4.9 displays thermocouple amplifier circuit
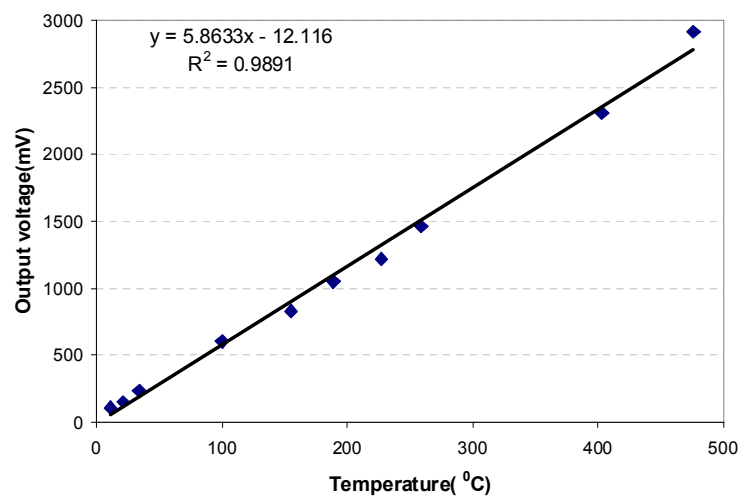
Figure 4.10 CMSX4 thermocouple measurements of output voltage vs. temperature

Chapter 5 Digital Signal Processing Techniques

5.1   Introduction to Digital Signal Processing

Signal processing is a process of extracting information into meaningful information to thus correlate with other physical phenomena, such as material defects or material anomalies for example. It can be argued that Digital Signal Processing (DSP) is perhaps one of the most important aspects within process monitoring and provides the transition from the real world to the computer world representation. Signals can have many different attributes such as changing in intensities, the frequencies of those intensities change, the mixture super imposing of several signals merging into one signal and of course, the addition of unwanted noise. DSP has four main technologies that systematically follow on from each other namely; acquisition of signal, the preparation and transformation of the signal, filtering of the signal and lastly, the analysis and synthesis of the signal (Lai 2004). This Chapter will look at the different attributes posed by signals and an in-depth discussion breaking up the four main technologies of DSP.

To gain signals of interest the different attributes need to be segregated, for instance, the signal of interest may be overwhelmed by noise at first investigation. This kind of scenario is indicative within grinding process monitoring with the application of high pressure coolant. Or the noise can be from other internal machining or external sources such as the mechanical machining noise experienced by the fast rotating spindle or, electromagnetic interference from white noise experienced in most places on a daily basis. This kind of segregation presents a problem to signal processing. With the use of

filters, it is possible to remove these unwanted characteristics and look at signals of interest with much clearer phenomenon providing clear features of interest. This feature extraction can then be carried out in the time domain, frequency domain or a combination of both, time-frequency domain. The extracted signal can be either a deterministic signal or a stochastic signal, the deterministic signal is broken down to either a periodic signal (simple and complex signals) or aperiodic signal (quasi-periodic and transient signal), where the stochastic signal is broken down to either a stationary (ergodic and non-ergodic processes) or non-stationary (random sporadic burst information). This thesis is primarily concerned with stochastic hi-frequency non-stationary signals. This is perhaps the most difficult type of signal to provide analysis for and therefore requires a good DSP technique to identify the key features of interest; such techniques are STFT and Wavelet Transform technology (WT). These techniques will be discussed at length as they are both used in the thesis, the technique of WPT is superior in terms of resolution to STFT however for some analysis work (if the noise is considered not too great and computational power is not a concern). STFT can be used in place of WPT (WPT provides more resolution analysis than that of WT) and still provides accurate and useful results.

5.2 Signal Properties and Representation

A signal can be expressed as a physical quantity which can change with time. The signal maybe periodic in which certain intensities occur at fixed intervals in time. The data in its raw form can be difficult to quantify and therefore requires the conversion to physical quantities that are both easier to measure and analyse. The signal itself is usually

The University of Nottingham

combined with both useful (correlated signal information to observed physical phenomena) and non-useful data (noise). Signal processing is required to extract the useful information and limit or even discard the useless information.
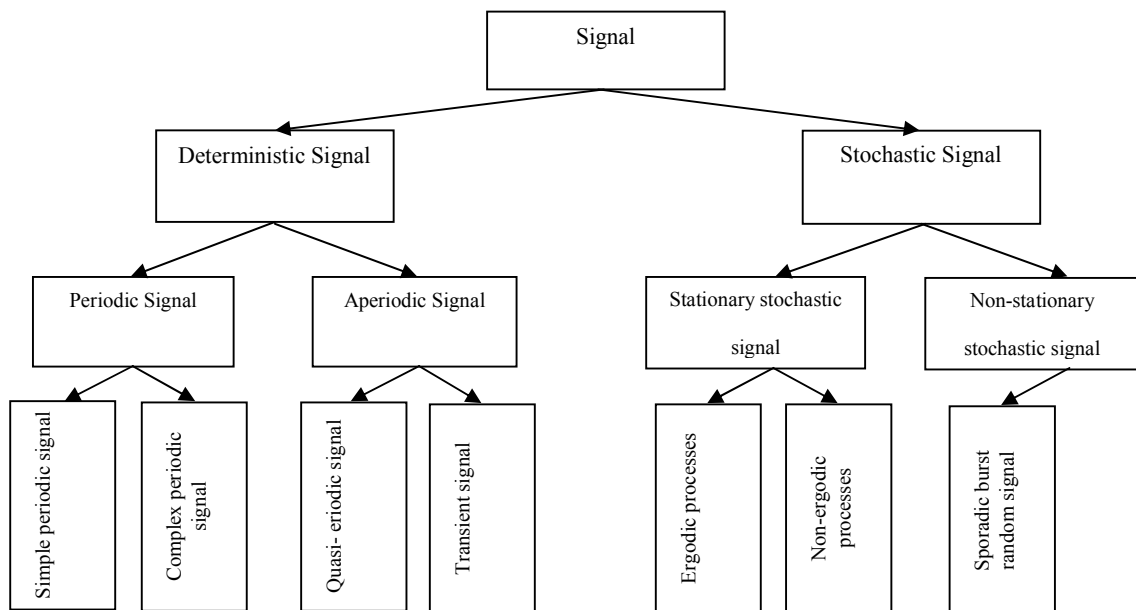
Figure 5.1 Signal characterisation

Signals can be deterministic or non-deterministic in nature. Deterministic can be represented by a mathematical function over time. For example; the electrical mains supply signal (UK) is deterministic in that the voltage amplitude is fixed at 240V (normal operation) and the sinusoidal signal carrying that voltage has a period of 20mS in which a rise and fall occurs from the zero reference norm (during the period, the signal passes through '0' three times). This signal is now represented as a 240V magnitude with an infinite occurring rise and fall in sinusoidal manner every 20mS which represents a 50 Hz signal or 50 cycles per second. Only if other external factors

The University of Nottingham

act on the signal will the properties and characteristics change thus; it is a highly predictable and easy mathematical function to model. Non-deterministic signals are the converse of deterministic signals in that the signal cannot easily be defined by a mathematical expression and their future values are very difficult or even impossible to predict. Non-deterministic signals are quantified as random signals characterised by uncertainty or unpredictability. To analyse and make use of these signals, signal processing techniques along with probability and statistics is used to draw out meaningful data. All signals have the physical quantity of time and amplitude and they can be segregated in terms of continuous (analogue tending towards infinity) and discrete signals (computer tending towards specified DC voltage levels).

Digital Signal Processing (DSP) is more concerned with the conversion from continuous (analogue/real world) to discrete (computer world). DSP is where the signal is transformed into discrete-time and discrete amplitude signals. Digitisation is carried out from sampling at a defined constant rate and equal step intervals (with amplitude quantification). There is a trade-off with analogue-to-digital (A/D) conversion and this is between the sampling interval and the sampling rate. The sampling interval has to be enough to ensure good resolution for computer interpretation and the sampling rate has to obey Shannon's sampling theorem (Liu 2004).

If this is not obeyed and the sampling rate is less than twice the bandwidth of the signal under process then aliasing of the reconstructed signal will occur. The accuracy of A/D conversion is also very important in that the difference between two quantified voltages

The University of Nottingham

neighbouring each other should have small associated quantified voltage errors. This is due to the noise getting superimposed onto the signal sampling values. If this is the case, an increase in resolution from an increase in the number of processing bits (within the A/D process) will overcome this problem.

Once the signal has been converted from the real to the computer world, analysis is then required regarding the transferred signal into different domains through mathematical functions (Stephenson 1988). These transformations allow interesting features to be more readily visible. For example; if the signal remains in the time domain the user will not have an idea which are the dominate frequencies; instead he/she will see a rise in amplitude and compact sinusoidal and, nothing more! If however the signal is converted to just the frequency-domain, the user will only see the dominant frequency bands and not when the dominant frequency bands occurred. One of the most useful signal transformations is from the time domain to the time-frequency domain displaying both time and frequency information at the same time. The signals itself can be broken down into different levels of detail this is to segregate the simple from complex signal composition. This hierarchical structure of data can then be used to look at key phenomenon of interest. The mathematical transforms allows techniques such as STFT and WPT to see the signals represented on three axis of interest; time, frequency and amplitude domains.

Reference ergodic stochastic signals; there are small similarities with the deterministic type of signal. These similarities can be accessed from using probability and statistical

functions. Some of these statistical functions work with the amplitude part of the signal and are listed as follows; mean, Root Mean Squared (RMS), standard deviation, Probability Density Function (PDF) and Joint Probability Density Function (JPDF).

Looking at the time domain part of the signal there are two statistical functions that can be used such as autocorrelation (AR) and cross correlation functions (CCF). Lastly, for the frequency domain there are four main statistical functions that can be used; transfer function, spectral correlation function, cross spectral density function and the power spectral density function.

A hierarchical road map is displayed in Qiang's thesis (Liu 2004) which provides an overview of DSP (procedures and methods) used within the area of grinding. Today in signal processing techniques, the arsenal of advanced functionality that is used more frequently than in previous process monitoring regimes are; chaos, fractal, maximum entropy spectrum, high-order spectra, AR coefficients and wavelet amplitude mean square (Lezanski 2001).

For the successful processing of signals there needs to be a trade-off between computerised complexity and accuracy suitable for application. For example; in the early trial work with radial scratch tests, a single AE sensor was used. During this trial work there was more noise extracted and this was due to using a less sensitive sensor to grinding AE emission. During the last trial work (horizontal scratch tests), more sensitive sensors were used that hadn't been previously been used in harsh environments

The University of Nottingham

(this could have affected the sensitivity with the previous sensor – note the use of sensor housing in experimental set-up). It was also observed that the grit made approximately 1µm depth cuts with the SG radial scratch tests. The set-up allowed more accurate 1µm advancements than what was experienced with SG horizontal scratch tests. The SG horizontal scratch tests set-up had the workpiece fixed as flat as possible, however, to accurately get 1µm flatness in an A55 machine centre is very difficult and therefore the SG horizontal scratch tests had depth cuts ranging from 0.25µm to 2.5µm. To separate the unwanted noise in the early work proved to be a challenge at first; this was due to the intensities of interaction being low and less sensitive and the sensor being more susceptible to noise. This meant the use of WT had to be used to segregate such signals and focus on the phenomenon of interest. For the main SG horizontal scratch tests, the noise was negligible and STFT were used instead; this technique still afforded good results. In addition to the technique used, the greater the sampling rate applied, the better the signal resolution for locating phenomenon of interest.

5.3 Filtering Techniques for DSP

Digital filters are used on discrete-time systems and when applied to a raw signal they take a snap shot of that signal in time, in short, the snap shot is the finite look at the analogue world. Through convolution calculations an output signal is provided with the necessary filtering made across the total snap shot raw extracted signal. From the conversion of analogue-to-digital signal the calculated output should have minimal energy loss. For example; the main part of the signal with rich information regarding the phenomena is still present although the noise component is removed or reduced to

negligible effects. There is therefore, a trade-off between filtering the unwanted noise and minimising the signal energy in terms of valuable signal information present in the raw extracted signal.

The window function within filtering and spectral analysis is mainly used to truncate signals and mitigate Gibbs phenomenon (Strang and Nguyen 1996). Such window functions allow the calculations for filtering or time-frequency analysis to exist in manageable/high resolution segments (if quantified and selected accurately). Window functions can be used in many DSP areas, filters and time-frequency analysis is just a few that are mentioned in giving relevant example to the window function. Outside of the chosen interval, the window function is zero-valued and within this interval the function is constant. Outside of the interval it is zero valued and this is why a window is known as a rectangular window. If however a signal or function is multiplied by the window outside its interval, the value still remains zero. It can be said a rectangular window works very well with signals of comparable intensity; however, it fails to provide a good realisation when the signals are of disparate amplitudes. This is known as low-dynamic-range window. With a high-dynamic-range and low resolution window, these are the poorest for sensitivity, if random noise exists closed to the signal frequency, the random noise signal would be more prominent. With a high resolution window this caters for a number of different signals at different strengths, this type of windowing is used in wideband applications. The common types of window techniques used in DSP are the Hamming window, Hamming window, rectangular window, Blackman window, and Kaiser window (Lai 2004). All these windows are described as

The University of Nottingham

moderate windows used in narrowband applications. When dealing with transforms, the properties can have infinite values converting from the time domain to the frequency domain. This is due to such mathematical functions like Fourier Transforms looking for every frequency component present between a lower and upper specified sampling rate bandwidth. Some of these components can be approximated and even so small can be ignored. From using the window function the impulse response is truncated to a finite duration and therefore no unnecessary computation is made and good approximations relating to the frequency bands exist. For a successful window function; the narrower the transition bandwidth across the raw extracted signal the larger the stop band attenuation. The better the resolution between the time domain. The most suitable window functions are the Hamming and Kaiser (Cohen 1995) window functions when compared with others. The processing gain is where the signal to noise ratio (SNR) is improved from uniformly distributing the noise signal across the whole signal, and at the same time focusing the sinusoids energy around one frequency.

For digital filters there are some parameters that need to be calculated to ensure the filter operates to correct specifications in stopping defined frequencies and allowing other defined frequencies to pass through. The Butterworth filter is used as an example for parameter selection of a digital filter.

5.3.1 Filter parameter selection for DSP

This section looks at how a Butterworth filter is used to ensure low frequencies pass through and high frequencies are stopped. For the correct filter response, some filter

parameters need to be calculated such as the order and quality coefficients. Figure 5.2 displays the design of the filter and magnitude response using the Matlab digital signal processing toolbox®. For AE signals, bandpass filters are used to ensure the low and high frequencies are removed giving a resultant quality signal in the middle of these filters. The midpoint between the pass-band and stopband limit frequencies is the midpoint f_c and known as the ideal cut off frequency. The filter equation breakdown can be referenced from (Cohen 1995).

The following filter design uses equations given by Cohen (Cohen 1995) to calculate the order of a Butterworth filter which is used to filter out grinding force.
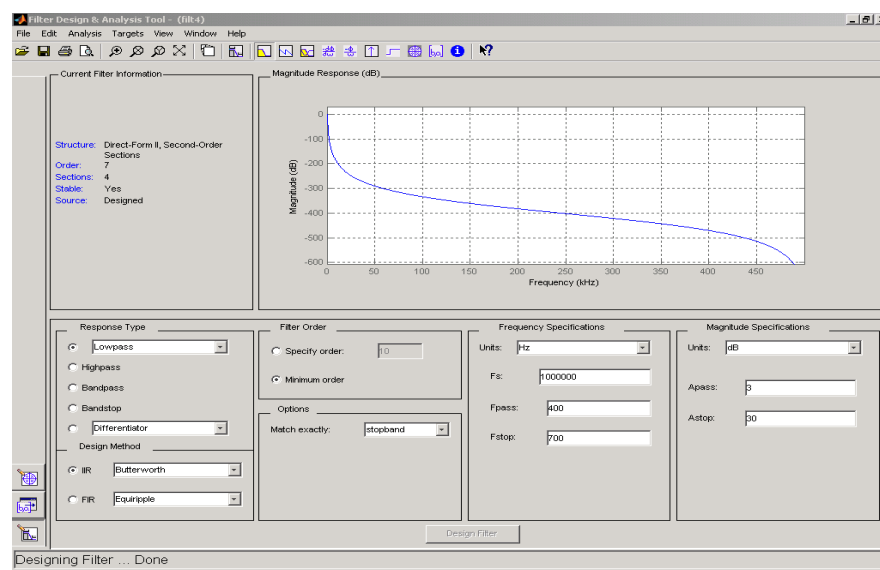
Figure 5.2 displays the design of a Butterworth filter

The design parameters of Figure 5.2 correlate with the previously discussed equations. For instance; f_{pass} = 400 Hz, f_{stop} = 700 Hz, K_s= 30dB, K_p. Using the above equations Ω=1.63, M=31.68, n $\geq$ 7.07.

The University of Nottingham

5.3.2 Filter Selection

There are many different filters available within the Matlab Signal Processing Toolbox®
ranging from FIR/IIR (Finite Impulse Response/Infinite Impulse Response) to adaptive
filters. The FIR filter takes averages from the interval window of the analysed signals
and is often described as a moving average filter. FIR filter is a non recursive filter that
is easy to design and use, in addition it has good stability characteristics. The IIR filters
have infinite duration impulse responses which is the converse to that of a FIR filter. If
the phase response is ignored, for the same magnitude response characteristics, the IIR
filter will have a lower order of operation when compared with FIR filters. Based on
Qiang's work (Liu 2004) 15 filters were tested in terms of the signal mean across the
extracted signal and standard deviation showing the fluctuation of the gained mean
signal value. The best filters were the Ellips, Chebysev I and Chebysev II filters, overall
the Chebyshev II provided most robust and consistent results. Chebyshev II bandpass
filters were used during the signal processing throughout all the grinding trial work
mentioned within this thesis. The following list displays desirable features when
designing a filter system, the filter should have:

- A specific frequency function
- A specific impulse response
- Should be causal (not affect the system)
- Should be stable
- Should be localised
- Low computational complexity

- The filter should be implemented in a particular hardware or software.

- High signal to noise ratio

The filter can be designed to have different frequency characteristics, such as a low pass filter only allows low frequency components to pass through; the converse is true for a high pass filter. The band stop filter is where the filter does not allow a certain bandwidth of frequencies to pass through, the converse to this is a band stop filter where a certain bandwidth of frequencies are not permitted to pass through and all others other than that defined pass through. An important parameter is the frequency response of a filter. This is determined by the steepness and complexity observed from the response curve. This observation gives a clear indication of the chosen feasibility and filter order for a designed filter. For instance, a first order filter has a single frequency-dependent component and the slope of the frequency response is limited to 6dB per octave thus not sufficient for most general filtering requirements. With steeper slopes within the frequency response the filter needs to be of a higher order.

5.4 Frequency Domain

The background to Fourier transformation is a mathematical one based on Fourier series analysis of continuous and infinite functions (detailed in most higher-level mathematics textbooks (Stephenson 1988)). In practice, data is sampled in time and thus digitised. To achieve a Fourier transformation for this case, a Discrete Fourier Transform (DFT) is required. This is usually achieved using a Fast Fourier Transform (FFT) which has a greatly reduced number of arithmetic operations compared with a direct DFT method (Cohen 1995; Oppenheim and Schafer 1999). The FFT is particularly important for

The University of Nottingham

condition monitoring and therefore this section provides detail on its practical application.

5.4.1 Converting from the Time to Frequency Domain

With Fast Fourier Transforms (FFT) however, it is possible to get the frequency band components. The FFT estimates the frequency components as well as their associated amplitudes based on the trigonometric family functions (Smith 1997). FFTs have been used for condition monitoring in the past, however they do not give any time information of when the event occurred. This is fundamental to the very nature of spontaneously released transient elastic energy (Acoustic Emission) when materials undergo deformation or fracture or, a combination of both. FFT calculates the frequency average over the duration of the extracted signal and can be applied to a non-stationary AE signal, however, the results do not adequately describe the transient features in terms of frequency resolution (Li and Wu 2000), instead, FFT has to be used with a another technique that produces both the time and frequency band information.

With this weakness in mind there was a need for FFT to be represented in the time domain and this paved the way for STFT.

5.5   Time-Frequency Domain

The AE wave is described as a non-stationary stochastic signal. Traditionally AE signals obtained from material tests were; Root-Mean-Squared (RMS) level detection, event-count, energy distributions, amplitude and the powers of dominate frequency bands. These techniques were broadly used and applied to general non destructive condition

monitoring (tests based on events that were recorded in days instead of seconds). With the grinding AE phenomenon producing both short-high frequency and long-low frequency components, there is a need to have a continual wave-stream extraction facility, as opposed to an event driven one based on a threshold which triggers the system into action. The continual wave stream was required as short burst high frequencies can be missed with the event driven method. Fast Fourier Transforms (FFT) already introduced in the last section have been used for condition monitoring in the past, this was for estimating the frequency band components based on a particular extraction moment in time. FFTs provide amplitudes based on the trigonometric family functions (Smith 1997). FFTs however, have a drawback; they do not have any time information of when the event occurred, which is fundamental to the very nature of spontaneously released transient elastic energy. This is where materials undergo deformation or fracture. It is because of this no time component that they are hard to distinguish. FFT calculates the frequency average over the duration of the extracted signal and can be applied to a non-stationary AE signal, however, the results do not adequately describe the transient features in terms of frequency resolution (Li and Wu 2000).

Another technique that emerged from the family of FFT is that of STFT. This technique is similar to FFT however it addresses the issue of considering time as well as the frequencies and their associated amplitudes. The STFT gets round the problem of representing when a particular phenomenon occurred, however, it still does not get round the problem of resolution which is needed for accurately distinguishing SG

The University of Nottingham

features. That said, and with the extra dimension of time, the STFT still offers a good solution when required to characterise an AE signal. If a suitable window function (such as Hamming or Kasier window) is chosen to fully represent the non-stationary stochastic signal then STFT can provide quick and accurate results.

Wavelet Transforms (WT), a family of orthogonal basis functions, can overcome some of the limitations posed by both FFT and STFT. This is based on WT representing non-stationary signals through scaled time-frequency analysis. WT provides both an approximate and a detailed representation of scaled time-frequency analysis. The scaled localised time-frequency analysis characterises AE signals in terms of high frequency burst of short duration and low frequency components of longer duration (Cohen 1993; Cohen 1996; Li and Wu 2000; Staszewski and Holford 2001).

There is a trade-off between choosing WT or STFT, this is due to the requirement of the signal analysis; if the signal is clear, with clear energy bands, STFT can be applied with a suitable window function parameterised for the application at hand. WT provides a higher resolution however; it can suffer in terms of computational complexity. Although WT is perhaps the best (DSP Time-Frequency) technique this is based on its ability to have a high resolution at any incremental point along the original time-frequency extracted signal (Chui 1992). The Fourier Transform for instance gives the frequency components of a non-stationary signal however it does not give the event information in the time domain. The STFT is somewhat similar to the WT although there are subtle differences in why WT are chosen over STFT. The STFT works in a similar manner to

The University of Nottingham

WT in that the signal is broken up into frequency bands with integer powers of two ($N=2^p$). For example; a 1000 Hz signal can be broken up into two frequency bandwidths of 0-500 Hz and 500-1000 Hz respectively. This however is not a good frequency resolution and instead the resolution window can go down to very small frequency components. For instance, the next level down from the last example would have the window function set to 250 Hz which would produce a further 4 resultant frequency bands of 0-250 Hz, 250-500 Hz, 500 – 750 Hz and 750 – 1000 Hz thus giving greater frequency resolution for each respective time interval. This would carry on to 8 resultant frequency bands if the STFT window was set 125 Hz and so on. The difference between STFT and WT is that the STFT window represents a specific frequency band with respect to time. The user however cannot get an exact time reading at a specific point of phenomenon, instead it's an approximation. The WT on the other hand breaks the signal up into smaller frequency components with high-short and low-long frequency components and the user is more able to read the exact point of phenomenon start or finish. Therefore the WT resolution is much better than that of STFT. That said, if an optimized window is found (not too small for reduction of frequency resolution and not too big for reduction of time resolution) good STFT results can still be afforded and within a quicker time frame than that of WT.

The following equations display the differences between FT, STFT and WTs techniques (Strang and Nguyen 1996):

$$X(f) = \int_{-\infty}^{\infty} x(t) \bullet e^{-2j\pi ft} dt \qquad (5.1)$$

where f is the frequency, t is the time, x denotes the signal under transform where $x(t)$ is the signal in the time domain and $X(f)$ is the signal in the frequency domain (FT of $x(t)$). Even though the transform is from $\pm \infty$ the FT computed function will sum up all the Sine waves that are within a particular time step and output a finite value. Hence the function name; Fast Fourier Transform. Next the STFT will be introduced (Strang and Nguyen 1996):

$$STFT_x^{(\omega)}(t', f) = \int_{-\infty}^{\infty} [x(t).w*(t - t')] \bullet e^{-j\pi ft} dt \qquad (5.2)$$

As with equation (5.6), $x(t)$ is the time domain signal under transform, $w(t)$ is the main difference from equation (5.6) and is known as the window function and $*$ is the complex conjugate. Based on the increment value of t' will determine the resolution between the frequency and time domains (this is always chosen as a tradeoff between each domain). Essentially the STFT is FT multiplied by a discrete window function along the length of the original time domain signal. The WT is based on equations (5.1) and (5.2) however, the scaling variable minimizes the tradeoff resolution problem between both the time and frequency domain as seen in STFT. The WT is introduced below (Strang and Nguyen 1996):

The University of Nottingham

$$Ws[x(\tau)] = |s|^{-\frac{1}{2}} \int_{-\infty}^{\infty} x(t)\psi * \left(\frac{t - \tau}{s}\right) dt \qquad\qquad (5.3)$$

τ and s are the translation and scale parameters, respectively. $\psi(t)$ is the transforming function, and it is called the mother wavelet (* is the complex conjugate). The term mother wavelet gets its name due to two important properties of wavelet analysis, for instance, the term wavelet means a small wave. The small wave is based on the window function method of a wavelet that is of finite length and compactly supported. The wave is based on the wave motions of the sea because of its oscillatory nature. The term mother function is based around all windows using this wavelet function. Translation is the location of the window as it is shifted along the original time extracted signal. Within the equation above there is no frequency parameter as in STFT & FFT, instead there is a scale parameter which is the inverse of frequency and more in line with phenomenon occurring in nature.

Nevertheless, the acoustic waves are often mixed with other acoustic waves such as grain fracture and both mechanical and white noise. The present investigation is motivated by the expectation that AE features of SG cuts can be extracted clearly by using STFT and more accurately with WT. Investigation and classification of such waveforms provides a profound initial step in understanding and distinguishing the very fundamentals grinding interaction which can ultimately increase the effectiveness of grinding monitoring.

5.5.1 STFT Analysis

This section will look at the STFT in greater depth as this technique was predominantly used throughout the signal analysis. For Time-Frequency analysis STFT is the most widely used; this is due to its support and ease of use (Cohen 1995). This was used due to it being the least computationally demanding when compared with Wavelet Transforms (WT) and WPT. Although if considerations were made regarding the signal had a good level of signal-noise-ratio and, the STFT Kaiser Window function was chosen optimally, then the differences between the two time-frequency transform techniques would be negligible. This in-depth discussion will look at the derivation of the STFT mathematical equations, followed by examples displaying the transformation from the time to the time-frequency domain. The STFT has already been introduced in section 5.5, looking at this equation 5.7, it is possible to see that STFT is an FFT from equation 5.6 and is made for a given interval window that increments across the total extracted signal. It is also worth knowing that both FFTs and STFTs are invertible in that original signal can always be retrieved from inverting the STFT function.

Looking at the mathematic principles behind this technique, firstly the window function used by STFT is investigated. In using the STFT window the one parameter that is of paramount importance is the interval of the window function, whether it be narrow band, mid-range band or wide band, this selection dictates the resolution trade-off between both time and frequency resolution. There is another important feature that is often over looked; this is the height of window function and what scaling parameter it will use to adequately represent the signal under analysis. Thus:

$$\int_{-\infty}^{\infty} w(\tau)d\tau = 1 \tag{5.4}$$

Following on:

$$\int_{-\infty}^{\infty} w(t-\tau)d\tau = 1, \forall t$$

and:

$$x(t) = x(t)\int_{-\infty}^{\infty} w(t-\tau)d\tau = \int_{-\infty}^{\infty} x(t)w(t-\tau)a$$

Where τ is an interval amount defining a constant window across the single w(t), $d\tau$ is the change in the interval value.

To analyse the signal at time τ, the emphasis is made at that time and the signal is suppressed at all other times. To do this the signal is multiplied by a window function w(τ), centered at τ, to produce the modified signal:

$$x(t) = x(t)w(t-\tau) \tag{5.5}$$

This modified signal is now a function of two times, the fixed time of interest τ and the running time t. The window function is chosen to leave the signal around time τ unaltered and suppress it with respect to times that are distant to τ. Thus:

$$x_t(t) \sim \begin{cases} x(\tau) \\ 0 \end{cases} \quad \text{for t near } \tau \tag{5.6}$$

The University of
Nottingham

The modified signal now refers to a time around τ, equation 5.12 displays the Fourier transform reflecting the frequency around that time, thus:

$$x_t(w) = \frac{1}{\sqrt{2\pi}} \int e^{-jtw\tau} x_t(t) dt$$

(5.7)

$$x_t(w) = \frac{1}{\sqrt{2\pi}} \int e^{-jtw\tau} x_t(t) w(t - \tau) dt$$

(5.8)

Equation 5.13 displays how the FFT (Equation 5.7) is multiplied by the window function to give the short time frequency analysis at around time τ. From this STFT mathematical expression it is easy to the get the spectrogram of the signal which was used in the Matlab® DSP Toolbox, see equation 5.9.

$$P_{SP}(\tau, w) = |x_t(w)|^2 = \left| \frac{1}{\sqrt{2\pi}} \int e^{-jwt} x(t) w(t - \tau) dt \right|^2$$

(5.9)

All dependent on what interval the window is decided on is whether the STFT is more favourable towards frequency or time analysis. The spectrogram is used to see the frequency bands occurring at specific time intervals across the extracted time domain signal. To go from one segment to the next segment, the window interval is incremented at optimised constant amounts thus; $w(t - \tau_0)$, $w(t - 2\tau_0)$…$w(t - n\tau_0)$ when $n\tau = t-\tau_0$. The FFT segments can then be used to describe phenomenon/event occurring at a specific time in space. For instance, a range of FFT from STFT would be used to signify cutting,

The University of Nottingham

ploughing or rubbing (this was due to measurements for the three phenomenon's have longer duration than the window lengths chosen at 1024 pts). Equation 5.9 however used the Discrete Fast Fourier transform thus equation 5.8 transfers into equation 5.10 and equation 5.9 transfers into equation 5.11:

$$x_{m,n}(w) = \int dw . x_t(t) . w(t - n\tau_0) e^{-imw_0 t} \tag{5.10}$$

$$P_{SP}(m,n) = \left| x_t(w) \right|^2 = \left| dw . x_t(t) . w(t - n\tau_0) e^{-imw_0 t} \right|^2 \tag{5.11}$$

Where w is compactly supported and from equation 5.9, τ and w are assigned regular spaced values; $\tau = nt_0$ and $w = mw_0$, where m, n range over the extracted signal.

5.5.2 Wavelet Analysis

Wavelets are considered more superior than STFT due to its ability to decompose data into different frequency components with the resolution matched to a scale which represents the functionality of the signal extracted. It can be said that wavelet analysis is more locally supportive in terms of the wavelet functions and are localised in both space and time and, the frequency, third domain is also localised in both space and time. For noisy signals or signals that are difficult to represent (non-stationary, random signals), the orthogonal basis functions can overcome limitations posed by other time-frequency analysis techniques such as STFT. For instance, STFT uses a single set of basis functions such as the Sine and Cosine function and with Wavelet Transforms (WT) there is a very large set of possible functions. It is true therefore WT can give better access to information that is otherwise obscured in using other methods. In addition, WT uses a dynamic window function where STFT uses a static window that has been optimised

between the frequency and time resolutions. Instead of using harmonics e^{-iwt}, as that seen in FFTs, the WT uses *wavelet basis*:

$$\psi_{ab}(t) = \frac{1}{\sqrt{a}}\psi\left(\frac{t-b}{a}\right)$$

(5.12)

This is where 'a' is a scaling factor and 1/a represents the frequency (frequency bands decrease in bandwidth with respect to the different levels of WT). The *translation factor* 'b' is a time shift function and ψ(function) is known as the mother wavelet and is compactly supported. Equation 5.18 displays an equation for the continuous wavelet function where a signal of interest x(t) is converted to the time-frequency domain with a scale a and position b (Mallat 1999).

$$w_f(a,b) = \frac{1}{\sqrt{a}}\int_{-\infty}^{\infty} x(t)\psi *\left(\frac{t-b}{a}\right)dt$$

(5.13)

Where * is a complex conjugation. Both $w_f(a,b)$ and x(t) constitute a pair of wavelet transforms. X(t) can be reconstructed by the following:

$$x(t) = \frac{1}{C_\psi}\int_{-\infty}^{\infty}\int_{-\infty}^{\infty}\frac{1}{a^2} w_f(a,b)\psi\left(\frac{t-b}{a}\right)dadb$$

(5.14)

Equation 5.14 displays a good local support in terms of frequency and time domains. With a decrease in 'a' allows $\psi_{a,b}(t)$ to focus on the higher frequency components for that segment in space, thus the narrower the time window the more resolution obtained. To obtain a discrete wavelet transform, $a = a_0^q$, $b = nb_0a_0^q$ in this case with 'm' and 'n'

The University of
Nottingham

ranging the length of the extracted signal. As with the discrete STFT of equation 5.10 and equation 5.11, $a_0 > 1$, $b_0 > 0$ fixed for discrete wavelet transform which is introduced in Equation 5.15:

$$\Psi_{q,r}(t) = a_0^{-q/2} \psi(a_0^{-q} t - n b_0) \qquad (5.15)$$

Signal x(t) can then be decomposed into the form of a wavelet coefficient $C_{q,r}$:

$$C_{q,r} = \int_{-\infty}^{\infty} x(t) \Psi *_{q,r}(t) dt \qquad (5.16)$$

'cm' and 'n' now becomes a 2D time frequency map of the orginal signal x(t).

Signal x(t) can be reconstructed:

$$x(t) = C_\psi \sum_{-\infty}^{\infty} \sum_{-\infty}^{\infty} C_{q,r} \psi_{q,r}(t) \qquad (5.17)$$

Where C is an independent constant of the signal.

5.5.2.1   Wavelet Packet Transforms

WPT is very similar to WT such as that seen by the Continuous Wavelet Transforms (CWT). WPTs is a time-scale representation of a digital signal obtained using digital techniques. For instance, when using the CWT this was computed from changing the scale of the analysis window, shifting the window in time, multiplying by the signal, and iterating over all times. With respect to computing in the discrete case, filters with cut-off frequencies are used to analyse the signal at different scales. For high frequencies the signal is passed through high pass filters and for low frequencies, the signal is passed through low pass filters. WPTs has a higher resolution space to work with this is due to the increase of the scaling parameter 'q' used throughout this discussion of Wavelets.

The filters are conjugate quadrature mirror filters and used to split the frequency bandwidth into equally spaced sub-band signals otherwise known as the filtered sub-band technique (Daubechies 1992; Strang and Nguyen 1996). The break up of how many sub-bands are present depends on the chosen level of decomposition. The more detail that is required the more levels are chosen and the greater the sub-band representation. The WPT process can be compared to a binary tree in that the properties of depth 'q' and nodal branch junctions 'p' define the level of detail reached. The nodal branch junction is referenced to a space W_q^p and is indicative of an orthonormal basis $\left\{ \psi_{q+1}^{2p}(2t-n)_{n \in Z} \right\}$. By using recursive relations (Mallat 1999), Equation's 5.18 and 5.19 display the wavelet packet numerical bases used at the child nodes used in the WPT tree representation:

$$\psi_{q+1}^{2p}(t) = \sum_{n=-\infty}^{\infty} h[n] \psi_q^p (2t-n) \tag{5.18}$$

$$\psi_{q+1}^{2p+1}(t) = \sum_{n=-\infty}^{\infty} g[n] \psi_q^p (2t-n) \tag{5.19}$$

From the introduction of these two equations a short hand representation of the two orthogonal spaces can be represented this is where the signal is split by divisions of 2 from the parent node:

$$W_q^p = W_{q+1}^{2p} \oplus W_{q+1}^{2p+1} \tag{5.20}$$

For a time varying signal x(t) recursive splitting is used to produce the binary tree of different levels of detail. Looking at equations 5.21 and 5.22, the parent node is split into two orthogonal spaces through the use of the high and low frequency pass filters (see

g(n) and h(n) respectively). By dividing the parent node signal into two equally spaced sub spaces of the original signal, the two resultant signals are down sampled by an order of two respectively with one sub space occupying the mid to high-end frequencies of the original parent node signal and the other, occupying the low to mid-end frequencies.

$$x_{q+1}^{2p}(t) = \sqrt{2}\sum h(n)x_{q+1}^{2p}(2t-n) \tag{5.21}$$

$$x_{q+1}^{2p+1}(t) = \sqrt{2}\sum g(n)x_{q+1}^{2p}(2t-n) \tag{5.22}$$

Thus the expanding coefficients of h(n) and g(n) are provided below displaying the orthogonal relationship between the two filter representations:

$$h[n] = \left\langle \psi_{q+1}^{2p}(t), \psi_q^p(2t-n) \right\rangle \tag{5.23}$$

$$g[n] = \left\langle \psi_{q+1}^{2p}(t), \psi_q^p(2t-n) \right\rangle$$

Equation 5.23 is represented in the frequency domain by:

$$H\{\bullet\} = \sum_{n=-\infty}^{\infty} h(n-2t) \tag{5.24}$$

$$G\{\bullet\} = \sum_{n=-\infty}^{\infty} g(n-2t)$$

The University of Nottingham

The following equations are used to show the steps of the WPT recursive algorithm where $x_j^p(r)$ relates the pth packet with the qth resolution. Equation 5.25 is equivalent to equation 5.20.

$$x_0^1(r) = x(t) \qquad\qquad (5.25)$$
$$x_q^{2p-1}(r) = Hx_{q-1}^p(r)$$
$$x_q^{2p-1}(r) = Gx_{q-1}^p(r)$$
$$x_q^p(r) = x_q^{2p-1}(r) + x_q^{2p}(r)$$

Where $r = 1, 2, \ldots, 2^{q-p}$, $p = 1, 2, \ldots, q$ and $q = \log 2\ N$.

The sub-band coding algorithm can be seen from the tree representation of Figure 5.3 where each level node is filtered and down-sampled by a factor of 2 for example, if the original signal had 512 sample points, the spanning frequency tends from 0 to π rad/s (note with the discrete computation frequency is calculated in radians as opposed to Hz). The first decomposition level, the signal is passed through high pass and low pass filters, followed by down sampling with a factor of 2. The output of the high pass filter has 256 points (half the time resolution) with the frequency span tending from $\pi/2$ to π rad/s (double the frequency resolution). These 256 samples constitute the first level discrete WPT coefficients. For the output, from the low pass filter this also has 256 samples and spans the other half of the frequency band; frequencies from 0 to $\pi/2$ rad/s. The second level of the tree is achieved by passing the signals through further low and high pass filters. At the 2nd level the output from the 2nd level low pass filter, there is down sampling and the length of the packets here are 128 samples respectively across the level. At this level, the 4 packets make up the frequency bandwidth and signal length of the original signal at the root node. Looking at Figure 5.3 it can be seen that frequencies

The University of Nottingham

span in 4 segments across the original signal bandwidth thus; (1) 0 - π/4 (2) π/4 - π/2 (3) π/2 - 3π/4 (4) 3π/4 – π. It is true at the second level the signal has half the time resolution, but twice the frequency resolution of the first level signal.

In short, time resolution has decreased by a factor of 4, and the frequency resolution has increased by a factor of 4 compared with the original signal. This process goes on until the defined 'M' level or, when the coefficient level is so small there is no further information available. It can be said that some of the information at the M level is redundant as the AE sensor picks up a signal bandwidth range of 1 MHz and using a sampling rate of 5MHz the signal is up sampled with 1 MHz to 5 MHz useless information. By using algorithms such as best tree or best within 50 KHz to 1000 KHz is more appropriate for a more focused signal analysis.

One point to also note here WPT can be used for data compression and therefore the greater the level achieved; the less data presented to the computer although rich summary data is presented.

Mallet (Mallat 1999) expresses the inner product theorem[3] in terms of energy E_q^p for each packet displayed in equation 5.26 (refer to Figure 5.3).

$$E_q^p = \sum_{t=1}^{2^{M-q}} (x_q^p(t))^2 \qquad (5.26)$$

Then the energy for each level based on the addition of all the segments in that level are displayed in equation 5.27.

---

[3] Moyal Formula

The University of Nottingham

$$E_q = \sum_{p=1}^{2^q} E_q^p = \sum_{p=1}^{2^q} \sum_{t=1}^{2^{M-q}} (x_q^p(t))^2 \tag{5.27}$$

Where $M = \log_2 N$; $j \, \varepsilon \, [1, M]$ and N is the length of the signal. From these signals being broken up into signal energies with different frequency ranges the reconstruction then commences as the next stage. The reconstruction is made to the decomposed coefficients. The total energy is obtained from summing all the segmented frequency bands into one energy, and then normalised for further use in terms of analysis or classification.

The University of Nottingham
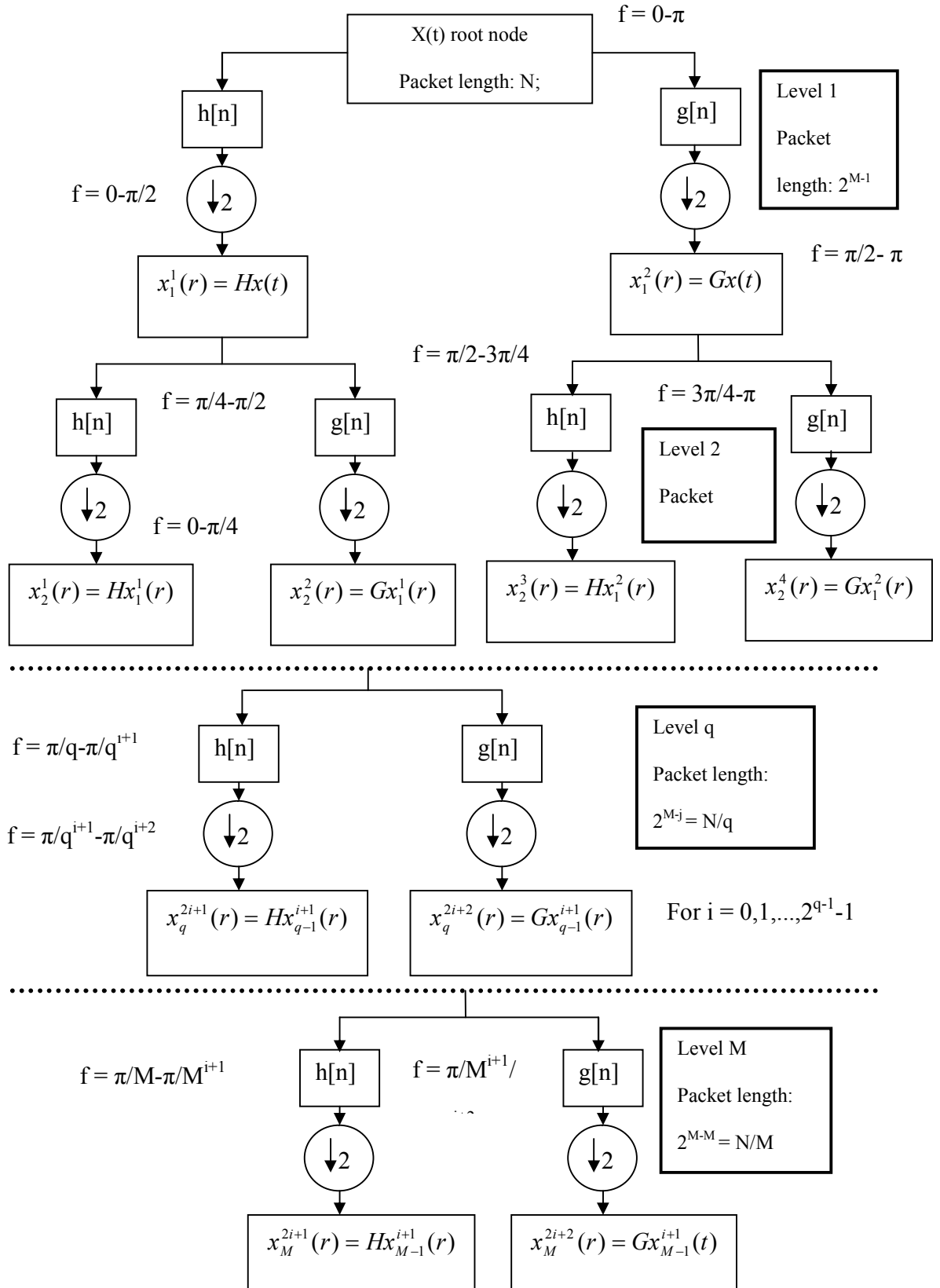
Figure 5.3 Wavelet packet decomposition tree

5.6   Signal Normalisation

For single grit analysis regarding the horizontal scratch cuts most AE signals should be normalised to a standard level to avoid misclassification. For instance, if a measured 4 μm cut existed then the decibel level for that associated AE signal would be much stronger than the decibel level of an AE gained by a 1μm cut. Here the decibel magnitude level of the AE for a 1 μm cut was taken as the basis throughout the tests. This is done by multiplying by a factor to ensure the level is in line with the 1μm cut level. This normalisation is necessary as the AE gained from ploughing with a 4μm cut has greater FFT magnitude intensities when compared with the AE gained from cutting within a 1μm cut. Based on these different intensities from measured different depth of cuts it was deemed necessary to normalise the signal to then be able to compare like with like signals.

Figure 5.4 displays raw extracted time series AE signals that have not been normalised and have been normalised respectively. Following on is the STFT representation before and after normalisation. Figure 5.4 Top left displays Hit 2 of a non AE normalised signal with a measured depth of cut of 0.25 μm. After the signal has been multiplied by a factor of 4 to bring it in line with a 1 μm cut (Bottom left) the new normalised signal is displayed at the top right of Figure 5.4. The bottom right displays the FFT vectors extracted from the STFT of Hit 2 both before normalisation and after normalisation together with the addition of a STFT vector of Hit 4. The normalised FFT magnitudes are of similar levels and can be compared without causing a problem during segregation and classification.
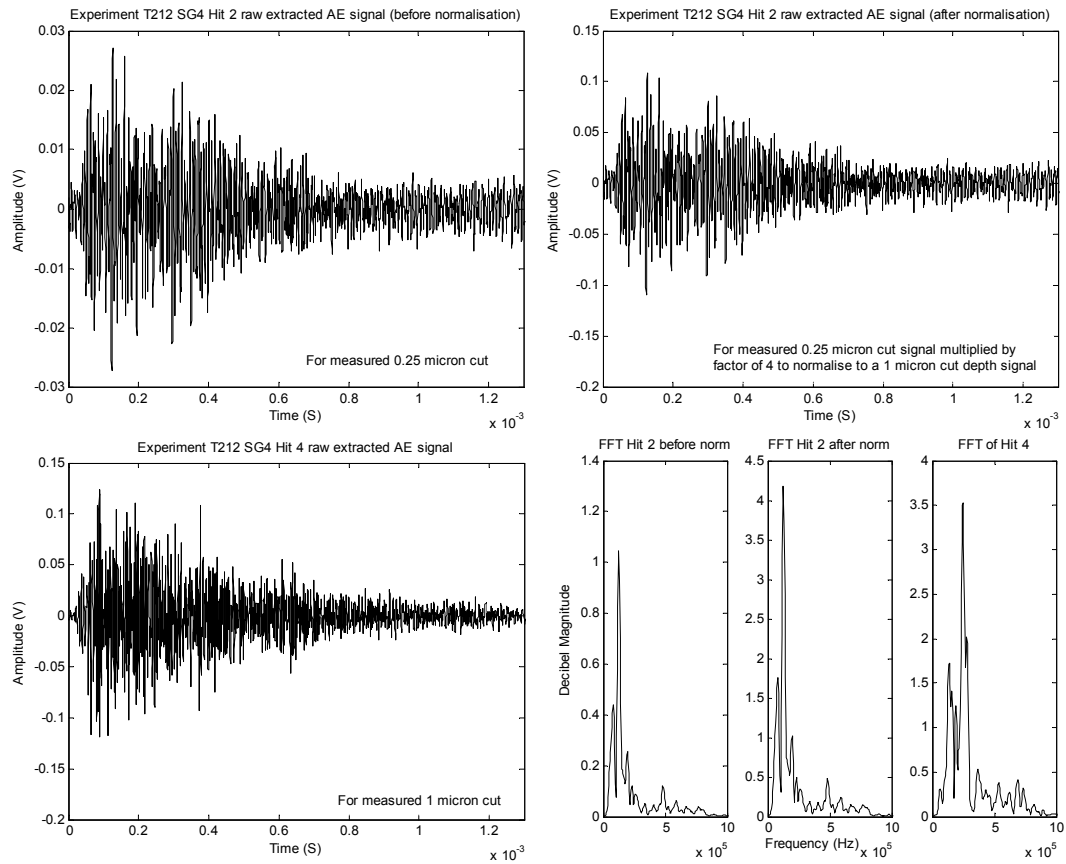
Figure 5.4 Normalisation of AE signal and cutting phenomenon FFTs after normalisation

To verify and normalise the AE extracted signals, an AE pencil lead break test (Barbezat, Brunner et al. 2004) was used to ensure the AE sensors were calibrated on a daily basis during the tests. AE Signal normalisation was only applied to plastic deformed phenomenon to ensure the segregation between cutting and ploughing phenomenon, although with the rubbing phenomenon this was not required. This was due to rubbing phenomenon having no recognisable depth of cut.

5.6 Data Reduction Techniques

For some of the grinding trials for ease of classification it was necessary to use statistical techniques in order to reduce the time varying signal to rich summary data with subtle differences to distinguish different phenomenon. For such data reduction techniques a moving window similar to that used in time-frequency analysis of STFT was used to apply the statistical measures of mean (Equation 5.28), standard deviation (Equation 5.29), Skewness (Equation 5.30) and the Kurtosis (Equation 5.31).

The origin moment of order 1 where x is the sensory signal:

$$\mu = \frac{1}{N}\sum_{i=1}^{N} x_i = \frac{1}{\omega}\int_{0}^{\omega} |x| dt \tag{5.28}$$

The centre moment of order 2: (5.29)

$$\sigma = \sqrt{\left(\frac{1}{N-1}\right)\sum_{i=1}^{N}(x_i - \mu)^2}$$

The centre moment of order 3:

$$S_k = \frac{1}{N}\frac{1}{\sigma^2}\sum_{i=1}^{N}(x_i - \mu)^3 \tag{5.30}$$

The centre moment of order 4:

$$Kr = \frac{1}{N}\sum_{i=1}^{N}\frac{(x_i - \mu)^4}{\sigma^2} \tag{5.31}$$

Concatenated to this rich summary data the time varying signal would be summarised in terms of the 5 highest peaks and the 5 lowest troughs and their relative measures of rise time from the highest peak to the both sides of the zero norm. This information gives an

The University of Nottingham

indication of the AE burst reaction in terms of the rise and decay time after the high peak burst. This information along with the statistical information was used to obtain good results in distinguishing grinding phenomena. For some signal analysis the power (Equation 5.32) and RMS (Equation 5.33) quantities were calculated for the time varying signal and used as way to substantiate the results.

The power representation of the signal:

$$P = \frac{1}{N} \sum_{i=1}^{N} x_i^2 \tag{5.32}$$

RMS representation of the signal:

$$u_{RMS} = \sqrt{\frac{1}{N} \sum_{i=1}^{n} x_i^2} = \frac{1}{\sqrt{N}} \left(\sum_{i=1}^{n} x_i^2 \right)^{\frac{1}{2}} \tag{5.33}$$

5.7   Summary and Gaps

This chapter has introduced and discussed in great depth the Digital Signal Processing (DSP) techniques used during the work of this thesis. DSP is considered one of the most important aspects of process monitoring. This is due to a lot of information within the signal possessing being that of redundant information; this is in terms of low continuous frequencies such as that experienced by mechanical machine noise. In addition there is high-end frequency components also experienced from magnetic interference such as white noise. Through using IIR filters such as Chebyshev II filters it is possible to filter out those identified noise components. The noise signals were obtained from a free

moving spindle with no other mechanical interaction. For the single grit scratch tests however no coolant was used and therefore was not considered. For grinding pass tests, coolant was used and both the spindle and coolant noise components had to be removed from the signals as a first priority. This chapter has looked at frequency analysis and more specifically into time-frequency analysis utilising the STFT and WT functions. By transforming the time extracted signals into the time-frequency domain it has been possible to identify significant grinding phenomenon; such as cutting, ploughing and rubbing. In addition with grinding pass work, it has been possible to identify grinding anomalies such as workpiece chattering and burn. AE extracted signals coupled with DSP techniques have proved to be a very successful strategy in trying to obtain optimised efficient grinding techniques. Not to mention some of this work can be directly transferred into nano/micro-machining work as most of these measurements were carried out at this level. The gaps that have been covered in this thesis are as follows:

- Using STFT to identify cutting, ploughing and rubbing AE footprint signatures.

- Using STFT and WT to segregate macro grinding anomalies such as burn and chatter.

- An AE to force calibration method such as the pencil break calibration method coupled to a force measurement could be used as an initial material standard practice.

- Using WT technique to identify and verify the grinding phenomenon, namely cutting, ploughing and rubbing AE footprint signatures.

- Signal normalisation with measured cut depth to ensure the accurate classification between cutting and ploughing AE footprint signatures.

- Data reduction techniques supplying rich summarised accurate data to a classifier system in terms of anomalies distinction.

Chapter 6 Classifier Technologies

6.1 Introduction to Classifiers

This chapter is primarily concerned with the classification of different grinding phenomena used in process monitoring of grinding technologies. Specifically, the classification of single grit scratch phenomena segregating the grinding mechanics of cutting, ploughing and rubbing through AE extracted signal analysis. There are many facets to pattern recognition. The classifier can be a general purpose classifier, for segregating the data it is presented with or, the classifier can have add on functionality to pre-prepare classification in terms of finding significant similarities and dissimilarities between similar or non similar data presented to the classifier. In addition to a pre-processing add on functionality there is also post processor add-on functionality, this is where the classifier outputs need to be converted to the real meaningful world from the computed classifier representation. Such pre-processing layers to a classifier are data normalisation; to convert the data into statistical variance and mean combinations throughout the data set. Or the data can be reduced from the 'curse of dimensionality' to more summary rich data through the use of Principle Component Analysis (PCA). This is where the principle components are rank listed in terms of the greatest significance first and the least significant at the end. There is however other information reduction pre processors such as; Independent Component Analysis (ICA) technique which are more advanced than PCA and Kernel Support Vector Machines (k-SVM) information reduction pre-processors. These provide excellent summary features to a classifier. ICA uses blind separation and is not sensitive to outliers which can promote the noise

The University of Nottingham

elements instead of the rich signal elements. Post processing techniques such as the inverse statistical mean and variance measures need to be applied to the output to then convert back to the real world or even the use of fuzzy rules to convert a range of outputs giving different intensities to one crisp value. The next section discusses pattern recognition and its techniques and technologies.

6.2   Pattern Recognition

To understand what pattern recognition is two definitions are introduced; Friedman discusses (Friedman and Kandel 1999):

> "Any pattern which can be classified in some categories must possess a
>
> number of features and the so-called pattern recognition is to distinguish
>
> these different patterns (Friedman and Kandel 1999)"

The American Psychological Association dictionary (APA 2007) gives the following definition of pattern recognition:

> "Pattern recognition aims to classify data (patterns) based on either a
>
> prior knowledge or on statistical information extracted from the patterns.
>
> The patterns to be classified are usually groups of measurements or
>
> observations, defining points in an appropriate multidimensional space."

It also discusses a complete pattern recognition system which consists of sensory devices that extract information, in terms of measurements or observations that are to be

classified or described. The extraction process is the mechanism of feature extraction that converts the raw analogue signal data or observation into numeric or symbolic meaningful information. The classifier is the system that provides the action of classifying or describing the observations that relate to the extracted features.

The classification techniques can be wide and varied both supervised and unsupervised techniques. If the classifier incorporates knowledge regarding the closing error at each stage this is referred to as supervised training. Training methods that rely purely on inherent distributions within the training set are referred to as unsupervised techniques. There are many different types of classifier concepts such as; Knowledge Based Systems (KBS), Data Mining and Data Warehousing (DM and DW), Knowledge Discovery in Database (KDD), Machine Learning (ML), statistical processing and probability networks to mention a few. Machine Learning techniques are perhaps the most common types of classifiers and there are many techniques within this facet of classifier technology namely; Support Vector Machines (SVM), Artificial Neural Networks (ANN), Genetic Algorithms (GA), Genetic Programming (GP), Clustering (Hard and soft clustering methods such as K-means and Fuzzy-c clustering respectively), Simulated Annealing (SA), Reinforcement Learning (RL), Liquid State Machines (LSM), particle swarm and, Chaos and Maximum Entropy (ME) (Mitra and Pal 2002).

The two core classification techniques that were used to classify these different types of data are; Neural Networks with back-propagation training algorithms and Fuzzy-c clustering with Genetic Algorithm (GA) optimisation. Artificial Neural Networks

(ANN) are statistical computational structures that are loosely modelled on brain tissue. These simple processing units are connected together and information about a problem is processed to produce a result, such as detection probability. This type of ANN is based on supervised training where the output is based on the learning of the presented training data. On the other hand both GA and Fuzzy-c clustering belong to the unsupervised training algorithms where rules are achieved from the presented data. In this case the presented data consists of both the training and test data vectors, and classification occurs for both training and test data. As the training data is already known with prior information the test data can be checked against which cluster centre data points they have already been assigned to.

6.3 Advantages and Disadvantages of Chosen Classifiers

There are advantages as well as disadvantages associated with GAs, ANNs and Fuzzy c-clustering and these should be observed when using the algorithms for classification purposes.

6.3.1 Fuzzy-c Clustering

Some of the problems faced in fuzzy-c clustering are where parameters (such as the 'b' term in equation) within the algorithm tend towards 1 or infinity. This is where the classifier becomes a hard clustering technique partitioning the clusters based on absolute similarities and a classifier that is too fuzzy and has very low values of similarity respectively. The hard partitioning is where the attributes are classed as either 1 or 0 in terms of similarity and not in between values. For instance, this is not taking into consideration boundary classification points, where the points can have attributes on

The University of Nottingham

both sides with different intensities. With total fuzzification, the similarities are very low and this has a major impact on classification where there are many cluster centres to many data points with little similarities, and therefore little classification. The trade-off here is to use the algorithm 'b' term value to 2 in that it's in-between hard partitioning and total fuzzification algorithm. With the support of GAs being used in concert with the fuzzy-c clustering algorithm it is possible to search for the fittest cluster paradigm(s). With both the GA and fuzzy-c attributes taken into consideration, fuzzy-c clustering with GA optimisation is an extremely powerful and accurate technique when classifying the data of interest. More will be discussed about this during the latter part of this chapter. An introduction to GAs is discussed next.

6.3.1.1   Genetic Algorithms

The GA tends towards a more random search in the beginning of execution, with the fitness however, the measure or rule constraints the search towards that objective goal. There are problems with speciality in obtaining the fittest and most efficient search path during the population generation. During the early part of the twentieth century, Sewell Wright (Wright 1932a; Wright 1932b) attempted to characterise the space of genetic possibilities as an 'adaptive landscape' and drew attention to the local optima that it must contain. For organisms to have evolved towards higher 'peaks', he argued, would require the traversal of 'valleys' of lower fitness which was possible because of the presence of multiple isolated populations that exchanged material periodically. Such research in genetics noted this behaviour as the 'Shifting Balance Theory' (SBT) and through genetic drift, an isolated population ('deme') could experience a temporary

reduction in fitness that would not be possible in a large pervasive population. This might then enable the population to traverse a region of the 'adaptive landscape' that would lead to an even higher peak, and having done so, it would increase in size – enabling genes to eventually pass to neighbouring demes. Like with most classification algorithms there is a trade-off here to be observed; this is between *isolation* and *interaction* this is articulated by Hartl and Clark (Hartl and Clark 1997):

> "…While migration between demes is necessary, neighbouring demes must be sufficiently isolated for genetic differentiation to occur, but sufficiently connected for favourable gene combinations to spread."

This suggests that the GA should try to maintain an evolutionary process. However to ensure it records certain material along the generations it needs to encourage lower fitness in certain runs, moreover it gains a better optimisation at the end of the specified generations. This particular problem is also seen in simple GA realisations where the solution space tends towards local optima instead of the global optimum and it's therefore very difficult for the GA to bounce out of the local optima into more global optima orientated surroundings. There is another important aspect of the SBT that has not had a great deal of attention in the field of evolutionary algorithms – the impact of a diverse environment, or what Wright calls 'ecological opportunity'. This is neatly summarised by Martin et al. (Back, Fogel et al. 2000):

> "…to follow the fundamental analogy, the island model should have differing

The University of Nottingham

fitness functions at the various subpopulations…we are not aware of any

systems that have made use of this facet…"

This suggests that the diversity of migration in nature has a greater significance than simply the wider propagation of favourable genes that have arisen in a single deme. Therefore, the evolutionary algorithm needs to copy both winning gene material and even a low fitness gene material. That said, with human evolution we evolved from genetically simpler ancestors. In addition to gene duplication being copied into the off-spring more than once (Carroll 1995; Stanley, Keller et al. 1998; Force, Lynch et al. 1999; Martin 1999; Back, Fogel et al. 2000) to ensure more advanced evolution, there is also the competing or co-evolving of several chromosomes with multiple GA realisations. These are some of the problems faced with evolutionary algorithms and specifically GAs. The GA used in this classification process was fit for purpose in optimising the Fuzzy-c clustering paradigm, even though this is a novel approach to fuzzy clustering, it can be further improved to ensure more advanced optimisation. In addition, such advanced algorithms can be used to provide a generic classifier in classifying many different grinding phenomena; be that from single grit scratches, to more abusive machining in monitoring grinding passes. Thus the classifier would be able to intelligently recognise hierarchical data (see Appendix A.25 for GA and A.26 for Fuzzy-c clustering algorithms).

The University of Nottingham

6.3.2 Neural Network

Neural Networks also possess similar problems to that found in GAs where the neural network can get stuck in local optima. This is where the neural network weights start off at a particular area of the solution space and if not directed intelligently with advanced algorithms, they can fall into a local minimum which is undesirable as the network needs to search for the global minimum. There are provisions within Artificial Neural Networks (ANN) (Bishop 1995; Haykin 1999) where the momentum can be set to 1 this ensures the neural network weights tends towards the nearest minimum valley of the search space in which it was started from. If the momentum tends towards 0.5 or lower the ANN training algorithm becomes more random based with many jumps occurring during training. Although the solution space gets a good overall picture around the information space it does not search for the global optimum as the algorithm has fewer tendencies to stay in gradient descent for the required time to find the optimum value within the searching the surrounding valleys. The best value used in the classification process tends between 0.8 and 0.9 giving both gradient descent as well as a random type jumping traits which is experienced in random search algorithms such as simulated annealing. In addition, there is a trade-off between sufficiently training the ANN and overtraining the ANN thus over fitting the data. If the data is over trained it over-fits the data hindering flexibility and it's much harder to predict the correct output of presented unseen data. Both these disadvantages are taken into consideration and provisions are made to ensure the network segregates the data to highest accuracy rates possible. In addition, the representation of the ANN provides a graphical linear plot of presented unseen data which provides a powerful picture to the observer.

The University of Nottingham

6.4 Single Grit scratch and grinding anomaly classifiers

Elastic waves such as that emitted by Acoustic Emission (AE) can be used for monitoring many machining processes and/or material non-destruction tests (Webster, Marinescu et al. 1994; Chen and Xue 1999; Coman and Marinescu 1999; Holford 2000; Liu, Chen et al. 2005). Once the raw extracted AE has been transformed into the time-frequency domain it can then be presented to the classifier. Here the work looks at the single grit (SG) scratch classification of cutting, rubbing and ploughing using two classifiers: ANN and Fuzzy-c Clustering/GA. The characteristics of cutting, ploughing and rubbing through both material profile measurements and DSP of AE extracted signals were discussed in Chapters 3, 4 and 5 respectively. It was found in the Chapter 5 that the STFT of an AE signal can represent different characteristics of cutting, ploughing and rubbing in grinding, which may be used as input parameters for the classification. The classification of the three phenomena is of particular importance to the fundamental understanding of grinding mechanics. From the accurate classification of cutting, ploughing and rubbing for SG tests it was then possible to classify $1\mu m$ and $0.1mm$ grinding wheel cuts in terms of the three phenomena. In addition, the Neural Network was used to distinguish grinding pass anomalies such as burn and chatter with the associated results discussed in chapter 7. The classification process is essentially the same however techniques such as reduction techniques mentioned in Chapter 5 were used to reduce the 'curse of dimensionality,' although the process of applying the processed signals is essentially the same as that used to classify single grit scratch cuts.

6.4.1 Neural networks for classification of cutting, ploughing and rubbing in grinding

Neural Networks have existed for over 50 years now, however in recent years an explosion of popularity has surrounded the research and development of neural computing methods. This is mainly due to recent advances in computer processing and storage capacity. A large number of researchers have reported the application of using ANN models for the classification of phenomena of interest when applied to tool condition monitoring (Sick 2002; Ozel and Karpat 2005; Karpat and Ozel 2006; Karpat and Ozel 2006). A feed-forward neural network model was used with the back-propagation learning strategy to provide the segregation of data (Rumelhart, Hinton et al. 1986). Commonly ANNs are used for pattern recognition in image analysis or sound waves of signal analysis. The ANN consists of a complex interconnection of units which are otherwise known as nodes or neurons. The general layout for a ANN consists of a set of neuron layers connected together through complex connections; this layout and features is known as the network architecture.

A two-layer ANN model can map the basic logic functions of OR, AND, and NOT however, a hidden layer is required when mapping non-linear functions such as that of exclusive-OR or the much more complex functions such as the data presented by STFT and WPT signal processing techniques. This type of data is not only non-linear but also n-dimensional. The basic logic function network classifiers use a linear data separation approach. With the separation of much larger data sets there is need for a more dynamic

learning system that takes all the information into consideration and maps the data in both parallel and gradient descent segregation, such as that seen by the back-propagation feed-forward networks (McCulloch and Pitts 1943).

Original Neural Networks were inspired by the human brain; they are based on crude mathematical and biological models of the human brain. A network is constructed from connections and neurons which simulate the function of biological neurons. The networks that exist today do not bare much resemblance to the human brain. Modern networks generally consist of layers of neurones connected together with a complex network of connections.

The next section looks at the ANN type used in this research this is in terms of either supervised or unsupervised networks and their respective different training regimes.

6.4.2 ANNs for non-linear problems in grinding monitoring

This section looks at the Multi-Layer Perceptron (MLP) with the back-propagation learning rule. This was the chosen ANN system used for classifying both single grit scratch tests and grinding pass anomaly detection. Such a system was chosen as it is simple to use and has been used in many research scenarios giving good confidence as a robust classifier. As mentioned in Section 6.3.3, ANN suffers with n-dimensional problems where they search in the local minima space instead of the global minima space. Bearing these constraints in mind if the data if sufficiently processed into good distinguishing classes of phenomenon, this ANN strategy is fit for purpose and provides intuitive graphical outputs.

A Multi-layer Perceptron (MLP) utilising the back-propagation learning rule is presented in Figure 6.1 for illustration purposes.
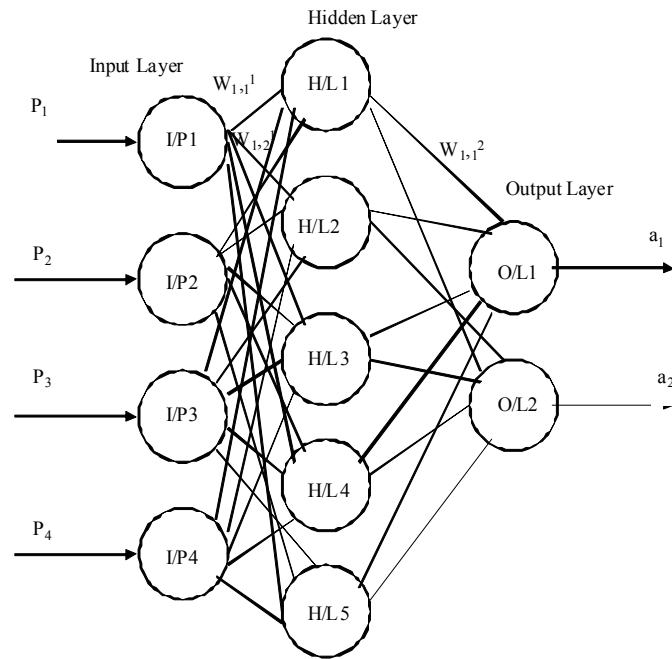
Figure 6.1 A 4 input ANN with one hidden layer.

As displayed in Figure 6.1 each of the inputs P_1 to P_4 are multiplied by a changing weight function and are associated to a target vector, in this example a_1 to a_2 respectively. This is called the associations of input-output pairs and provides the supervised training data. Test and verification data sets have both data that has been seen by the network in training (supervised) and data that has not been seen (testing the generalisation of the network).

Each Neuron has a summation function which sums up the weighted (for example $w_{1,1}{}^{1}$ and $w_{1,2}{}^{1}$ to $w_{n,n}{}^{2}$ reference to Figure 6.1) and input bias (bias input variable) connections. The transfer function (for non-linear problems a differential transfer function; such as Tan-sigmoid is used) is required to map the non-linear input-output relations these are obtained for each neuron and updated in an iterative fashion towards the desired target set. Back-propagation is so called as the weights are updated from the error between the actual output and the desired output. In short, the learning occurs from the back of the network to the front. This method segregates the different classes based on the supervised training data given to the ANN. The summation of weights and bias values are multiplied by a differential transfer function to give a neuron output.

The summation of weights and bias values are multiplied by a differential transfer function to give a neuron output. The differential and linear transfer functions used in network are displayed in Figure 6.2.

Tan-Sigmoid Transfer Function   Pure-linear Transfer Function
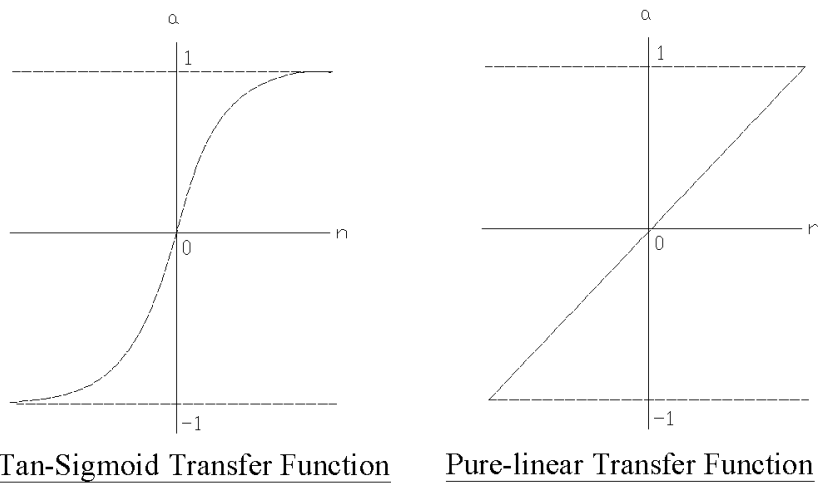
Figure 6.2 displays the two transfer functions used in the multi-layer ANN

Table 6.1 samples vs. features

	Features					
Samples	L_1	L_2	…	L_i	…	L_n
P$_1$	p_{11}	p_{12}	…	p_{1j}	…	p_{1n}
P$_2$	p_{21}	p_{22}	…	p_{2j}	…	p_{2n}
…	…	…	…	…	…	…
P$_j$	p_{i1}	p_{i2}	…	p_{ij}	…	p_{in}
…	…	…	…	…	…	…
P$_m$	p_{m1}	p_{m2}	…	p_{mj}	…	p_{mn}

Reference Table 6.1, let $\vec{P} = \left\{ \vec{P}_1, \vec{P}_2, ..., \vec{P}_i, ..., \vec{P}_m, \right\}, \vec{P} \subset L$, where

$\vec{P}_i = (p_{i1}, p_{i2}, ..., p_{in}) \in L$ is a feature vector and p_{ij} is the ith feature of individual phenomenon signal sample P_i. From P_1 to P_m is the total number of samples. Note for each signal sample there are features (variables) from L_1 to L_n. These samples with their respective features are realised in a matrix form ready for input to the ANN. Normalisation of the data was not used for the ANN presentation as this suppressed certain salient features used to signify some features over less significant features. Equation 6.1 displays what was presented to ANN for training purposes:

(6.1)

$$P(m \times n) = \begin{bmatrix} p_{11}, p_{12}, ..., p_{1j}, ..., p_{1n} \\ p_{21}, p_{22}, ..., p_{2j}, ..., p_{2n} \\ \vdots \qquad\qquad \vdots \\ p_{i1}, p_{i2}, ..., p_{ij}, ..., p_{in} \\ \vdots \qquad\qquad \vdots \\ p_{m1}, p_{m2}, ..., p_{mj}, ..., p_{mn} \end{bmatrix}$$

$$T(m) = \left[t_1, t_2, ..., t_i, ..., t_m \right]$$

Where T(m) is the single dimension target vector(s) corresponding to each individual sample, this class (target value) should be output when the samples are input into the network as a test set.

The University of Nottingham

To ensure the ANN had a clear indication of the minimum and maximum values input from the matrix P, a 'min_max' function would be applied to the matrix P to give a two dimensional column matrix of min and max values see Equation 6.2.

$$P(\text{min\_max}) = \begin{bmatrix} p_{1\min}, p_{1\max} \\ p_{2\min}, p_{2\max} \\ \vdots \qquad \vdots \\ p_{j\min}, p_{j\max} \\ \vdots \qquad \vdots \\ p_{m\min}, p_{m\max} \end{bmatrix} \tag{6.2}$$

The output of each neuron is a function of its inputs. Specifically, output of the jth neuron is described by the following equations:

$$U_j = \sum (Pi * w_{ij}) \tag{6.3}$$

$$a_i = F(U_j + t_j) \tag{6.4}$$

For every neuron, 'j,' in a layer, each of the 'I' inputs, P_i to that layer is multiplied by a previously established weight, w_{ij}. These are all summed together, resulting in the internal value of the operation, U_j. This value is then biased by a previously established threshold value t_j, and sent through an activation function, F (Sigmoid non-linear input and hidden layer and Linear at the output layer) giving the ANN output; a_i. Equation (6.5) describes the output error obtained from each neuron.

$$ME = \frac{1}{\Omega} \sum_{i=1}^{\Omega} (t_i - a_i)^2 \tag{6.5}$$

Where ME is the mean squared error, a_i (refers to a_1 and a_2 in the example illustrated by Figure 6.2) is the output of the network corresponding to i^{th} input P_1 to P_4. The error

The University of Nottingham

term of network is given from $(t_i - a_i)$ where t_i is the target vector or the desired value for given input vectors P_1 to P_4. The error function can be applied to the ANN in a batch training fashion at the end of data presentation or, sequentially after each input-output pair.

For the back-propagation algorithm the weight and bias update equations are as follows:

$$\Delta w_{ij}^k = -\alpha \frac{\partial ME}{\partial w_{ij}^k} \qquad (6.6)$$

$$\Delta b_i^k = -\alpha \frac{\partial ME}{\partial b_i^k} \qquad (6.7)$$

where α is the learning rate, which has a trade-off in value to ensure it is small enough to gain a true convergence but large enough to separate the data space in adequate time. Equations 6.6 and 6.7 are iteratively changed across the network along with other functions to provide learning sensitivity. This process of weight and input, and error calculation propagates through the ANN to provide the segregation rules which separates the data according to class (target vector). The 'b' is a bias term used to influence the training weights and for ANN training. Figure 6.3 displays this process of backward propagating the error term through the network architecture.

The University of Nottingham
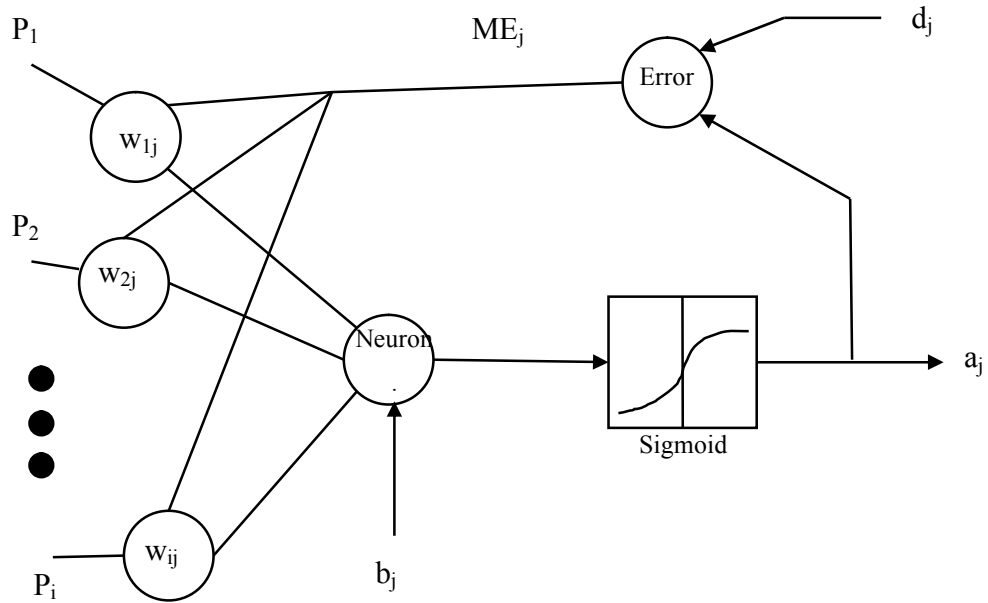
Figure 6.3 Illustration of how the error term propagates back through MLP network

The ANN error term back propagation illustration of Figure 6.4 is an extension from Figure 6.2 multi layer network, within this representation the focus is on the error term ME_j and how this is derived from desired output d_j minus the actual output a_j (see Equation 6.5). This error term propagates back through the network to the influence the weights which have a rate of change gained from Equations 6.4 and 6.5. For illustration purposes this is a two layer network and the classification networks used for classifying single grit scratch and grinding pass phenomena used four layer network(s).

P_t and T_t are both 'mn' dimensional and 'm' dimensional matrix used to test the ANN against the learnt weights and is made up of both unseen and seen, sample AE signal data.

The University of Nottingham

$$P_t(m \times n) = \begin{bmatrix} p_{t11}, p_{t12}, \ldots, p_{t1j}, \ldots, p_{t1n} \\ p_{t21}, p_{t22}, \ldots, p_{t2j}, \ldots, p_{t2n} \\ \vdots \qquad\qquad \vdots \\ p_{ti1}, p_{ti2}, \ldots, p_{tij}, \ldots, p_{tin} \\ \vdots \qquad\qquad \vdots \\ p_{tm1}, p_{tm2}, \ldots, p_{tmj}, \ldots, p_{tmn} \end{bmatrix}$$ (6.8)

$$T_t(m) = [t_1, t_2, \ldots, t_i, \ldots, t_m]$$

Both P_t and T_t are presented to the ANN as test vector matrices and for the single scratch tests classifying; cutting, ploughing and rubbing data the classification would look something like the representation in Figure 6.5. The output of the ANN is based on the desired and actual classification of correct classes and the classification boundary which is not shown.
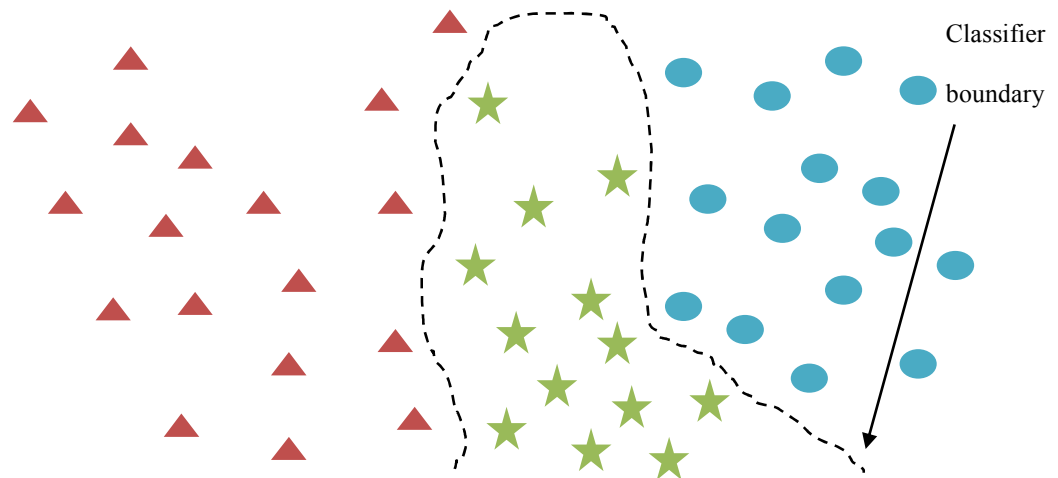
Figure 6.4 illustrates the MLP back-propagation ANN segregating 3 classes of data

Figure 6.4 illustrates a data segregation example where the three classes (class 1 triangles, class 2 stars and class 3 circles) are segregated after sufficient training. The curved surface is gained from iterations starting from an initial state to a very low error

The University of Nottingham

mapping value (Sum Squared Error). For the computation to pass from the input to the output and update the weights is known as one epoch. The ANN process can be stopped by user intervention, the amount of epochs trained for, or getting MSE below a certain error threshold.

Table 6.2 ANN parameters for experiments

ANN Parameters	Value
hidden layers	2
Input size	(1) STFT: 256 Neurons (2) WT & Statistical window: 72 Neurons (8 windows with 6 values across the set of coefficients + 24 time constants (8 windows))
Transfer function for layer 1,2,3	Tan-sigmoid
Transfer function for output layer	Pure-linear
Epochs	10000 for (1) Time: 25 minutes 10000 for (2) Time: 5 minutes
Type	Back-propagation
Learning rate	0.1^{-10}
Momentum	0.9
Training	(1) STFT: 60 different *C, P and R cases (2) WT: 60 different *C, P and R cases

*C = cutting, P = Ploughing and R = Rubbing

Tables 6.2 and 6.3 display the parameters used for classification of the both the radial scratch tests and the horizontal scratch tests respectively.

Table 6.3 ANN parameters for ANN classifications

ANN Parameters	Value
hidden layers	2
Input size	STFT processed data: 207 Neurons
Transfer function for layer 1,2,3	Tan-sigmoid
Transfer function for output layer	Pure-linear
Epochs	10000 for (1) Time: 37 minutes
Learning rule	Back-propagation
Learning rate	0.1^{-9}
Momentum	0.9
ANN Training performance	$5.2423e^{-31}$
Training	STFT: 148 equally applied as phenomenon cases*

*C = Cutting, P = Ploughing and R = Rubbing as equally applied phenomenon cases

Once the network had learnt the training data, the test data would be applied to the ANN and tested for classifications and misclassifications. The results for this classifier can be found in Chapter 7. The weights would be initialised in random manner and from the back-propagation learning rule they would change with respect to mapping the desired from the obtained target values (see Appendix A2.6 for ANN code listing).

6.5 Clustering method for classification of cutting, ploughing and rubbing in grinding

Another pattern recognition technique used for classification is through Fuzzy-c clustering (Li 1998; Liu 2004; Liu, Chen et al. 2005). Pattern Recognition can select features of interest based on all data features. The technique of fuzzy clustering provides rules in the form of distance measurements that segregate the different cluster sets from each other, in this case; the cutting (C), ploughing (P) and rubbing (R).

Clustering techniques have emerged from work carried out in statistical probability (Hartigan 1985; Cuevas, Febrero et al. 2001). When looking at real world phenomena most cases are not finite and instead possess a lot of in between values such as that seen with fuzzy sets. Fuzzy c-mean algorithm is an iterative technique for clustering data sets in a soft rule set fashion. It is a technique for grouping data and finding structures within data. Essentially clustering techniques use a distance measure to segregate like data from other presented data into classes or datasets (clusters).

There are two main types of clustering techniques; the conventional way of clustering is through hard clustering where partitions are formed, representing each pattern similar to a threshold measure used for pre-processing the ANN outputs. The difference in hard clustering is the data belongs to only one cluster. With non linear data there is no sharp classification between clusters, especially at the boundaries; this is why fuzzy clustering is better as it can assign clustering between 0 and 1 and not just one fixed value,

The University of Nottingham

therefore giving cases for both cluster sets. The classification here is based on the set input data having more similarities when compared with other data clusters and is known as soft clustering, if however, there were no similarities or little similarities, the data set would more than likely belong to another cluster set.

6.5.1 Hard Clustering

A hard cluster algorithm that uses hard partitioning is displayed in Figure 6.5. Here the Hierarchical Clustering Explorer (HCE (Jinwook and Shneiderman 2002)) uses the Minkowski distance function to cluster like data samples based on the minimum similarity threshold. The hard clustering technique is unlike soft clustering, in that a sample is classified under a particular cluster this is when the minimum similarity is considered too close when compared with other members of similar cluster(s). Looking at the 1st and 2nd clusters the end cases in both clusters appear to have similarities i.e. there is membership in both clusters. With fuzzy clustering, the clustering would be assigned differently taking more in-between factors into consideration. The HCE tool is very useful for displaying data, non-relationships/relationships before using a more advanced classifier such a Fuzzy-c clustering technique. In addition, at the bottom of the window pane there is a 'parallel co-ordinates realisation' this is very useful for analysing the data outliers and for use with tree based classifiers such as that seen by GP.
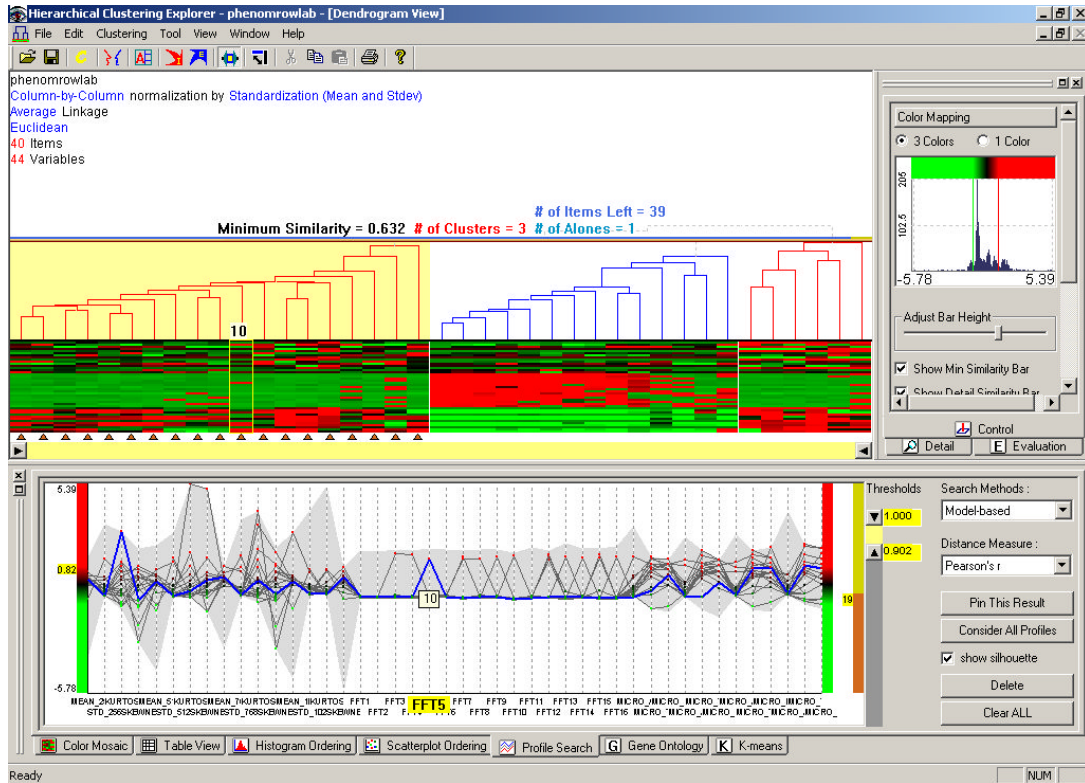
Figure 6.5 displays HCE – clustering cutting, ploughing and rubbing AE data.

6.5.2 Soft Clustering

Fuzzy rules look at the membership between the crisp values such as the maybe situation or grey area instead of black and white 'yes' and 'no' answers. The following illustration describes fuzzy rules for classifying cutting, ploughing and rubbing in terms of AE emitted signal intensities.
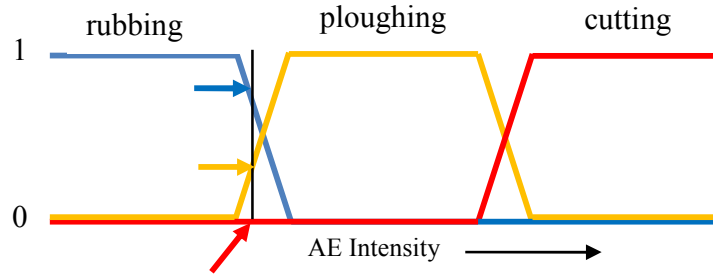
Figure 6.6 displays the fuzzy relationship between cutting, ploughing and rubbing

For instance, looking at Figure 6.6 where the slider is positioned there are high intensities of rubbing and low intensities of ploughing therefore, the rubbing classification would occur for this illustrated example. Border line cases having half rubbing and half ploughing occur very infrequently and if by the off chance they did, they would be removed to ensure safe classification or, an upper/lower bound would be used to ensure no confusion during classification. The transitive closure method is fundamental to fuzzy discrimination; where the relationship between one set of data based on the similarities to another set of data. This similarity relationship is more of a proximity relationship, rather than a similarity relationship. This similarity relationship has 3 features; reflexive $m_{ij} = 1$, symmetric, $m_{ij} = m_{ji}$ and min-max transitive,

$m_{ij} \geq \overset{n}{\underset{k=1}{\wedge}}(m_{ik} \wedge m_{ki}),$ this is where the fuzzy relationship is both reflexive and symmetric in nature. It is here where the min-max relationship is with the sign reversed however this is difficult to come by.

6.5.3 Fuzzy-c Clustering
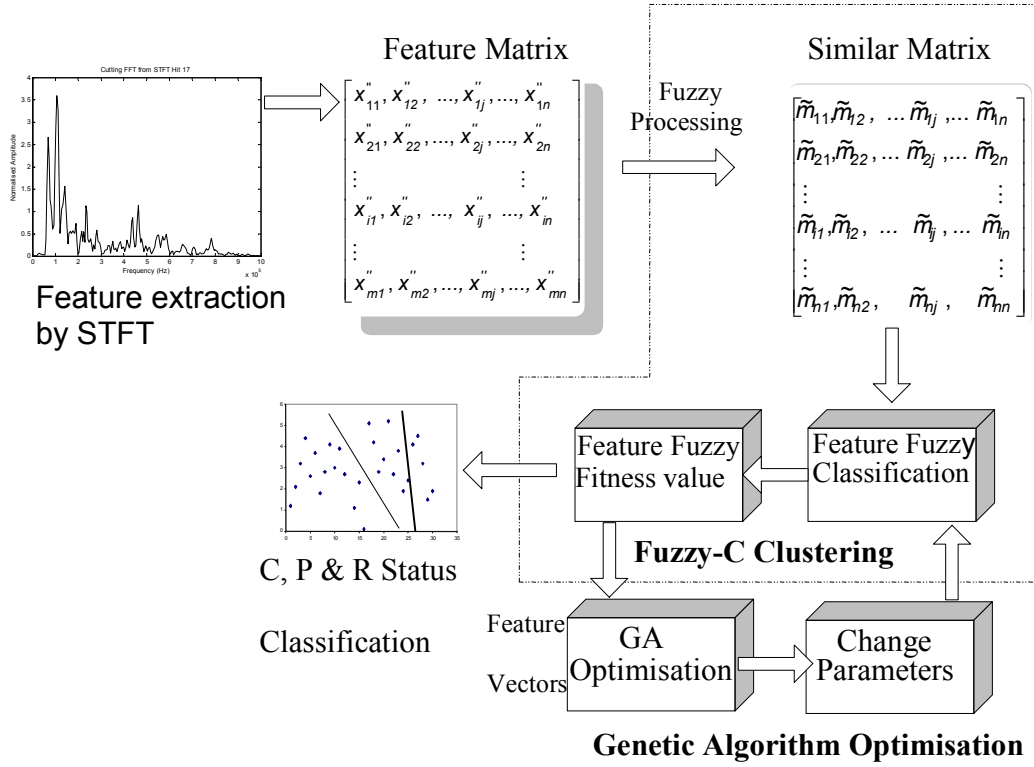
Figure 6.7 Block diagram of the C, P and R classification

Figure 6.7 displays a block diagram of the fuzzy-C/GA is based on work carried out by (Liu 2004; Liu, Chen et al. 2005) however in this case a GA is used for optimisation and it's the clustering of the cutting, ploughing and rubbing. The first step in this process is to convert the STFT vectors into a fuzzy similarity matrix defining the relations of similarity. The next process is to then define the fuzzy variable similarity matrix which evaluates each coefficients $\tilde{r}_{ij}$ degree of membership between the element 'i' and element 'j.' Following on, the cluster centres are determined; the centres segregate and categorise one cluster from another. The centre cluster is the representing function of a

particular cluster. Input test data that has a membership close to a particular centre than other measured mean-centres means that input data belongs to that particular centre.

As displayed in the Table 6.1 in Section 6.4.3, the samples vs. feature matrix is the same for presentation to Fuzzy-c clustering, as that applied to ANN however, let P_1 is X_1 and U_1 is V_1. Note that test set P_t of Equation 6.8 is concatenated with the training set P (equation 6.1) and both the target vectors; T_t and T are used to verify the correct clustering outcome. Let $X = \{X_1, X_2, ..., X_m\}, X \subset V,$ where X_1 to X_m are feature vectors make up the total feature matrix set and $X_i = (X_{i1}, X_{i2}, ..., X_{in}) \in V$ is a feature vector (element of total feature matrix set V); X_{ij} is the *jth* feature of individual X_i the feature matrix are made up from 1 to n feature vectors. To ensure there is normalisation across the feature matrix; Equation (6.9) is used which calculates the normalised mean for each input value divided by the variance.

$$x'_{ij} = m_j \cdot X_{ij} \ \& \ x''_{ij} = (x'_{ij} - \bar{x}'_i)/\sigma_i \tag{6.9}$$

Where:

$$m_j = \max(X_{11}, X_{12}, ..., X_{1n})/X_{1j}, \quad \bar{x}'_i = \frac{1}{n}\sum_{j=1}^{n} x'_{ij} \ \& \ \sigma_i = \left|\frac{1}{n}\sum_{j=1}^{n}(x'_{ij} - \bar{x}'_i)^2\right|^{1/2}$$

The normalised feature matrix is then represented by the feature matrix below in equation (6.10):

The University of Nottingham

$$X(m \times n) = \begin{bmatrix} x''_{11}, x''_{12}, ..., x''_{1j}, ..., x''_{1n} \\ x''_{21}, x''_{22}, ..., x''_{2j}, ..., x''_{2n} \\ \vdots \qquad\qquad \vdots \\ x''_{i1}, x''_{i2}, ..., x''_{ij}, ..., x''_{in} \\ \vdots \qquad\qquad \vdots \\ x''_{m1}, x''_{m2}, ..., x''_{mj}, ..., x''_{mn} \end{bmatrix} \qquad (6.10)$$

The Fuzzy similarity matrix is the next calculation required for the fuzzy clustering of the input data set. The similarity matrix uses a distance measure to show similarities within the matrix set. There are many distance functions available; however, Fuzzy-c clustering uses Equation (6.11). The index of similarity is based on the minimum distance that equates to the maximum similarity.

$$(6.11)$$

$$m_{ij} = \frac{\sum_{k=1}^{n} \left| (x_{ik} - \bar{x}_i)(x_{kj} - \bar{x}_j) \right|}{\left\{ \left[\sum_{k=1}^{n} (x_{ik} - \bar{x}_i)^2 \right] \cdot \left[\sum_{k=1}^{n} (x_{kj} - \bar{x}_j)^2 \right] \right\}^{\frac{1}{2}}}$$

By using the correlation coefficient Equation (6.11) the normalised feature matrix is converted into a fuzzy proximity matrix M:

$$M = \begin{bmatrix} m_{11}, m_{12}, ..., m_{1j}, ..., m_{1n} \\ m_{21}, m_{22}, ..., m_{2j}, ..., m_{2n} \\ \vdots \qquad\qquad \vdots \\ m_{i1}, m_{i2}, ..., m_{ij}, ..., m_{in} \\ \vdots \qquad\qquad \vdots \\ m_{m1}, m_{m2}, ..., m_{mj}, ..., m_{mn} \end{bmatrix} \qquad (6.12)$$

The University of Nottingham

The fuzzy proximity matrix 'M' is then converted into a fuzzy similarity matrix M^K, as the proximity relationship does not have enough similarities for fuzzy clustering to be carried out. From the using the fuzzy algorithm such as transitive closure, the fuzzy matrix 'M' can be converted into the fuzzy similarity matrix M^K.

$$M^K = \begin{bmatrix} \tilde{m}_{11}, \tilde{m}_{12}, \ldots, \tilde{m}_{1j}, \ldots, \tilde{m}_{1n} \\ \tilde{m}_{21}, \tilde{m}_{22}, \ldots, \tilde{m}_{2j}, \ldots, \tilde{m}_{2n} \\ \vdots \qquad\qquad \vdots \\ \tilde{m}_{i1}, \tilde{m}_{i2}, \ldots, \tilde{m}_{ij}, \ldots, \tilde{m}_{in} \\ \vdots \qquad\qquad \vdots \\ \tilde{m}_{m1}, \tilde{m}_{m2}, \ldots, \tilde{m}_{mj}, \ldots, \tilde{m}_{mn} \end{bmatrix} \tag{6.13}$$

$$\min\left\{ J_m = \sum_{j=1}^{m} \sum_{i=1}^{n} \left| \mu_j(x_i) \right|^b \left\| x_i - c_j \right\|^2 \right\} \tag{6.14}$$

Looking at Equation 6.13, $\tilde{m}_{ij}$ in the matrix M^k is the similarity between feature 'i' and feature 'j'. The maximum value of similarity is when $i = j$ and the feature itself equates to 1. After ranking the features in the order of similarity values, it is then possible to segregate these features using the closest cluster distance membership function and distinguish the AE STFT data in terms of cutting, ploughing and rubbing phenomenon. The closest distance membership function of fuzzy-c clustering is based on the squared loss cost function (see Equation 6.14) for each point. For Equation 6.4, x_i is the samples ($i = 1, 2, \ldots, n$), 'm' is the number of known clusters, c_j is the cluster centre point where ($j = 1, 2, \ldots, m$), $\mu_j(x_i)$ is the fuzzy membership of sample x_i to cluster 'j.' The 'b,' term

The University of Nottingham

if equals 1, tends more towards k-means clustering, similar to city-block distance statistical measure and if 'b' tends towards ∞ it becomes completely fuzzy similar to Chebyshev maximum distance clustering. Moreover if the term 'b' takes the value of 2, it is similar to the Euclidean distance technique which was used in this work. The fuzzy algorithm iterates through Equation 6.4 until it can no longer best fit the separation of one cluster from another.
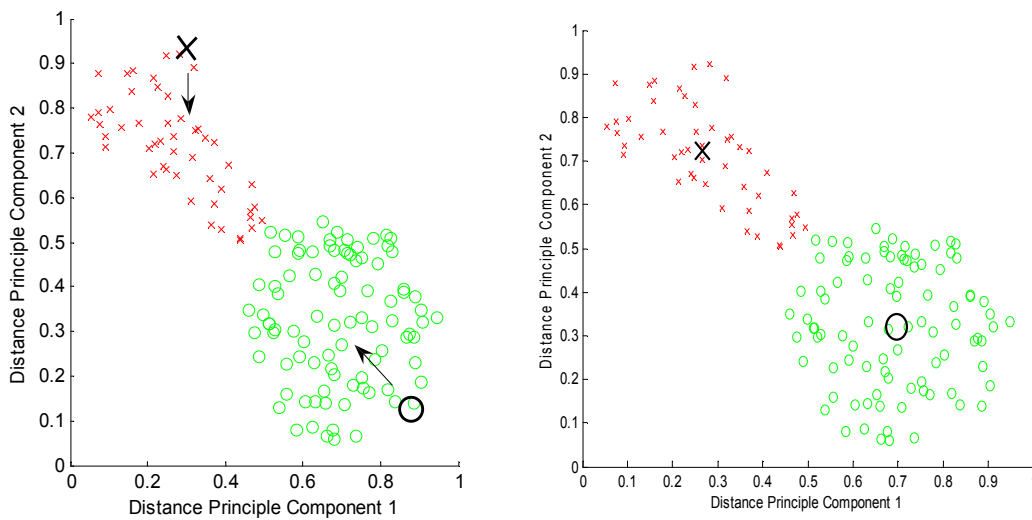
Figure 6.8 displays where the cluster centres start (left) and finish (right)

From Equation 6.14 the clusters initially start away from their actual cluster centres; they are then calculated in terms of the best cluster centre representation for its respective cluster set. Once the cluster sets have iterated to the best fitness for a set number of iterations (Figure 6.8); it would represent the datum for that specific cluster set ensuring correct classification for the presented data set.

6.5.5 Genetic Algorithm for cluster optimisation

The Genetic Algorithm (GA) is also a biologically inspired technique that optimises the evolutionary process of living organisms. The pioneering book 'Adaption in Natural and Artificial Systems' by Holland, (Holland 1975; Booker, Goldberg et al. 1989; Holland 1992) paved the way for genetic algorithms in proposing an evolutionary process that can solve problems by means of a highly parallel technique.

They were invented specifically to avoid getting a solution stuck in a local minimum, also to cover as much of the solution space as possible. The essential feature of a GA (Johnson, Picton et al. 1993) is the group of chromosomes that contain the genetic information. The genetic information is in the form of strings which define a particular solution. For instance, a six bit binary number would be represented by the following string and stored as a chromosome: 1 0 1 0 0 1. The GA randomly produces strings forming a population. Once there are a significant number of strings in the population, a fitness function is used to test whether a particular chromosome is used to influence a new population, or, whether it is to be discarded. The better of these chromosomes is kept in the population for the next generation. Thus each successive population of the chromosomes will have a greater cumulative fitness compared with its predecessor. The fit chromosomes are then chosen for breeding; this then allows the fit chromosomes to influence the next population.

The breeding mechanism is known as cross-over and can be seen from the example below:

Parent 1   **1 0 1 | 0 1 0** →   offspring 1   **1 0 1** | 0 1 1

Parent 2   1 1 0 | 0 1 1 →   offspring 2   1 1 0 | **0 1 0**

The result is two offspring chromosomes; combining the digits of the parents according to the crossover point chosen (the middle of the chromosome was chosen here).

Another influencing factor on a population is mutation, this is where a point is chosen on the chromosome and that genetic material is changed, in this case inverted. Mutation only occurs on randomly selected chromosomes, this random feature is dependant on the mutation rate (higher the rate, the more random mutation becomes). The example below will show mutation being applied to the 5th bit of offspring 1.

Offspring 1   1 0 1 0 1 1

↓

Mutated offspring 1   1 0 1 0 0 1   (5th bit inverted)

The last influencing factor is based on genetic reproduction; this is where the Darwinian principle of reproduction is applied in terms of 'survival of the fittest.' In this reproduction operation, an individual is probabilistically selected from a population; (on the basis if fitness with reselection permitted the best evaluated fitness measure) the individual is copied without change, into the next generation of population.

There are four main preparatory steps to consider when setting up a GA of fixed length character string representation, namely:

- The representation scheme.

- The fitness measure.

- The algorithm controlling parameters and variables.

- A strategy to determine a solution or met goal and criterion for terminating a run.

The GA was used to interact with the Fuzzy-c clustering set, by searching the solution space with a Darwinian fitness approach. The GA would convert the best individual from a population (genotype function) into two variables (phenotype functions) being: the cluster number and, the number of iterations. From the returned fitness value of the Fuzzy-c clustering algorithm; the GA can evaluate the best individual. The Fuzzy-c clustering algorithm is executed for each best individual presented. If the fitness value is less than the fitness function returned, it is discarded as genotype material for the next GA pass, otherwise, it used in the next GA pass. By continually simulating the Fuzzy-c clustering algorithm the best fitness gained would result as the given classifier. If the GA was not used, the Fuzzy-c clustering algorithm is less likely to gain the optimised cluster set. The flow chart below displays how the GA works and interacts with the Fuzzy-c clustering algorithm.

With Figure 6.10 the P_r, P_c and P_m stands for probabilistic reproduction, probabilistic crossover and probabilistic mutation respectively. This is consistent with the idea that GA is a probabilistic search technique.

The Fuzzy-c algorithm would have the data applied to the paradigm. Iteratively searching for the best cluster of data the algorithm would look for the nearest clusters and associate a data set to that chosen cluster. The algorithm would stop once the best mapping of data would have occurred. The GA would optimise both the amount of iterations and number of clusters for the Fuzzy-c algorithm, based on the overall fitness function this would contain the most optimised parameters in terms of the number of clusters and iterations. The GA would run the Fuzzy-c algorithm many times to obtain this optimisation. Once the set criteria had been met with a specific number of GA runs, the algorithm optimisation would stop and the optimised data mapping would exist.
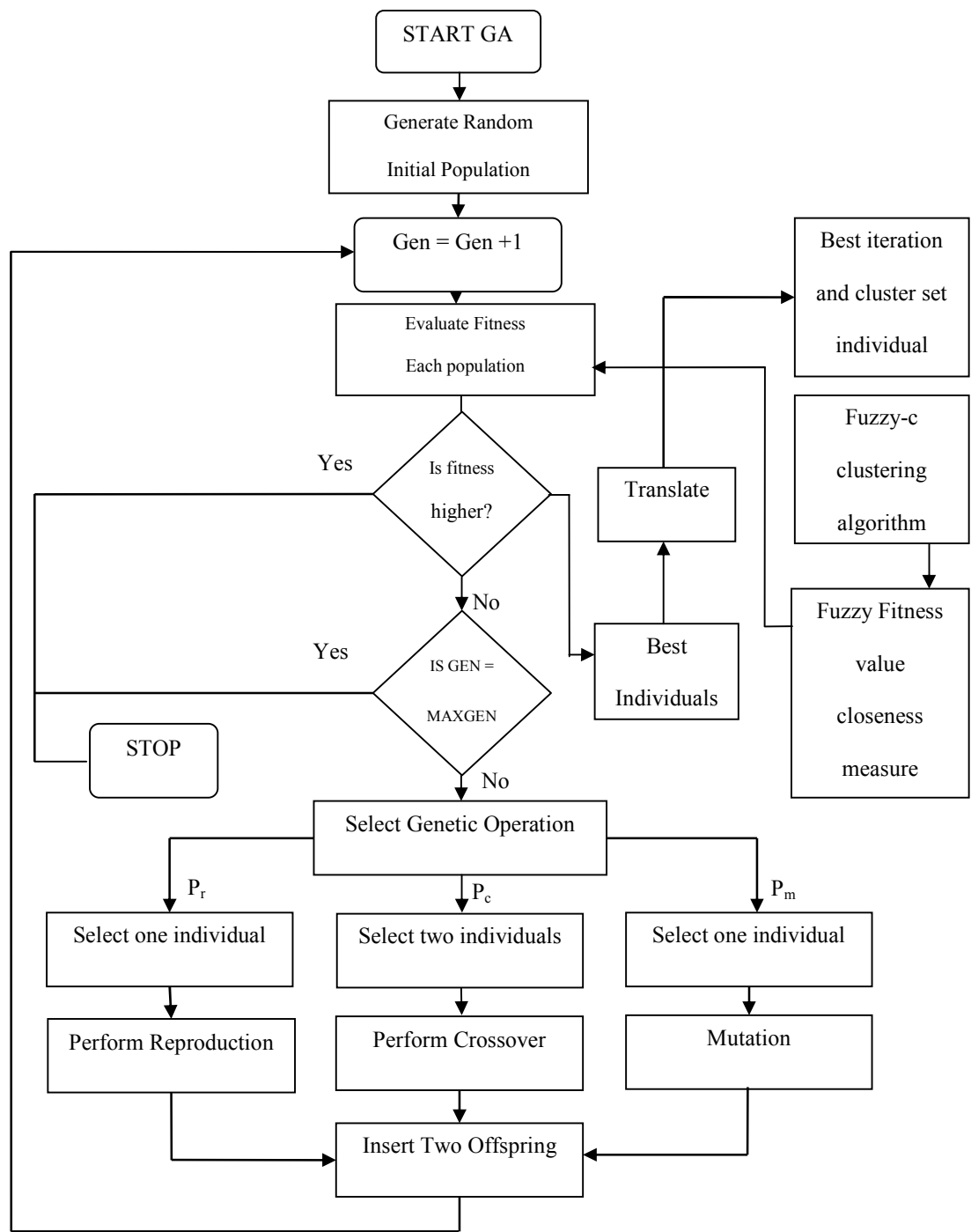
Figure 6.9 Genetic Algorithm Flow Chart interactions with Fuzzy-c Clustering Algorithm

The resulting outputs of this optimised fuzzy-c mapping classification can be found in Chapters 7 and 8 displaying the thesis results (see Appendix A.25 for code listing).

6.6 Generic Grinding Classifier

It was decided early in the research project that the achievement of a generic classifier would be advantageous to industrial monitoring systems. Such a system was decided to be hierarchical in distinguishing different characteristics in grinding, such as different presented material, efficient grinding in terms of cutting, ploughing and rubbing utilisation and, pre diagnose the onset of unwanted grinding phenomenon such as chatter or burn. This work however, requires far more work than what is presented in this thesis. This thesis has already provided novel findings and already added to knowledge in terms of publications in both machine learning and grinding technologies, but to take this work further towards a fully operational generic classifier would require a significant amount of work-beyond the scope of this thesis. Such a research concept would be based around classifying three different materials, (for example; aerospace materials such as Inconnel 718, CMSX4, MARM-002 and Titanium-64) in terms of hardness characteristics, different wheel and feed speeds, different depth of cuts correlated with force, accelerations, acoustic emission, power and temperature signal data as well as measured surface roughness, wheel wear and Material Removal Rates (MRR). The efficient grinding condition monitoring would require the use of further single grit to single grit multi-array research work, with further scratch indentation measurements and the further correlating of the AE energy levels of cutting, ploughing rubbing. This model analysis work would grow in terms of bridging the gap (for four materials) between single grit

analyses with actual grinding pass analysis. With all this information present and a powerful hierarchal rich summary classifier system, the generic classifier for industry may just become a realisation. Next is the discussion regarding the two classification techniques.
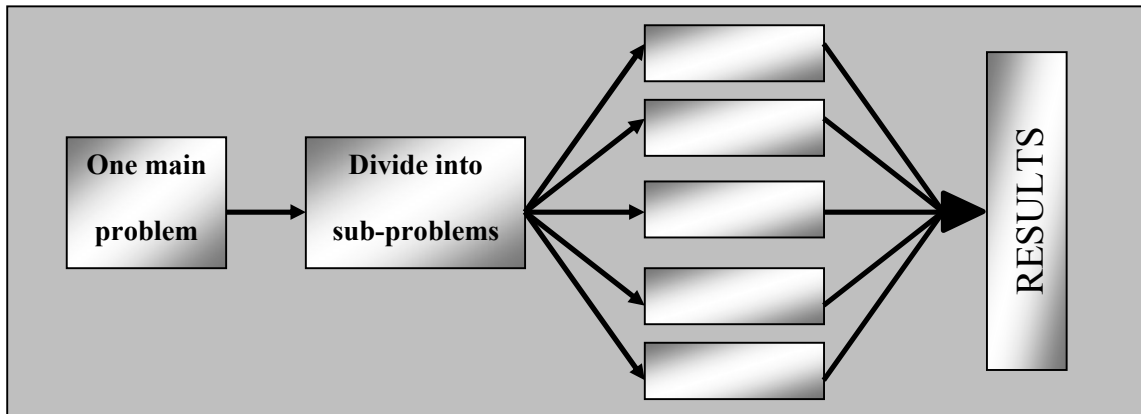
Figure 6.10 Hybrid classifier system made up of subsystems

Looking at Figures 6.10 it is possible to see that the classification problem can be broken up into smaller subsystems, with one main classifier making the distinction between what anomalies have been identified and using one powerful single system. The subsystems in this case were proposed to use Independent Component Analysis (ICA); this acts as a non-linear n-dimensional data reduction process, where the data is converted into rich summary data. The Genetic Program (GP) is then used to make the hierarchical classification, based on evolutionary rules. The next sections give a brief introduction to both ICA and GP respectively.

6.6.1 Independent Component Analysis

Originally for n-dimensional reduction analysis Principle Component Analysis (PCA) through least squares regression was to be used. This would be provided by the Support

Vector Machine (SVM) kernel. The Least Squares Support Vector Machine (LSSVM) toolbox was obtained from the Katholieke Universiteit Leuven (Peleckmans, Suykens et al. 2003). Even if the data is highly non-linearly separable then the quadratic function such as the oval segregating the class points (Vapnik 1998; Tay, Francis et al. 2001) can be used to provide non-linearity to the SVM. The only problem with using SVM and other PCA pre-processors (both linear and non-linear variants) is that they seek directions in the feature space that best represent the data in a sum-squared error sense. Independent Component Analysis (ICA) instead seeks directions that are most independent from each other. The goal behind ICA is blind separation of the signal using mixing weights to separate the signals with no correlations. ICA works in the following way; a number of independent signals are presented for classification, these signals are known as 'd' independent scalar source signals $x_i(t)$ (for i , ..., d and t is considered a time index between $1 \leq t \leq T$).

Figure 6.12 displays the ICA steps in terms of the actual signal which in this example is two independent signals A and B at the top left, top right, the mixing non-linear functions such as Sigmoid, Hyperbolic or power functions are used to rotate the two, and separate the signals (Hyvarinen and Oja 1996; Hyvarinen and Oja 1997; Hyvarinen and Oja 1998). The bottom is where whitening is applied to ensure the mixing transformation is normalised.
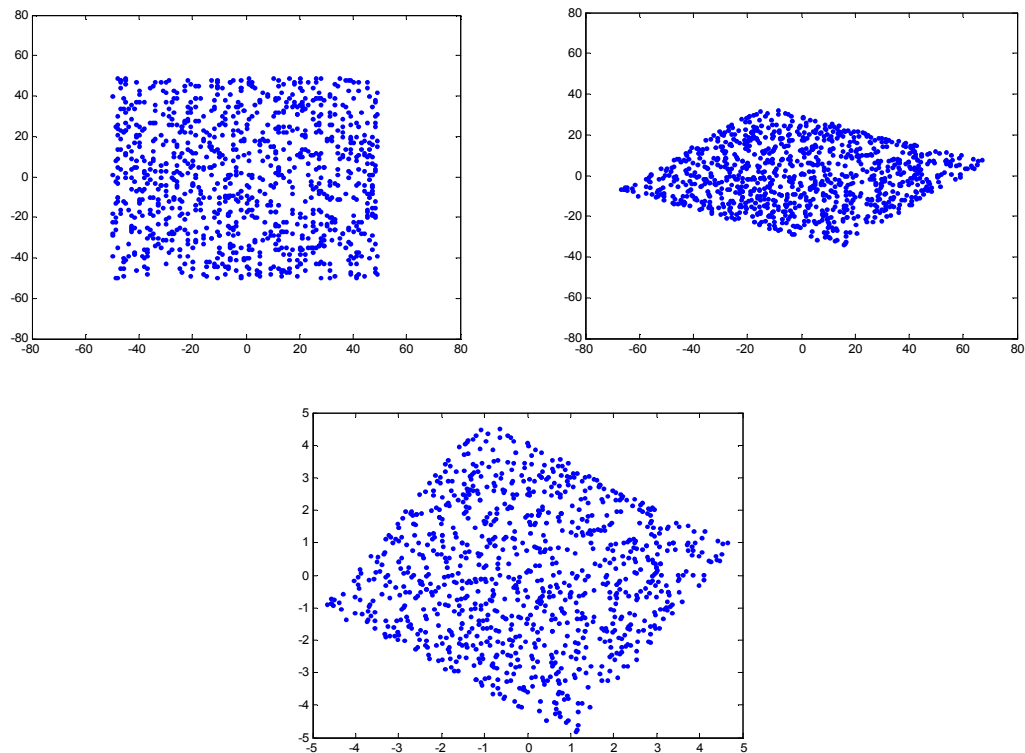
Figure 6.11 displays top left: signals before ICA, top right: Signals with ICA and bottom whitened ICA signals

Figure 6.11 is an example of a random data set which in its raw form and can be seen in

Figure 6.11 (top left). Figure 6.11 (top right) displays the signals mixed with random

non-linear functions to rotate and separate the original (random) data set. This is where

the blind separation of the signals exists. Figure 6.11 (bottom), is where the rotated-ICA

signals are normalised. From the rotation of non-linear functions the signals are

separated and through this blind separation can be confidently applied to the chosen

classifier system.
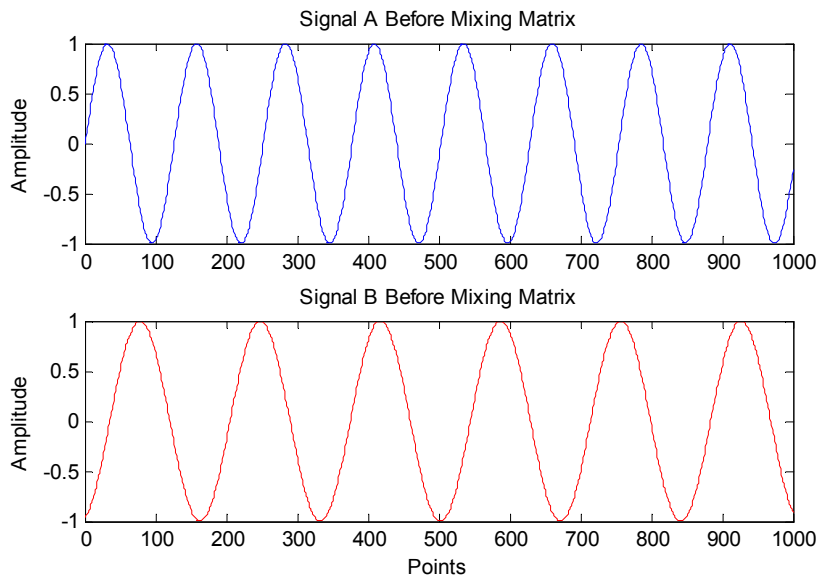
Figure 6.12 displays two original signals A and B before the mixing matrix is applied
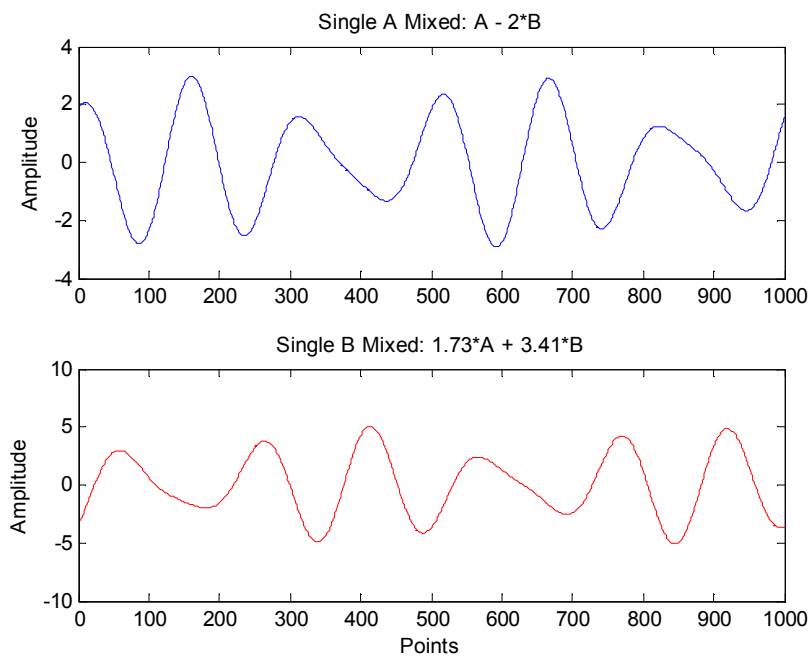
Figure 6.13 displays two signals A and B after having a mixing matrix applied
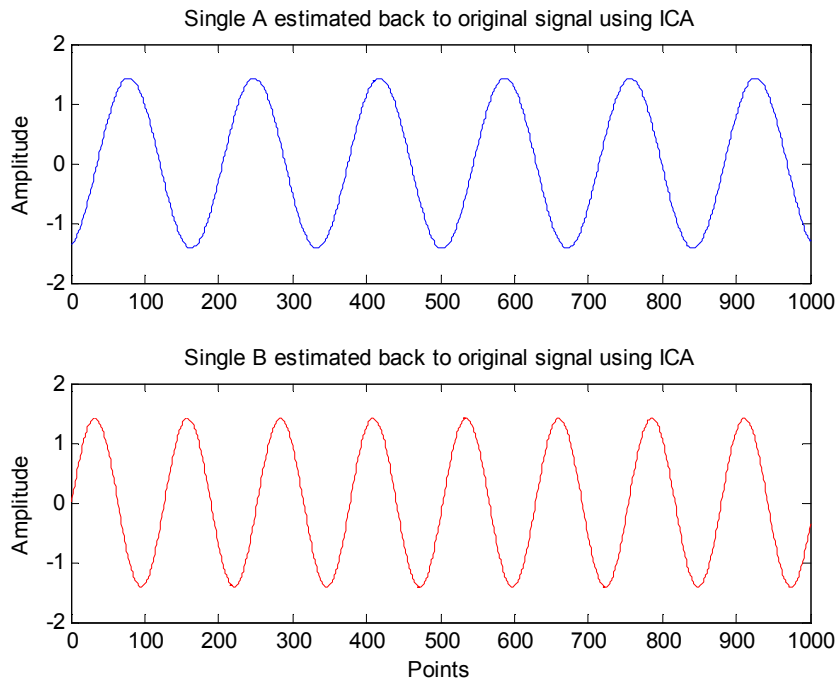
Figure 6.14 displays two signals A and B estimated to their originals (Figure 6.14) by ICA

Figure 6.12 to Figure 6.14 displays the process of ICA from original signals given by the two example sinusoids: 'A' and 'B' in Figure 6.12. Figure 6.13 displays the mixing matrix resultant signals which are rotated from their normal axis to diagonal axis these are displayed in Figure 6.12 (top right figure). The mixing matrix here is given for signal A = A-2*B and signal B = 1.73*A + 3.14*B. There are no rules for the mixing functions as they are chosen to ensure the data set is rotated accordingly. The final state is where the signal is whitened and transformed by the inverse mixing matrix this is to obtain an estimated signal A and B (Figure 6.14) of the original signal A and B of Figure 6.12.

The following Equation 6.13 provides a multivariate density function based on the assumptions of no noise and source independence:

$$p[x(t)] = \prod_{i=1}^{d} p[x_i(t)] \tag{6.15}$$

If a k-dimensional data vector or sensor is observed at each time step, the following equation would exist:

$$s(t) = Ax(t) \tag{6.16}$$

This is where 'A' is a 'k * d' matrix (k sensed signal * d source signals). If 'x' represents acoustic sources, and 's' the signals in 'k' microphones, then the matrix 'A' depends upon the attenuations due to the source sensor separations. Therefore the goal of ICA is to extract 'd' components in 's' that are independent. For instance, the data is represented by the random vector x =$(x_1(t),\ldots,x_d(t))$ and the components as the random vector s(t) = $(s_1(t),\ldots,s_k(t))$. The task is to transform the observed data x(t), using the a linear static transformation 'A' as seen in Equation 6.14. Where 'A' provides the transformation into maximally independent components s(t) these are measured by some function $F(s_1(t),\ldots,s_k(t))$ of independence.

Such a realisation is made from the following equations to provide the algorithm of ICA providing the best independent blind separation based on the maximised joint entropy through gradient descent based weight matrix.

$$P_y(y) = \frac{P_s(s)}{|J|} \tag{6.17}$$

Where J is the Jacobean matrix

The University of Nottingham

$$J = \begin{pmatrix} \dfrac{\partial y_1}{\partial s_1} & \cdots & \dfrac{\partial y_d}{\partial s_1} \\ \vdots & \ddots & \vdots \\ \dfrac{\partial y_1}{\partial s_d} & \cdots & \dfrac{\partial y_d}{\partial s_d} \end{pmatrix}$$

(6.18)

and

$$|J| = \left\| W \right| \prod_{i=1}^{d} \frac{\partial y_i}{\partial s_i} \right|$$

The last part of this ICA equation realisation is in the form of a linear transform of the source signals multiplied by a static non-linear function (Equation 6.19):

$$y = f\left[W_s + W_0 \right]$$

(6.19)

This is where 'W$_0$' is a bias vector and $F(\cdot)$ is a non-linear function such Sigmoid, Hyperbolic Tangent or odd powers for example. By finding parameters for 'W' and 'W$_0$' to ensure the outputs y$_i$ are as independent as possible is the key aim behind ICA.
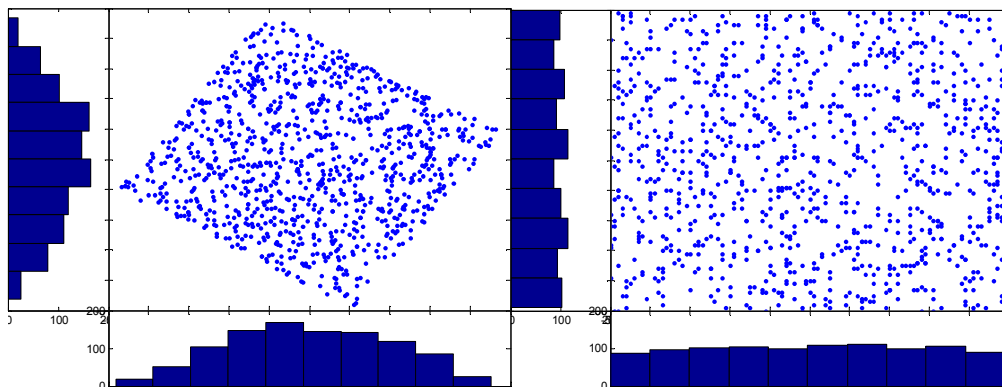
Figure 6.15 left: whitened mixed signals, right: ICA projection of original

The University of Nottingham

Looking at Figure 6.15 (Left) displays whitened mixed signals where the points within the diagonal have a gaussian distribution. For ICA, the signals are required to be independent and not just uncorrelated points along the signal(s) of interest. As non-Gaussian is discussed as independent in terms of signal segregation (Comon 1994; Hyvarinen and Oja 2000) there are several methods used to ensure independence. The first statistical measurement of nongaussianity looks at the kurtosis (fourth-order cumulant). Kurtosis however has some drawbacks in practice, such as its value has to be estimated from a measured sample and this can give rise to problems where kurtosis is very sensitive to outliers (Comon 1994). A second measure of nongaussianity is given by negentropy, this is based on the information theoretic quantity of differential entropy. Where entropy is the basic concept of information theory and in this case, its entropy of the "random variable," can be interpreted as the degree of information that the observation of the variable gives. Thus, the more unpredictable and random the variable, the larger its entropy will be. Such entropy measures are calculated from using Equation 6.20. See Figure 6.16 (right) for non-Gaussian representation using maximum blind separation entropy measure.

To ensure maximum independence the joint entropy method criterion is maximised.

$$H(y) = -\varepsilon[\ln p_y(y)]$$

$$= \varepsilon[\ln|J|] - \varepsilon[\ln p_s(s)]$$

(6.20)

This maximum entropy equation is taken over the full set of samples t = 1, …, T. The bottom right hand side of the equation is independent of weights. The learning rule for

weight matrix using Equation 6.20 and is based on gradient descent. Thus maximum entropy is found from set number of iterations (1000 iterations chosen for current algorithm), and the goal here is to achieve maximum independence. The following Equation 6.21 is used to give the criteria for learning rule behind ICA:

$$\Delta W \alpha \frac{\partial H(y)}{\partial W} = \frac{\partial}{\partial W} \ln|J| = \frac{\partial}{\partial W} \ln|W| + \frac{\partial}{\partial W} \ln \prod_{i=1}^{d} \left| \frac{\partial y_i}{\partial s_i} \right| \qquad (6.21)$$

Equation 6.18 was used to achieve Equation 6.21. Equation 6.22 is the component form from the 1st term on the right hand side of Equation 6.21.

$$\frac{\partial}{\partial W_{ij}} \ln|W| = \frac{cof[W_{ij}]}{|W|} \qquad (6.22)$$

This is where the cofactor of W_{ij} is $(-1)^{i+j}$ multiplied by the determinant of the (d - 1) by (k – 1) dimensional matrix (note: the ith row and jth column of 'W' is deleted) to give Equation 6.23:

$$\frac{\partial}{\partial W} \ln|W| = \left[W^t \right]^{-1} \qquad (6.23)$$

A non linear function is used to rotate the 'W' matrix set and one common nonlinear function that is used is the sigmoid nonlinearity function, this gives the update rule as follows:

$$\Delta W \alpha \left[W^t \right]^{-1} + (1 - 2y)s^t{}_g \qquad (6.24)$$

Where 1 is a d-component vector of 1s.

The learning rule for bias weights is as follows:

The University of Nottingham

$$\Delta w_0 \alpha 1 - 2y \qquad\qquad (6.25)$$

Equations 6.24 and 6.25 give the learning rule for ICA. When using such an algorithm, without prior knowledge of the number of categories this can be difficult to use as an unsupervised technique. If however there are categories of unknown quantity which is equal or near in length to other information 'd,' then this should be segregated independently. For the reason of independently separating signals based on nonlinear functions and random variables it ensures ICA blindly separates the signals. Other linear and nonlinear PCA techniques can be ineffective in separating classes this is based on the noise component giving more salient features within a dataset.

Pseudo Code for ICA

  (1) Whiten the data to zero mean and unit covariance.
  (2) Move data to the range of [-1,1].
  (3) Find the weight matrix Set W matrix to random matrix of size n rows of input patterns.
  (4) While loop until iteration exceeds 1000.
  (5) update W matrix with non-linear activation function.
  (6) Calculate new patterns by multiplying by updated W matrix.
  (7) Increment iteration.
  (8) If the algorithm converged to maximum entropy of signal separation then exit.
  (9) Stop.

This concludes an introduction into ICA (see Appendix A.1 for ICA code listing) and its advanced features for use as a pre-processor within a generic classifier. The independent components achieved from the ICA mapping of the data sets can be used to summarise

The University of Nottingham

n-dimensionally huge data sets. This can then be introduced into the hierarchical hybrid classifier system such as a data mining strategy or GP. The next section looks at GP.

6.6.2 Genetic Programming

GP is a very important breakthrough in conventional programming techniques and came from the advancement of Genetic Algorithms. The idea behind GP came from the 1950s when Arthur Samuel asked the following questions on computer systems (Kosa 1994):

"…How can computers learn to solve problems without being explicitly programmed?"

In other words, how can computers be made to do what is needed to be done, without being told exactly how to do it? GP answers this question in that the computer program has many different computer programs that evolve and even in parallel, GP paradigms co-evolve producing bi-polar solutions to one problem. This realism is found from the evolution strategy of sexual recombination and fitness of many sub programmes evolving complex search criterion based around Darwinian fitness strategies. This brief introduction will discuss significant aspects regarding GP and how the evolutionary strategy is initialised and run against a problem domain environment. Very much based on the concepts of GAs where reproduction and crossover operations are fundamental to this programming paradigm. The mutation function is difficult to implement in a tree based search strategy which is indicative of GP. GA uses binary strings and therefore mutation operators are very easy to establish for this type of strategy search paradigm. Note the following five initial steps required before applying a GP:

The University of Nottingham

- The set of terminals.

- The set of primitive functions.

- Fitness measure.

- Parameters for controlling the algorithm and generation.

- Method for providing an understandable output and criterion for terminating a generation.

A precondition for solving problems with GP is that the terminal set of functions adequately satisfies the sufficiency requirement in the sense that they are capable of expressing a solution to the problem. Within the function set, the individual functions should be able to accept any arguments that possibly maybe generated by a function set. This is also true of any terminal within the terminal set. Both a function and terminal set that satisfies this requirement are said to satisfy the closure requirement. An example node and functional set for determining the correct representation of burn and no burn grinding classification when using AE, force, accelerations, power and temperature measurements are displayed. The terminals can be any number or random number; this defines levels of distinction such as the signal voltage levels for example. The functions that verify closure fit for use with GPLAB (Silva 2004) are;

- Plus, minus, times.

- Sin, cos.

- And, or, not, xor.

- Ceil, floor.

- Min, max.

- Eq (equal), gt (greater than), le (less than or equal).

For the grinding signal anomalies, the following functions should be used; plus, minus, times, sin, min and max. The GPLAB is a toolbox developed for the Matlab environment (Silva 2004). The fitness measure for the grinding signal anomalies is given by the training data set and correlating vector set. This is a kind of supervised approach where the test vectors can be applied to the GPLAB environment for tree based classification output. The following example gives a representation of how crossover occurs with a simple mathematical set of tree based functions.
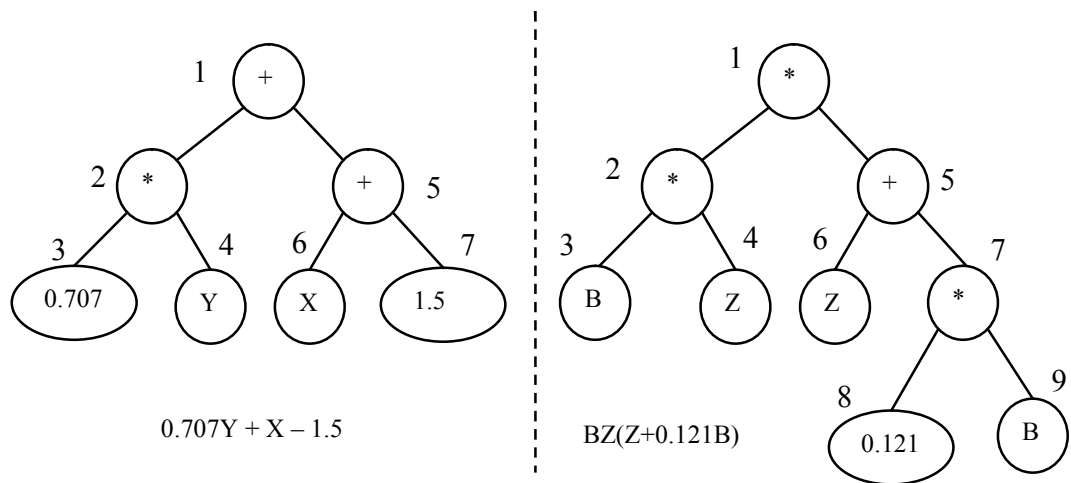
Figure 6.16 Two parent computer programs
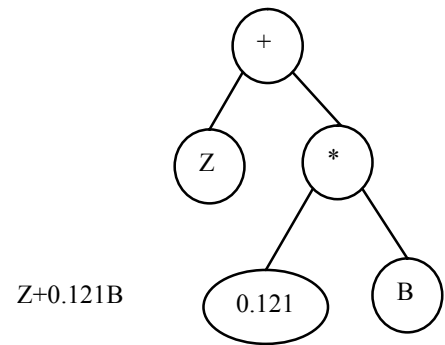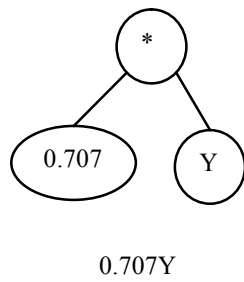
Figure 6.17 Two crossover fragment programs
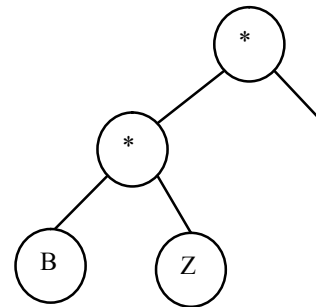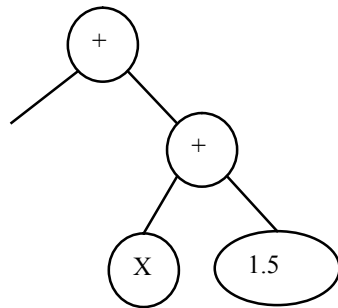
Figure 6.18 Two remainders

Z +0.121B+ X − 1.5

BZ(0.707Y)
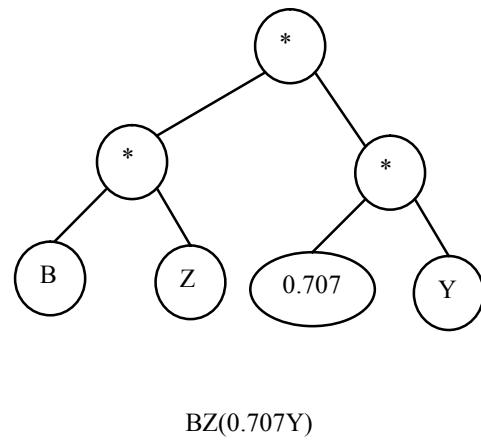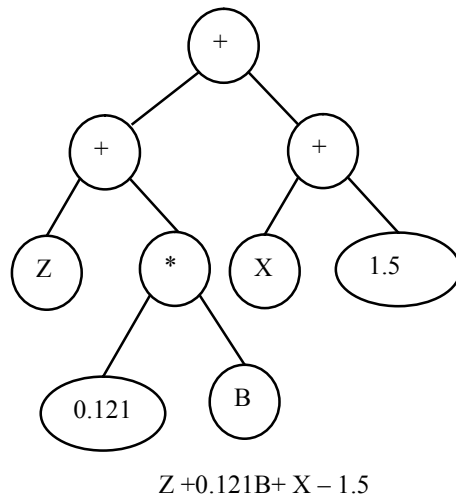
Figure 6.19 Two child programs (made from cross over operation)

The University of Nottingham

Originally, Figure 6.16 starts off with a computer program on the left and another on the right. Separations are made at both nodes 2 and 5 respectively. These crossover fragment programs are represented in Figure 6.17. From the separation, there are missing nodes and functions respectively seen in Figure 6.18. The crossover fragment programs are swapped over with node 2 tree becoming node 5 tree and vice/versa. These crossover fragment programs are attached to the new node 2 and node 5 respectively this is as seen in Figure 6.19 and thus two child programs result. The flowchart of Figure 6.20 displays how the GP iterates through its evolutionary process in determining the best individuals based on evolutionary strategies.
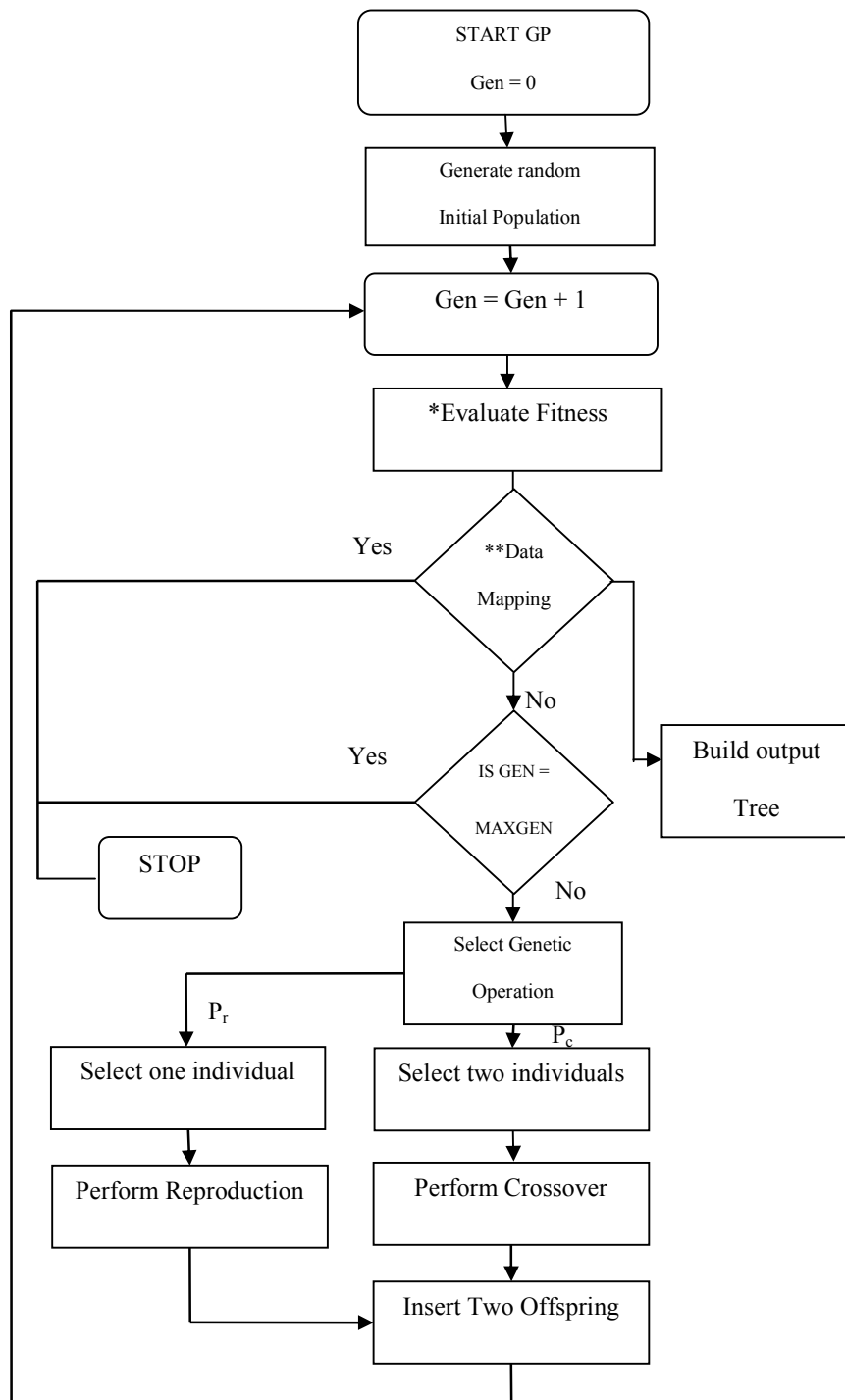
Figure 6.20 Displays the flowchart for GP

The chosen operator function for the GP paradigm were as follows; protected divide, plus, minus and multiplication for integer classification and 'if greater than' or 'if less than' for rule based classification. The terminal nodes were from X1 input to X20. From the flow chart displayed in Figure 6.20 the following rule was obtained for chatter in the following string format:

mydivide(X20,plus(X8,plus(X10,mydivide(X14,plus(X8,mydivide(plus(X10,plus(X8,plus(X10,mydivide(X14,mydivide(X14,plus(X8,mydivide(X13,X20))))))), X20))))))

Reference Figure 6.20 (fitness*), the fitness is obtained from calculating the obtained verses the desired outputs. This is with regard to the target vectors and from selecting random crossover points (see Figures 6.16 to 6.19) each time; the string output is evaluated in terms of its fitness. The crossover operation in this case changes the operator function and values of terminal nodes. The output string maps the two classes (GP can only map two classes at any one time) within the data set (data set** reference Figure 6.20) and when there can be no more mapping the fitness would have converged to its optimal minima, the GP paradigm would stop. The random crossover is based on manipulating the string (through crossover) to give the best output string representation and thus GP strives towards a Darwinian type fitness strategy. This type of fitness is based on the neural network back propagation learning rule in mapping the desired to the actual outputs. For the ICA reduced data set a more advanced fitness measure is used to give a more focused and accurate mapping between the segregation of the two data sets. The pseudo code for such a fitness function is as follows (Silva and Tseng 2005):

Nclasses = number of classes

Nsamples_i = number of samples in class i

Min_i/Max_i = minimum/maximum value plotted in class i

Overlapped = 0

For i = 1 to nclasses

      For j = 1 to nsamples_n

            Value_j = value plotted for sample j

            For nc = 1 to nclasses, nc <> i

                  If value_j between min_nc and max_nc

                        Overlapped = overlapped + 1/nsamples_i

Fitness = 100 * overlapped / nclasses

This pseudo code is not focused on the notation of distances between, and within classes. Instead it calculates the percentage of points within a plot that fall within the range of more than one class. By minimizing this percentage it allows the GP system to have the freedom to devise any possible discrimination strategy and arrive at an optimal or near optimal goal of segregating the data sets. It was decided to provide rules for two data sets at any one time and using the different rules merged together to make the multiple classification strategy. This type of evolutionary rule strategy can be developed for different grinding parameters and for the more generic classification system. Different evolutionary rules can be developed for different machining technologies such as milling, drilling or turning. This type of fitness is used to map difficult to separate

The University of Nottingham

data sets in terms of data overlap. The greater the overlap of the data set, the greater the % fitness would result.

This concludes GP which has a very promising future although more research is going into more advanced topics such as bootstrapping (bolting on computer programs to the tree nodes) and suppressing bloating (where the program tree grows to unmanageable sizes and tends away from solution closure). GP can be considered as a tree based search program similar to those seen in Data-mining. However, GP has the added advantage of being able to search in an evolutionary manner and on a mass parallel scale. The full results can be found in Chapter 8 of this thesis. The code listing for GP and its respective fitness class measurements can be found in Appendix A.2.

6.7 Summary

This chapter has presented four classification techniques some of which were used for the main body of research and the others used for concept realisation of a powerful generic hybrid classifier. This chapter has provided an introduction and discussion of both novel classifiers and mature classifiers. The novel classifiers that have not been used in literature before is the Fuzzy-c clustering algorithm with GA optimisation and GP with ICA as a hybrid classifier. These paradigms have produced some very encouraging results when compared and verified against a mature classification technique such as a Neural Network. The Neural Network give a two-dimensional resolution and can be used to show cutting, ploughing and rubbing surface profiles when applied to single grit scratch tests. The Fuzzy-c/GA gives an n-dimensional view and

The University of Nottingham

considers the data classes in terms of different intensities from 0 to 1 cluster membership (0 being no membership and 1 being an exact membership). With the GA optimising the best number of iterations against the number of clusters it is possible to say the returned Fuzzy-c clustering is the most optimised data realisation. The values experienced by these two classifiers (ANN and Fuzzy-c/GA clustering) provided similar results for the introduced non-linear AE signal grinding data. SVM with GA optimisation has seen numerous applications in grinding monitoring used to provide the best feature set. Although this is considered the incorrect way round. SVM does best with n-dimensional data, so it was proposed to use SVM as a data reduction technique providing rich summary data for a hierarchical classifier such as that seen by GP, however the SVM provided principle components which were sensitive to noise and gave erroneous n-reduction data. This therefore lead to the introduction of ICA where its non-Gaussian, blind separation method proved very powerful for the introduction to the GP classifier system. This hybrid classifier approach is realised in Chapter 8 and is certainly a topic for future work discussion. The ideas discussed in this chapter and Chapters 4 and 5 provide the very essence for a generic monitoring system in anomaly(s) detection and, the control of efficient grinding. This type of hybrid classifier has not been used in machine monitoring before. The novel classifiers that have been used within this thesis are summarised below:

- Fuzzy-c clustering GA classification system.
- A Fuzzy-c/GA clustering system that classifies rubbing, ploughing and cutting AE signals for both single grit scratches and 1μm and 0.1mm grinding pass cuts.

The University of Nottingham

- A ANN system that classifies rubbing, ploughing and cutting AE signals for both single grit scratches and 1μm and 0.1mm grinding pass cuts.

- A hybrid classifier system using ICA and GP providing a multi anomaly classification system for the detection of burn and chatter.

Chapter 7 Single Grit Scratch Test Results

7.1 Introduction

This chapter looks at the fundamental research carried out in this thesis in looking at the material removal rates experienced during both radial scratch cuts and horizontal scratch cuts. Work has already been carried out in this area looking at the correlation between both radial and horizontal scratch cuts in terms of material removal and force extracted information. The research has provided SG grinding models however there has been no research looking at the differences in cutting, ploughing and rubbing mechanics in terms of acoustic emission (AE) signatures. This work has looked at a number of different materials with different material characteristics as this will have an effect on the emitted AE signature extracted data. The first part of the results will look at radial scratches (Griffin and Chen 2006) and the second part the horizontal scratch tests (Griffin and Chen 2007).

7.2 Radial Scratch Results

The first part of this chapter looks at the radial scratch results already discussed in depth within Chapter 2 of the thesis. The radial scratch used a specially designed rig to ensure surface scratch was made against two highly polished aerospace surfaces.

7.2.1 Signal Analysis of cutting, ploughing and rubbing

Figure 7.1 displays a breakdown of Inconel 718 SG cut AE time extracted signal (top of figure), the STFT representation of the signal (middle of figure) and FT of start, middle and end segments of STFT (bottom of figure). Looking at these representations, it is

possible to see similar frequency bands between 100 kHz and 300 kHz at the start and end, which shows a higher intensity of rubbing at the start when compared to that of the end of the cut. The ploughing phenomenon was found to exist in the middle of the signal and there was no cutting measured in this particular test.

Removal or non-removal of materials during SG pass depends on the cutting action of grit to workpiece interaction. The groove is ideally created from a starting rubbing grit action followed by a ploughing/cut combination, then actual cut action followed by another ploughing/cut combination and then lastly, a rubbing action. Figure 7.2 shows the performance of a single piece of grit interacting with the workpiece material. Depending on the obtained cutting depth, the grit may experience rubbing, ploughing and cutting phenomenon that engages with the workpiece materials. The proportion of rubbing, ploughing or cutting in a grit pass depends on the amount of engagement between grit and workpiece material (quantified in terms of the material and groove area). The SG engagement can be displayed by the profile of the material groove cut, the measurement of the SG before and after the experiment and, the constant monitoring of first touch which is sensed by the calibrated AE sensor (set to 40dB) and is very sensitive to grit-workpiece touch (this is optimised to ensure lack of noise and grit phenomenon extraction). It is also noted that the stress under the grit depends on the undeformed chip thickness. The larger the undeformed chip thickness, the higher the force needed to remove the chip. Therefore higher stresses would be initiated.

Time Series Plot for Inconel 718 Single Grit Cut Test

STFT of AE from Single Grit Cut of Inconel 718

Start STFT Signal (above)   Middle STFT Signal (above)   End STFT Signal (above)
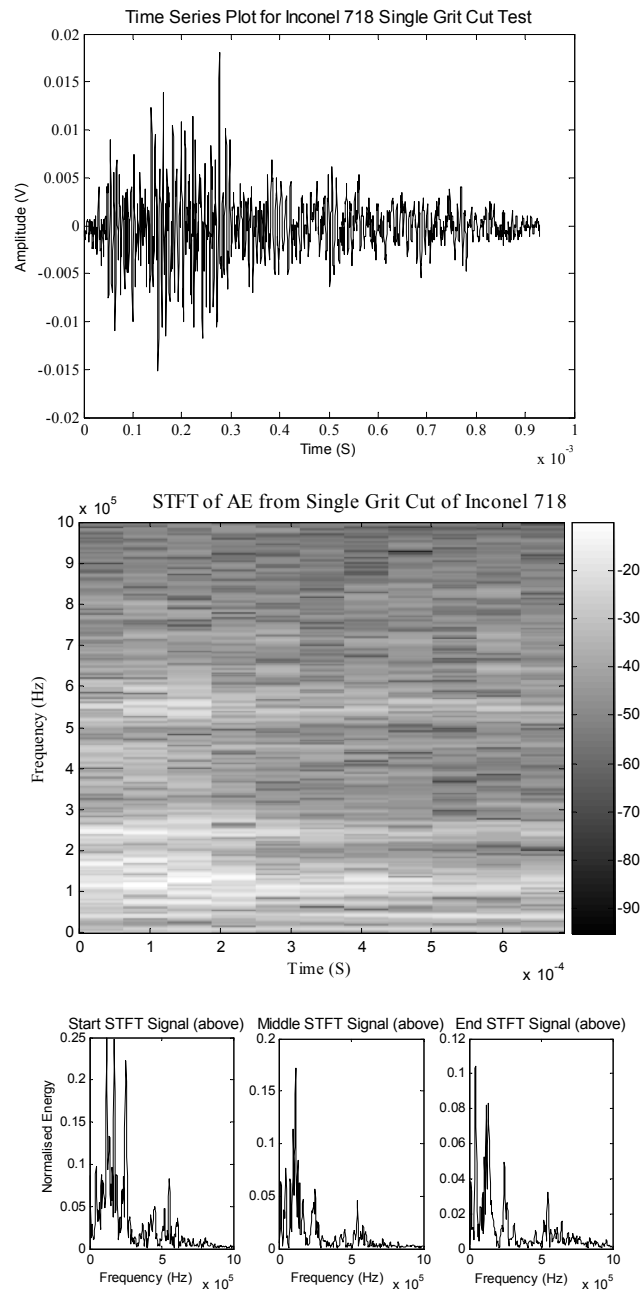
Machine: Makino A55; SG Material: Al$_2$O$_3$; Workpiece: Inconel 718;

Single Grit Dimensional depth and width appx. 1.5μm;

Figure 7.1. Time series, STFT analysis for extracted AE signal of Inconel 718 SG scratch

The University of Nottingham
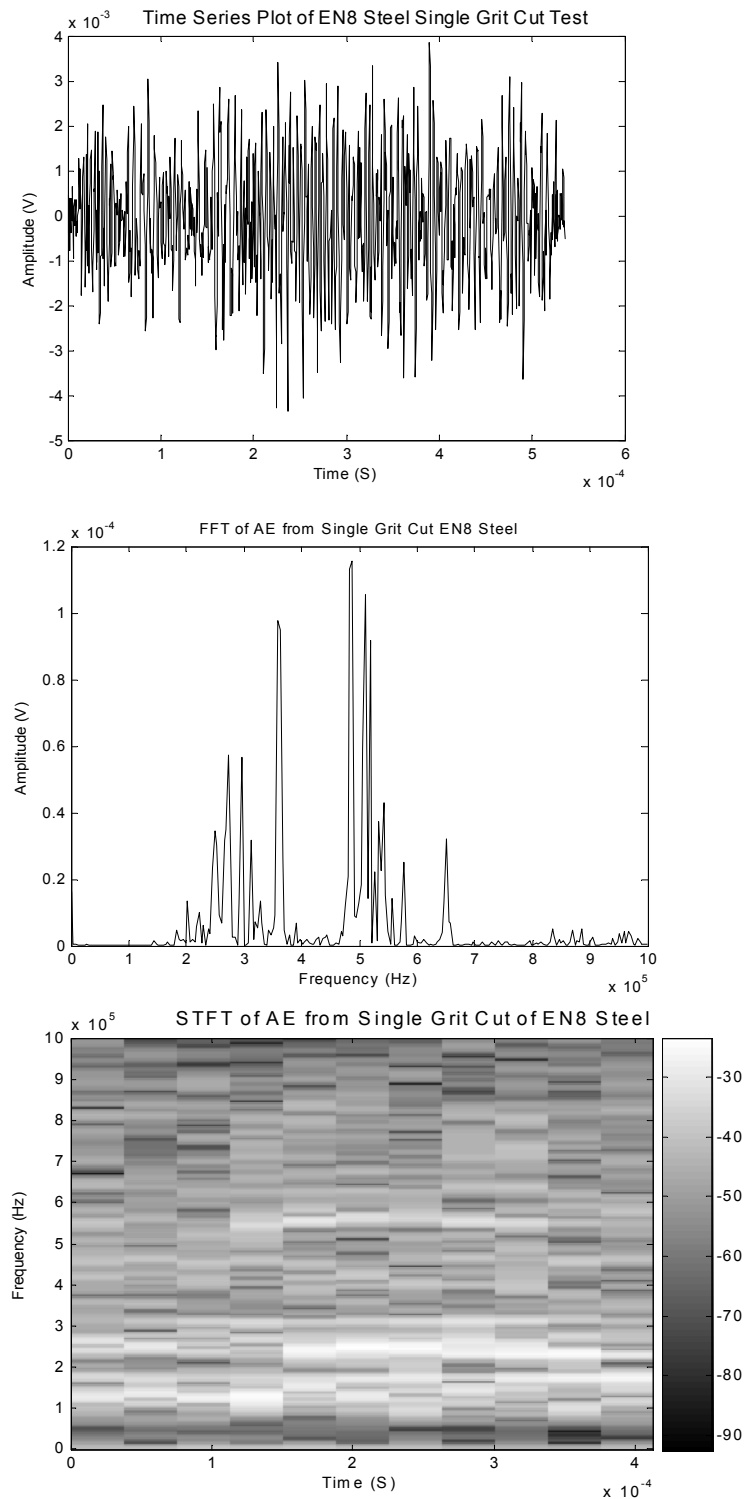
Figure 7.2 Top: EN8 Steel SG Cut AE Times series, Middle: FFT, Bottom: STFT

Figures 7.2 and 7.3 display a test which consisted of a SG Cut AE for EN8 Steel. Looking at the two figures, it is possible to see that the FT offers only frequency information, the STFT offers additional time information although with a of time resolution trade-off and the WT which offers the most information with scaled time-frequency information across the extracted signal. With reference to Figure 7.3 (a) and (b), they display the WT components that have been decomposed from the original signal with an approximate signal of low frequencies at level 3 and a detailed decomposition from levels 1 to 3. This information is then converted to normalised signals displayed in Figure 7.3 (b) for illustration purposes. Figure 7.3 (c) displays the continuous wavelet transform (CWT) of the EN8 SG cut with all time, scale and amplitude information. Each scale starting from 2 is divided by two from sampled frequency (2 MHz) and both high and low frequencies can be seen across the SG cut.

(a)

Nottingham

(b)

(c)
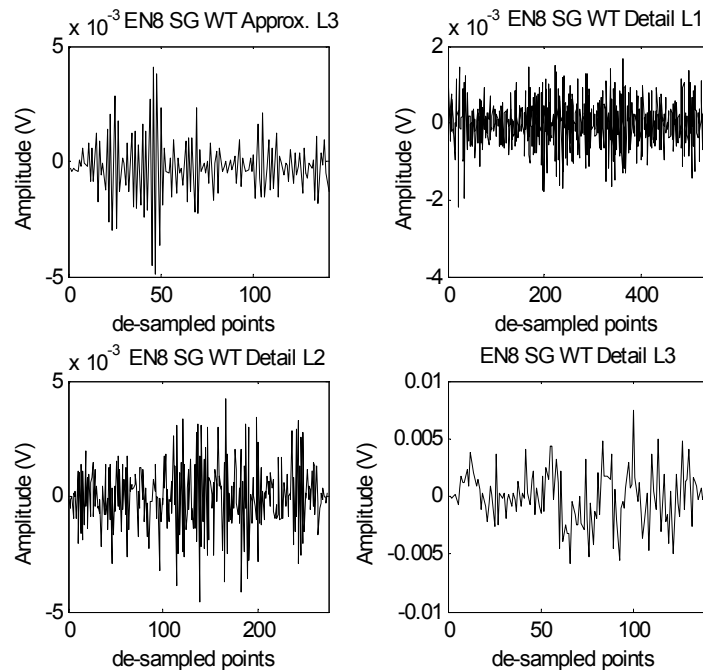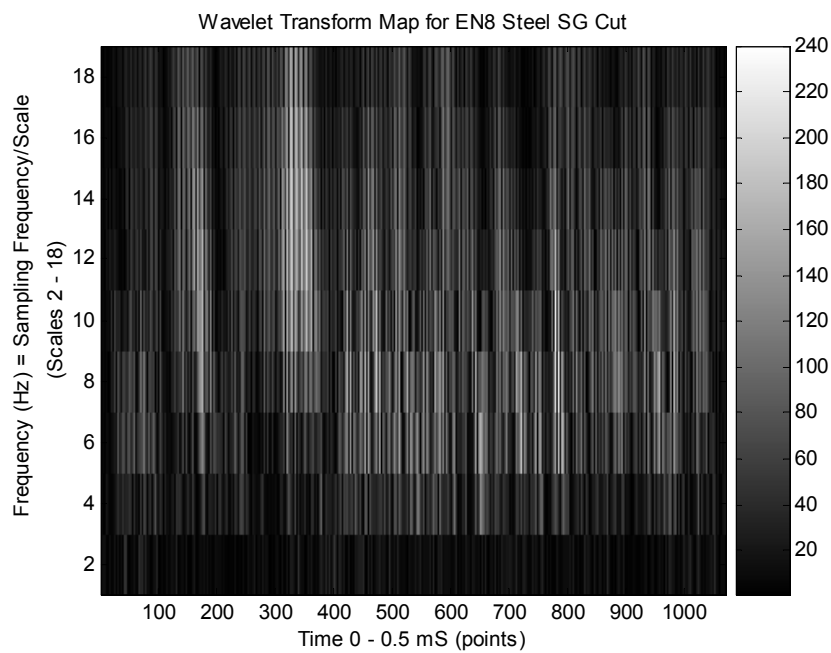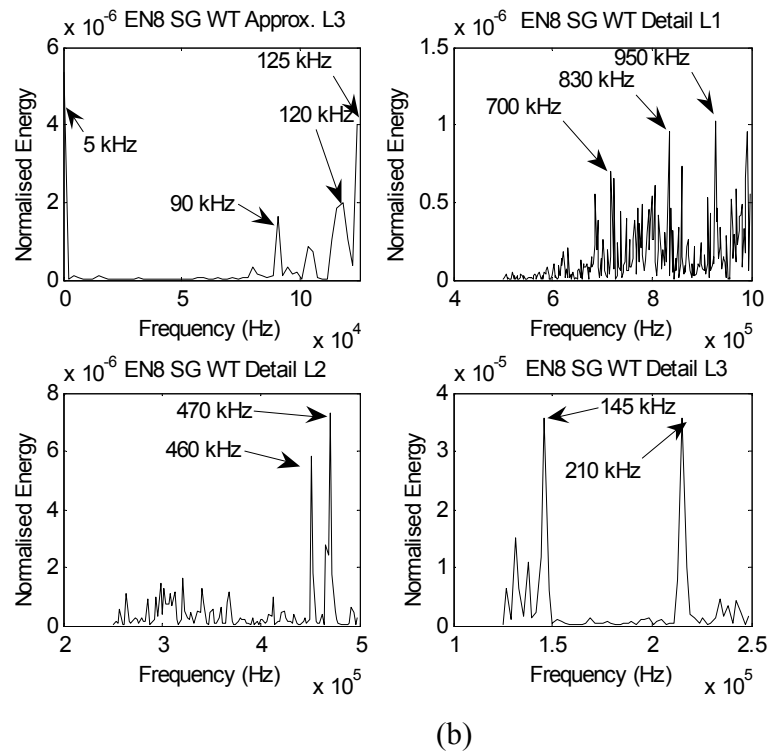
Figure 7.3 EN8 Steel SG Cut AE WT (a), (b) and (c)

Further looking at Figure 7.3, due to the size of the signal, three levels were considered more than enough to represent the required information; any further levels would not display any more features of interest.

With the different energy signatures occurring from the SG interacting within the workpiece, WTs provide a good solution for separating the cutting, ploughing and rubbing phenomenon. Ploughing and cutting both provide different energy signatures where the energy is consumed from surface deformation. In the rubbing case however there is surface friction (Kalpakjian and Schmid 2003) which suggests therefore, that different AE signatures should be apparent between the two different phenomena. Ploughing and cutting are somewhat similar in that both push and slide to one side or, remove material respectively; as these predominately cause material plastic deformation. Whereas rubbing does not remove or slide any material away instead, it touches the surface with no visible markings where rubbing just has elastic material characteristics in that the material deforms and returns back to its original state (this is after a SG pass has occurred). In short, the boundaries are much closer in terms of ploughing and cutting AE distinguishing features. Ploughing and cutting are perhaps the most difficult phenomenon to separate based on this assumption. The technique of both STFT and WT needs to be as accurate as possible to ensure the time constants as well as the sharpness of the waveforms are accurately represented when trying to distinguish the frictional energy and material deformation energy in the form of plastic or elastic energy.

7.2.2 Material to Signal Signatures

Once the profile cut measurements had been taken, the next step of the experiment was to convert the AE signals into STFT with no reduction techniques and then, WT with statistical reduction techniques. The reduction technique (reference Figure 7.3 (c) and (d)) was needed to provide principal components from the rich albeit large wavelet coefficient dataset. The reduction technique employed used statistical windowing with the calculation of mean, standard deviation, kurtosis, skewness, maximum and minimum values. This richness of information obtained by small windows across the dataset provides the basis for an accurate classification by neural networks.
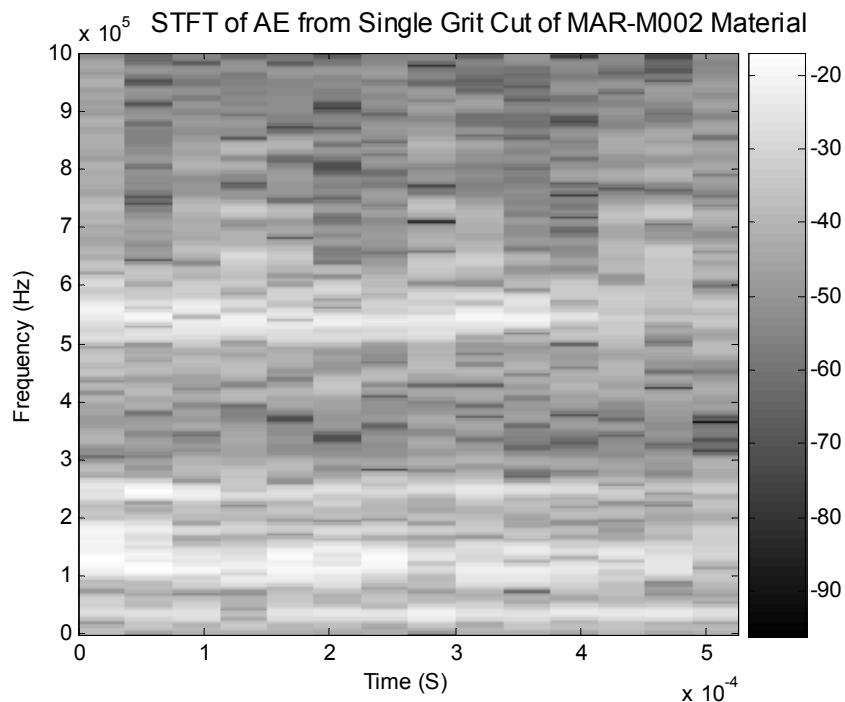
Machine: Makino A55; Single Grit Material: Al2O3; Workpiece: Inconel MAR-M002;

Single Grit Dimensional depth and width appx 1.5μm;

Figure 7.4 Top: Time-Frequency representation (STFT) for SG scratch test MAR-M002

Looking at Figure 7.4 it is possible to see ploughing and cutting has intense amplitudes at 100 kHz to 200 kHz and 250 kHz to 550 kHz frequency bands (0 – 0.1 ms and 0.23 – 0.33 ms respectively). For rubbing however there are only frequency components at the 100 kHz and 250 kHz range in this example (0.43 – 0.53 ms).

In comparison to STFT Figures 7.5, 7.6 and 7.7 display the WT energy spectrums for levels 1-3 signifying ploughing, cutting and rubbing respectively. These results were taken from the same scratch (SG cut) and the same piece of material (MAR-M002).
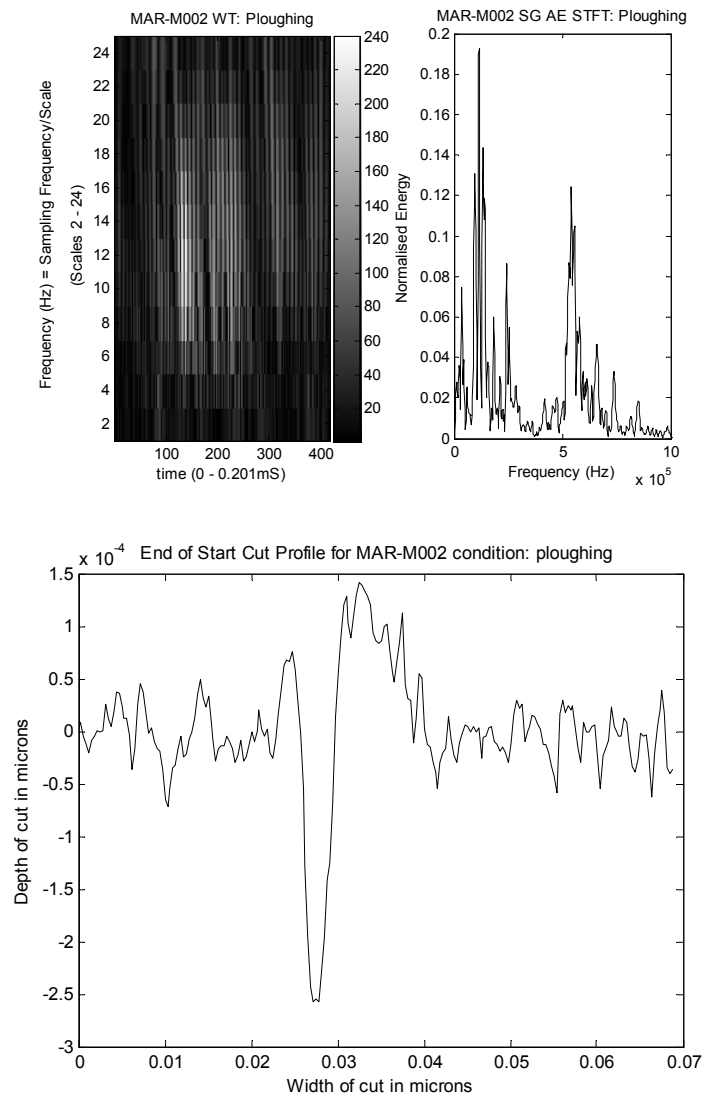
Figure 7.5 Top AE WT (MAR-M002), Bottom corresponding Profile cut for ploughing

Looking at the WTs, ploughing consists of mainly large amplitude, high frequencies between 100kHz and 600kHz although with smaller amplitude components at 50 kHz and 750 kHz.
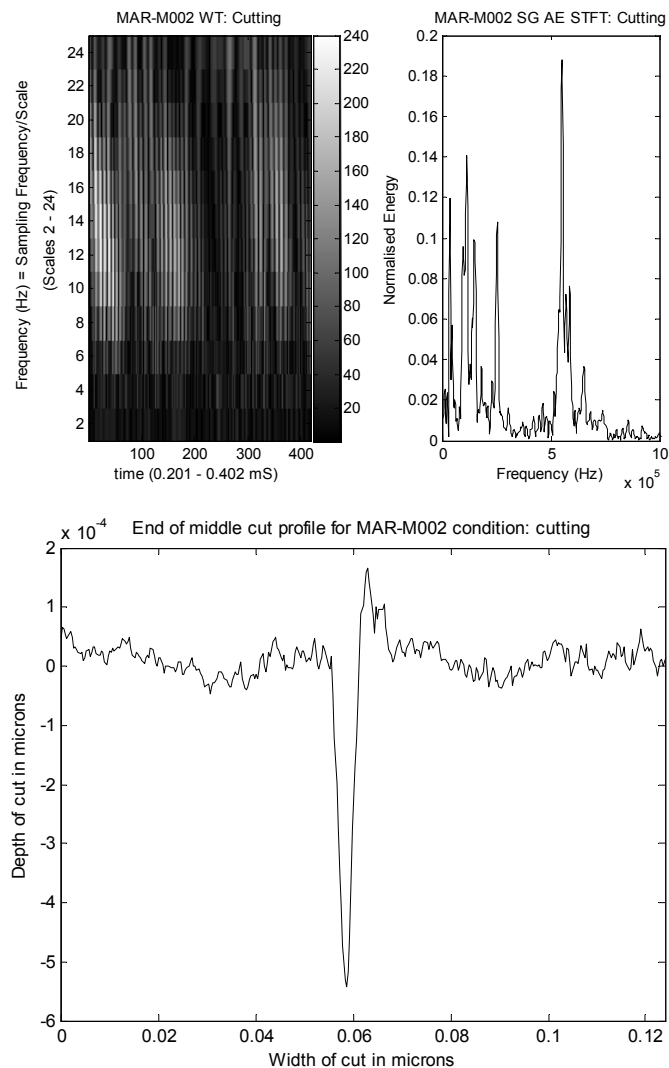
Figure 7.6 Top WT AE (MAR-M002), Bottom corresponding Profile cut for Cutting

When looking at Figures 7.5 and 7.6 we can see some similarity in that both cutting and ploughing produce some material deformation and have plastic material characteristics. Looking at the three detailed WT levels for the cutting phenomenon there are large amplitudes for 50 kHz, 100 kHz, 250 kHz and 600 kHz (much larger amplitude when compared to ploughing cut).
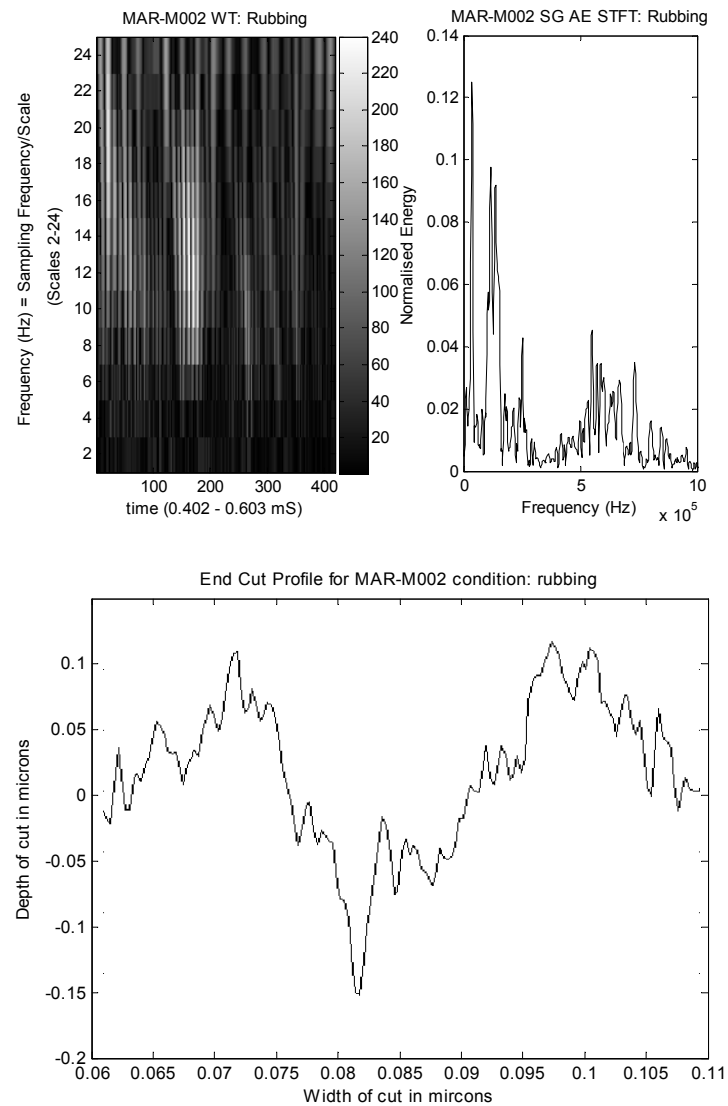
Figure 7.7 Top WT (MAR-M002), Bottom corresponding Profile cut for rubbing

Figure 7.7 show that rubbing has high amplitudes ranging from 50 KHz to 100 KHz with some smaller amplitudes although still significant (when compared to ploughing and cutting phenomenon) between 600 to 750 KHz. Looking at the energy spectrums in terms of features and amplitude levels it is possible to segregate the phenomena however there are a lot of overlaps in the signals that have to be ignored from distinguishing

similar characteristics across one phenomenon border to another. All AE extracted signals were tested against an AE pencil lead break test (Barbezat, Brunner et al. 2004) where the AE signals could be normalised on a day to day basis. The rubbing case in Figure 7.7 and others not displayed here were found not to be pure rubbing due to slight indentation marks which should not occur during rubbing. No scratch or mark is based on the rubbing phenomenon's elastic material properties. This rubbing phenomenon identified in this thesis is more of rubbing with plastic deformation, however more experiments have been carried out to verify pure rubbing from rubbing with plastic deformation.

The observations from the tests provided generalised frequency bands for the different phenomena which were as follows: Rubbing phenomenon occupied the frequency bands of 116 kHz, 172 kHz, 256 kHz, 320 kHz 536 kHz, 780 kHz and 844 kHz. For the three frequencies of 116 kHz, 172 kHz and 320 kHz the normalised energy peaked twice as much as it did with ploughing and cutting phenomena.

The cutting phenomenon had dominant frequency bands at 60 kHz, 90k Hz, 116 kHz, 172 kHz, 416 kHz, 516 kHz and 650 kHz. The lower frequencies of 60 kHz and 90 KHz had normalised energy peaks that were twice that of ploughing and three times that of rubbing phenomenon.

Having properties of both cutting and rubbing phenomenon, ploughing dominated the following frequencies of 96 kHz, 144 kHz, 160 kHz, 172 kHz, 190 kHz, 256 kHz, 536

kHz, 560 kHz and 608 kHz. Where the 560 kHz had a normalised energy peak twice that of cutting and three times that of rubbing. In addition both 144 kHz and 172 kHz had three times normalised energy peaks when compared with cutting and rubbing phenomena.

7.2.3 Neural Network Classification Results

A neural network (ANN) was developed to identify different phenomena involved in SG scratch tests. The parameters used for the ANN for different experiments are listed in Table 7.1. There were a total of 6 scratches made 2 mm apart for each material with a total of 24 scratches existing for all the materials. The materials used in the following tests consisted of EN8 steel, Inconel 718, CMSX4 and MAR-M002. The ANN results were only displayed for Inconnel 718 material. This is to give an indication of cutting, ploughing and rubbing classification, however all the materials with their different signatures displayed segregations and similar ANN results.

The supervised training method would consist of twice as many training examples than examples used in the test case. The test case uses a rule of confidence, where the cases are split up between seen and unseen data, in the seen case the data has already been presented from the training data and is the unseen case it has not (see Table 6.2). The classification accuracy is based on correct classifications against misclassifications. A High value of momentum was used which ensures the ANN can search outside a located minimum to see if the point obtained is a local or global minimum, which is ultimately required.

Looking at Figure 7.8 the first initial results for STFT are very encouraging although the data set is limited in size (due to small data sets for each material used to display initial method capability) and the ploughing and cutting phenomenon combined. This experiment gives a confidence milestone and paves the way for the classification between all SG phenomena, cutting, ploughing and rubbing.
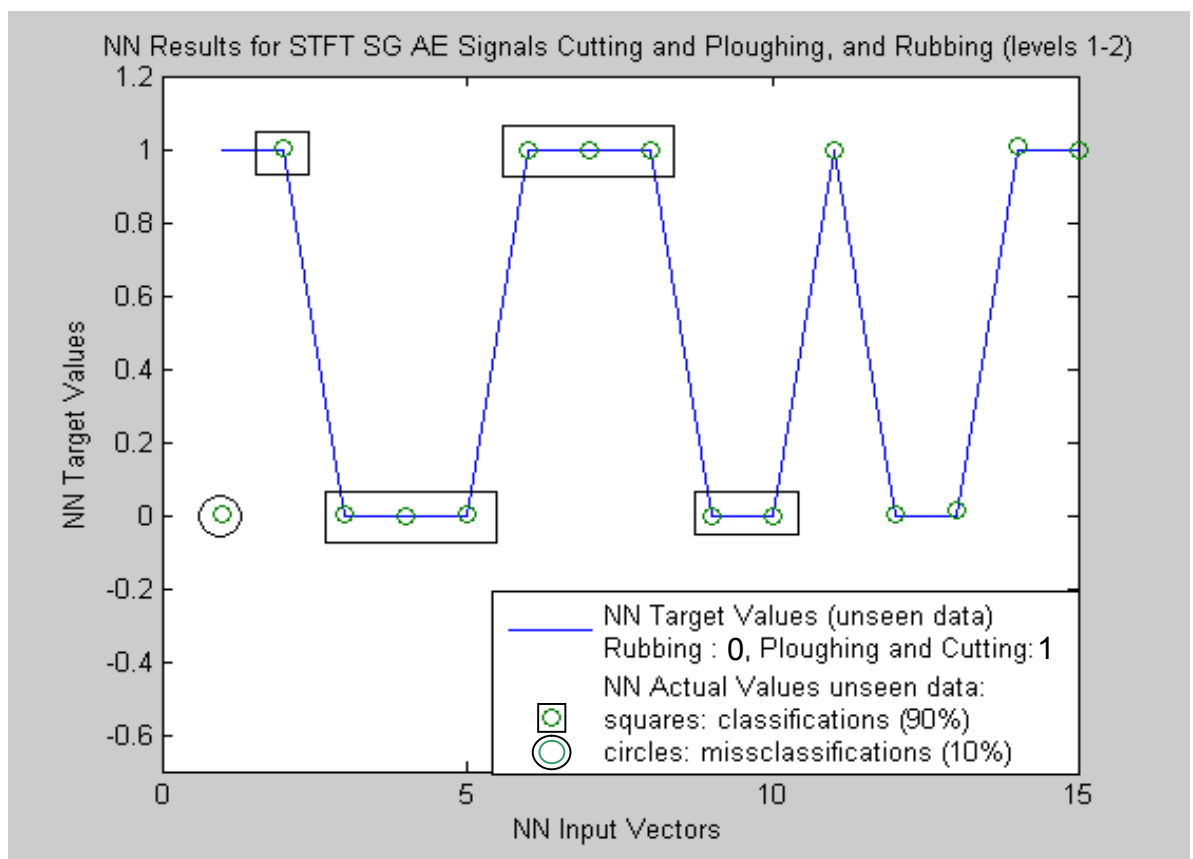
Figure 7.8 ANN Results for STFT AE of Cutting and Ploughing versus Rubbing

Figure 7.9 displays results that are again very encouraging with only 1 misclassification. The ANNs size were based on two hidden layers with the input layer having 256 inputs

(length of the STFT vector inputs) and the two hidden layers consisting of one and a half times the input neuron amount. The output layer was set to one to ensure a crisp output answer was obtained.
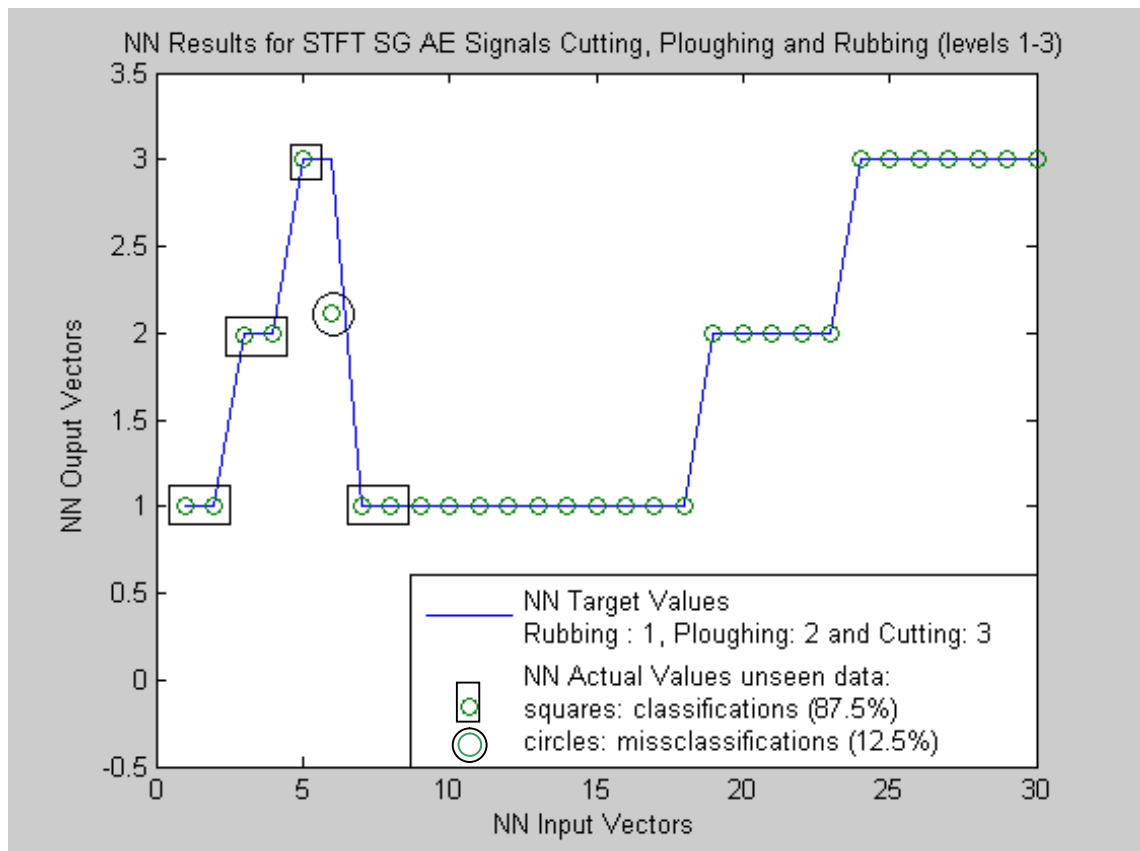
Figure 7.9 ANN Results STFT AE Rubbing (1), Ploughing (2) and Cutting (3)

Using a combination of WT and statistical windowing it was possible to get the salient principle components and obtain 100% classification for identifying both the two phenomenons' (Figure 7.10) and three phenomenon (Figure 7.11). Though there are two points slightly off the line.
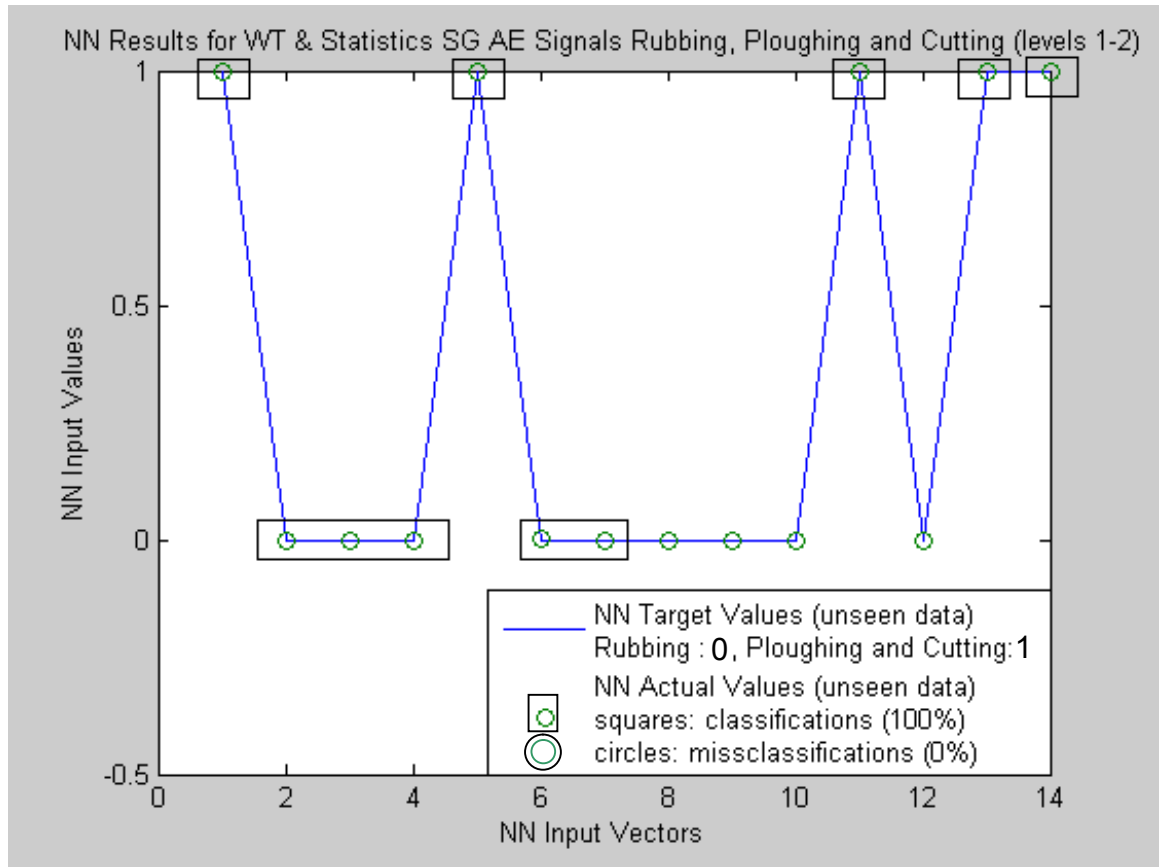
Figure 7.10 ANN Results WT & Statistics AE Cutting and Ploughing versus Rubbing
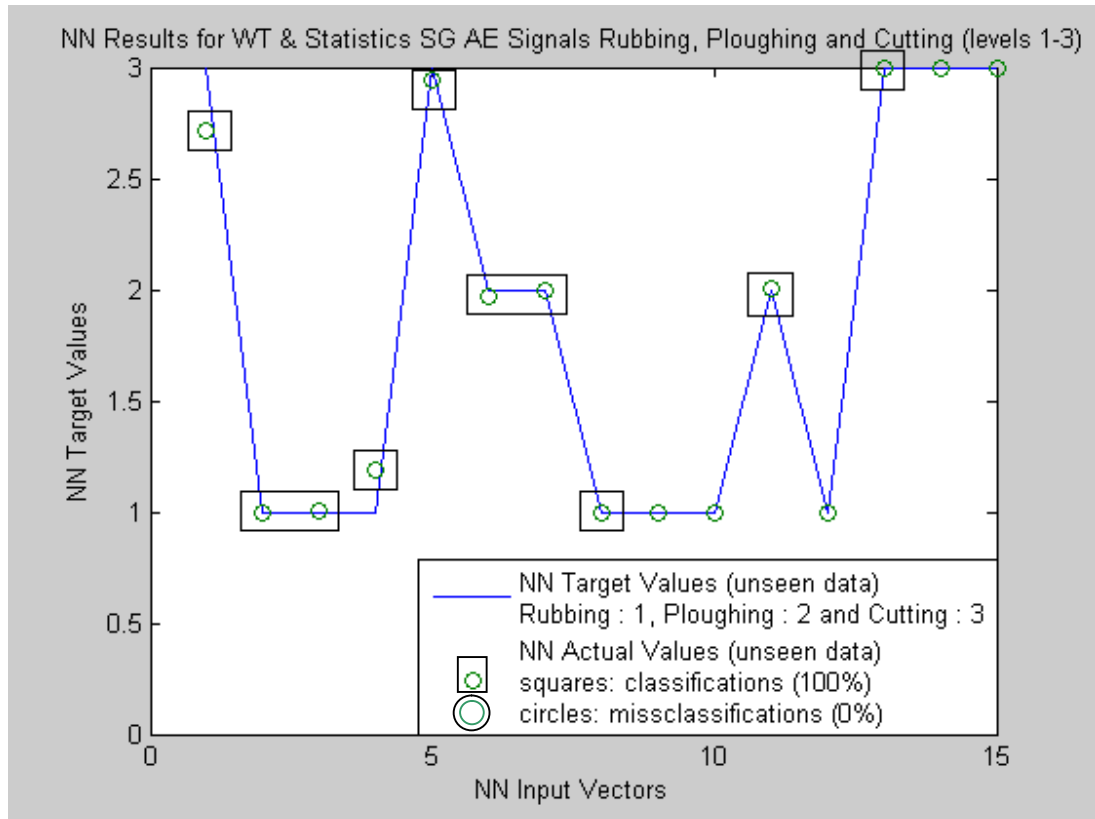
Figure 7.11 ANN Results WT & Statistics AE Rubbing (1), Ploughing (2) and Cutting (3)

The intensities are based on the area cut values between the surface cut material and the groove cut depth (reference Chapter 3 Figure 3.13 and Equations 3.1 to 3.4). This was considered as small data set although it encourages further experiments based on a larger cross section of different SG phenomenon cases which is more indicative of grinding with horizontal scratch cuts.

7.3   Horizontal Scratch Results

7.3.1 Signal Analysis of Cutting, Ploughing and Rubbing
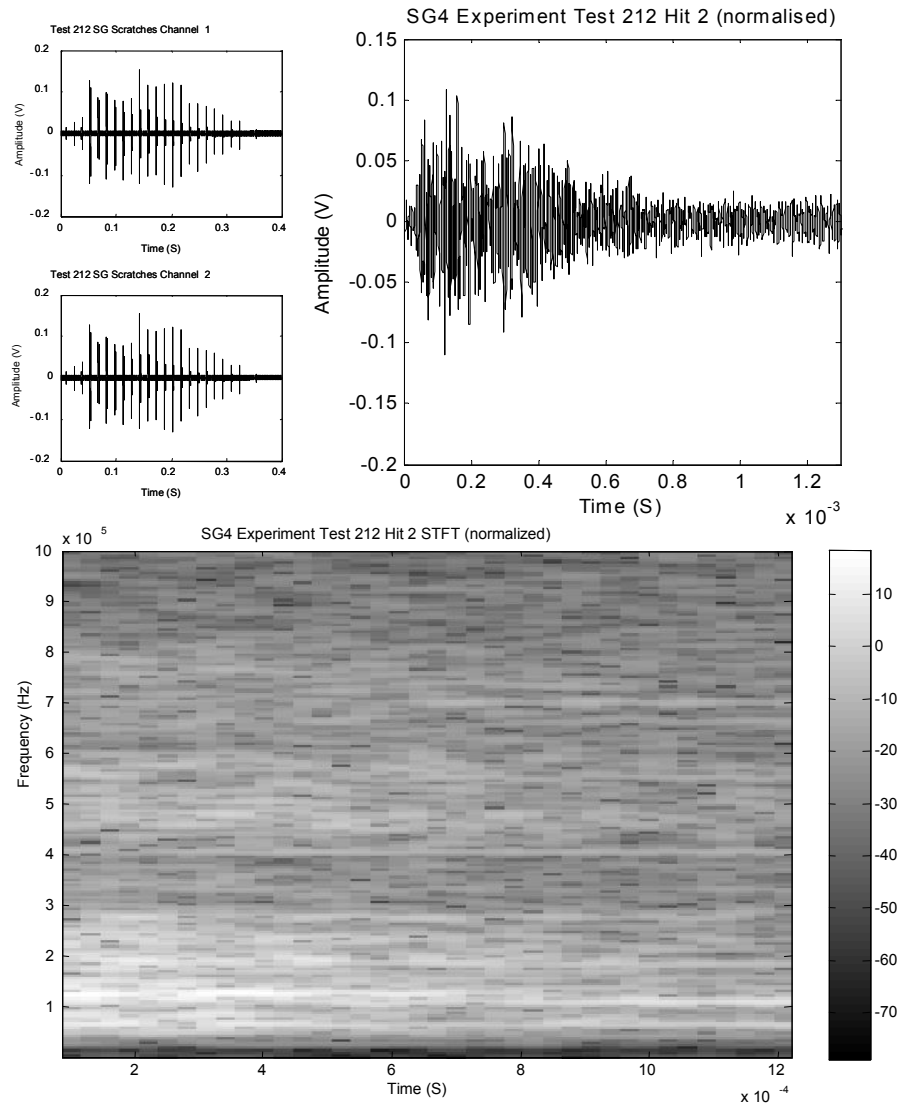
Machine: Makino A55; SG Material: Al$_2$O$_3$; Workpiece: CMSX4;
Single Grit Dimensional depth and width appx. 1μm;
Dry down grinding: Vs= 4000 RPM; Vw=4000 mm/min; Ap= 0.001 mm

Figure 7.12 Hit 2, Top: raw extracted time signal, Bottom: STFT

Looking at Figure 7.12, it was noticed that the changing feature of the intensity of AE signals was similar to shape of grit scratch. Therefore both amplitude of AE in time domain and the frequency band intensities could correlate to the material interaction characteristics identified as rubbing, ploughing, cutting, ploughing and then rubbing, though the AE wave response takes much longer than the actual mechanical interaction. Under such assumptions, the grit to workpiece interaction and AE extracted signal are consistent for calculations. The signal, through stretched, is still representative of the scratch interaction and the three phenomena could still be located as long as careful scratch map measurements are taken and the correct ratio measurements are applied to the STFT representation.

Machine parameters for the SG experiments were as follows: Single grit material was Al_2O_3, SG dimensional depths and widths were approximately 1.5µm. The SG advanced towards the workpiece with a one micron incremental step.

By slicing up the STFT representation of Figure 7.12, Figure 7.13 gives the relative FFT at different moments. The slice number correlates to a point in time along the STFT and displays the normalised energy for ploughing, cutting and rubbing. Predominately around the 100 KHz range, cutting has high magnitude intensities. Ploughing is similar to cutting however it just has one peak and two side band peaks either side of its feature frequency. The feature frequency of ploughing is approximately half the intensity found with that in cutting. Both cutting and ploughing have relatively similar amplitude intensities for 500 KHz although cutting appears to have more slight peak intensities

from 600 KHz to 750 KHz. Rubbing on the other hand has major frequency band peak intensities that are both above and below the machine noise level (see bottom right Figure 7.13). Rubbing can have higher magnitudes up to 0.9 and in some cases less magnitude than that seen from the extracted noise signal (major frequency band peak 0.6). This is where rubbing appears to damp the noise signal (see bottom left Figure 7.18).
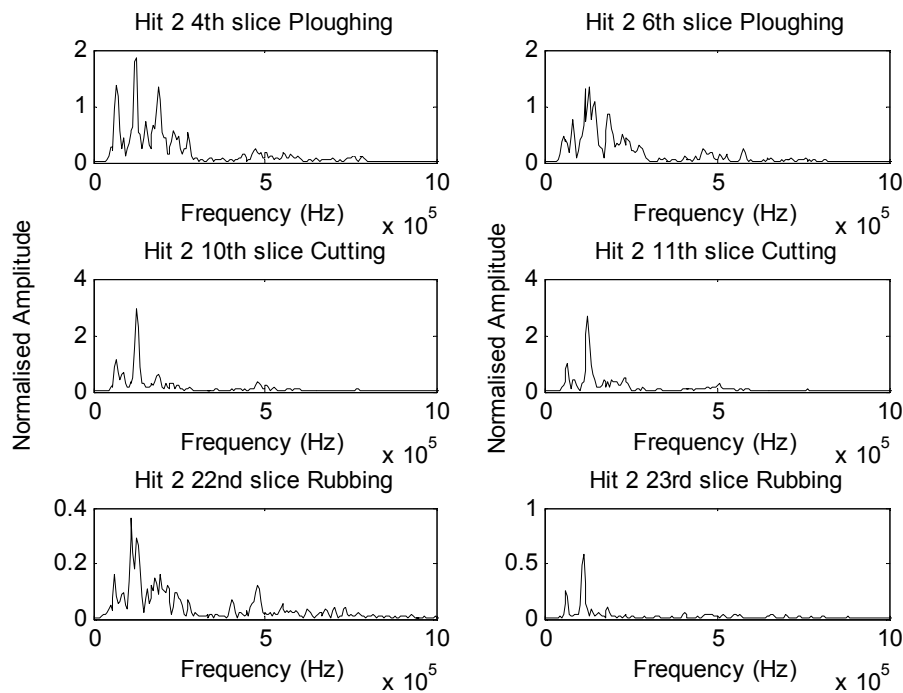
Figure 7.13 Test 212 Hit 2, Top: Ploughing, Middle: Cutting, Bottom: Rubbing

Figure 7.14 displays the AE signals of rubbing phenomena as there was no mark on the workpiece for the pass (test T211) just before the next incremental machine pass (test T212) which left scratch marks on the workpiece. The STFT analysis results shown in

The University of Nottingham

Figure 7.14 is similar to the rubbing features displayed in Figure 7.17. Note the scratch hit obtained for Test 212 contain all three phenomenon of cutting, ploughing and rubbing. Although most of the rubbing extracted signals came from Test 211 where 5 hits were extracted and no visible mark was made on the workpiece. This interaction gave good confidence of rubbing without plastic deformation.
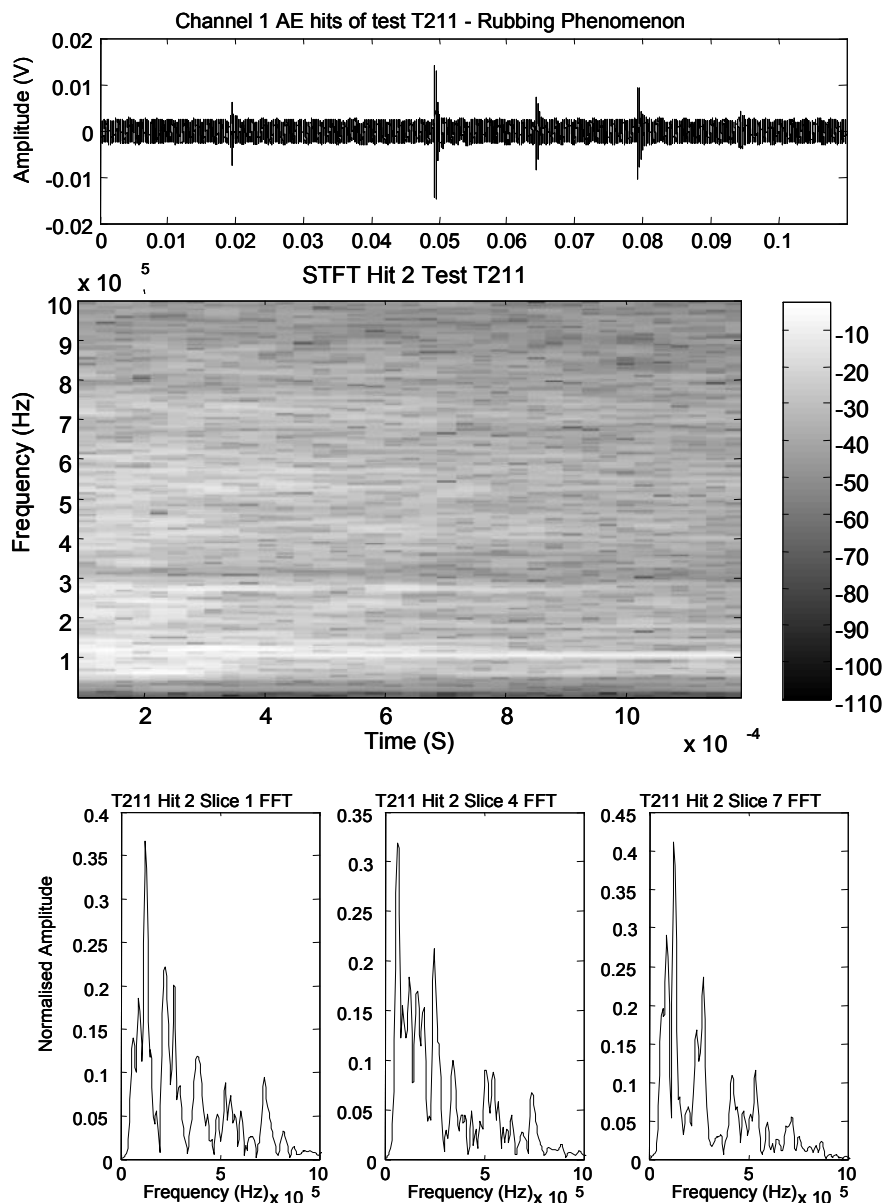
Figure 7.14 displays the hit before T212 contact (T211)

A STFT spectrum of the noise signal can be seen in Figure 7.15. The noise here displays constant frequencies although the intensities are fairly low and they are clearly different from rubbing signal phenomenon.
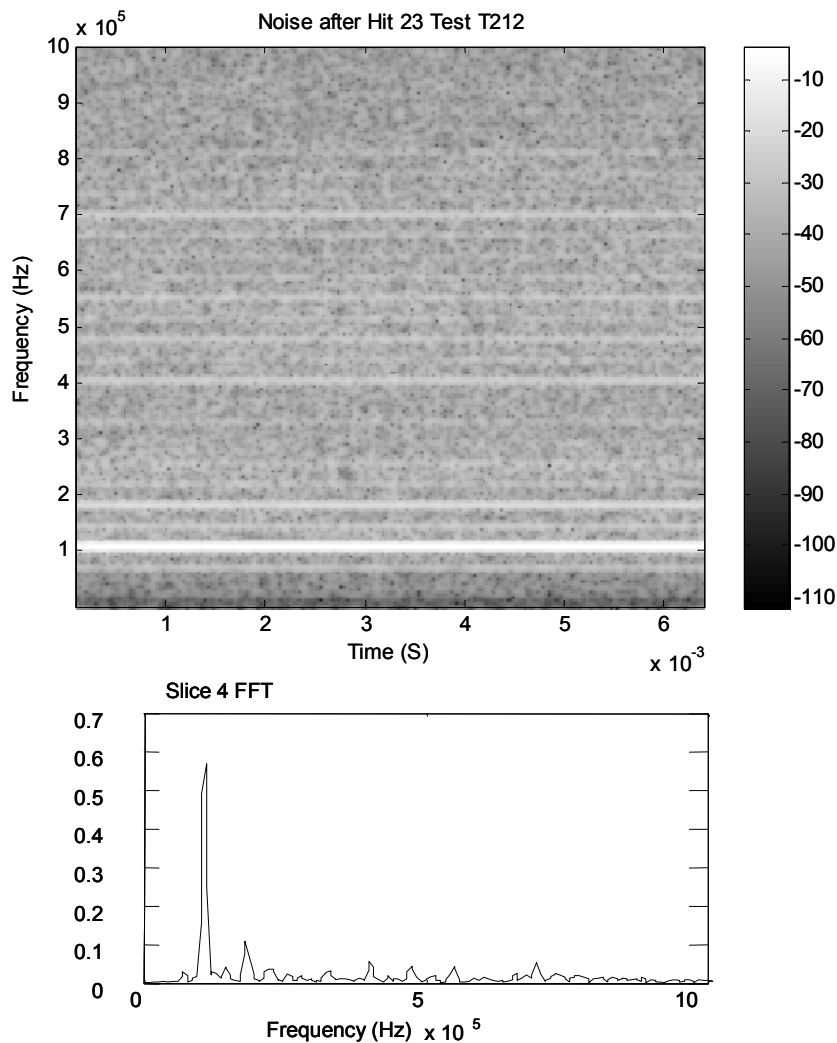
Figure 7.15 The noise signal extracted at the end of Test 212

With the different energy signatures occurring from the SG interacting within the workpiece the STFT provides a good solution for separating the cutting, ploughing and

rubbing phenomenon. Ploughing and cutting are somewhat similar in that the material is push/slide to one side or material removed which predominately cause material plastic deformation. The energy is consumed from surface deformation. In the rubbing case however there is surface friction (Kalpakjian and Schmid 2003) this suggests therefore, that different AE signatures should be apparent between the two different phenomena. Rubbing does not remove or slide any material away, instead, it touches the surface with no visible markings which signifies elastic material characteristics in that the material deforms and returns back to its original state after a SG pass has occurred. In short, the boundaries are much closer in terms of AE distinguishing features of ploughing and cutting. Ploughing and cutting are perhaps the most difficult phenomenon to separate based on this assumption. The classification technique need to be as accurate as possible to ensure the sharpness of the waveforms are accurately represented when trying to distinguish the frictional energy and material deformation energy in the form of plastic or elastic energy.

7.3.2 Material and Signal Signatures

Figure 7.16 Top displays the STFT for T212 Hit 17. The middle of the figure represents the FFT slices obtained from the STFT thus relating to the horizontal cross section cut profiles (Figure 7.16 bottom) which signify whether the signal is cutting, ploughing or rubbing. Equation 3.1 from Chapter 3 was applied to the material measurements along with general observations to decide the segregation of the identified phenomenon. For cutting phenomenon there are much higher amplitudes experienced than with ploughing and rubbing. For this particular material of CMSX4 all phenomena occupy the same

peak frequency bands however the higher amplitudes are for cutting, then ploughing and lastly, in between the machine noise (normalised magnitude of 0.6) with a magnitude of approximately 0.3 to 0.9 is the rubbing phenomenon. Each signal AE hit was normalised to a 1µm cut signal therefore ensuring with deeper/shallower cuts there was no crossover from the designated ploughing and cutting signals.

From those patterns ploughing occupied between 50 KHz and 300 KHz of the major frequency band peaks. The normalised FFT magnitude was between 1 and 2 with side bands either side of the largest frequency band between 0.7 and 1.4 normalised magnitudes. Cutting also had similar major frequency band peaks between 50 KHz and 300 KHz. The normalised magnitude for the major band peak was between 2.4 and 4 with side bands the same or slightly less than that of the ploughing side bands magnitudes. Both ploughing and cutting have slight frequency band peaks around the 500 KHz range and cutting has slightly larger peaks when compared with rubbing and ploughing at the 750 KHz range. Rubbing has major frequency bands between 30 KHz and 500 KHz with the major peaks ranging from 0.3 to 0.8 magnitude. With rubbing there are a range of energy bands either side of the dominant frequency band which are half the magnitude of the dominant frequency band for rubbing.

The University of Nottingham
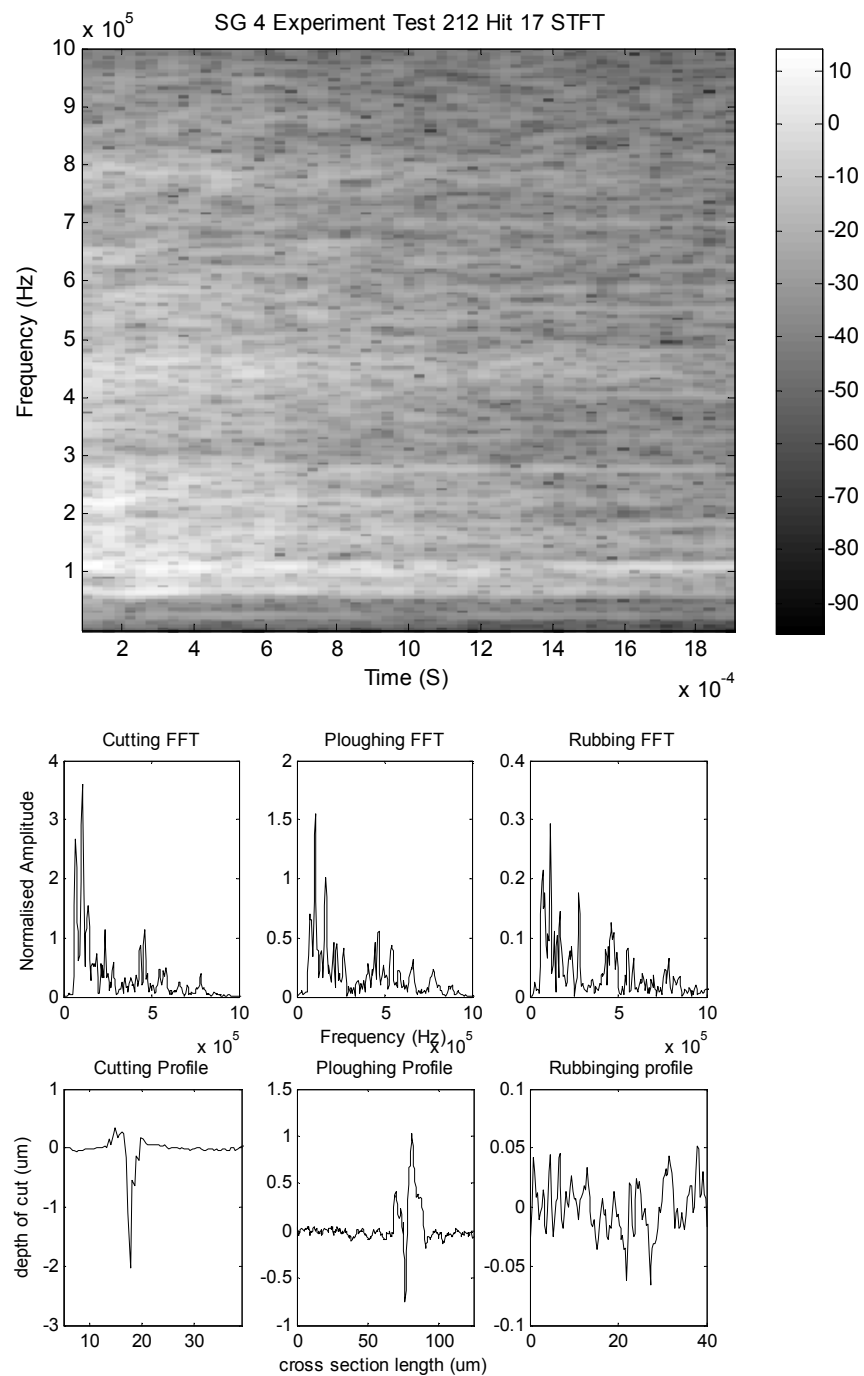
Figure 7.16 SG4 Test 212 Hit 17 displays the STFT (Top) and FFT slices (Middle) and profiles relating to cutting, ploughing and rubbing phenomenon (bottom)

7.3.3 Cutting, Ploughing and Rubbing Distinction for 1 μm and 0.1 mm grinding wheel passes

This section of the horizontal scratch cut results presents hit data taken from 1 μm and 0.1 mm grinding cut wheel data to classify against already identified cutting, ploughing and rubbing data extracted and analysed from the single grit scratch test results. This is where unknown data is presented to classifiers with no verified results and are based on the already presented training data. This section displays results for two classifiers, MLP Back propagation ANN and Fuzzy-c clustering. In addition, there was comparison with SVM, ANN with reduction time-frequency techniques and Fuzzy-c/GA clustering, this comparison looked at single grit scratch tests with Titanium-64 material.

7.3.3.1   ANN classification results

The supervised training method uses three times more examples than that of the examples used in both the test and verification data sets (in terms of vector numbers; 180 for training and 60 vectors for testing and verification data sets respectively). The network verification test set is similar to the test set although slightly different to ensure the network provides a good confidence when presenting its classifications. The classification accuracy is based on correct classification against misclassification data. The network momentum value was set to a high value to ensure the ANN can search beyond localised minimum and stick to the minimum post near global minima. Table 6.3 lists the parameters used in the ANN to classify the cutting, ploughing and rubbing phenomenon.

Figures 7.17 and 7.18 represent both the ANN test and test verification data sets. The STFT Signal ANN test results are very encouraging with an 87% unseen classification (out of total 60 test vector set) and overall network classification of 93%. To give further confidence (Peterson and Gerald 1992; James 1994), the STFT signal ANN test verification results give an 83% unseen classification accuracy and total network accuracy of 92%. These two sets of results are conclusive when classifying SG cutting, ploughing and rubbing phenomenon; two sets of similar test data are used to check consistency of results. The training data was 148 cases which were considered sufficient for data generalisation of the Neural Network.
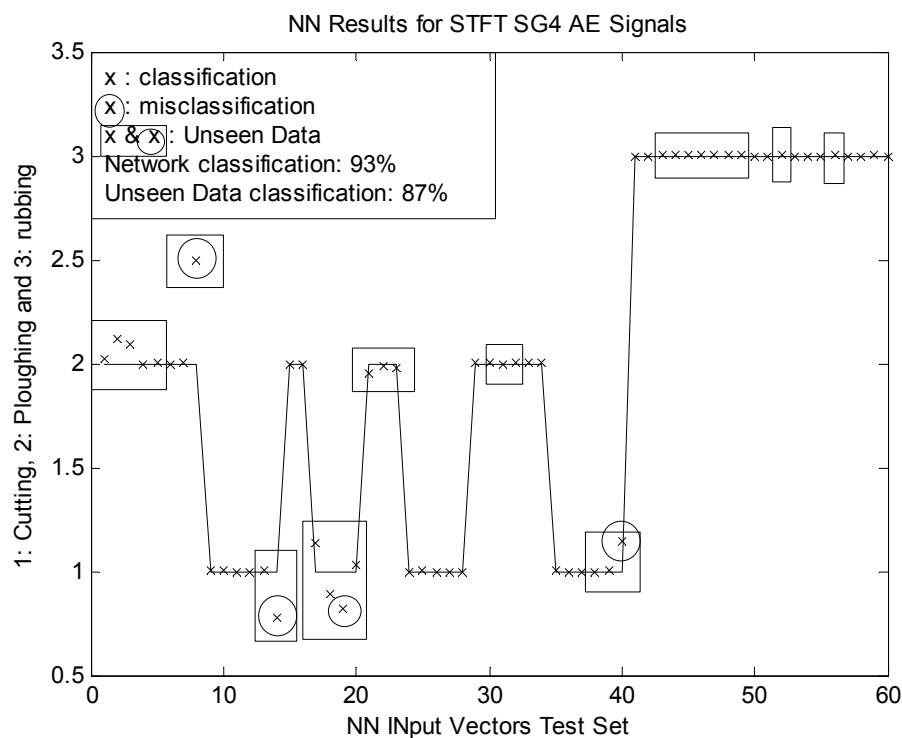
Figure 7.17 Displays the ANN Results for Cutting, Ploughing and Rubbing Test Set
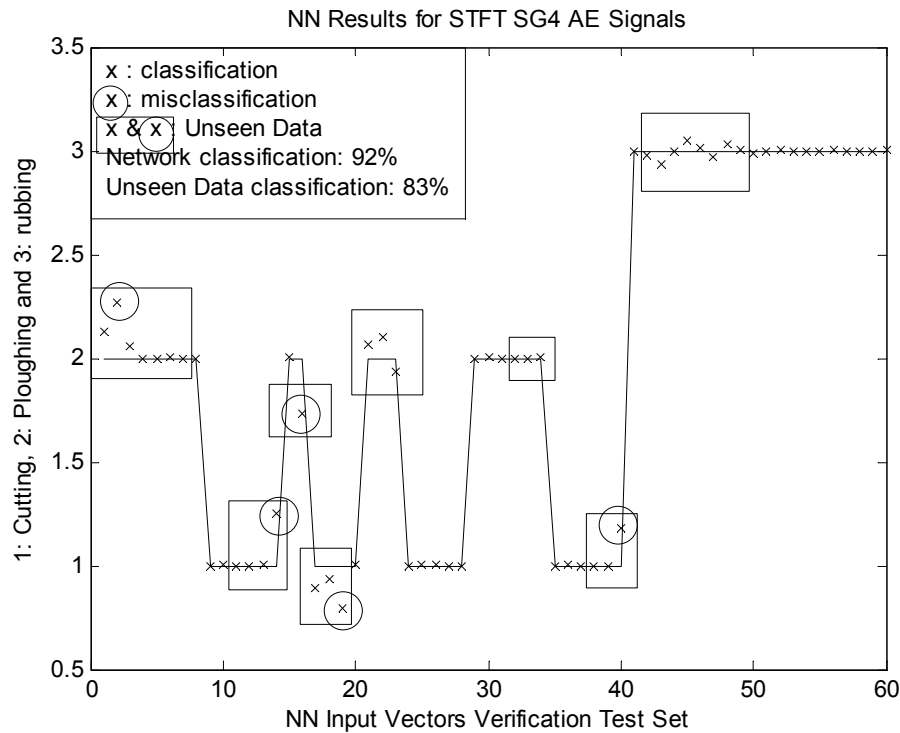
Figure 7.18 Displays the ANN Results for Cutting, Ploughing and Rubbing Verification Set

The next results present Hit 4, Hit 14 and Hit 15 of 1μm grinding cut pass and, Hit 20 of the 0.1 mm grinding cut pass respectively. In addition to the above, the third hit taken from the rubbing signal before Test 212 (Test 211) is also tabulated to show the classification of pure rubbing. Here a STFT of the hit data was taken from start of the hit AE profile to the finish. Table 7.3 represents the amount of hit data classified as cutting, ploughing or rubbing and the percentage amounts of cutting, ploughing and rubbing. Figure 7.19 displays the neural network outputs starting with the top left as hit 4, top right hit 14 and bottom left hit 15 for a 1 μm grinding wheel cut. Bottom right displays the ANN output for hit 20 of a 0.1 mm grinding cut. All grinding cuts had no coolant present. It is possible to see the profile of cut from the ANN outputs of Figure

7.19. Table 7.1 classifications used a rule based threshold system to gain a crisp cutting, ploughing and rubbing output, the rule being; if greater than 2.5 then rubbing, if less than 2.5 and greater than 1.5 then ploughing and if less than 1.5 then its cutting phenomenon. T212 Hit 2 data is total hit data and not segments used for training and test (top row). 1µm to 0.1mm cuts are for grinding wheel passes and not SG scratch experiments (both ANN and Fuzzy-c/GA results).

Looking at Figure 7.19 and Table 7.3 further, there appears to be more of a percentage of cutting for the more interaction between workpiece and grit. There is a higher percentage of cutting compared with ploughing and rubbing when the depth of cut is increased for grinding wheel passes (middle parts of the 1µm cuts had greater depth of cuts when measured against the beginning and end grit hits of the grinding pass – this is due to a greater surface area being present during the cut rather than at the start or end).

Table 7.1 displays ANN Test Vector Outputs for grinding wheel cuts

Test Set	ANN Cutting (C)	ANN Ploughing (P)	ANN Rubbing (R)	Total Vectors	C % correct/ total	P % correct/ total	R % correct/ total
Hits 1 to 23 T211/T212	17/20	18/19	21/21	60	27/33	30/32	35/35
Hit 3 T211 (rubbing)	0	0	21	21	0	0	100
Hit 2 T212	13	20	5	38	34	53	13
Hit 4* (*1µm cut)	14	17	16	47	30	36	34
Hit 14*	26	17	15	58	45	29	26
Hit 15*	28	29	5	62	45	47	8
Hit 20 0.1mm cut	34	24	2	60	57	40	3

With a pure rubbing extracted signal there is hardly any interaction between grit and workpiece which is also displayed by Table 7.1 results. The ANN Sum Squared Error (SSE) for the cutting, ploughing and rubbing tests was $5.24e^{-31}$ and the number of training epochs was 10000. This ANN engine was used throughout the applied hit data tests of 1μm cuts and 0.1mm cuts. The hit tests were applied to the ANN engine that had already gained 93% classification accuracy from cutting, ploughing and rubbing tests and was considered a good accuracy for applying the hit data tests. For instance; as the hits are classified from the 1st interactions (hit 4) to the mid interactions (hit 14 and hit 15) appears to have a higher percentage of cutting. Certainly with a mid hit of a 0.1mm depth cut there is a lot more cutting interaction and a lot less rubbing when compared to the 1μm cuts (more so with hit 4 than hit 14 and hit 15 as it is at the beginning of grit/scratch interaction). This signifies that cutting, ploughing and rubbing changes in ratio as there is more interaction between workpiece and grinding wheel (depth of cut increases therefore more grit interaction between material surface and grit). Note that AE of all depth-cut hits were normalised to a 1μm cut to compare the cutting, ploughing and rubbing training/test set (see Chapter 5, Section 5.6). The normalisation is used to distinguish between different material deforming phenomena. Looking at the lower right of Figure 7.19, the 0.1mm cut have more crisp cutting classifications than with other displayed grinding pass cuts this is due to the training data and 0.1mm grinding cut pass data being very similar in characteristics. With the other grinding pass cuts the ANN output displays linear regression with respect to the groove being cut.
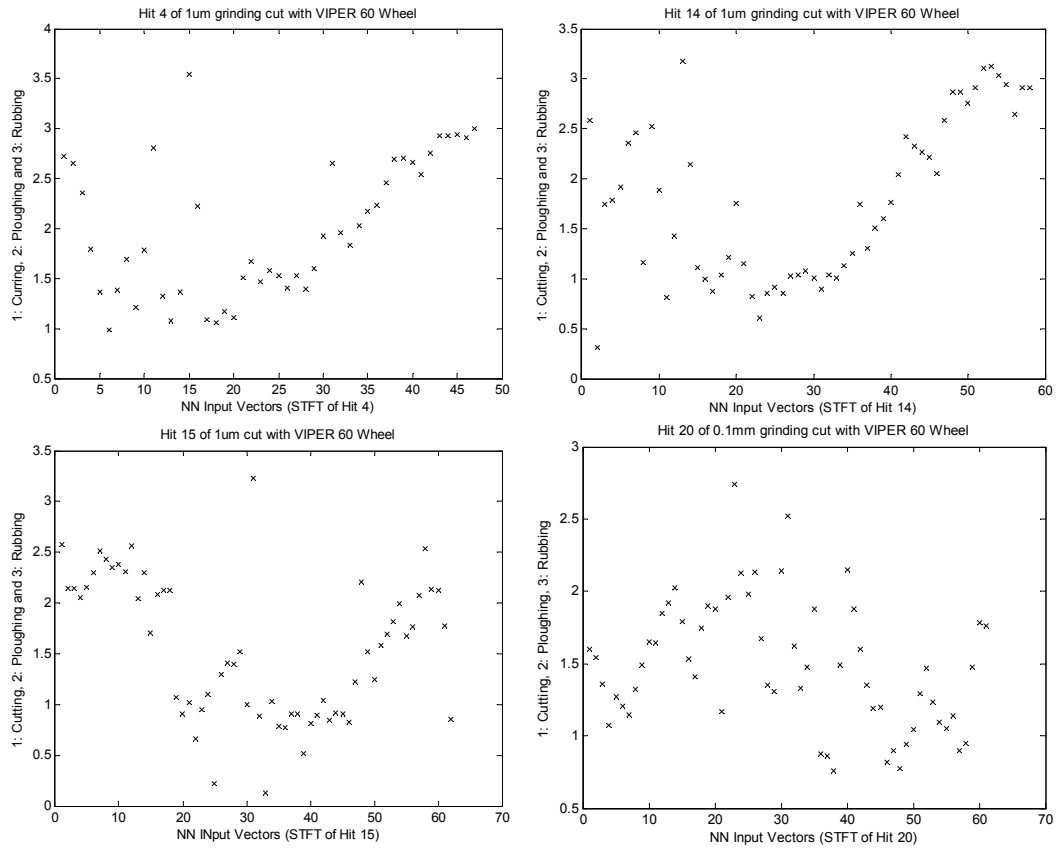
Figure 7.19 Top Left Hit 4, Top Right Hit 14, Bottom Left: Hit 15 (1µm cuts) and Bottom Right: Hit 20 (0.1mm cut)

7.3.3.2 Fuzzy-GA classification results

Figure 7.20 displays the equivalent fuzzy-c/GA cluster outputs to the ANN outputs of Figure 7.19. Figure 7.21 displays the first two principle components (which contain 65% of the total variance of the ~300 cases with 205 elements for each case (SG training and test data and unseen grinding pass data)). The fuzzy-c/GA outputs are mapped onto these two principle components which are based on the highest evaluated data cluster centre membership. For cutting data, 2 cluster centres were output based on the optimised criteria between fuzzy-c algorithm and GA.

The University of Nottingham
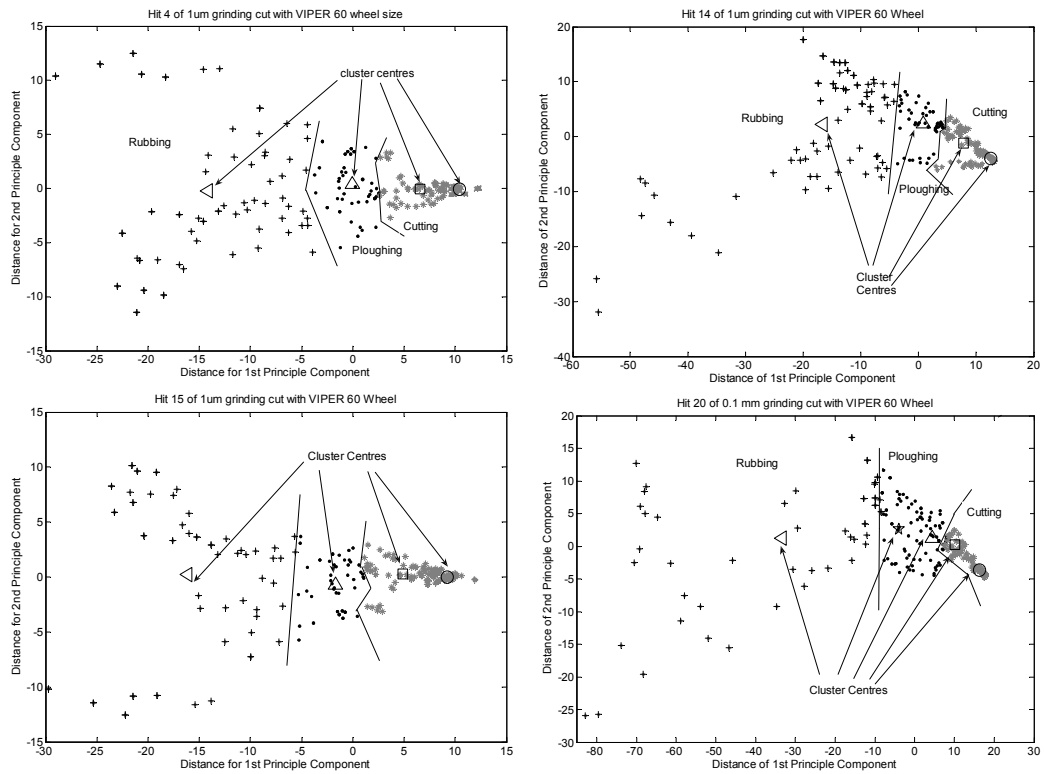
Figure 7.20 Fuzzy-c Clustering, Top Left: Hit 4, Top Right Hit14, Bottom Left: Hit 15 of 0.1um cut and Bottom Right: Hit 20 of 0.1mm cut

Table 7.2 displays the known classification accuracy of fuzzy-c/GA clustering. Here the correct/incorrect clusters were checked against the known phenomenon and a percentage of classification was determined. Table 7.3 displays the percentage of cutting, ploughing and rubbing phenomenon for Hit 4, Hit 14 and Hit 15, 0.1μm cuts and Hit 20, 0.1 mm cut.

Table 7.2 Fuzzy-c Clustering results for 0.1um cuts and 0.1 mm cut

Test Set	FuzzyGA Cutting (C)	FuzzyGA Ploughing (P)	FuzzyGA Rubbing (R)	Classification Accuracy %
Test SG4	61/62	43/47	81/97	90% (185/206)
Hit 3 T211 (rubbing)	53/55	51/66	84/85	91% (188/206)
Hit 2 T212	52/55	60/66	84/85	95% (196/206)
Hit 4* (*1μm cut)	69/69	41/50	71/87	88% (181/206)
Hit14*	42/48	58/59	68/99	82% (167/206)
Hit15*	46/46	72/96	55/64	84% (173/206)
Hit 20 0.1mm cut	39/44	82/85	77/77	96% (198/206)

Table 7.3 The Fuzzy-c cluster for the percentage of C, P and R phenomenon

Test Set	C %	P%	R%	Iterations & clusters	Fitness
Test SG4	33% (20/60)	23% (19/60)	44% (21/60)	78/4	0.7245
Hit 3 T211 (rubbing)	0% (0/21)	0% (0/21)	100% (21/21)	190/6	0.822
Hit 2 T212	32% (12/38)	61% (23/38)	8% (3/38)	153/5	0.1305
Hit 4 (1μm cut)	19% (9/47)	26% (12/47)	55% (26/47)	135/6	1.659
Hit 14 (1μm cut)	52% (30/58)	23% (13/58)	21% (12/58)	81/4	0.8862
Hit 15 (1μm cut)	58% (36/62)	24% (15/62)	18% (11/62)	165/6	1.85
Hit 20 0.1mm Cut	76% (48/60)	22% (13/60)	2% (1/60)	120/5	0.968

From looking at Table 7.3 it is again possible to see more utilisation of cutting, than ploughing and rubbing when the depth of cut increases leading to more interaction (more pressure/force exerted) between grit and workpiece. The fuzzy-c/GA classifier was first

The University of Nottingham

tested for the SG4 data (T212 & T211 cutting, ploughing and rubbing data) and the classifier produced a , 90% classification accuracy). Then the output of the hit data (for 1 µm and 0.1 mm cuts respectively) using the fuzzy-c/GA clustering classifier is displayed in Figure 7.21, this is in comparison with the ANN output displayed in Figure 7.19. For each individual hit, the classification consisted of both the training single grit scratch data and test set(s) used in the ANN experiments.
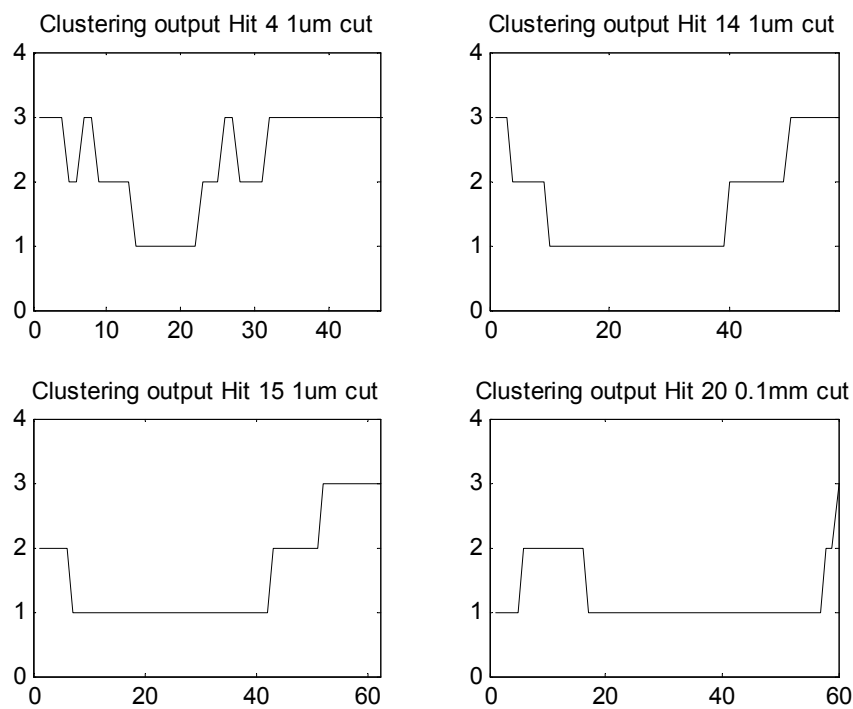
Figure 7.21 displays the Fuzzy-c Clustering and GA classification for grinding wheel cuts

When the associated hit data for 1 µm and 0.1 mm cuts were concatenated with the training and test data, the classification had to be recalculated each time a different hit was presented, this is due to the training and test (single grit scratch test and correlated measurements) data being of known phenomenon distinction and the 1 µm and 0.1 mm

The University of Nottingham

being of unknown phenomenon distinction. This creates a problem for verification purposes in that the more unknown data the less to check the recently added, additional test data. By calculating each individual test case to the known cluster memberships the more accuracy and confidence is gained in phenomenon distinction. It would appear that both the ANN and fuzzy-c/GA clustering techniques have given similar results and therefore the findings in this research are conclusive of the cutting, ploughing and rubbing phenomenon distinguished by the energy released from the workpiece and grit interaction in the form of an AE signal. That said, where the results are slightly in favour of one phenomenon than another when compared between the two classification techniques this can be attributed to incorrectly classifying a cluster set (hence no hard separation rule with fuzzy-c clustering, or cluster sets with low similarity membership intensities) or a lower returned fitness value. In short, if the classifier produces 90% or more for the known data set then there is more confidence when the rubbing, 1µm and 0.1mm cuts are introduced to the classifier.

7.4   Discussion of Results

7.4.1 Radial SG Scratch Tests

The Radial scratch tests were investigated to provide an initial look at the feasibility in obtaining AE footprints of cutting, ploughing and rubbing phenomenon and, to look at this phenomenon in terms of different material characteristics. The ANN results in this thesis are based on a small subset of classified results for Inconel 718 SG scratch cuts. The other materials provided similar classification results. Looking through this section it can be seen that the different materials provide different AE footprints for all

associated grinding phenomenon. This is consistent with Clausen's work (Clausen, Wang et al. 1996) in single grit cutting of granite rock. The Radial scratch tests provided more work in terms of material measurements as two workpieces 180 degrees apart provided the scratch cut measurement for material removal analysis. This work provided some very interesting initial results in using STFT and WT which both provided rich data representations of the raw extracted signals. There was a need for a more focused repeated set of SG scratch tests in the form of looking at one material and horizontal scratch tests are more akin to grinding pass tests.

7.4.2 Horizontal SG Scratch Tests

Comparing the results between the two classifiers (fuzzy-c/GA and ANN) there are differences between the given outputs. These differences can be attributed to the different methods of classification. For instance; looking at Figure 7.24 the ANN outputs for the rubbing, 1μm and 0.1mm cuts, have levels between 1 and 3 and were not identified as crisp integers. This is due to the presented data being similar albeit different to the training and test data set of the original ANN data set. The varying levels display linear patterns with reference to the interaction between the workpiece and grit. A threshold rule based system was used to classify which was cutting, rubbing and ploughing. The thresholds used were any input vector less than 1.5; cutting, greater than 1.5 but less than or equal to 2.5; ploughing, and >2.5 classified as rubbing. This hard classification rule based system segregates the boundaries based on absolute outputs. The fuzzy-c clustering/GA classification system looks at all the data points and works

out a crisp output although the identified cluster may have the same distance as another cluster or be very near to another cluster and therefore has attributes for both classes. It was noted that some of the outputs for the fuzzy-c clustering/GA classification system had data points belonging to two cluster pairs however the one absolute cluster was chosen based on its position in the identified fuzzy matrix. The output differences have correlations with each other in that the more workpiece and grit interaction through measured depth of cut the more cutting phenomenon occurs followed by ploughing then lastly, rubbing. Both classifiers had a high confidence in terms of classifying both the training and test data with 93% and 90% respectively for the ANN and fuzzy-c clustering/GA classifiers. That said, the hit data presented to the ANN had close boundary conditions and with the hard rule based threshold post-processor, the data applied to the ANN for 1μm and 0.1mm cuts, could have had output cases classified as cutting when instead they were ploughing and the same for ploughing with rubbing. With fuzzy-c/GA the results that were significantly different to the ANN results had a higher fitness function, when a lower fitness function returns higher classification accuracy. In addition, more clusters are returned which can easily be classified incorrectly giving an incorrect classification. Even with some similar but slightly different results gained by the comparison of the two classifiers a pattern can be seen in the classification of the three phenomena. This pattern is summarised as greater intensities towards rubbing when grinding wheel passes with slight touch and, greater intensities towards cutting when operational conditions for a grinding wheel pass exists.

7.5 CMSX4 and Titanium-64 SG horizontal scratch test

The results discussed in this section looks at the comparison of two AE footprints for two different materials in terms of cutting, ploughing and rubbing phenomenon. In addition comparisons between three classifiers are made to see which classifier is better at mapping n-dimensional non linear data sets. The Classifiers are the ANN, Fuzzy-c/GA assisted clustering and Support Vector Machines (SVM) using the radial basis kernel functions (see end of Chapter 6). The same set-up as the horizontal scratch tests was applied to the Titanium-64 scratch tests. However the SVM classified multiple data in the following way, classified two classes of cutting and ploughing (accuracy of segregations tabulated) and then two classes with cutting and ploughing as one class and rubbing as the other (accuracy of segregation tabulated) two data sets in two different classifications thus cutting and ploughing

Figure 7.22 displays the FFT slices taken from the STFT representation of a filtered AE signal for the CMSX4 material the same as those presented in Figure 7.16, of the CMSX4 horizontal SG scratch tests.

The University of Nottingham
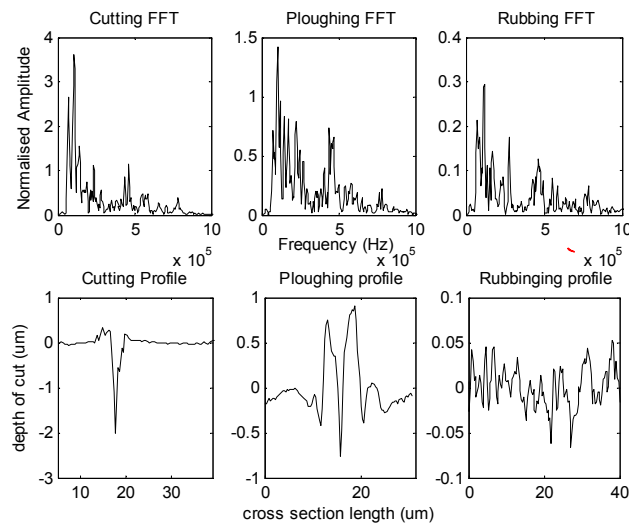
Figure 7.22. Top: CMSX-4 FFT of phenomenon on, Bottom: material cross section profile

For comparison purposes Figure 7.22 displays the FFT slices obtained from STFT representation of the extracted AE signal. Figure 7.23 results were obtained from the SG tests of the Titanium-64 aerospace alloy. As expected, the FFT representing the cutting data has much higher magnitudes when compared with both ploughing and rubbing phenomenon. Cutting has higher magnitudes at frequency bands 100 KHz, 250 KHz and 600 Khz with a major peak at 500 KHz. Ploughing on the other hand has a similar utilisation of the frequency bands however the magnitudes are lower when compared with the cutting phenomenon. One interesting observation is that there are two major frequency bands at 450 KHz and 550 KHz for ploughing. The rubbing phenomenon has much lower magnitude intensities when compared with both cutting and ploughing phenomena however the major frequency bands occupy 100KHz and 250 KHz where a shift is observed compared with the other phenomenon. Looking at both CMSX4 and Titanium-64 results it is possible to see that two materials (diverse material

characters) exert different AE signatures during the SG scratch test which is consistent with AE research (Clausen, Wang et al. 1996).
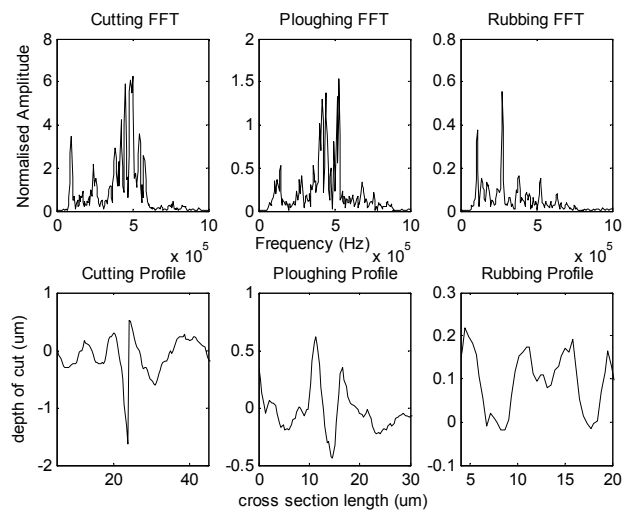
Figure 7.23. Top: Titanium-64 FFT of phenomenon on, Bottom: material cross section profile

The Tables 7.4 and 7.5 display the classification totals for unsupervised as 100% and unsupervised out of the correct classification %, miss classifications have not been counted in the cutting, ploughing and rubbing % utilisation.

Table 7.4 displays ANN and Fuzzy-GA CMSX4 results

Test Set	Cutting (C)	Ploughing (P)	Rubbing (R)	Total correct classification
ANN Test SG	27%	30%	35%	92%
ANN 1μm cut	45%	46%	8%	92%
FuzzyGA TestSG	30%	23%	47%	90%
FuzzyGA 1μm cut	22%	46%	31%	88%

The Training data vectors used 160 cases of cutting, ploughing and rubbing with 60 cases of cutting, ploughing, rubbing for both test and verification data sets. Within the 60 cases half were unseen by the classifier and determined the classifiers generalized behaviour. The 1um cuts were extracted straight from the hit data of a 1um grinding wheel pass and presented directly to the classifier.

Table 7.5 displays ANN and SVM Titanium results

Test Set	Cutting (C)	Ploughing (P)	Rubbing (R)	Total correct classification
ANN Test SG4	25%	25%	50%	90%
ANN 1μm cut	36%	28%	36%	91%
SVM Test SG4	17.5%	17.5%	50%	95%
SVM 1μm cut	35%	32%	24%	93%

From looking at the results presented in Tables 7.4, there is no real difference in terms of classification accuracy between the ANN and Fuzzy-c/GA clustering. For Table 7.5 the SVM out performs the ANN this is based on the superiority of SVM when dealing with n-dimensional intensive data sets.

7.6 Conclusions

The gaps that have been addressed in this chapter are as follows:

- Using STFT technique to identify cutting, ploughing and rubbing AE footprint signatures.

- Using WT technique to identify and verify the grinding phenomenon, namely cutting, ploughing and rubbing AE footprint signatures.

- Distinguishing and classifying both radial and horizontal single grit scratch tests in terms of AE footprint signatures correlated to measured material removal rates.

- Classifying 0.1µm and 0.1mm horizontal grinding pass cuts when presented to classifiers with previously trained and classified SG scratch cuts.

- Looking at the AE signatures correlated to cutting, ploughing and rubbing phenomenon for different materials with diverse material characteristics.

- Produced accurate and comparable results for a novel Fuzzy-c/GA clustering algorithm against conventional ANN MLP classifier.

The University of Nottingham

Chapter 8 Classification of Grinding Anomolies

8.1   Grinding Anomalies Parameters

This chapter discusses the grinding conditions, the extracted experimental signals and classifications carried out during multiple classification research work within this thesis. Within this section the first grinding parameters that will be discussed are grinding burn trials. The trials are dependent on keeping the wheel speed and feedrate constant and increasing the depth of cut to obtain the grinding burn anomaly. For the grinding burn phenomenon trials the parameters of Table 8.1 were used. Not all the tests gave burn as this was to compare burn and no burn. With the parameter increase in depth of cut, the more % surface burn was observed.

Table 8.1 Grinding conditions for burn trials

Grinding Parameter	Condition
Depth of cut	0.1mm – 0.6mm & 1mm
Feedrate	1000 mm/s
Wheel speed	35 m/S
Wheel diameter	134.94 mm
Wheel Material	Al_2O_3
Work piece Material	Inconnel 718
Lubricant	None

The research presented in this chapter looks at several types of extracted signals taken from both the dry grinding environment to obtain burn characteristics and the use of coolant for chattering characteristics (both trials used the same machining parameters and Inconnel 718 material, however chattering trials used faster wheel speed). Coolant burn trials were then investigated which looked at different materials such as CMSX4

The University of Nottingham

and Titanium-64. The signals of these two experiments will be discussed and displayed in terms of feature classification. The extraction and signal processing techniques of each sensory signal will be discussed further as they play an important role when presenting the information to the classifier system. The main focus of the work in this chapter is to display multiple classifications for a novel hybrid classifier to display a generic classifier looking at different demes of information. The dry burn tests used the parameter of depth of cut change to experience from no burn to increasing levels of burn. The first dry cuts with low depth of cut provided normal grinding cut signals and this resulted in both burn and no burn extracted signal waveforms.

Chattering or chatter however is another grinding machining phenomenon that needs to be identified and monitored. Chatter is caused from machine vibration during high speed manufacturing (Chen, Rowe et al. 1996; Fu, Raja et al. 2002; Li, Gracewski et al. 2002; Oscar, Eduardo et al. 2006). The Chatter is identified through force, acceleration, power and acoustic emission signal extraction. This research also looks at the investigation and classification of chatter through Acoustic Emissions (AE). The AE signals are verified with force, acceleration, power signals, roughness measurements, observations and audible chatter detected by the trained ear.

Chattering produces surface waviness and can be measured from surface roughness measurements with a talysurf measurement system. This investigation looked at both STFT and WPT to convert the raw extracted AE time signal into a time based signal, segmented into different frequency bands.

The classifier systems are presented with rich although prolix range of information and therefore the transformed information from the time domain is further cut down by statistical windowing techniques and then presented to the classifier. With some of the classification techniques presented, other n-dimensional reduction techniques were also used in place of statistical windowing techniques such as independent component analysis (ICA). Table 8.2 displays the grinding conditions used for the chatter phenomenon trials. Chatter would be achieved from the increasing levels of wheel loading by making several passes with the conditions presented in Table 8.2 with only pre-trial wheel dressing carried out for each individual chatter trial.

Table 8.2 Grinding conditions for Chatter trials

Grinding Parameter	Condition
Depth of cut	1mm
Feedrate	1000 mm/s
Wheel speed	55 m/s
Initial wheel diameter	138 mm
Wheel Material	Al_2O_3
Work piece Material	Inconnel 718
Lubricant delivery	Yes

For both trials (chatter and burn) the machine was set-up with a fixed workpeice and grinding wheel attached to the spindle. Instrumentation sensors were initially checked for reliability and correct amplifier sensitivities to ensure the signal intensities would not saturate and render the results unusable. The wheel diameter was measured followed by the dressing of wheel. The sensors would then be fastened to the workpeice and protected from the harsh grinding environment. The AE sensor system would be calibrated by a 2H, 5mm automatic pencil (Barbezat, Brunner et al. 2004). Grinding conditions were adjusted as required for the experiment (in this case increasing depth of

cut with no lubricant in order to gain burn and more intense burn characteristics). The extracted signals would then be logged and saved to files. The thickness of the wheel would be measured along with surface integrity images of wheel and workpeice. For image data in regard to wheel loading; a microscope image (25x magnification) was taken after every third cut. The sample thickness would be measured and noted along with observations of the temper colour change signifying physical burn characteristics. These steps would be repeated for successive depth cuts and the measurement of the wheel diameter at the end of a trial would be carried out. For validity of the experiments, duplication of the experiments would exist in a sequential manner. The signal processing techniques ranged from using the raw extracted temporal AE signal to using the STFT/WPT of the raw extracted signal along with statistical measures of the force extracted data. Both the dry burn runs and chattering experiments used Inconnel 718 material, for the grinding burn trials with coolant, two different materials were used; CMSX4 and Titanium. The grinding signal analysis for burn of CMSX4 and Titanium will be discussed at the end of this chapter along with CMSX4 trials accompanying thermocouple heat measurements.

8.2   AE and Force Identification

Figure 8.1, top, displays the raw extracted AE signal representing grinding chatter and bottom displays grinding burn. This raw form of the AE signal is then converted into both the frequency and time domains through DSP techniques such as WPTs and STFTs. These transformed signals are then ready to be applied to classifier technologies however in some cases the transformed data may be still too large for application to the

classifier and therefore require further reduction in terms of concise, salient components. Such reduction techniques have already been discussed at length in Chapters 5 and 6 and are significant for multiple robust process monitoring classifiers.
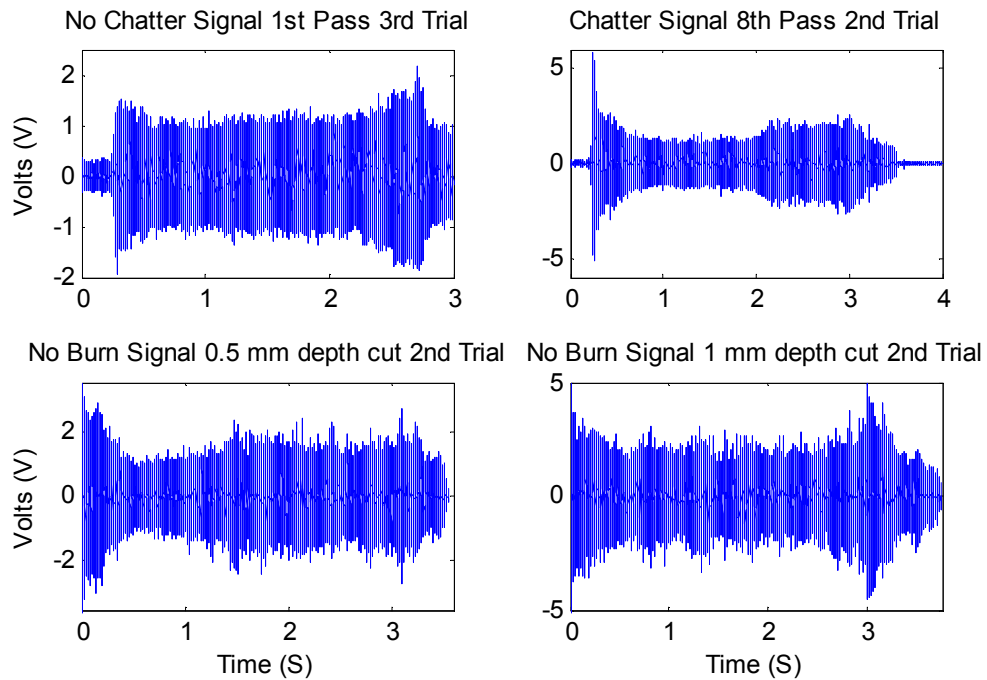
Machine: Makino A55; Grinding Wheel: Al_2O_3; Workpiece: Inconnel 718; Burn trials A_p 0.1mm → 0.6mm and 1mm, wheel thickness 15mm ; Chatter trials A_p 1mm; Dry down grinding: Vs= 35 m/s; Vw= 1000 mm/min; Coolant down grinding: Vs= 55 m/s; Vw= 1000 mm/min;

Figure 8.1 Top: No chatter and chatter raw AE extracted signal Bottom: no burn and burn

Figure 8.1 displays the raw extracted AE signals for no chatter/chatter and no burn/burn respectively. With respect to both phenomena the AE signal tends to rise for different phenomenon, however DSP techniques are used to distinguish which frequency bands are more prominent for which particular anomaly. Figure 8.2 displays the conversion of the raw extracted time signals displayed in Figure 8.1 to the STFT representation. This displays both the time and frequency information at the same time. Looking at the top

The University of Nottingham

representations the chatter intensities are higher than the non-chatter intensities. This is displayed more in the actual segmentation of the FFT strip taken from the STFT representation displayed in Figure 8.3. A pattern that is generally indicative of burn is displayed at the bottom half of Figure 8.3 where the AE intensities are higher in magnitude when compared to that of no burn. In addition, AE intensity bands increase in the mid bands of the AE sensor frequency response bandwidth. For many materials signifies burn/severe burn. The Chatter frequency components are more salient and defined when compared with no chatter, however the intensities are confined to lower frequency band components. Also for chatter signal analysis, the higher frequency band at 500 kHz is more prominent (less mechanical noise present in the chatter case) when compared with no chatter. With burn, both the lower and higher intensity frequency bands (100 kHz and 550 kHz) are much higher than no burn. There is also a chatter frequency band at 850 KHz where burn has frequency components across the whole signal spectrum unlike grinding with no burn.

STFT and FFT slices are a simple yet effective way of representing the time-frequency domain information and are often the DSP choice based on its ease of use and non computationally demanding algorithms. As mentioned in Chapter 5 STFT lacks the resolution in either the time or the frequency domain. If however a number of trial and error signals are carried out then a good trade-off between both the time and frequency domains can be achieved. WPT answers the problems in terms of individual domain resolution and the technique compactly supports the signal where the windowing

technique is dynamic for both high and low frequency components providing good resolution for both time and frequency domains.
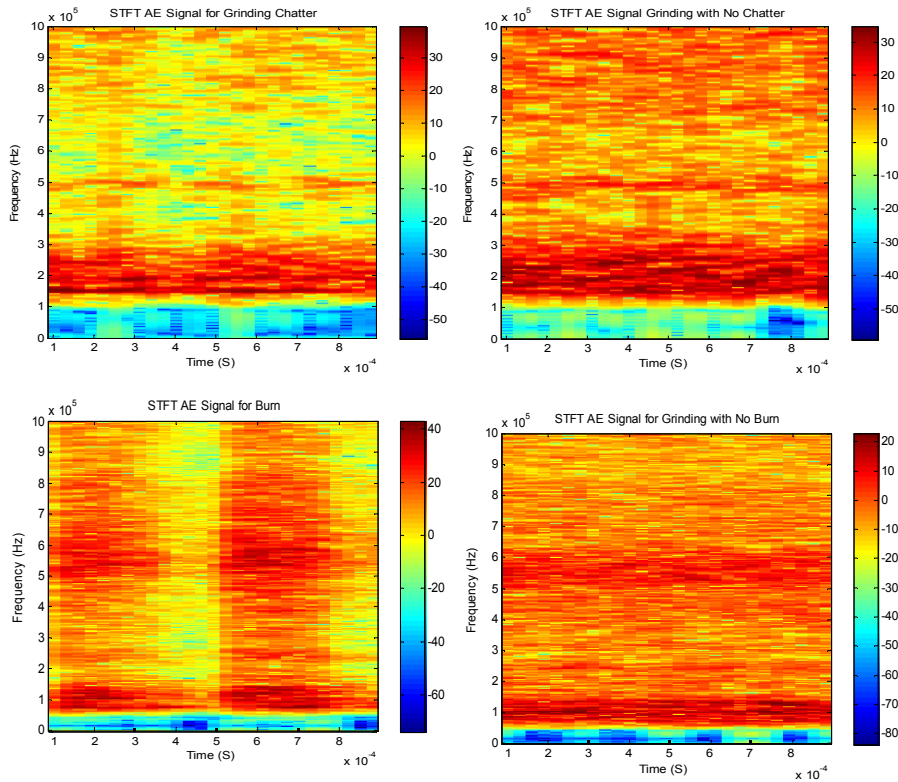
Machine: Makino A55; Grinding Wheel: Al_2O_3; Workpiece: Inconnel 718; Burn trials A_p 0.1mm → 0.6mm and 1mm ; Wheel width 15mm; Chatter trials A_p 1mm; Dry down grinding: Vs= 35 m/s; Vw= 1000 mm/min; Coolant down grinding: Vs= 55 m/s; Vw= 1000 mm/min;

Figure 8.2 Top: STFT for burn and no burn and Bottom: STFT for chatter and no chatter

WPT coefficients are displayed in Figure 8.4, this rich information can provide more domain orientated information however when presented to the classifier can present a problem in that the classifier may be overwhelmed from correlating too many dimensions of information. Following on from Figure 8.4, Figure 8.5 displays the WPT tree composition of the chatter and burn with normal grinding displayed in Figure 8.6.

The University of Nottingham

Such information can be too large and for application to the classifier a reduction technique such as Principle Component Analysis (PCA) or Independent Component Analysis (ICA) is required before classifier introduction.
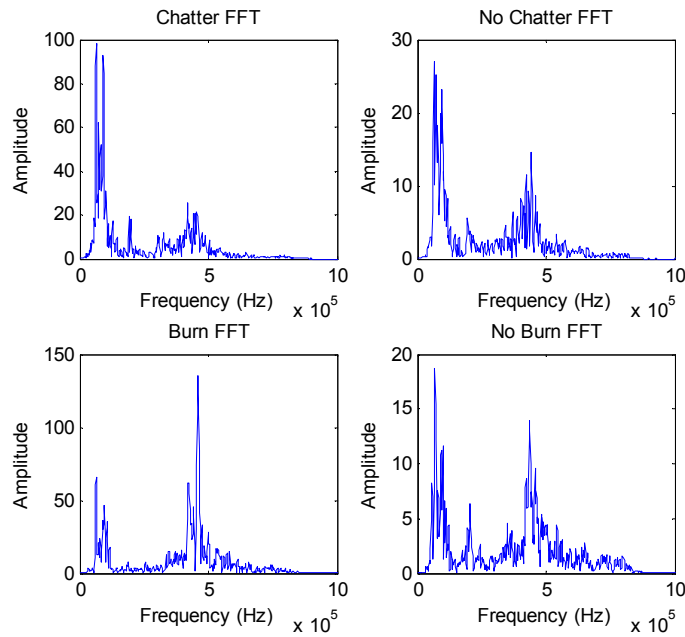
Figure 8.3 Top: FFT chatter and non chatter Bottom: FFT burn and no burn amplitudes*
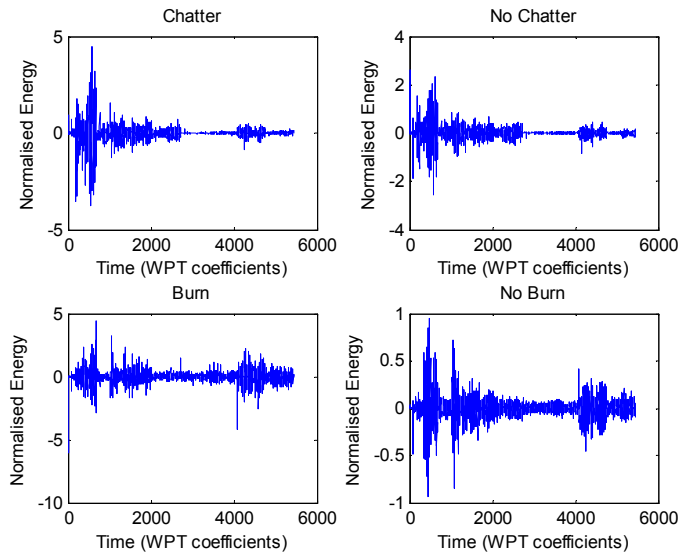
Figure 8.4 Top: WPT coefficients chatter and non chatter Bottom: WPT coefficients burn and no burn*
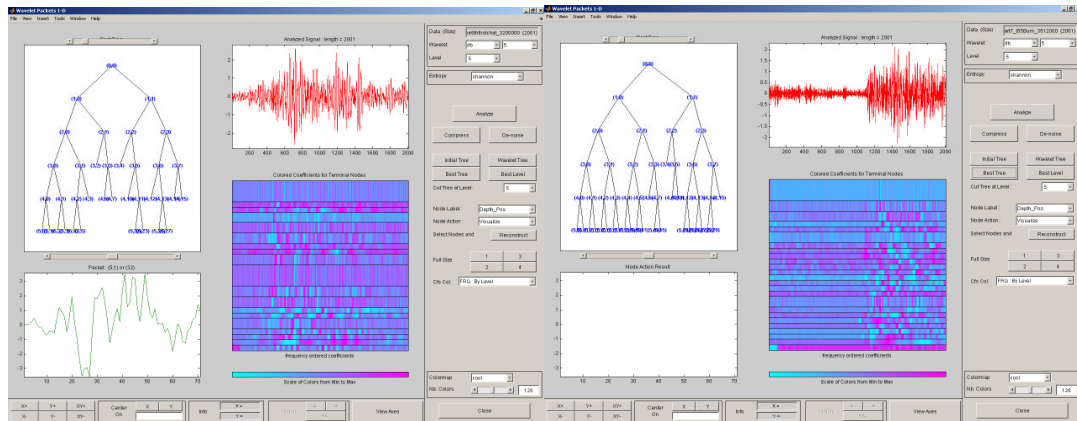
Figure 8.5 displays WPT Composition Tree for grinding chatter and burn*
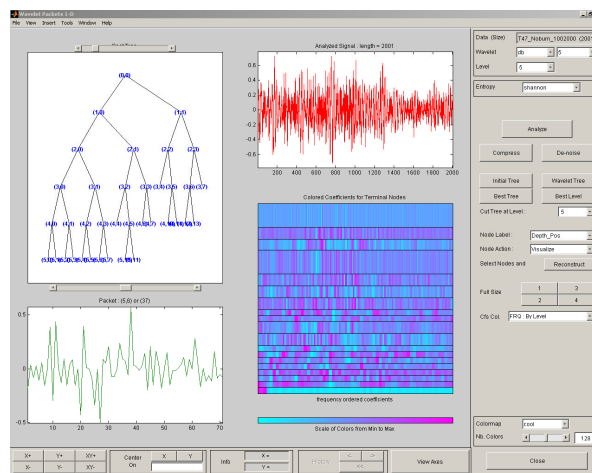
Figure 8.6 displays WPT Composition Tree for normal grinding*
*Grinding Conditions: Machine: Makino A55; Grinding Wheel: Al_2O_3; Workpiece: Inconnel 718; Burn trials A_p 0.1mm $\rightarrow$ 0.6mm and 1mm ; Chatter trials A_p 1mm; Dry down grinding: Vs= 35 m/s; Vw= 1000 mm/min; Coolant down grinding: Vs= 55 m/s; Vw= 1000 mm/min;

Generally speaking, WPT representations provide a 10% increase in accuracy when compared with using STFT representations although there is the undesirable aspect of an increase in computation. This factor of being computationally demanding and extra preparation for the introduction to the classifier can hinder the practicality in using such algorithms for robust industrial manufacturing environments. That said, WPT can be

used to verify STFT results and search for very difficult phenomenon in providing the outlier signal cases presented by extracted signals.
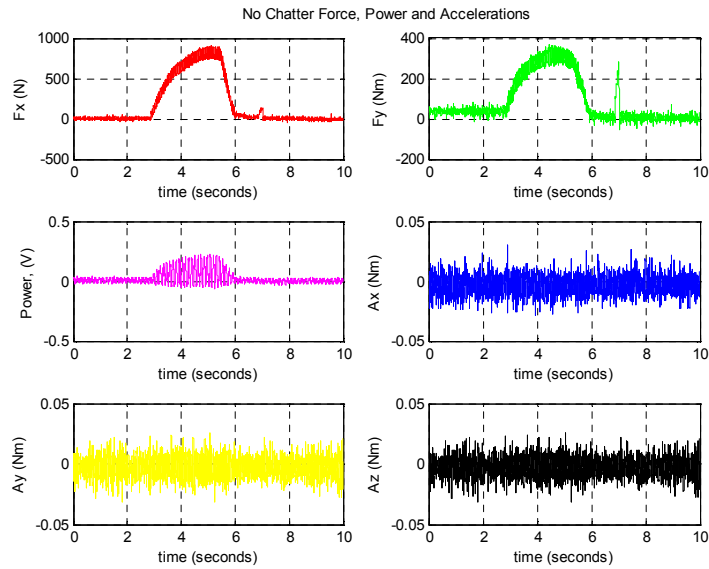
Figure 8.7 Inconnel 718 No chatter force, power and acceleration measurements
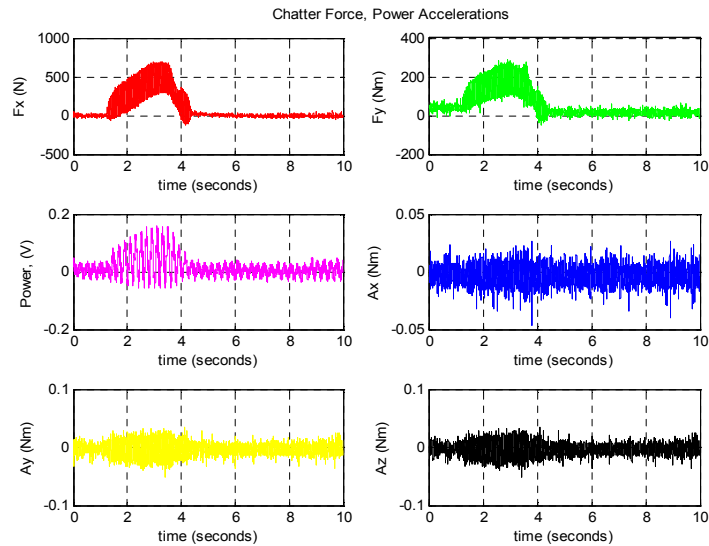
Figure 8.8 Inconnel 718 chatter force, power and acceleration measurements
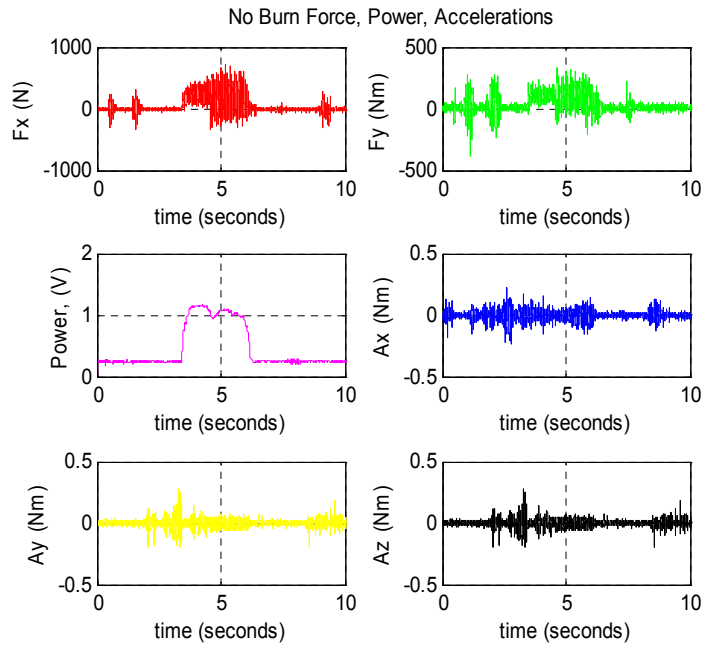
Figure 8.9 Inconnel 718 no burn force, power and acceleration measurements
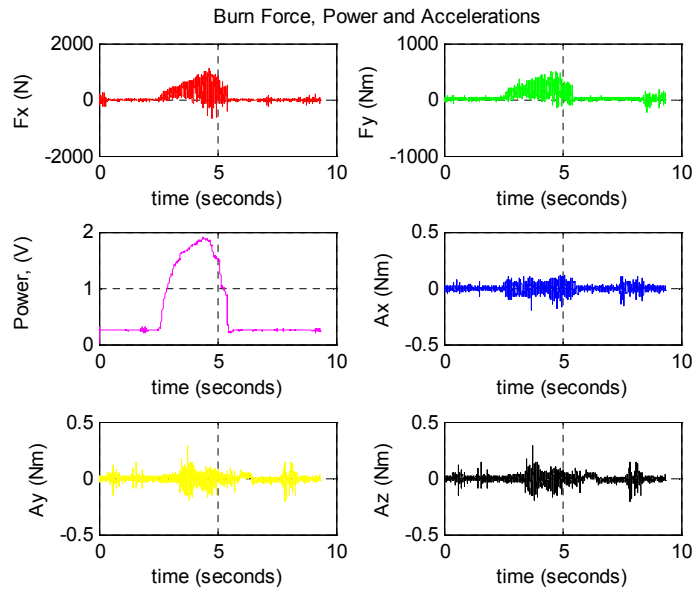
Figure 8.10 Inconnel 718 burn force, power and acceleration measurements

Figures 8.7 to 8.10 display the force, power and acceleration measurements for chatter and burn phenomena trials. For the multi-classification, AE signal extraction was used as well as AE, force, power and accelerations. Both sets of results will be displayed and discussed however with the other burn trials, only the signal synthesis will be discussed and not the classification of such signals. This is due to the signal synthesis displaying good segregation between burn and no burn signal phenomenon.

8.2.1 N-dimensional Analysis

For multiple classifications of many classes it is important to reduce the data into the major salient components that generalise the different data sets. There are some classification techniques that are most suited towards n-dimensionally large data sets however they suffer from multi-classification characteristics. Such techniques are Support Vector Machines (SVM) and hard rule based clustering methods for example. There are other classification techniques that are very good at accurately classifying many different datasets albeit they cannot look at n-dimensionally large datasets. Such classification techniques are GP Multi-Rule Paradigm, Fuzzy Clustering Techniques and Multi-Layer Perceptron Neural Networks (MLPANN). This chapter looks at statistical data reduction signal windowing techniques, Support Vector Machines (Kernel Principle Component Analysis (k-PCA)) and ICA. Out of the three techniques, the best results for n-dimensional realisation were gained by statistical data reduction techniques and ICA. These techniques provided the salient data summary sets to the Genetic Program classifier. The statistical data reduction techniques used the most sensitive AE statistical measures in a windowed fashion (every 100 pts along the STFT signal). These statistical

measures were the standard deviation, the kurtosis and the max (window every 50 pts) which provided 20 points summarising the STFT signal. This data reduction technique was only applied to the AE extracted signals reference the burn and chatter phenomena trials. The ICA technique is similar to K-PCA although the salient parts are not based on promoting unwanted noise signals and instead, just the signals of interest. ICA was applied to a concatenated grinding data set namely; the STFT AE signal, the STFT thrust force (force in Z direction), the STFT power and the STFT thrust accelerations (acceleration in Z direction). The data set here was again reduced from 800 points to 20 points; which ensures the data rows with the highest variance of data between the classes are introduced to the classifier system. With the statistical windowing technique the STFT data displayed in Figure 8.3 is reduced to 20 points based on the most salient components and are therefore distinguishable across the different classes. Figures 8.11 and 8.12 display the Fuzzy-c/GA clustering of ICA reduced data sets. Looking at chatter there is a 95% accurate segmentation between the actual grinding and chattering signals. The overlap between the two classes can be seen at the boundary conditions and this is where the few inaccuracies occur which is either grinding or very slight chattering.

Fuzzy-c GA Clustering of ICA Of Chatter AE and Force Data

Legend: grinding: normal grinding conditions (pink), chatter: chatter grinding conditions (blue).
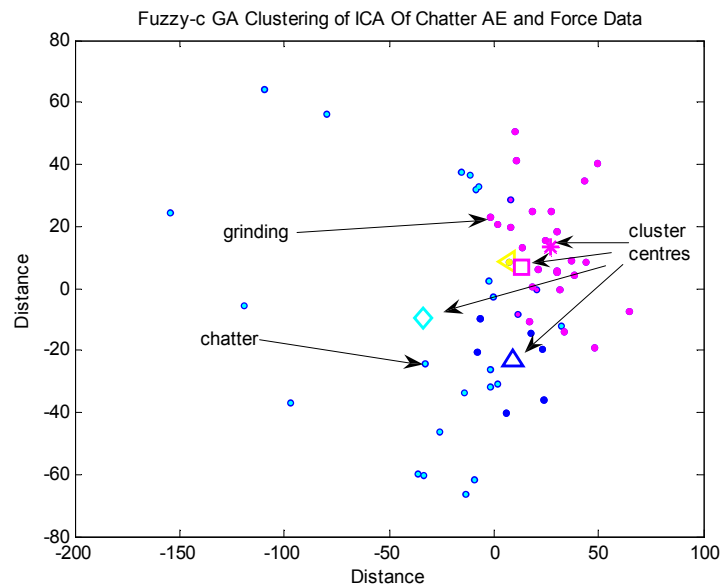
Figure 8.11 Fuzzy-c/GA clustering of Chatter concatenated signals with ICA reduction

Fuzzy-c/GA Clustering of ICA AE and force burn data

Legend: grinding: normal grinding conditions (blue), burn: burn grinding conditions (pink).
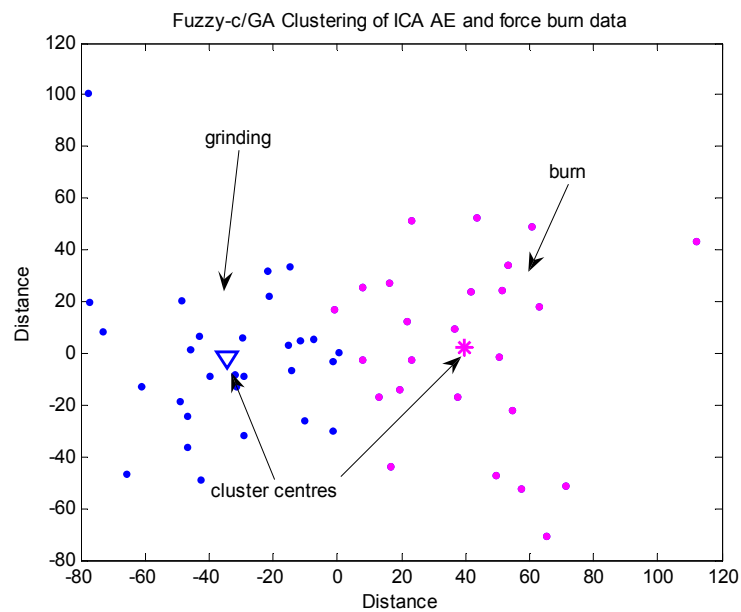
Figure 8.12 Fuzzy-c/GA clustering of Burn concatenated signals with ICA reduction

PhD thesis by James Griffin   [280]

Figure 8.12 displays the perfect 100% accurate segregation between the two classes and displays how useful ICA is at reducing such high-dimensional data sets into rich accurate summary data sets.

8.3 Classification

8.3.1 Observational distinguishing features for classification

The first set of results were omitted from this investigation as some of the extracted signals were found to have a lot of noise present due to a faulty AE power amplifier, this however was rectified for the second set of results. Figure 8.13 displays the physical observed properties from the two successive trials. These properties are based on the recorded percentage of burn which occurred more towards the end of cut where the severity of burn increased (more friction present from wheel loading).
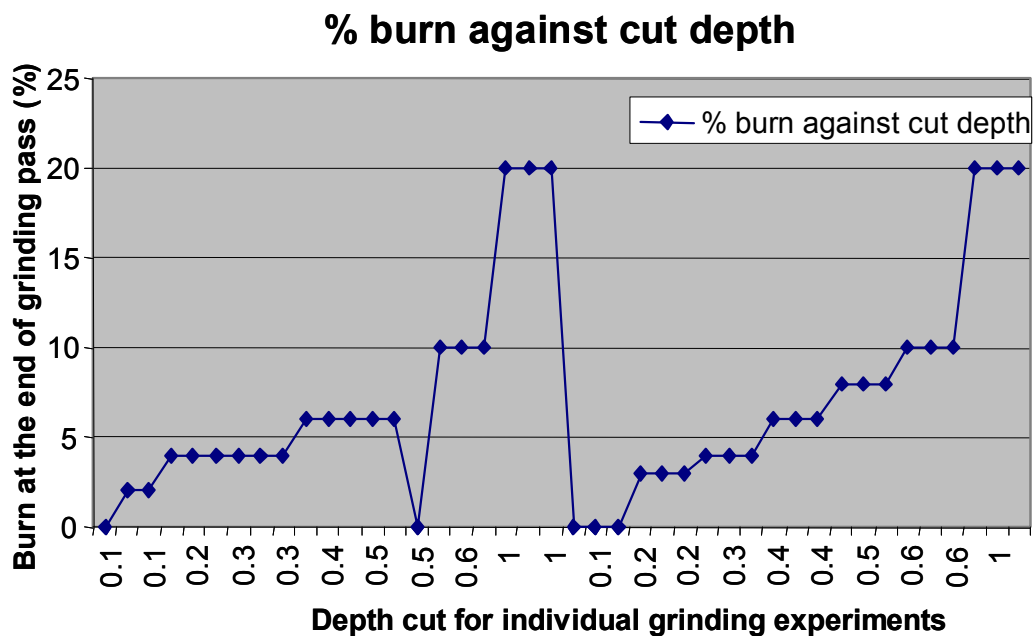
Figure 8.13 Displays the Relationship of Burn and Depth of Cut

This burn phenomenon was observed after each grinding pass. The two sets of similar data are based on the repeatability of trials to ensure the results were true and reliable. Through using segmentation of the burn digitised image it was possible to work out the different percentages of burn. The severe cases of burn were certainly much deeper in terms of surface anomalies when compared with other minimal percentage burn cuts such as the 0.1mm depth of cut.

Grinding conditions were adjusted as required for the experiment (increasing depth of cut with no lubricant in order to gain burn) or in the chatter case, ensure a 1mm cut for each grinding pass and listen for chatter noise and visible chatter marks to identify chatter phenomenon. The extracted signals would then be logged and saved to files. The thickness of the wheel would be measured along with images of wheel and workpeice. For image data of wheel loading, a microscope image (25x magnification) was taken after every third cut for the burn experiment and after every cut for chatter experiment. The sample thickness would be measured and noted along with observations of the temper colour change signifying physical burn characteristics. These steps would be repeated for successive depth cuts and the measurement of the wheel diameter would be carried out at the end of each trial. For chatter however, the wheel diameter would be measured after each cut to quantify the material removal rate. For validity of the chatter experiments, triplication of the trials would be carried out in a sequential manner.

8.3.2 Material Analysis for distinguishing grinding phenomena

Figure 8.14 left, displays the intensities of a burn sample (20%) with all the burn occurring from the middle section (very slight) to the end section (severe). Figure 8.14 right displays the corresponding loading of the wheel for a 1mm depth of cut (20% burn) grinding pass.
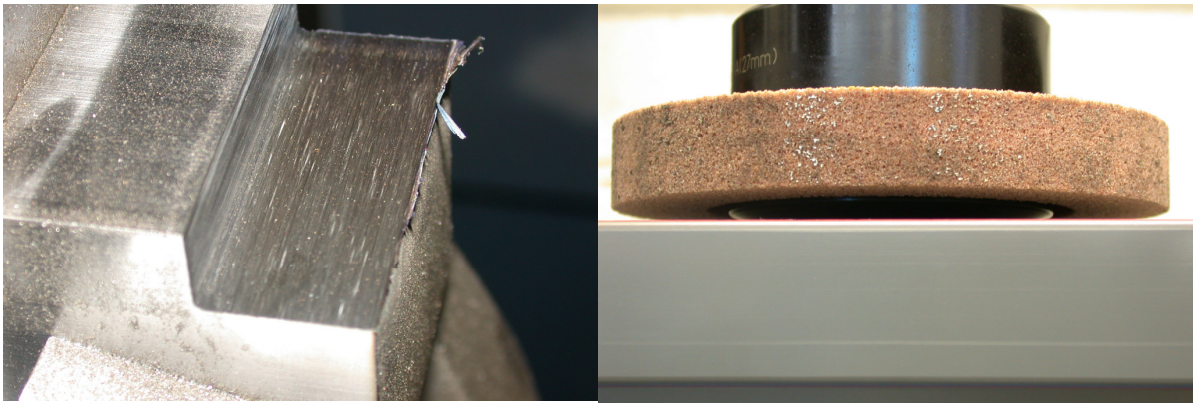
Figure 8.14 left, Inconnel 718 burn end of dry cut 1mm (a_p), Right, material Al_3O_2 wheel-loading

In some cases such as that seen in the CMSX4 trials there is a need for material etching and high magnification surface analysis. This is due to the burn being very difficult to see in some experimental cases (see Figure 3.2). Sometimes slight surface colouration is not enough to establish burn and conducting further material analysis will show if there is material hardening with a white layer present.

Figure 8.15 displays the results gained from the chatter experiment. It is possible to see that chatter is experienced from 6th- 8th cut, 13th-16th cut and, 20th – 24th cut (the Ra values are approximately 2.6> µm for chatter). Note the lines between the 8th, 16th and 24th cut segregate trial 1 to trial 3 respectively, where dressing operations were carried

The University of Nottingham

out within these intervals. For each cut, the actual cut length of the workpiece was measured. The middle part of Figure 8.15 displays the wheel wear which endured a constant near linear removal from one trial to the next. The bottom part of Figure 8.15 displays a decrease in cut length as each cut is passed during the 3 trials.
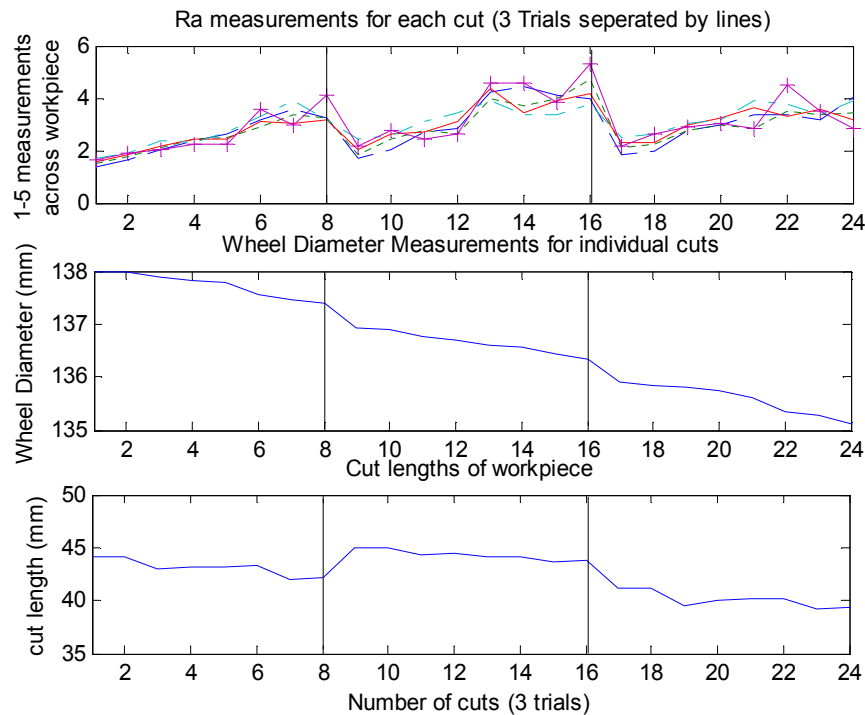
Figure 8.15 Displays roughness, wheel wear and cut lengths for chatter tests

8.3.3 Machine Learning Classification

Figure 8.16 displays the fuzzy-c/GA classification of the full grinding data set with an 81% classification accuracy. Most of the misclassifications are made between the boundaries of chatter and grinding data clusters. Figure 8.16 shows that the data can be separated in a multi class fashion with a reasonably high level of confidence.
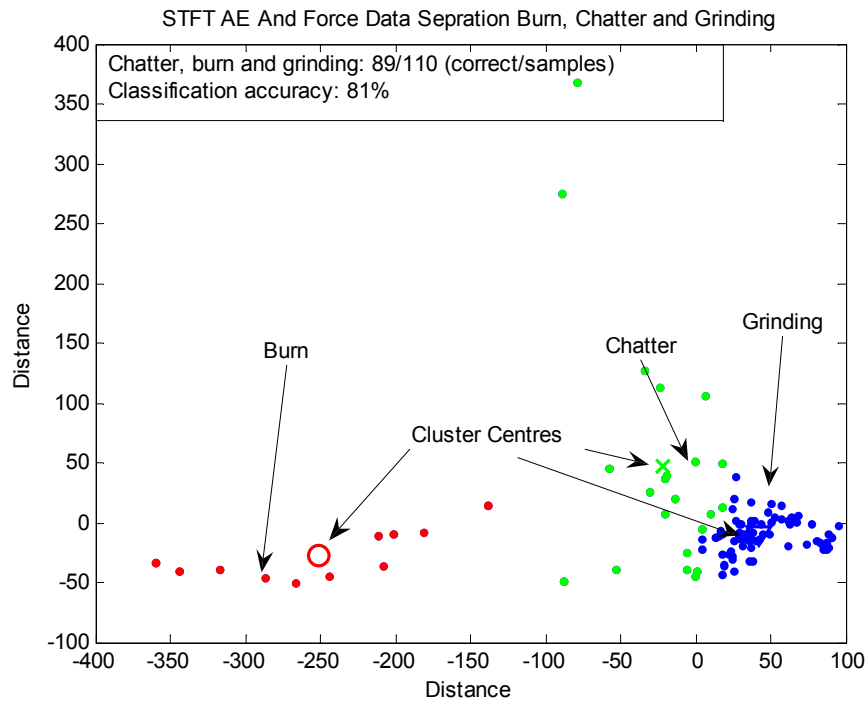
STFT AE And Force Data Sepration Burn, Chatter and Grinding

Chatter, burn and grinding: 89/110 (correct/samples)
Classification accuracy: 81%

Grinding Conditions: Machine: Makino A55; Grinding Wheel: Al_2O_3; Workpiece: Inconnel 718; Burn trials A_p 0.1mm $\rightarrow$ 0.6mm and 1mm ; Wheel width 15mm;
Chatter trials A_p 1mm; Dry down grinding: Vs= 35 m/s; Vw= 1000 mm/min; Coolant down grinding: Vs= 55 m/s; Vw= 1000 mm/min;

Legend: Burn: burn phenomenon (red), Chatter: chatter phenomenon (green) and grinding: normal grinding conditions (blue)

Figure 8.16 Multi-classification of AE, force, power and acceleration concatenated signals

Figure 8.17 is based on the same full concatenated data set used in the results displayed by Figure 8.16 however the burn and grinding classification were separated as one set of results and another is the superimposed chatter and grinding classification on top of those results. It can be seen that running Fuzzy-c/GA clustering for two dual class classifications obtained results close to the one triple class classification. Again,

reasonably high levels of classification accuracy are obtained which bodes well for the GP classification as a generic classifier. These results show it is possible to separate burn and chattering grinding conditions with DSP and classification techniques.
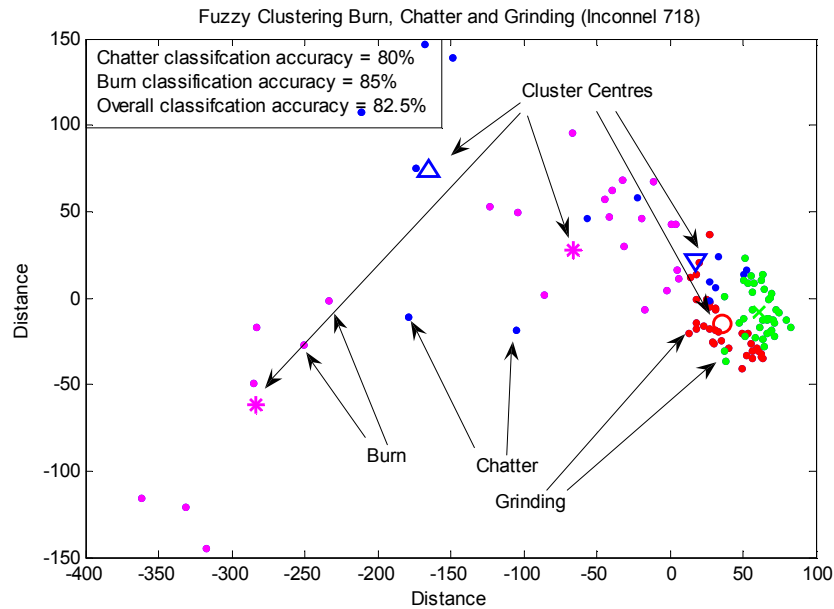
Figure 8.17 superimposed burn classification with chatter classification

Grinding Conditions: Machine: Makino A55; Grinding Wheel: Al_2O_3; Workpiece: Inconnel 718; Burn trials A_p 0.1mm → 0.6mm and 1mm ; Wheel width 15mm;
Chatter trials A_p 1mm; Dry down grinding: Vs= 35 m/s; Vw= 1000 mm/min; Coolant down grinding: Vs= 55 m/s; Vw= 1000 mm/min;

Legend: Burn: burn phenomenon (red), Chatter: chatter phenomenon (green) and grinding: normal grinding conditions (blue)

Figure 8.17 superimposed burn classification with chatter classification
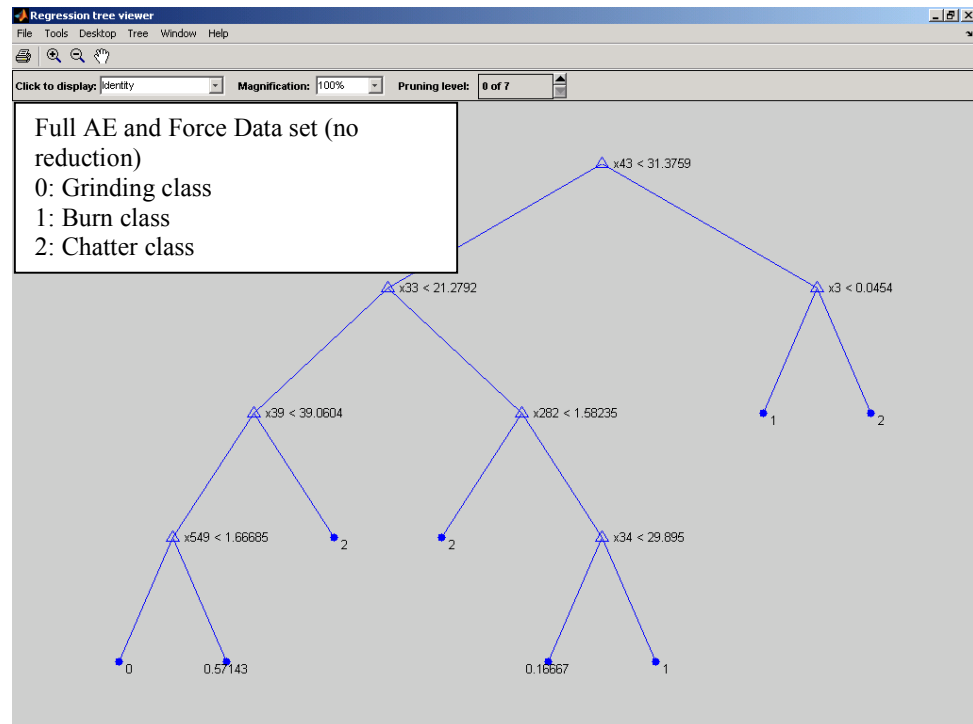
Figure 8.18 displays tree regression multi classification for AE and force, power and acceleration data

Figure 8.18 displays tree regression applied to the full signal data set of chatter, burn and grinding data sets. Tree regression is based on data minimizing by probability and data tree rules. These rules have also classified the multi-data sets with a high level of accuracy however they can become unmanageable when the amount of classes increases. There are however some cases where the classification is in between classes and not distinct. This can cause certain misclassifications or don't know states (in-between cases). Figure 8.18 is based on the full data sets of AE and, grinding force, power and accelerations for the dual grinding anomalies.
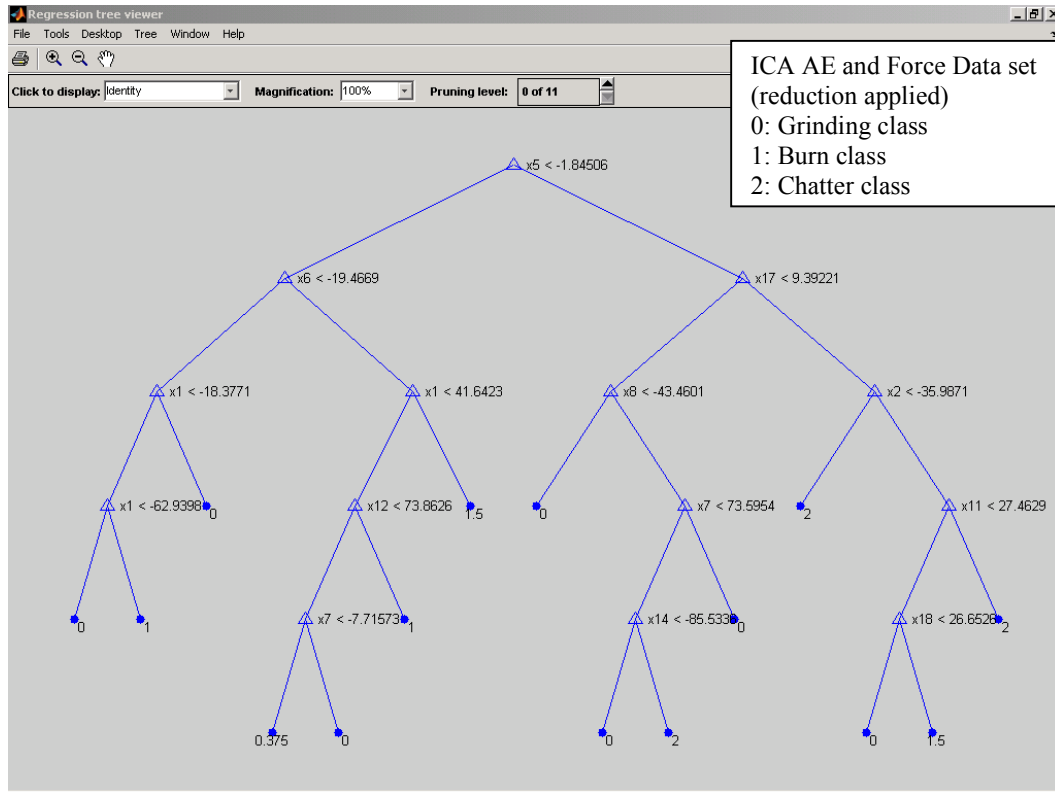
Figure 8.19 displays tree regression ICA n-dimensional reduced multi classification for AE and force, power and acceleration data

Figure 8.19 displays the tree regression for ICA reduced full grinding AE, force, power and acceleration data sets. Again a high confidence of the classification accuracy can be established here which bolsters the distinction between three classes of chattering, burn and normal grinding conditions. These trees are also used to display what GP could achieve in terms of a generic classifier. With the merge between tree regression and GP, a generic classifier can exist. For instance, the tree regression could separate the dual phenomena or triple phenomena for a defined set of conditions. These rules and many other similar phenomena conditions could be learnt by GP, or even different machining phenomena giving a generic classifier type system. For example; several rules for a

specific parameter setting, and several other rules for another parameter setting, and finally a set of hierarchical evolutionary based rules controlling both the two rule states. The next set of results displays how such a realisation can be made. The first set of results displayed by Figure 8.20 display the GP output for learning the segregation between burn and no burn cases using a statistical window reduction AE data set.
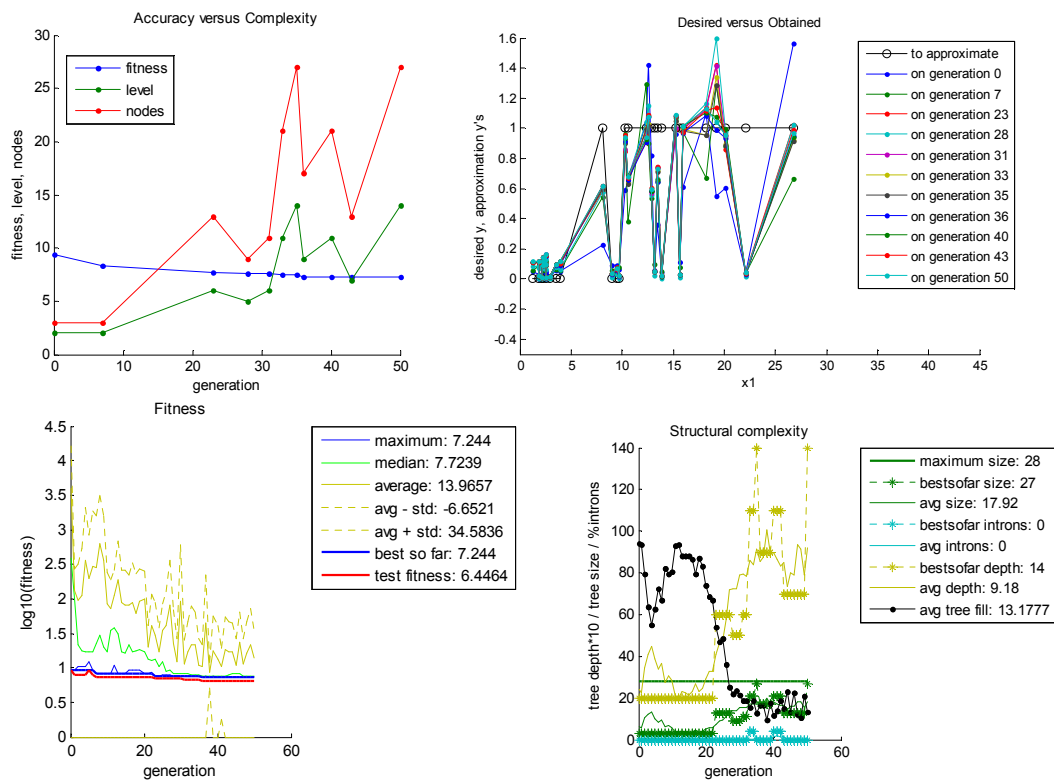
Figure 8.20 GP outputs for burn statistical window reduced AE data set
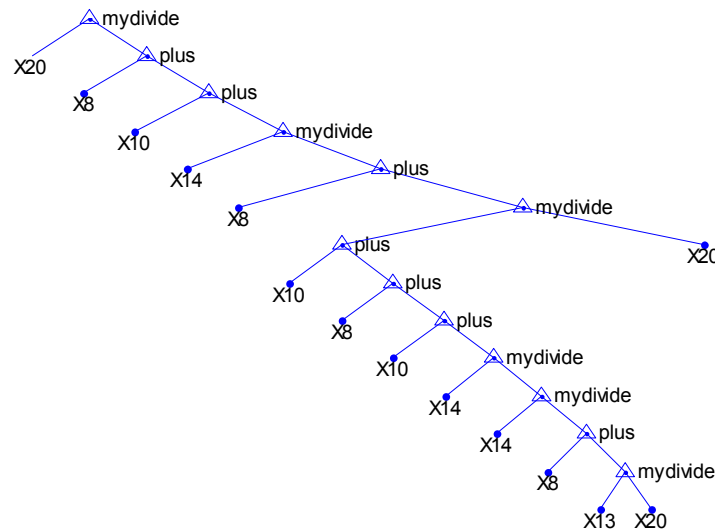
Figure 8.21 GP tree output for burn and no burn statistical window reduced AE data set

Figure 8.21 displays the tree output for classifying the burn and no burn statistical window reduced set. The fitness measure used was based on the error between the desired and actual obtained outputs from applying the tree rule for the 'best individual so far.' The results of these experiments will be displayed in Tables 8.3 and 8.4.

The rule obtained from the tree displayed in Figure 8.21 is as follows:

mydivide(X20,plus(X8,plus(X10,mydivide(X14,plus(X8,mydivide(plus(X10,plus(X8,plus(X10,mydivide(X14,mydivide(X14,plus(X8,mydivide(X13,X20))))))),X20))))))

The fitness displayed in Figure 8.20 Top left is based on the amount of correct values obtained for that generation run (see Figure 8.20 Top Right). Each case within the

training data set or test data set is transferred to the rule and the computed output will give either a '1' or '0' or very near to either of these classification values.
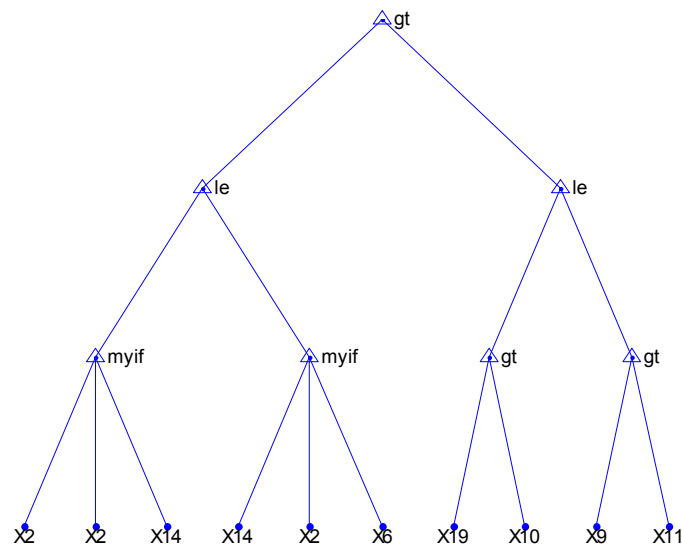
Figure 8.22 same parameters and data set as in Figure 8.21 however different GP function set

Figure 8.22 displays the same tree rule set as that seen in Figure 8.21 however the function set used in this example is not between +, -, * and / and instead; it is more of data mining functions (as seen by tree regression) using 'if less than' or 'if greater than' do type functions. These two realisations would see which is the more useful for segregating the data sets. This type of GP paradigm could work directly with tree regression as a hierarchical multi classifier. The rule obtained from the tree displayed in Figure 8.22 is as follows:

gt(le(myif(X2,X2,X14),myif(X14,X2,X6)),le(gt(X19,X10),gt(X9,X11))).

The University of Nottingham

The rules displayed above are examples obtained from the GP program and are used to segregate the two data sets when applied to data. The output of the data and rule give either class '1' or class '0'. With greater than or less than rules, either logical 'TRUE' or logical 'FALSE' is output.
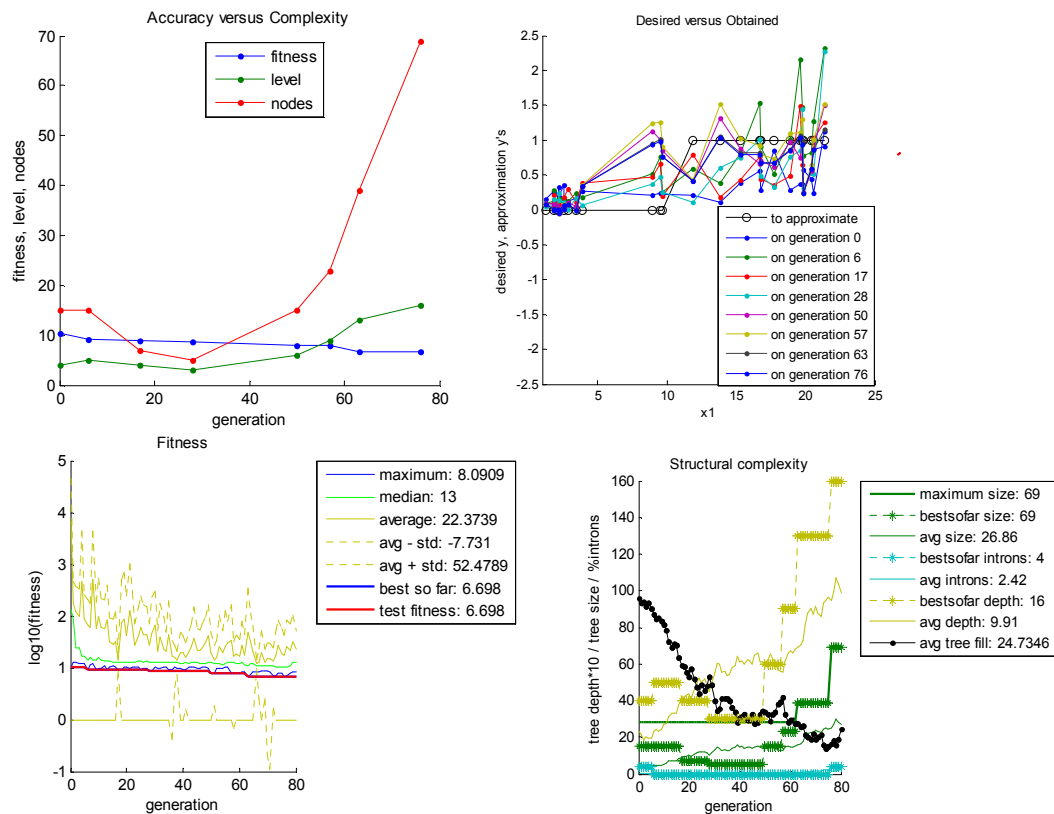
Figure 8.23 GP outputs for chatter statistical window reduced AE data set

Figure 8.23 displays the GP output similar to Figure 8.20 although this time the output is based on learning the chatter and no chatter data set. Looking at Figure 8.23 these four outputs give the most information in regard to the GP progression for a specific data set. Top left, accuracy vs. complexity is as important as the fitness (accuracy) decreases (fitness measure gets smaller) over the number of generations, the depth of nodes

The University of Nottingham

increase which can give a more comprehensive and detailed classification solution. Top right, shows the progression of learning between the desired set of results and currently obtained results (dynamic error surface graphical output). Bottom left is based on the fitness and how accurate the tree rules are at evaluating the presented datasets. Bottom right, the structural complexity verses the number of generations.

Figure 8.24 GP tree output for chatter and no chatter statistical window reduced AE data set
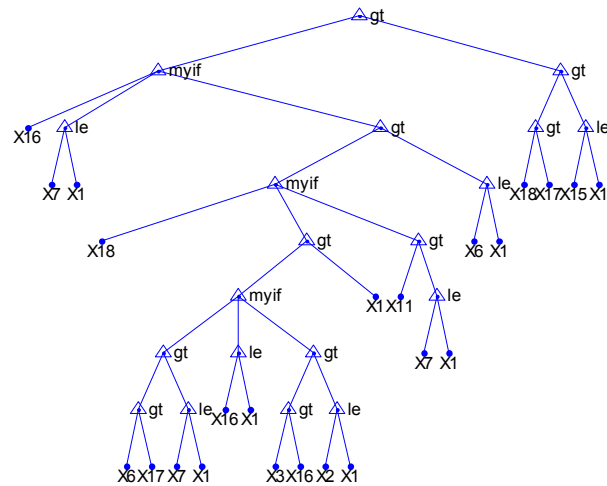
Figure 8.25 same parameters and data set as used in Figure 8.24 however with different functions

The results displayed in Figures 8.24 and 8.25 displays accurate segregation of the chatter data set which is also based on the fitness function of sum difference error between the actual and obtained outputs during each population evaluation. The output trees and rules are examples of these cases however many more tests were made and tabulated in Tables 8.3 and 8.4.
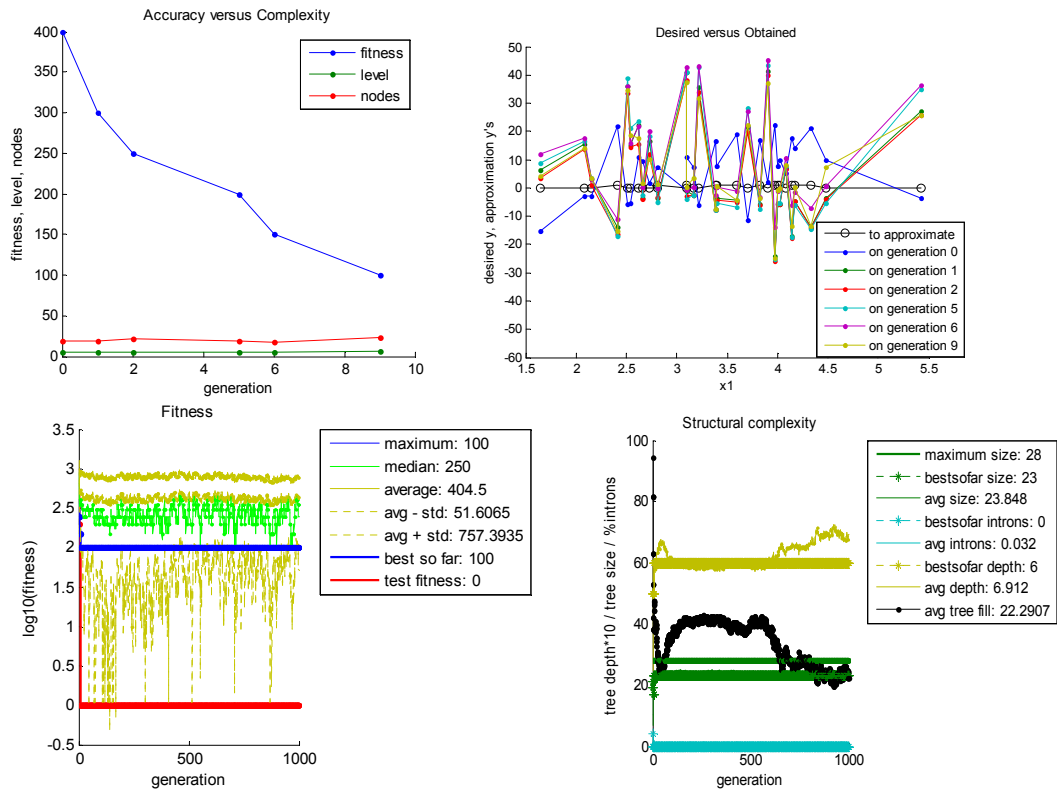
Figure 8.26 GP o/p for burn/chatter ICA reduced AE, force, power and accelerometer data set

Figure 8.26 displays the GP outputs for ICA (Duda, Hart et al. 2001), reduced AE, force, power and accelerometer data sets. The fitness function used here is based on the percentage overlapping between the data points of the two class sets. With this fitness measure the errors are much larger at the beginning of learning and then get smaller with respect to the increased generations. The fitness measure already discussed is based on the back propagation error minimisation from the desired minus the actual output values.
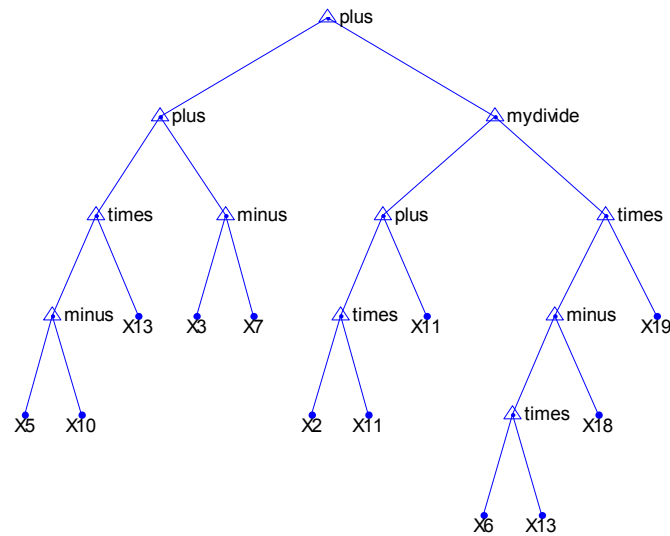
Figure 8.27 GP tree o/p for chatter/burn ICA reduced AE, force, power and acceleration data set

Figure 8.27 displays the output tree made by the GP engine at the end of 1000 generations, 500 population program execution. This improved fitness function ensured the ICA data set of burn and chatter had an accuracy classification of 95% which is very encouraging for both ICA and GP. The if, greater and less rules were displayed previously with the statistical window reduced sets and this was for illustration and discussion purposes, however, they were thought inappropriate for these classifications with the different fitness function in place.
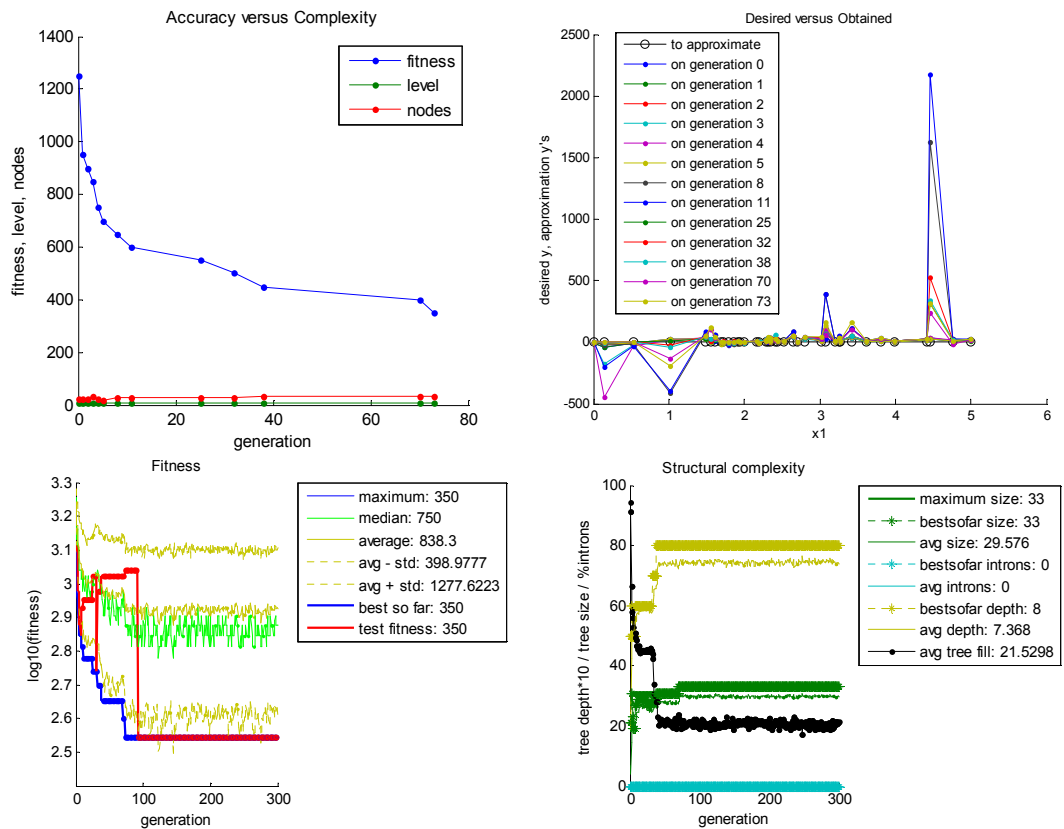
Figure 8.28 GP o/p for burn/grinding ICA reduced AE, force, power and accelerometer data set
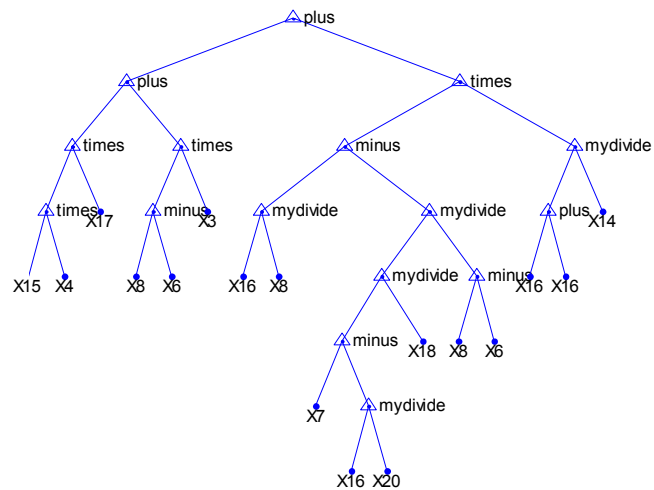
Figure 8.29 GP tree for burn/no burn ICA reduced AE, force, power and acceleration data set
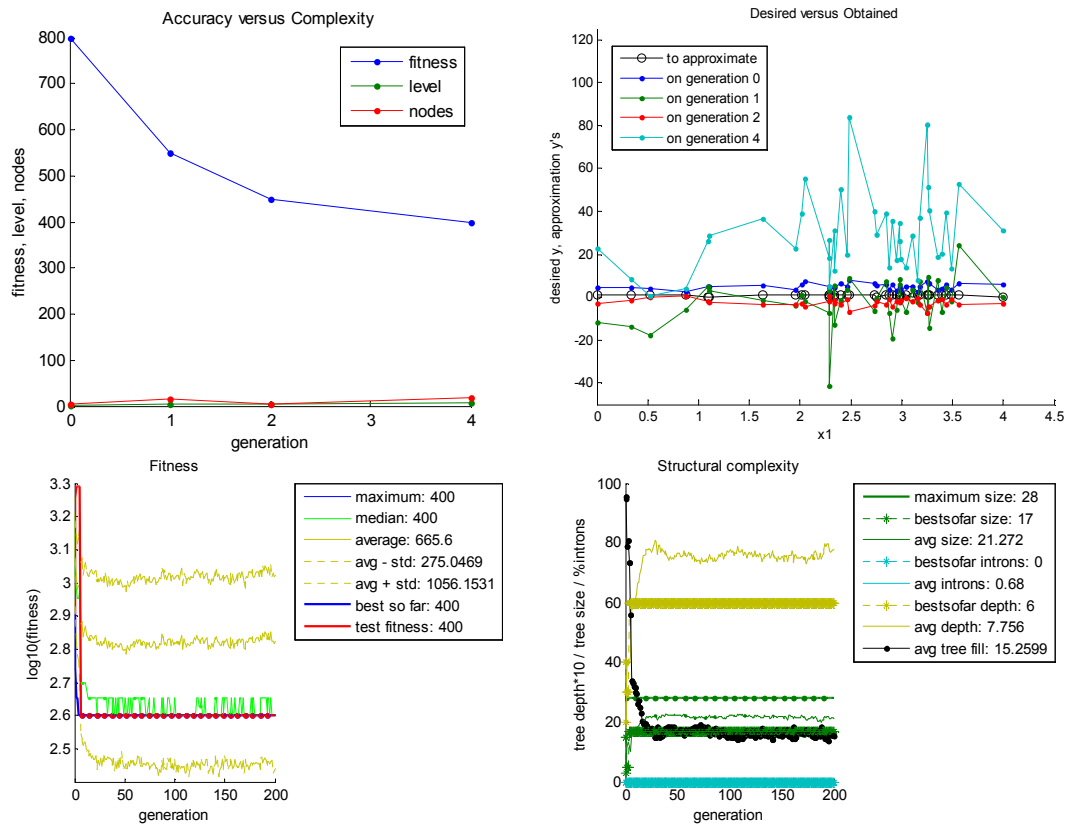
Figure 8.30 GP o/p chatter/no chatter ICA reduced AE, force, power and accelerometer data set

Figure 8.28 to Figure 8.31 displays the GP outputs for classifying ICA reduced AE, force, power and acceleration concatenated data. Figures 8.28 and 8.29 display GP outputs for ICA reduced burn and no burn data, from these results a fairly high confidence is achieved with a classification accuracy of 82.5%. Sometimes the fitness of minimising the percentage overlap between the two classes is undesirable and the fitness of decreasing the error between the desired and actual outputs is more desirable, hence this learning strategy is analogous to the back propagation learning rule used in Neural Networks and suitable for classification or regression problems. The trade-off between the GP fitness function is based on the fitness achieved and rule complexity. The sum

The University of Nottingham

difference fitness function is for easy partition datasets. This trade-off is analogous to finding local optima instead of the desired global optima.
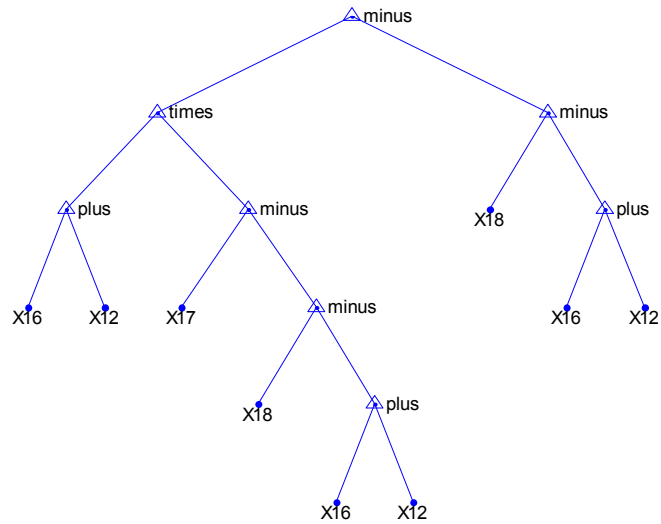
Figure 8.31 GP tree o/p for chatter/grinding ICA reduced AE, force, power acceleration data set

Figure 8.31 displays the GP output tree for chatter and no chatter classification. Using the class overlap fitness function, a classification accuracy of 80% is achieved. From these results it can be noted that GP and n-dimensional reduction techniques are useful for classifying difficult to segregate signal data.

Figures 8.20 to Figure 8.31 displays some of the GP outputs displayed in Table 8.3 and Table 8.4. The overall results displayed by GP and n-dimensional reduction techniques are very encouraging especially when compared with other classifier techniques such as Fuzzy-c/GA clustering displayed in Figure 8.16 and Figure 8.17 where the classification

The University of Nottingham

accuracy was 81% and 82.5% respectively. That said, all the classifications made from

GP were at worst 80% classification or at best, 100% classification.

Table 8.3 GP Results set Part 1

Exp No.	GP Fitness function	Data set	Function Nodes	Data test score	accuracy %
1	sum diff fitness	ICA Chatter and burn	+,' -, '/, '*	32/40	80
2	sum diff fitness	*reduction burn and no burn	+,' -, '/, '*	36/40	90
3	sum diff fitness	*reduction burn and no burn	=<, '=>, if	36/40	90
4	sum diff fitness	*reduction burn and chatter	+,' -, '/, '*	36/40	90
5	sum diff fitness	*reduction burn and chatter	=<, '=>, if	38/40	95
6	classes overlap	ICA Burn and no burn	+,' -, '/, '*	33/40	82.5
7	classes overlap	ICA chatter and no chatter	+,' -, '/, '*	32/40	80
8	classes overlap	ICA chatter and no chatter	+,' -, '/, '*	40/40	100
9	sum diff fitness	ICA chatter and no chatter	+,' -, '/, '*	36/40	90
10	classes overlap	ICA Burn and no burn	+,' -, '/, '*	40/40	100
11	classes overlap	*reduction burn and no burn	+,' -, '/, '*	40/40	100
12	classes overlap	*reduction chatter and no chatter	+,' -, '/, '*	40/40	100

*reduction burn and no burn: is based on the statistical window n-dimensional reduction technique

Table 8.4 GP Results set Part 2

Exp No.	class 1 min	class 1 max	class 2 min	class 2 Max	Generations	Population	fitness
1	1.1484	0.9292	-0.0484	0.0332	100	200	9
2	0.5953	1.0877	0.0089	0.1664	100	200	6
3	FALSE	TRUE	TRUE	FALSE	100	300	6
4	0.8207	0.9675	0.0132	0.3546	100	300	6
5	FALSE	TRUE	TRUE	FALSE	100	300	6
6	11.949	319.4126	188.4734	10.8819	200	700	350
7	13.3406	55.1572	0.2907	12.565	200	700	400
8	1.2287	37.3007	-24.8803	1.2287	1000	500	0
9	0.9921	1.0051	-0.0159	0.0074	1000	500	3
10	4.7712	205216.7424	-3.5706	4.6128	1000	500	0
11	0.6145	3.2685	3.6544	16.7413	1000	500	0
12	0.4305	3.3461	4.1047	7.3781	1000	500	0

The University of Nottingham

8.3.4 Discussion of Results

The classifier results displayed in section 8.3.3 display some encouraging results for a multiple grinding phenomena classifier system. The WPT AE signal representation was expected to outperform the STFT AE signal representation which on initial tests it did by a 10% increase however this was to the detriment of time consuming signal post preparation and computational complexity. Further tests were thought not to be necessary as STFT and n-dimensional reduction techniques worked just as well and were more user-friendly with less demands made on computer resources. It is thought that if the signal suffers from extremely fast burst information or poor signal to noise ratio then WPT can be better a choice than STFT representation otherwise, STFT representation satisfies the requirement for identifying grinding phenomena such as burn and chatter.

The Statistical windowing techniques have proved to be just as useful as when they were used in previous trials (Griffin and Chen 2006). A lot of research looks at identifying singular phenomenon such as Burn or No Burn, this research however looks at a more generic classifier system which is more useful to industry in being able to identify a multitude of phenomena and carry out the necessary maintenance based on that classification. The GP implementation provides very accurate results when compared with other robust classifiers such as Fuzzy-c/GA clustering. By using GP as a hybrid classifier with n-dimensional reduction techniques such as ICA and statistical window reduction techniques, this bolsters GP as a powerful hierarchical classification system. These results in Chapter 8 display how useful GP is at classifying chatter, burn and

normal grinding. This may have been set-up for a chosen set of cutting parameters however the results show that many rules can be evolved looking at several different cutting conditions, even a mix of different machining strategies such as those seen with defined cutting edges such as milling, drilling and turning. Such a mix of rules for different demes of data sets would allow the intelligent monitoring of all the tasks carried out in manufacturing a turbine disk. GP along with other classifier techniques such as fuzzy-c clustering to enhance the evolving rules could be a very powerful investigation for future work. Such rules could be extremely robust and reliable and introduced to an integrated chip (IC) with the required DSP and n-dimensional reduction logic. Such a system could prove to answer the requirements of an online intelligent generic classifier monitoring system.

8.4 CMSX4 and Titanium Burn Signal Analysis

The last part of this chapter looks at other burn signals taken from different aerospace materials however some of these materials were machined with coolant and to the higher end of manufacturing 'speeds and feeds.' One material that required coolant was Titanium-64, being a highly combustible material. The CMSX4 signal analyses are merged with thermocouple measurements made at the beginning of this research. Table 8.5 and Table 8.6 display the machining parameters for both trials; CMSX4 and Titanium-64 burn respectively:

Table 8.5 Grinding Conditions for CMSX4 burn trials

Grinding Parameter	Condition
Depth of cut	0.1mm – 4mm
Feedrate	1000 mm/S
Wheel speed	35 m/S
Wheel diameter	134 mm
Wheel Material	Al_2O_3
Work piece Material	CMSX4
Lubricant	Hocut 3380 70 bar/None

Table 8.6 Grinding Conditions for Titanium-64 burn trials

Grinding Parameter	Condition
Depth of cut	0.01mm – 2mm
Feedrate	1000 mm/S
Wheel speed	35 m/S
Wheel diameter	134.85 mm
Wheel Material	Al_2O_3
Work piece Material	Titanium-64
Lubricant	Hocut 3380 70 bar

Looking at Figure 8.32, it is possible to see that the burn AE intensities are much greater than that of normal grinding AE intensities. CMSX4 is a specifically hard material with a hardness of HRB 60 and is difficult to obtain severe burn and therefore produces high intensities rising in the mid sensor frequency response levels (such as high AE intensities at the 500-600 KHz frequency bands).

CMSX4 No Burn FFT   CMSX4 Burn FFT
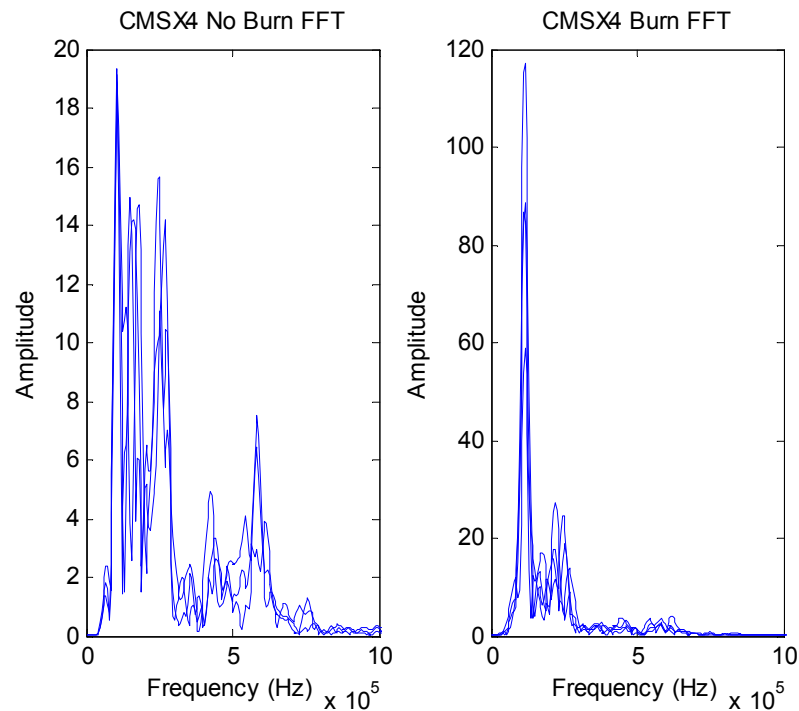
Grinding Conditions: Machine: Makino A55; Grinding Wheel: Al$_2$O$_3$; Workpiece: CMSX4; Burn trials A$_p$ 0.1mm → 4mm ; Wheel width 15mm; Coolant down grinding: Vs= 35 m/s; Vw= 1000 mm/min;

Figure 8.32 CMSX4 FFT AE signals

Figure 8.33 display very high AE intensities for Titanium-64 burn. This is due to the material properties of Titanium-64 when compared with the CMSX4 and Inconnel 718 which are nickel based and highly heat resistant materials. Titanium-64 is a highly combustible material and used for engine casing which requires the characteristics of strength and low density (light/tough material).

As a highly combustible material, the AE intensities are the highest out of all the material AE signatures and during the severe burn it is possible to see the high

The University of Nottingham

intensities in the mid sensor response range of the AE sensor (peaks around the 500 – 600 KHz).

Thermocouple experiments were performed on nickel alloy (CMSX4, HRB60) workpiece with vitrified aluminium oxide wheel (60E). These heat measurements were used to bolster visible burn identification techniques.

Grinding burn is detected at best by optical microscopic examination of the polished/chemical etched surface. Upon etching the surface, the martensitic layer usually shows up as a white phase occurring in patches. Such analysis is time consuming and can only be carried out in an off-line manner taking several hours if not days to ensure the sample is correctly polished and etched to required standards. A less time consuming method was applied to achieving heat detection and this demonstrates the critical temperatures of CMSX4 grinding burn with Al_3O_2 wheels.
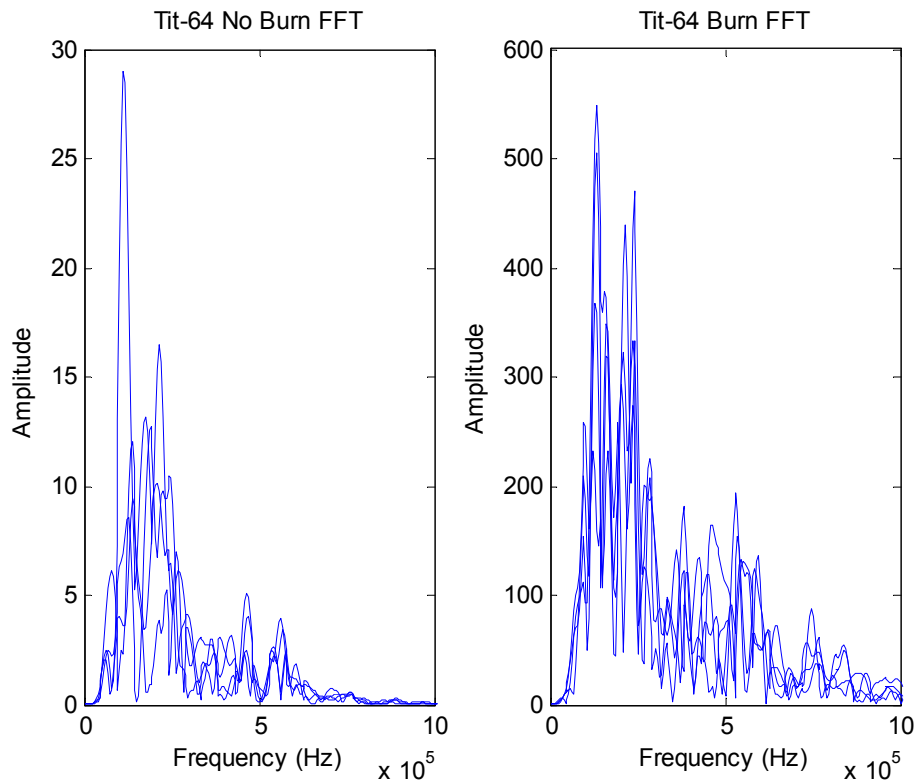
Grinding Conditions: Machine: Makino A55; Grinding Wheel: Al$_2$O$_3$; Workpiece: Titanium-64; Burn trials A$_p$ 0.01mm → 2mm ; Wheel width 15 mm; Coolant down grinding: Vs= 35 m/s; Vw= 1000 mm/min;

Figure 8.32 Titanium-64 FFT AE signals

The surface of the ground workpiece is evenly divided into 10 segment-areas. When the temper colour of grinding burn is pale yellow or light brown and only occurs on two segment-areas of the whole surface area, the burn is defined as the slight burn. When the colour of grinding burn is violet and occurs over five segment-areas of the whole surface area, the burn is classed as severe burn. The critical zone therefore of CMSX4 grinding burn is between 590 and 670 °C. See Figure 8.33 to display this burn and grinding zone temperature (Liu 2004; Liu, Chen et al. 2005).
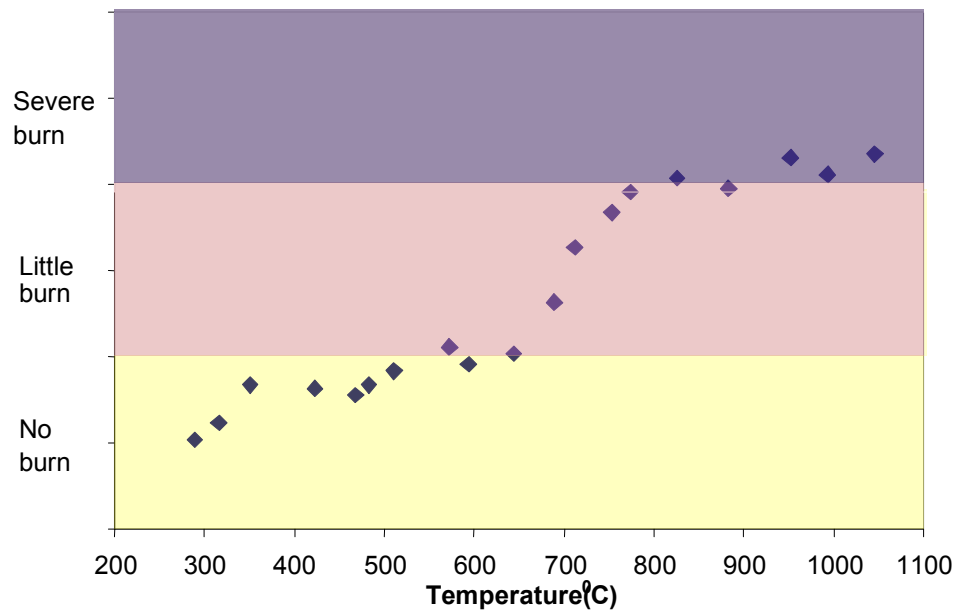
Figure 8.33 CMSX4 material properties with respect to temperature measurements

Figure 8.33 displays the critical burn zone for grinding nickel alloys such as CMSX4. These experiments are a further verification of burn taking place and correlates with the obtained AE extracted waveforms. These different materials and their different characteristics can be captured in terms of rules under a generic classifier system such as that seen by GP. These different material analyses can pave the way for the investigations and synthesis into providing monitoring for composite materials which is now becoming more and more important in an ever advanced hi-tech world.

8.5   Conclusion and Gaps

Chapter 8 has looked at the macro aspects of grinding and ties in with the research discussed in Chapter 7. This merge is provided in terms of developing a highly efficient cutting robust monitoring system. As already discussed, the work carried out in Chapter

7 can be directly used in micro machining (micro grinding) and with further work, it can be used to enhance efficient grinding such as that seen in the manufacture of aerospace disks/blades. In addition, such work can be used to assess the efficiency of the type of the wheel used for a specific material application. With this research in mind, Chapter 8 looks at macro grinding phenomena (burn, chatter and normal grinding conditions) and the accurate multiple classifications of such extracted signal data. The generic classifier used was predominately GP providing advanced and accurate evolved rules to provide the classification for a fixed, specified set of 'speeds and feeds.' These rules can then be evolved for several cutting states 'varying levels of speeds and feeds' giving rise to many types of grinding phenomena coverage. The work displayed in Chapter 7 can replace the phenomena identified in Chapter 8 this is after future work has proved the cutting, ploughing and rubbing identification for macro grinding ratios for burn and chatter. This generic evolving classification system can be extended for other machining such as the monitoring of milling, turning and drilling therefore providing a total monitoring solution for manufacture aerospace turbines. In the burn case it was noticed that the burn ratios increased due to the increased depth of cut. The generic classification can therefore identify both conditions as they are dependent on each other. The work of chapter 8 has displayed a novel generic classifier and due to time constraints; more involved burn, chatter with cutting, ploughing and rubbing ratios have not been possible and this is left for future work which in short combines both work displayed in chapters 7 and 8.

- Multiple classification system identifying chatter and burn grinding phenomena.

- Identifying burn with coolant present from using STFT and WPT DSP techniques.

- Investigating grinding temperatures through thermocouple and signal analysis for different materials with different material characteristics.

- Comparison of evolutionary classification techniques such as Fuzzy-c/GA, GP and Data Mining Tree Regression.

- Multiple classification of generic classifier system using GP.

- Multiple classification of generic classifier system using n-dimensional reduction techniques such a statistical window reduction, PCA and ICA.

Chapter 9 Future Work and Conclusions

The conclusions made are based on the results mainly accumulated in Chapter 7 and Chapter 8. There are however gaps experienced in the other chapters such as DSP techniques that incorporate both STFT and WPT technologies. These general gaps within process monitoring will also be discussed. The main findings of this thesis look at the AE signature in terms of cutting, ploughing and rubbing experienced from single grit scratch tests. This work looks at both radial and horizontal scratch tests at standard aerospace manufacturing 'speeds and feeds.' The horizontal scratch tests are more analogous to actual grinding and this allows the classification in terms of cutting, ploughing and rubbing utilisation for normal grinding passes using the already verified; single grit cutting, ploughing and rubbing data. The last section of results looks at providing a generic grinding classifier using a novel hybrid evolutionary computing technique. The work carried out in Chapter 7 requires more work to be able to look at the cutting, ploughing and rubbing utilisation for both chattering and burn, however when such work has been carried out, the burn and chattering conditions for various speeds and feeds can be classified providing an accurate robust generic grinding classifier. This paradigm could also be transferred to other machining technologies and the generic classifier could monitor all the extracted signals from machining the whole disk to standard features within a disk.

9.1   Conclusions to Radial Scratch SG tests

Identifying the fundamental signatures of Single Grit (SG) phenomenon is significant to the process of monitoring grinding materials; all parts of the research work were

specifically concerned with the manufacture of aerospace materials. Once the microscopic level of grinding activity has been identified and verified through a number of repeat tests it is then ready for identification at the macro level phenomenon (full grinding pass). This part of the research presents an investigation using Acoustic Emission signals to identify the SG phenomenon of cutting, ploughing and rubbing. The difficulty of using AE techniques for monitoring SG phenomenon is that AE signals are often weak and merged by other AE signals from other sources such as mechanical and white noise. The key point here is how to distinguish the AE signals of relevant phenomenon from other AE signals.

By using both the STFT and Wavelet Transforms (WT) with statistical reduction windowing techniques useful features can be extracted. The difference between SG phenomenons from extracted AE signals is distinguished in the form of cutting, ploughing and rubbing. Initially, rubbing was very difficult to identify in terms of the profile grit cut measurements. This is because rubbing has elastic material energy properties and ploughing/cutting has plastic material energy properties. With elastic material properties there should be no or minuscule marking on the workpiece, this is why this phenomenon has been difficult to identify in terms of its physical properties. With reference to the rubbing phenomenon cases they are identified as rubbing with slight plastic deformation this is due to most of the scratch depth measurements having some slight albeit consistent groove markings to quantify.

The University of Nottingham

The results show that AE energy for the three phenomena is concentrated between the frequency ranges of 50 kHz to 1 MHz (frequency response range for AE sensor). Cutting appears to have low to mid range frequencies with the greatest normalised energies residing in the lower frequency components. Whereas ploughing is more concentrated in the mid frequency ranges in terms of energy and rubbing, is weighted towards the mid to high frequency ranges. The results just mentioned were taken from the WT signal analysis. With less resolution the STFT displays similar properties to that found with WT. For STFT analysis reference ploughing and cutting phenomenon; the results were similar although they did not contain as much detail as found in the WT case.

Even though the STFT lacks resolution in both the time or frequency domain it can still be used with WT as a check to see if the salient bands of information have been identified. Looking at the ANN results; both STFT and WT have a high confidence in segregating the different phenomenon. Looking at different classification results it is possible to see the elastic and plastic energy signatures can be segregated, however the results were not fully conclusive to identify pure rubbing phenomenon. This initial work found some very encouraging results however it was considered that a new approach was needed to ensure actual rubbing phenomenon could be obtained and an approach that could be directly transferred into an actual grinding pass (macro grinding) which lead to a new approach; the Single Grit Horizontal Scratch Tests. The radial scratch tests made four main classification data sets for cutting, ploughing and rubbing based on four different materials; CMSX4, EN8 Steel, Inconnel 718 and MAR-M002 material. It was true of all materials having different characteristics and emitting different signatures for

cutting, ploughing and rubbing. In general material terms, the AE intensities were highest for cutting, then ploughing and very small for rubbing. This initial work of identifying different grinding mechanics through rotational scratch tests has provided a clear indication that this work is very useful in the identification of material removal process at the unit event and whether the grit material is suitable for application to the workpiece material. In addition, the work can be directly applied to micro grinding in controlling efficient cutting. The novel work presented here is the radial scratch classification using Neural Networks to distinguish between the three levels of grinding phenomena through the extracted AE emitted signals. This is the first work of its kind and leads to follow on work that is more analogous to actual grinding.

The next part of this work investigates single grit horizontal scratch tests and investigates two different materials with diverse material properties; CMSX4 (hard heat resistant aerospace material) and Titanium-64 (a more ductile, combustible, less hard aerospace material). The majority of the work was carried out with CMSX4 material however the Titanium-64 results were used for comparative purposes.

9.2   Conclusions to SG Horizontal Scratch tests

9.2.1 Signal and Material Analysis Perspective

For the horizontal scratch test work the aerospace material; CMSX4 was mainly investigated. Once the microscopic level of grinding activity had been identified and verified through a number of repeat tests it was then ready for identification at the macro

level phenomenon (full grinding pass data identification). Similar to the radial scratch tests, acoustic emission (AE) signals were used to identify the SG phenomenon of cutting, ploughing and rubbing. With the use of two AE sensors that were more sensitive to grinding activity, the noise therefore was less of a problem than that experienced with the radial scratch tests. There was still a need to use filtration techniques to ensure the phenomenon of interest was crisp however, with the horizontal scratch cuts the majority of signal belonged to the material emitted AE signal.

The work demonstrated that STFT as a useful technique to distinguish the frequency bands occupied by cutting, ploughing and rubbing phenomena (WPT used to verify STFT signal analysis). The results show that the AE energy for the three phenomena is concentrated between the frequency ranges of 50 kHz to 1 MHz. HCE Parallel co-ordinates were used to see the general patterns for cutting, ploughing and rubbing phenomena. From those patterns it was possible to see all three phenomena occupied peaks between 50 and 500 KHz frequency range. Cutting had the most dominant peaks and next, ploughing, followed lastly by rubbing.

Cutting and ploughing were difficult to distinguish due to their similar plastic material energy properties. Rubbing was difficult to distinguish from noise, this is due to the noise occupying peak frequency levels in-between the identified levels for rubbing phenomenon. To that end, as some rubbing cases consisted of noise it was thought the extra classification of noise would be confusing for the classifier and hinder classification accuracy. The rubbing phenomenon was seen to either have slightly higher

amplitudes than that of noise (occupies a wider range of frequency bands than that of noise) and in some cases having less magnitude than that of noise which was assumed due to the damping of the AE signal experienced in some of the identified rubbing cases. This is verified from the obtained AE hit data with no mark being present on the workpiece, the next 1μm depth cut increment provided both the scratch hit phenomenon for cutting, ploughing and further rubbing. In the case of the scratch hit phenomenon the rubbing was determined from the AE time span covering more of a signal when compared with the actual distance travelled of the scratch groove (the surface here was consistent with the general roughness of the workpiece). The rubbing phenomenon is different from both cutting and ploughing phenomenon as it only possesses elastic deformation energy properties. Ploughing and cutting has both plastic and elastic deformation energy properties. With elastic deformation there should be no or miniscule marking (smear like mark) on the workpiece.

9.2.2 Horizontal SG Scratch Classification

The first part of horizontal single grit scratch tests was concerned with identifying the fundamental signatures of Single Grit (SG) phenomenon. The second part of the work concludes the horizontal SG scratch investigation by classifying cutting, ploughing and rubbing phenomena using classification techniques such as Artificial Neural Networks (ANN) and Fuzzy-c clustering/Genetic Algorithm (GA) classification techniques. Other techniques were used to verify the signal results such as Support Vector Machines (SVMs) however this involved the dual classification of the cutting and ploughing then the dual classification of cutting and ploughing verses rubbing (the results here were

The University of Nottingham

encouraging too). This work has demonstrated STFT as a useful technique to distinguish the frequency bands occupied by cutting, ploughing and rubbing phenomena.

Both the ANN and Fuzzy-c clustering/GA classifiers were found to have a high confidence in distinguishing cutting, ploughing and rubbing phenomenon. The ANN classified the phenomena at 87% classification accuracy for the unseen test data set and, 93% for the total test classification accuracy. The Fuzzy-c clustering/GA had a 90% total data set classification accuracy (both training and test sets was presented to the classifier for this accuracy result). Fuzzy-c clustering algorithm with GA optimisation is a novel approach to classification problems and has not been discussed in literature before.

Further tests investigated hit data taken from grinding passes with 1μm and 0.1mm depth cuts (actual wheel passes), both classifiers indicated more percentage of cutting utilisation when the process had more interaction between workpiece and grit (i.e. from an increased depth of cut). The rubbing and first hit for 1μm scratch had more rubbing percentage utilisation when compared with both ploughing and cutting phenomenon. Looking at the general patterns from the three different grinding passes both classifiers provided encouraging results. There were classification differences attributed to different classification strategies such as with the increased cluster sets for the dynamically changing Fuzzy-c/GA classifier between one data introduction and the next. Whereas with the ANN engine this remained static in its classification throughout all the applied grinding pass data. There will always be slight differences between the two

The University of
Nottingham

classifiers as Fuzzy-C/GA is a non-supervised technique and ANN is a supervised technique. These differences are based on Fuzzy-c/GA clustering providing classification for data that has membership to many clusters albeit the chosen cluster has the most membership intensity for the specific data point under test and on the converse; ANN is a parallel statistical process that makes hard, crisp classifications of data, i.e. either 1 or 0 and not in-between. Therefore, there are subtle differences between the classifiers however they should both give the same general patterns of regression or classification in terms of results and assumptions. This was the first kind of work into the investigation and classification of AE intensities emitted from the different states of a horizontal single grit scratch. This novel work has confidently identified and classified the three grinding phenomena namely, cutting, ploughing and rubbing through AE extracted signal footprints. The research discussed here can be directly applied to controlling efficient micro grinding strategies and is the initial work to identifying the macro ratios of cutting, ploughing and rubbing experienced in grinding anomalies such as chattering and burn. In addition, this initial work can change the face of grinding by using AE signal footprints to test whether the unit material event (grit and workpiece) gives a good indication to the general material removal rates (MRR) and, efficient grinding energies before being used within the macro grinding event. For example, different grit material can be tested on the workpiece material for specific MRR. With future work merging the gap between the unit and multiple grinding events (micro to macro grinding event) more generalised grinding patterns will be obtained. This is reference to the in-between understanding of grinding efficiencies in terms of cutting, ploughing and rubbing through the intelligent identification of unwanted phenomena

such as chattering and burn. This 'bridging the gap' between the unit and multiple grit event can be achieved through the use of multi grits occupying more space along the steel wheel and increasing the grit length to investigate the changing effects. In addition, these tests could provide the way to deciding new grinding wheel architectures be it the use of new grit materials or even the strategy of how they are bonded together to make the wheel topography. Both the work on radial and horizontal scratch tests are novel and can set future standards in the way difficult to cut materials is machined. This is based on different grinding mechanics, signatures obtained for different hardness materials and therefore ensuring the cutting parameters are both controlled and optimised for that specific material.

9.3   Conclusions Anomalies Tests

Chapter 8 displayed some novel work in terms of multiple grinding phenomena classification using both conventional and novel evolutionary classification techniques. There has been very little work in looking at multiple phenomena classification especially with multiple concatenated extracted signal analysis. The research presented in Chapter 8 looked at both aspects of multiple phenomena classification. Accurate multiple classification machining strategies are useful for current manufacturing environments this is due to the manufacturing requirements being able to identify different anomaly initiation. These results also investigated the AE signal characteristics of burn when exerted from different materials. In addition, thermocouple measurements were made to bolster burn identification results. The results displayed by Fuzzy-c/GA clustering and tree regression, displayed the chatter and burn extracted AE signal

analysis were separable. The GP Paradigm provided powerful rules to separate both chatter and burn to a high level of accuracy. The two datasets used for multiple classifications were (1) AE and (2) AE, force, power and accelerations. GP suffers from large n-dimensional data problems and therefore requires n-dimensional reduction techniques to ensure the data applied to the classifier is both salient and rich in terms of describing the actual data. Independent Component Analysis (ICA) was used to reduce the transformed signal data of AE, thrust force, power and thrust accelerations. For the transformed AE data, statistical windowing techniques of the kurtosis, standard deviation and maximum were used to provide salient and rich data to the GP classifier. Both sets of data were accurately classified giving the minimum and maximum values between classes (see Table 8.4). The rules were given in regard to some of the GP executions (reference Table 8.3 and Table 8.4), these obtained rules would provide a classifier (be it in integrated circuit hardwire form or, rules on a dedicated on-line monitoring system) with the necessary information to identify anomalies of interest for specific sets of 'grinding speeds and feeds.'   With many different investigations into the range of anomalies for different 'speeds and feeds' the GP system can provide specific rules for segregating the data at specific cutting parameters and with many different rules; an advanced robust classification system can evolve. The work achieved in Chapter 7 can then be merged with the work in Chapter 8, this is where the generic classifier identifies anomalies through ratios of cutting, ploughing and rubbing. To prove these concepts in terms of macro cutting, ploughing and rubbing more future work is required.

9.4 Thesis Gaps Addressed

- Data reduction techniques supplying rich summarised accurate data to a classifier system in terms of anomalies distinction.

- Using STFT technique to identify cutting, ploughing and rubbing AE footprint signatures.

- Using WT technique to identify and verify the grinding phenomenon, namely cutting, ploughing and rubbing AE footprint signatures.

- Distinguishing and classifying both radial and horizontal single grit scratch tests in terms of AE footprint signatures correlated to measured material removal rates.

- Classifying $0.1\mu m$ and $0.1mm$ horizontal grinding pass cuts when presented to classifiers with previously trained and classified SG scratch cut data.

- Looking at the AE signatures correlated to cutting, ploughing and rubbing phenomenon for different materials with diverse material characteristics.

- Produced accurate and comparable results from a novel non-linear Fuzzy-c/GA assisted clustering algorithm against conventional ANN back-propagation MLP classifier.

- Multiple classification system indentifying chatter and burn grinding anomalies phenomena.

- Identifying burn with coolant present from using STFT DSP techniques and thermocouple measurements.

The University of
Nottingham

- Comparison of evolutionary classification techniques such as Fuzzy-c/GA, GP and Data Mining Tree Regression.

- Multiple classification of generic grinding classifier system using GP with dynamic sliding fitness functions.

- Multiple classification of generic classifier system using n-dimensional reduction techniques such a statistical window reduction and ICA.

9.5 Future work

This work has been carried out over the last three years and has found some very encouraging results for both SG cutting phenomena and the multiple classification of grinding anomaly phenomena. From carrying out this work, a number of areas were exposed for the first time and a lot of future work can result from the work carried out within this thesis. With reference to the SG scratch test (cutting, ploughing and rubbing identification work); the next part of this investigation could look at several pieces of grit being glued into equally spaced holes along a steel plate. This will show the AE signatures for several SG cuts made simultaneously. Again, the material evaluations can be made for this multi event and investigate whether the unit results of single scratch tests correlate with that of the multi grit event results. Following on, several experiments could be carried out by looking at increasing the amount of grit protruding from the steel plate and investigate the effects of such changes. From bridging the gap between the micro and macro grinding unit events, it is possible to gain both efficient and safe machining strategies.

The University of Nottingham

The actual work carried out in Chapter 7 looked at the classification of cutting, ploughing and rubbing using both; ANN and Fuzzy-c/GA clustering techniques. The classification of 0.1µm data and 0.1mm macro grinding data were classified from the measured cutting, ploughing and rubbing SG cut tests. This data can be extended towards controlling efficient micro-grinding strategies which is becoming more prolific in current hi-tech manufacture.

This research can lead onto providing wheels of different materials to work better with different workpiece materials. For example, the grit material could be tested with a specific workpiece material and evaluated in terms of Material Removal Rate (MRR), energy and surface finish. These results could be built-up in a special features database to give users a quick heads up of what is the best tool material for cutting a specific type of material. In addition, the wheel architecture could be changed in terms of total grit utilisation within the wheel profile. For instance; which architecture gives the most efficient cut in terms of MRR and wheel loading? This could also mean the wheel has more gaps than current wheels allowing it to disperse more heat, more quickly and, remove greater quantities of stock material in rough machining.

Other horizontal SG work could look at the difference between AE signatures of dull and sharp grits investigating the difference in grinding mechanics such as ploughing and rubbing utilisation becoming more apparent from the cutting utilisation which is expected to be more prominent when considering efficient grinding.

The University of Nottingham

With current acquisition cards and load cells it was not possible to extract the force and accelerations of the micro SG scratch event. AE is more sensitive to such burst events and therefore this was the only sensor technology to extract the signal material event and provide the analysis for the unit event of actual manufacturing grinding mechanics. By using a fast acquisition card it would be useful to verify the AE signals with force and acceleration measurements (tangential and normal respectively) and note when cutting, ploughing and rubbing takes place in terms of both force and accelerations. As with previous research, once this equipment had been set up, more experiments looking at the grinding mechanics in terms of material removal and extracted signals could exist giving the user and grinding community more information about current grinding strategies. Such tests could be to slow the machine down and investigate effects at different speeds and feeds. This maybe not useful for actual manufacturing monitoring however it would give more information about fundamental mechanics of SG scratch tests and the effects on the AE extracted signal analysis.

Future work could look at residual stress measurements made from the unit event and macro grinding wheel pass. This again is useful in promoting efficient and quality intensive grinding strategies. AE and the SG unit event could be further investigated in terms of slow rotational speeds to faster speeds understanding the gradual cutting, ploughing and rubbing mechanisms. This work used speeds that are based on industrial practices used in manufacturing aerospace parts. In addition, an FEA model could be useful in modelling the unit and macro grinding mechanisms. The future work discussed here is beyond the scope of this research and provides new insights into novel

approaches and understanding the grinding mechanisms promoting efficient grinding especially when considering more difficult to cut materials are emerging within the market today.

For future work the following gaps could be approached in sensor advancement:

- Compression algorithms for storing the huge AE data and ensuring rapid graphical display.

- An array of AE sensors to give a 3D image of the surface interaction

- Develop online monitoring system used for advanced AE signature analysis and other sensory features in a data fusion approach.

- For single grit scratch tests use a much higher sampling rate (2 MHz) than the current system and extract force, accelerations and power information.

- Use sensor fusion with optical fibre to acquire the heat gained from the grinding zone.

- Carry out trials with AE and residual test measurements and see if the signals and measurements correlate.

There are other gaps that were investigated but time constraints dictated they be left for future work:

- Providing dynamic intelligent adaptive filters based on Chenbyshev II filters, Linear Regression with Support Vector Machines or Independent Component Analysis (ICA) (See Chapter 6) and several noise signals normalised by variance throughout the signal.

- Providing a time-frequency analysis technique that is based on the dynamic window of WT and the ease of use with STFT; such a representation could be the Zhao-atlas-Marks distribution (Cohen 1995).

The generic classifier work looking at multiple classifications can be improved with Adaptive Dynamic Functions (ADFs) in terms of low level classifiers. For example, the classifier could use an n-dimensional reduction technique such as that used in Chapter 8 then use an auto correlation function to provide a weighted measure for GP rule classification. Instead of using an n-dimensional reduction technique, another classifier could be built into the GP functionality as another ADF namely; Fuzzy-c clustering. This dynamic generic classifier could then be used to provide a range of different grinding scenarios for 'varying speeds and feeds' and control both the efficiency preventing the occurrence of unwanted anomalies. These rules can then be introduced into a dynamic rule base firing system where the rules are weighted and based on different grinding scenarios. Such a system could be fused into integrated circuit electronics with real time characteristics and a system feedback loop to update the weights in terms of good or bad control (maximising efficiency, surface quality and anomaly elimination). This work has provided a lot of novel work and technology to the manufacturing arena and from this initial work can provide a fully operational generic monitoring tool.

References

Akbari, J., Y. Saito, et al. (1996). "Effect of grinding parameters on acoustic emission signals while grinding ceramics." <u>Journal of Materials Processing Technology</u> **62**(4): 403-407.

Al-Habaibeh, A. and N. Gindy (2000). "A new approach for systematic design of condition monitoring systems for milling processes." <u>Journal of Materials Processing Technology</u> **107**(1-3): 243-251.

Al-Habaibeh, A. and N. Gindy (2001). "Self-learning algorithm for automated design of condition monitoring systems for milling operations." <u>International Journal of Advanced Manufacturing Technology</u> **18**(6): 448-459.

Al-Habaibeh, A., F. Zorriassatine, et al. (2002). "Comprehensive experimental evaluation of a systematic approach for cost effective and rapid design of condition monitoring systems using Taguchi's method." <u>Journal of Materials Processing Technology</u> **124**(3): 372-383.

APA, A. P. A. (2007). "Pattern Recognition." <u>Dictionary.com, Unabridged (v1.1), Retrieved May 18, 2007 from Dictionar.com webste:</u> http://dictionary.reference.com/browse/pattern recognition.

Axinte, D. A. and N. Gindy (2003). "Tool condition monitoring in broaching." <u>Wear</u> **254**(3-4): 370-382.

Axinte, D. A., M. Kritmanorot, et al. (2005). "Investigations on belt polishing of heat-resistant titanium alloys." <u>Journal of Materials Processing Technology</u> **166**(3): 398-404.

Back, T., D. B. Fogel, et al. (2000). "Evolutionary Computation 1 & 2." <u>Institute of Physics Publishing, Bristol, UK</u>.

Badger, J. A. and A. A. Torrance (2000). "A comparison of two models to predict grinding forces from wheel surface topography."

International Journal of Machine Tools & Manufacture **40**(8): 1099-1120.

Barbezat, M., A. J. Brunner, et al. (2004). "Acoustic emission sensor properties of active fibre composite elements compared with commercial acoustic emission sensors." <u>Sensors and Actuators a-Physical</u> **114**(1): 13-20.

Baul R.H. and Shilton R. (1967). "Mechanics of metal grinding with particular reference to Monte Carlo simulation Proceedings." <u>8th MTDR Conference</u>: 923.

Bezombes, F. A., D. R. Burton, et al. (2006). <u>Fibre bragg grating temperature sensors for grinding application</u>. 4th International Conference on Manufacturing Research, Liverpool JMU.

Bishop, C. M. (1995). "Neural Networks for Pattern Recognition." <u>Clarendon Press, Oxford</u>.

Boczar, T. and M. Lorenc (2006). "Time-frequency Analysis of the Calibrating Signal Generated in the Hsu-Nielsen System, Physics and Chemistry of Solid State." **7.3**: 585-588.

Booker, L. B., D. E. Goldberg, et al. (1989). "Classifier Systems and Genetic Algorithms." <u>Artificial Intelligence</u> **40**(1-3): 235-282.

Brinksmeier, E. and C. Heinzel (1999). "Friction, cooling and lubrication in grinding." <u>CIRP Annals - Manufacturing Technology</u> **48**(2): 581-598.

Buttery, T. C. and J. F. Archard (1971). "Some Microscopical Investigations of Grinding and Abrasive Wear." <u>Journal of Microscopy-Oxford</u> **94**(Naug): 13-&.

Byrne, G. (1995). "Tool Condition Monitoring (TCM) - The Status of Research and Industrial Application." <u>Annals of the CIRP</u> **48**(2): 541-567.

Carroll, S. B. (1995). "Homeotic genes and the evolution of arthropods and chordates." <u>Nature, 376,</u>: 479-485.

Chen, M. and B. Y. Xue (1999). "Study on acoustic emission in the grinding process automation." <u>American Society of Mechanical Engineers, Manufacturing Engineering Division, MED Manufacturing Science and Engineering - 1999 (The ASME International Mechanical Engineering Congress and Exhibition) - Nashville, TN, USA</u>.

Chen, X., Z. Feng, et al. (2004). "Comparison of laser cleaning of Al2O3 and CBN grinding wheels." <u>Advances in Abrasive Technology Vi</u> **257-258**: 365-370.

Chen, X., Z. Feng, et al. (2004). "A study on laser cleaning of Al2O3 grinding wheels." <u>Advances in Abrasive Technology Vi</u> **257-258**: 359-364.

Chen, X., J. Griffin, et al. (2007). "Mechanical and Thermal Behaviours of Grinding Acoustic Emission." <u>International Journal of Manufacturing Technology and Management (IJMTM)</u> **12**(1-3): 184-199.

Chen, X. and Q. Liu (2004). "Grinding burn identification through AE monitoring." <u>3rd International Conference and Exhibition on Design and Manufacturing of Die and Moulds, ISAAT 2004</u>.

Chen, X., Q. Liu, et al. (2005). "Signal analysis of acoustic emission for laser imitating grinding burn." <u>Advances in Abrasive Technology Viii</u> **291-292**: 91-96.

Chen, X. and W. B. Rowe (1996). "Analysis and simulation of the grinding process .1. Generation of the grinding wheel surface." <u>International Journal of Machine Tools & Manufacture</u> **36**(8): 871-882.

Chen, X. and W. B. Rowe (1996). "Analysis and simulation of the grinding process .2. Mechanics of grinding." <u>International Journal of Machine Tools & Manufacture</u> **36**(8): 883-896.

Chen, X., W. B. Rowe, et al. (2002). "Precision grinding using CBN wheels." International Journal of Machine Tools & Manufacture **42**(5): 585-593.

Chen, X., W. B. Rowe, et al. (1996). "Grinding vibration detection using a neural network." Proceedings of the Institution of Mechanical Engineers Part B-Journal of Engineering Manufacture **210**(4): 349-352.

Chen, X., W. B. Rowe, et al. (2000). "Analysis of the transitional temperature for tensile residual stress in grinding." Journal of Materials Processing Technology **107**(1-3): 216-221.

Chiou, R. Y. and S. Y. Liang (2000a). "Dynamic modeling of cutting acoustic emission via piezoelectric actuator wave control." International Journal of Machine Tools & Manufacture **40**(5): 641-659.

Chiou, R. Y. and S. Y. Liang (2000b). "Analysis of acoustic emission in chatter vibration with tool wear effect in turning." International Journal of Machine Tools & Manufacture **40**(7): 927-941.

Chiou, Y. S., E. S. Chung, et al. (1995). "Analysis of Tool Wear Effect on Chatter Stability in Turning." International Journal of Mechanical Sciences **37**(4): 391-404.

Chui, K. C. (1992). "An Introduction to Wavelets." Academic Press, San Diego.

Clausen, R., C. Y. Wang, et al. (1996). "Characteristics of acoustic emission during single diamond scratching of granite." Industrial Diamond Review **56**(3): 96-99.

Cohen, L. (1993). "The Scale Representation." Ieee Transactions on Signal Processing **41**(12): 3275-3292.

The University of Nottingham

Cohen, L. (1995). "Time-Frequency Analysis." <u>Prentice Hall Signal Prcoessing Series, Alan V. Oppenhiem series editor, Englewood Cliffs, NJ</u>.

Cohen, L. (1996). "A general approach for obtaining joint representations in signal analysis .1. Characteristic function operator method." <u>Ieee Transactions on Signal Processing</u> **44**(5): 1080-1090.

Coman, R. and I. D. Marinescu (1999). "Acoustic Emission Signal - an effective tool for monitoring the grinding process." <u>Abrasives</u> **5**.

Comon, P. (1994). "Independent Component Analysis, a New Concept." <u>Signal Processing</u> **36**(3): 287-314.

Crisp, J., J. Seidel, et al. (1968). "Measurement of forces during cutting with a single abrasive grain." <u>Int. J. Prod. Res.</u> **7**(2): 159.

Cuevas, A., M. Febrero, et al. (2001). "Cluster analysis: a further approach based on density estimation." <u>Computational Statistics and Data Analysis</u> **36**: 441-459.

Cus, F. and J. Balic (2003). "Optimization of cutting process by GA approach." <u>Robotics and Computer-Integrated Manufacturing</u> **19**(1-2): 113-121.

Danzl, R., F. Helmli, et al. (2006). "Comparison of roughness measurements between a contact stylus instrument and an optical measurement device based on a colour focus sensor." <u>NSTI Nanotechnology Conference and Trade Show - NSTI Nanotech 2006 Technical Proceedings</u> **3**: 284-287.

Daubechies, I. (1992). "Ten Lectures on Wavelets." <u>CBMS-NSF Regional Conference Series in applied Mathematics</u>.

Deiva, N. and R. L. Vijayaraghavan (1999). "In-process monitoring of grinding burn in the cylindrical grinding of steel." <u>Journal of Materials Processing Technology</u> **91**(1): 605-611.

Demetriou, M. D. and A. S. Lavine (2000). "Thermal aspects of grinding: The case of up grinding." <u>Transactions of the ASME-Journal of Manufacturing Science and Engineering</u> **122**(4): 605-611.

Doyle E.D. and Samuels L.E. (1974). "Further Development of the model of Grinding." <u>Proceedings of the International Conference on Production Engineering, published by the Japenese Society of Precision Engineers</u> **Part 2**.

Duda, R. O., P. E. Hart, et al. (2001). <u>Pattern Classification</u>. New York, A Wiley-Interscience Publication.

Farmer, D. A. (1967). "Grinding." <u>Journal of Engineering for Industry</u> **89**(1): 15-&.

Fisher, R. M. and J. S. Lally (1967). <u>Canadian Journal of Physics, CJPHA</u> **45**(2, Part 3): 1147-59.

Force, A., M. Lynch, et al. (1999). "Preservation of duplicate genes by complementary, degenerative mutations." <u>Genetics</u> **151**: 1531-1545.

Friedman, M. and A. Kandel (1999). "Introduction to Pattern Recognition: Statistical, Structural, Neural, and Fuzzy Logic Approches." <u>River Edge, N.J., World Scientific</u>.

Fu, S., J. Raja, et al. (2002). "Recent advances in seperation in roughness, waviness and form,." <u>Precision Engineering</u> **26**(2): 222-235.

Graham, D. and R. M. Baul (1972). "An investigation into the mode of metal removal in the grinding process." <u>Wear</u> **19**: 301.

Griffin, J., . and X. Chen (2007). "The classification of rubbing, ploughing and cutting during grinding and the comparison of different evolutionary inspired classification techniques." <u>40th CIRP International Seminar on Manufacturing Systems, Department of Engineering, University of Liverpool,</u> : CD Proceedings PT2.

The University of Nottingham

Griffin, J. and X. Chen (2006). "Classification of the Acoustic Emission Signals of Rubbing, Ploughing abd Cutting during Single Grit Scratch Tests." International Journal of Nanomanufacturing **1**(2): 189-209.

Griffin, J. and X. Chen (2006). "Classification of the Acoustic Emission Signals of Rubbing, Ploughing and Cutting during Single Grit Scratch Tests." International Journal of Nanomanufacturing **1**(2): 189-209.

Griffin, J. and X. Chen (2006). "Classification of varying levels of ploughing, rubbing and cutting during single grit tests using evolutionary inspired computer techniques." ICMR, Liverpool John Moores University, : 217-222.

Griffiths, B. (2001). "Manufacturing Surface Technology - Surface Integrity and Fuctional Performance." Manufacturing Engineering Modular Series: 45-49.

Griffiths, B. J., R. H. Middleton, et al. (1996). "Condition monitoring of the grinding process using light scattering." Wear **198**(1-2): 39-45.

Guo, C. and S. Malkin (1994). "Analytical and experimental investigation of burnout in creep-feed grinding." CIRP Annals **43**(1): 283-286.

Guo, C. and S. Malkin (1995). "Analysis of transient temperatures in grinding." Journal of Engineering for Industry-Transactions of the Asme **117**(4): 571-577.

Guo, C. and S. Malkin (1996). "Inverse heat transfer analysis of grinding .1. Methods." Journal of Engineering for Industry-Transactions of the Asme **118**(1): 137-142.

Guo, C. and Y. Wu (1999). "Temperatures and energy partition for grinding with vitrified CBN wheels." Cirp Annals-Manufacturing Technology **48**(1): 247-250.

The University of Nottingham

Hamid, M. S. (1977). "Grinding Mechanics - Single Grit Approach." PhD Thesis, Leicester Polytechnic.
    single grit force models

Hartigan, J. (1985). "Statistical theory in clustering." Journal of classification **2**: 63-76.

Hartl, D. L. and G. Clark (1997). "Principles of population genetics." Sunderland, MA., Sinauer Associates.

Hashimoto, M., E. Marui, et al. (1996). "Experimental research on cutting force variation during regenerative chatter vibration in a plain milling operation." International Journal of Machine Tools & Manufacture **36**(10): 1073-1092.

Hassui, A. and A. E. Diniz (2003). "Correlating surface roughness and vibration on plunge cylindrical grinding of steel." International Journal of Machine Tools & Manufacture **43**(8): 855-862.

Haykin, S. (1999). "Neural Networks, A Comprehensive Foundation." Prentice Hall, NJ.

Hobson, T. (2003). "Exploring Surface Texture - A fundemental guide to the measurement of finish." Taylor Hobson Limited.

Holford, K. M. (2000). "Acoustic emission - basic principles and future directions,." Strain **36**(2): 51-54.

Holland, J. H. (1975). "Adaption in Natural and Artificial Systems: An Introductory Analysis with Applications to Biology, Control, and Artificial Intelligence." University of Michigan Press. Also second edition, The MIT Press 1992.

Holland, J. H. (1992). "Genetic Algorithms." Scientific American **267**(1): 66-72.

Howard, D. and S. C. Roberts (2002). "The prediction of journey times on motorways using genetic programming." Applications of Evolutionary Computing, Proceedings **2279**: 210-221.

The University of Nottingham

Howard, D., S. C. Roberts, et al. (1999a). "Target detection in SAR imagery by genetic programming." Advances in Engineering Software **30**(5): 303-311.

Howard, D., S. C. Roberts, et al. (1999b). "Target detection in SAR imagery by genetic programming." Advances in Engineering Software **30**(5): 303-311.

Howard, D., S. C. Roberts, et al. (1999c). "Evolution of ship detectors for satellite SAR imagery." Genetic Programming **1598**: 135-148.

Howard, D., S. C. Roberts, et al. (2006). "Pragmatic Genetic Programming strategy for the problem of vehicle detection in airborne reconnaissance." Pattern Recognition Letters **27**(11): 1275-1288.

Howard, L. M. and D. J. Dangelo (1995). "The Ga-P - a Genetic Algorithm and Genetic Programming Hybrid." Ieee Expert-Intelligent Systems & Their Applications **10**(3): 11-15.

Hyvarinen, A. and E. Oja (1996). "Simple neuron models for independent component analysis." International Journal of Neural Systems **7**(6): 671-687.

Hyvarinen, A. and E. Oja (1997). "A fast fixed-point algorithm for independent component analysis." Neural Computation **9**(7): 1483-1492.

Hyvarinen, A. and E. Oja (1998). "Independent component analysis by general nonlinear Hebbian-like learning rules." Signal Processing **64**(3): 301-313.

Hyvarinen, A. and E. Oja (2000). "Independent component analysis: algorithms and applications." Neural Networks **13**(4-5): 411-430.

Inasaki, I. (1998). "Application of acoustic emission sensor for monitoring machining processes." Ultrasonics **36**: 273-281.

The University of Nottingham

Inasaki, I., B. Karpuschewski, et al. (2001). "Grinding chatter - Origin and suppression." <u>Cirp Annals-Manufacturing Technology</u> **50**(2): 515-534.

James, S. D. (1994). "Verification and Validation of Neural Networks, Proceedings of the Neural Network Workshop for the Hanford Community, ." <u>Pacific Northwest National Laborartory, Richland, WA, USA</u>: 76-80.

Jemielniak, K. (2001). "Some aspects of acoustic emission signal pre-processing." <u>Journal of Materials Processing Technology</u> **109**(3): 242-247.

Jinwook, S. and B. Shneiderman (2002). "Interactively Exploring Hierarchical Clustering Results." <u>IEEE Computer</u> **35**(7): 80-86.

Johnson, J. H., P. D. Picton, et al. (1993). "Safety-Critical Neural Computing - Explanation and Verification in Knowledge Augmented Neural Networks." <u>Artificial Intelligence in Engineering</u> **8**(4): 307-313.

Kaiser, J. (1950). "Untersuchugeb uber das auftrten Gerauschen beim Zugversuch." <u>PhD Thesis, Munich University</u>.

Kalpakjian, S. and S. R. Schmid (2003). "Manufacturing Process for Engineering Materials." <u>Prentice Hall</u>: 510-520.

Karpat, Y. and T. Ozel (2006). "Predictive analvtical and thermal modeling of orthogonal cutting process - Part II: Effect of tool flank wear on tool forces, stresses, and temperature distributions." <u>Journal of Manufacturing Science and Engineering-Transactions of the Asme</u> **128**(2): 445-453.

Karpat, Y. and T. Ozel (2006). "Predictive analytical and thermal modeling of orthogonal cutting process - Part I: Predictions of tool forces, stresses, and temperature distributions." <u>Journal of Manufacturing Science and Engineering-Transactions of the Asme</u> **128**(2): 435-444.

Kato, T. and H. Fujii (1997). "Temperature measurement of workpiece in surface grinding by PVD film method." Journal of Manufacturing Science and Engineering-Transactions of the Asme **119**(4B): 689-694.

Kato, T. and H. Fujii (1999). "Energy partition in conventional surface grinding." Journal of Manufacturing Science and Engineering-Transactions of the Asme **121**(3): 393-398.

Kim, N. K. and C. Guo (1997). "Heat flux distribution and energy partition in creep-feed grinding." CIRP Annals - Manufacturing Technology **46**(1): 227-232.

Klumpen, T. H. (1994). "Acoustic Emission (AE) beim Schleifen." Dr-Ing Dissertation, RWTH, Aachen.

Kosa, J. R. (1994). "Genetic Programming II - Automatic Discovery of Reusable Programs." The MIT Press, Cambride MA, London, England.

Kwak, J. S. and M. K. Ha (2004). "Intelligent diagnostic technique of machining state for grinding." International Journal of Advanced Manufacturing Technology **23**(5-6): 436-443.

Kwak, J. S. and J. B. Song (2001). "Trouble diagnosis of the grinding process by using acoustic emission signals." International Journal of Machine Tools & Manufacture **41**(6): 899-913.

Lai, E. (2004). "Practical Digital Signal Processing for Engineers and Technicians." Oxford, Newnes.

Lezanski, P. (2001). "Intelligent system for grinding wheel condition monitoring." Journal of Materials Processing Technology **109**(3): 258-263.

Li, X. (1998). "Tool wear monitoring with wavelet packet transform-fuzzy clustering method." Wear **219**(2): 145-154.

Li, X. and J. Wu (2000). "Wavelet analysis of acoustic emission signals in boring Part B,." Journal of Engineering Manufacture **214**(5): 421-424.

Li, Y., S. M. Gracewski, et al. (2002). "Analysis of chatter in contour grinding of optical materials." International Journal of Machine Tools & Manufacture **42**: 1095-1103.

Liang, Y. N., S. Z. Li, et al. (1996). "Some developments for single-pass pendulum scratching." Wear **199**(1): 66-73.

Linderman, K., R. G. Schroeder, et al. (2003). "Six Sigma: a goal-theoretic perspective." Journal of Operations Management **21**(2): 193-203.

Liu, Q. (2004). "Pattern Recognition of Grinding Defects and Assessment Strategies of Grinding." Diss. University of Nottingham, School of M3.

Liu, Q., X. Chen, et al. (2005). "Fuzzy pattern recognition of AE signals for grinding burn." International Journal of Machine Tools & Manufacture **45**(7-8): 811-818.

Liu, Q., X. Chen, et al. (2006). "Investigation of acoustic emission signals under a simulative environment of grinding burn." International Journal of Machine Tools & Manufacture **46**(3-4): 284-292.

Lui, Q. (2004). "Pattern Recognition of Grinding Defects and Assessment Strategies of Grinding." Diss. University of Nottingham, School of M3.

Malkin, S. and N. H. Cook (1971). "Wear of Grinding Wheels .1. Attritious Wear." Journal of Engineering for Industry **93**(4): 1120-&.

Mallat, S. G. (1999). "A wavelet tour of Signal Processing." San Diego, London, Academic Press **2nd Ed**.

The University of Nottingham

Mardei, C. and R. Piotrkowski (2002). "Monitoring of the tool condition with acoustic emission signal analysis using wavelet packets, ." Insight: Non-Destructive Testing and Condition Monitoring **44**(12): 786-791.

Marshall, E. and M. C. Shaw (1952). "Forces in dry surface grinding Trans " ASME: 51.

Martin, A. P. (1999). "Increasing genomic complexity by gene duplication and the origin of vertebrates." The American Naturalist **154**(2): 111-128.

McCulloch, W. S. and W. H. Pitts (1943). "A logical calculis of the ideas immanent in nervous activity." Bulletin of Mathematical Biophysics **5**: 115-133.

Mitra, S. and S. K. Pal (2002). "Data mining in soft computing framework: A survey." IEEE Transactions on Neural Networks **13**(1): 3-14.

Mokbel, A. A. and T. M. A. Maksoud (2000). "Monitoring of the condition of diamond grinding wheels using acoustic emission technique." Journal of Materials Processing Technology **101**(1-3): 292-297.

Natarajan, D. R. (2004). "Investigation on the Use of Multiple Acoustic Emission Sensors to Detect Prcoess Disturbances in Machining." Diss. University of Nottingham.

Oppenheim, A. V. and R. W. Schafer (1999). "Discrete-Time Signal Processing." Prentice-Hall, Upper Saddle River, NJ.

Oscar, G. B., R. Eduardo, et al. (2006). "Chattering detection in cylindrical grinding processes using wavelet transform." International Journal of Machine Tools & Manufacture

Ozel, T. and Y. Karpat (2005). "Predictive modeling of surface roughness and tool wear in hard turning using regression and neural

The University of Nottingham

networks." International Journal of Machine Tools & Manufacture **45**(4-5): 467-479.

Pandit, S. M. and G. Lin (1991). "Data Dependent Systems Methodology for Validation of Simulation-Models Illustrated by End-Milling." International Journal of Production Research **29**(6): 1251-1261.

Peleckmans, K., J. A. K. Suykens, et al. (2003). "LS-SVMLab Toolbox User's Guide." ESAT-SCD-SISTA Technical Report 02-145, Katholieke Universiteit Leuven, Belgium, http://www.esat.kuleuven.ac.be/sista/lssvmlab/ **version 1.5**.

Peterson and Gerald (1992). "A framework for Neural Network Evaluation." McDonnel Douglas Technical Report MDRL TN-92-02, McDonnel Douglas Research Laboratories, St. Louis, Missouri.

Poli, R. and W. B. Langdon (2006). "Backward-chaining evolutionary algorithms." Artificial Intelligence **170**(11): 953-982.

Poli, R., W. B. Langdon, et al. (2005). "Extending particle swarm optimisation via genetic programming." Genetic Programming, Proceedings **3447**: 291-300.

Pollock, A. (1977). "Structural Calibration Technique for Quantitative Application of Acoustic-Emission." Acustica **38**(5): 281-284.

Pollock, A. A. (1973). "Acoustic Emission .2. Acoustic Emission Amplitudes." Non-Destructive Testing **6**(5): 264-269.

Pollock, A. A. (1976). "Acoustic-Emission." Machine Design **48**(8): 72-76.

Pollock, A. A. (1979). "Introduction to Acoustic-Emission and a Practical Example." Journal of Environmental Sciences **22**(2): 39-41.

Pollock, A. A. (2004). "Loading and stress in acoustic emission testing." Materials Evaluation **62**(3): 326-333.

The University of Nottingham

Prins, J. F. (1971a). "Single Diamond Particle Interaction on Steels." Industrial Diamond Review **31**(370): 364-&.

Prins, J. F. (1971b). "Study of Single Diamond Particle Interaction on Alumina." Industrial Diamond Review **31**(373): 497-&.

Qiang, L. (2004). "Pattern Recognition of Grinding Defects and Assessment Strategies of Grinding." PhD Thesis, University of Nottingham, School of M3.

Raj, B. and B. B. Jha (1994). "Fundamentals of Acoustic-Emission." British Journal of Non-Destructive Testing **36**(1): 16-23.

Roth, J. T. and S. M. Pandit (1999). "Monitoring end-mill wear and predicting tool failure using accelerometers." Journal of Manufacturing Science and Engineering-Transactions of the Asme **121**(4): 559-567.

Roth, J. T. and S. M. Pandit (2000). "Development of a cutting direction and sensor orientation independent monitoring technique for end-milling." Journal of Manufacturing Science and Engineering-Transactions of the Asme **122**(4): 671-677.

Rowe, W. B. (2001a). "Thermal analysis of high efficiency deep grinding." International Journal of Machine Tools & Manufacture **41**(1): 1-19.

Rowe, W. B. (2001c). "Temperature case studies in grinding including an inclined heat source model." Proceedings of the Institution of Mechanical Engineers Part B-Journal of Engineering Manufacture **215**(4): 473-491.

Rowe, W. B. and T. Jin (2001b). "Temperatures in high efficiency deep grinding (HEDG)." Cirp Annals-Manufacturing Technology **50**(1): 205-208.

Royer, D. and E. Dieulesaint (2000). "Elastic Waves in Solids I, II." New York, Springer Verlag, Berlin, Heidelberg.

Rumelhart, D. D., G. E. Hinton, et al. (1986). "Learning Representations by Back-Propagating Errors." <u>Nature</u> **323**: 533-536.

Samanta, B. (2004). "Gear fault detection using artificial neural networks and support vector machines with genetic algorithms." <u>Mechanical Systems and Signal Processing</u> **18**(3): 625-644.

Schofield, B. H., R. A. Bareiss, et al. (1958). "Acoustic Emission Under Applied Stress." <u>ASTIA Document AD 155674 Report</u>: 58-194.

Schulz, M. (2003). "Uncertainty of topography determination based on slope difference or curvature measuring systems in laboratory and industrial environment." <u>Proceedings of SPIE - The International Society for Optical Engineering</u> **v 5144**: 323-332.

Shaw, M. C. (1996). "Principles of Abrasive Processing."

Sherrington, I. and E. H. Smith (1988). "Modern measurement techniques in surface metrology: Part 1: Stylus instruments, Electron Microscopy and non-optical comparators." <u>Wear</u> **125**(3): 271-288.

Sick, B. (2002). "On-line and indirect tool wear monitoring in turning with artifical neural networks: a review of more than a decade of research." <u>Mechanical Systems and Signal Processing</u> **16**: 487-546.

Silva, S. (2004). "A Genetic Programming Toolbox for Matlab - version 2." <u>ECOS - Evolutionary and Complex Systems Group, University of Coimbra, Portugal, http://gplab.sourceforge.net/</u>.

Silva, S. and Y. T. Tseng (2005). Classification of Seafloor Habitats using Genetic Programming. <u>GECCO '05</u>. Washington.

Smith, S. W. (1997). "The Scientist and Engineer's Guide to Digital Signal Processing." <u>California Technical Publishing</u>.

Sri Namachchivaya N. and Beddini R. (2004). "Spindle Speed Variation Variation for the Suppression of Regenerative Chatter." <u>Journal of Nonlinear Science</u> **13**(3): 265-288.

Stanley, R. J., J. M. Keller, et al. (1998). "Data-driven homologue matching for chromosome identification." Ieee Transactions on Medical Imaging **17**(3): 451-462.

Staszewski, W. J. and K. M. Holford (2001). "Wavelet signal processing of acoustic emission data,." Key Engineering Materials **204-205**: 351-358.

Stephenson, G. (1988). "Mathematical Methods for Science Students." Longman.

Strang, G. and T. Nguyen (1996). "Wavelets and Filter Banks." Wellesley, MA, Wellesley-Cambridge Press.

Strang, G. and T. Nguyen (1996). "Wavelets and Filter Banks." Wesley Cambridge Press: 1-29 & 61-68.

Subhash, G., J. E. Loukus, et al. (2001). "Application of data dependent systems approach for evaluation of fracture modes during single-grit scratching, ." Mechanics of Materials **34**: 25-42.

Tawakoli, T. (2002). "An innovative system for grinding, dressing and milling." Industrial Diamond Review **62**(1): 37-40.

Tawakoli, T., E. Westkaemper, et al. (2007b). "A New Development in Dry Grinding." 40th CIRP International Seminar on Manufacturing Systems, Department of Engineering, University of Liverpool, : CD Proceedings PT2.

Tawakoli, T., E. Westkaemper, et al. (2007a). "Ultrasonic Assisted Dressing of Vitrified CBN Grinding Wheel." 40th CIRP International Seminar on Manufacturing Systems, Department of Engineering, University of Liverpool, : CD Proceedings PT4.

Tay, E., E. H. Francis, et al. (2001). "Application of support vector machines in financial time series forecasting." Omega **29**: 35-49.

The University of Nottingham

Tetelman, A. S. and R. Chow (1972). "Acoustic Emission Testing and Microcracking Processes." <u>ASTM Special Technical Publication</u> **505**.

Tonshoff, H. K. (1992). "Modelling and Simulation of Grinding Processes." <u>Annals of the CIRP</u> **41**(2): 677-688.

Tonshoff, H. K., T. Fremuth, et al. (1994). "Process Monitoring in Grinding." <u>Institute of Production Engineering and Machine Tools, **University of Hannover, Germany**</u>.

Tonshoff, H. K. and K. T. Friemuth (2002). "Process monitoring in grinding." <u>CIRP Annals - Manufacturing Technology</u> **51**(2): 551-571.

Tonshoff, H. K., M. Jung, et al. (2000). "Using acoustic emission signals for monitoring of production processes." <u>Ultrasonics</u> **37**(10): 681-686.

Tsukimoto, H. and H. Hatano (2003). "The functional localization of neural networks using genetic algorithms." <u>Neural Networks</u> **16**(1): 55-67.

Vapnik, V. N. (1998). "Statistical learning Theory." <u>John Wiley & Sons</u>.

Wang, H. and G. Subhash (2002). "An approximate upper bound approach for the single-grit rotating scratch with a conical tool on pure metal." <u>Wear</u> **252**(11-12): 911-933.

Wang, H. and G. Subhash (2002). "Mechanics of mixed-mode ductile material removal with a conical tool and the size dependence of the specific energy." <u>Journal of the Mechanics and Physics of Solids</u> **50**(6): 1269-1296.

Wang, H., G. Subhash, et al. (2001). "Characteristics of single-grit rotating scratch with a conical tool on pure titanium." <u>Wear</u> **249**(7): 566-581.

Wang, Z., P. Willett, et al. (2001). "Neural network detection of grinding burn from acoustic emission." <u>International Journal of Machine Tools & Manufacture</u> **41**(2): 283-309.

Webster, J., I. Marinescu, et al. (1994). "Acoustic Emission for process control and monitoring of surface integrity during grinding,." <u>Annals of CIRP</u> **43**(1): 299-304.

Wright, S. (1932a). "Evolution in mendelian populations." <u>Genetics</u> **16**: 97-159.

Wright, S. (1932b). "The roles of mutation, inbreeding, crossbreeding and selection in evolution." <u>Proceedings of the 6th International Conference on Genetics</u> **1**: 356-366.

Yan, J., T. Sasaki, et al. (2004). "Chip formation behaviour in ultra-precision cutting of electroless nickel plated mold substrates." <u>Advances in Abrasive Technology Vi</u> **257-258**: 3-8.

Yao, Y. X., X. L. Li, et al. (1999). "Tool wear detection with fuzzy classification and wavelet fuzzy neural network." <u>International Journal of Machine Tools & Manufacture</u> **39**(10): 1525-1538.

Zeng, Y. G. and E. Forssberg (1994). "Application of Vibration Signal Measurement for Monitoring Grinding Parameters." <u>Mechanical Systems and Signal Processing</u> **8**(6): 703-713.

Zeng, Y. G. and E. Forssberg (1994). "Monitoring Grinding Parameters by Vibration Signal Measurement - a Primary Application." <u>Minerals Engineering</u> **7**(4): 495-501.

Appendix

Appendix A

Appendix A looks at all the classifier computer code discussed in this thesis.

A.1   Independent Component Analysis

```matlab
function [patterns, targets, W, Aw, means] = ICA(patterns, targets,
params)

%Reshape  the  data  points  using  the  independent  component  analysis
algorithm
%Inputs:
%    train_patterns  - Input patterns
%    train_targets   - Input targets
%    params          - [Output dimension, Learning rate]
%
%Outputs
%    patterns        - New patterns
%    targets         - New targets
%    W               - Reshape martix
%    means           - The means vector of the patterns

[r,c]            = size(patterns);
[dimension, eta] = process_params(params);

if (r < dimension),
    error('Output dimension cannot be larger than the input dimension')
end

%Whiten the data to zero mean and unit covariance
means       = mean(patterns')';
patterns    = patterns - means*ones(1,c);
[v, d]      = eig(cov(patterns',1));
Aw          = v*inv(sqrtm(d));
patterns    = Aw'*patterns;

%Move data to the range of [-1,1]
minp     = min(patterns')';
maxp     = max(patterns')';
patterns = (patterns - minp*ones(1,c))./((maxp-minp)*ones(1,c));
patterns = patterns*2-1;

%Find the weight matrix
W           = randn(r);
iter        = 1;
while (iter < 1000),
    iter    = iter + 1;
    y       = W*patterns;
    phi     = activation(y);
```

```matlab
        dW       = (eye(r) - 1/c*phi*y')*W;

        %Break if algorithm diverges
        if (max(max(dW)) > 1e3),
            disp(['Algorithm diverged after ' num2str(i) ' iterations'])
            break
        end

        W        = W + eta*dW;

        update   = max(max(abs(dW)));

        %If the algorithm converged, exit
        if (update < eta),
            disp(['Algorithm   converged   after   '   num2str(iter)   '
iterations'])
            break
        else
            if (iter / 10 == floor(iter/10))
                disp(['Iteration  ' num2str(iter) ': Maximum  update  is  '
num2str(update)])
            end
        end
end

%Take only the most influential outputs
power        = sum(abs(W)');
[m, in]      = sort(power);
W            = W(in(r-dimension+1:r),:);

%Calculate new patterns
patterns = W*patterns;

W        = W*Aw;

%End ICA

function phi = activation(y)
%Activation function for ICA
phi = y.^3;
%phi = tahn(y);
```

A.2   Genetic Programming

This section displays the code used to conduct the GP classification using the GP Toolbox [ref].

A.2.1 Genetic Programming Main File

This code is used to set all the GP functions and parameters and calls a number of sub code either defined or actual toolbox provided code.

```matlab
function [v,b]=demostftburnchat9

%   Copyright (C) 2003-2007 Sara Silva (sara@dei.uc.pt)
%   This file is part of the GPLAB Toolbox


fprintf('STFT demo');    % The burn or chatter data is an STFT of raw
extrcated AE signal
p=resetparams;

%p.sampling='roulette';     in some cases roulette wheel evolution was
                            % used for test
p.survival='keepbest';      % keep best individual

p.sampling='tournament';
p.elitism='replace';
p.survival='fixedpopsize';
p.initpoptype='rampedinit';

%p=setfunctions(p,'gt',2,'le',2,'myif',3);      -functions  for  greater
than
                                        %or less than functions
p=setfunctions(p,'plus',2,'minus',2,'times',2,    'mydivide',    2);
%functions for GP rule
%p=setterminals(p,'0','1');
%p=setterminals(p,'1','2', '3');
p=setterminals(p,'X1','X2','X3','X4','X5','X6','X7','X8','X9','X10','X1
1','X12','X13','X14','X15','X16','X17','X18','X19','X20');

% terminal set used to represent cut down AE signal source

p=setoperators(p,'crossover',2,2,'mutation',1,1);
%p.calcfitness='regfitnessv11';  %used instead of class fitness for
                                %backpropagation type learning rule

p.calcfitness='classfitness';    % fitness function to learn overlap
between
                                % dataset presented data
```

[A3]

```matlab
p.lowerisbetter=1;                % if the fitness value is lower this is
best


p.operatorprobstype='variable';
p.minprob=0;

%p=setterminals(p);
p.datafilex='patterns_burnICA_40data.txt'; %ICA reduced test data set 1
burn phenomonon
p.datafiley='targets_burnICA_40data.txt';
p.operatorprobstype='variable'; %%%%%

p.usetestdata=1;
p.testdatafilex='patterns_burnICA_14_54data.txt';   %ICA   reduced   test
data set 2 burn phenomonon
p.testdatafiley='targets_burnICA_14_54data.txt';


p.calcdiversity={};

p.fixedlevel=0;
p.dynamiclevel='1'; %allows tree bloat if fitness increases


p.tournamentsize=0.1; %tournament size is 10% of designated population
set

p.hits='[100 0 50 10]';

%p.graphics={};        graphic GP output
p.calcdiversity={'uniquegen'};
p.calccomplexity=1;
p.graphics={'plotfitness','plotdiversity','plotcomplexity','plotoperato
rs'};
p.depthnodes='2';


[v,b]=gplab(200,500,p);        %population 200 and generations 500

desired_obtained(v,[],1,0,[]);        %desired v obtained graphical o/p
accuracy_complexity(v,[],0,[]);        % accuracy v complexity graphical
o/p

figure
plotpareto(v);                        % pareto GP plot

drawtree(b.tree);                     % plot GP tree representing best
found data separation rule
```

A.2.2 Test class fitness function

```matlab
function fitness=testclassfitnesssara(res,classes);
% fitness = number of points that belong to more than 1 class

nclasses=length(classes);
npoints=length(res);

% check max and min of all classes:
for i=1:nclasses
    maxclasses(i)=max(res(classes{i}));
    minclasses(i)=min(res(classes{i}));
end

% create matrix of belonging (for each point, 1 if belongs to class, 0
if not):
mb=zeros(npoints,nclasses); % initialize matrix with as many rows as
points, and as many columns as classes
for i=1:nclasses
    mb(:,i)=mb(:,i)+and(res<=maxclasses(i),res>=minclasses(i));
end

% sum belonging columns:
sumb=sum(mb,2);

% fitness function:
% locate the points who belong to more than one class:
sb=(sumb>1);
% now give equal weight to all classes:
for i=1:nclasses
    sb(classes{i})=sb(classes{i})./length(classes{i});
end

sum(sb);

%and finally give percentage of points belonging to more than one
class:
fitness=100.*sum(sb)./nclasses;
```

A.2.3 Class fitness function

This type of fitness function obtains a good fitness based on the mappings of mapping the overlap between two data sets.

```matlab
function ind=classfitness(ind,params,data,terminals,varsvals)

% same as regfitness.m
% -------------------
%X=data.example;
for t=1:params.numvars
```

[A5]

```
       % for all variables (which are first in input list), ie,
X1,X2,X3,...
   var=terminals{t,1};
   val=varsvals{t}; % varsvals was previously prepared to be assigned
(in genpop)
   eval([var '=' val ';']);
   % (this eval does assignments like X1=2,X2=4.5,...)
end


% evaluate the individual and measure difference between obtained and
expected results:
res=eval(ind.str);
% if the individual is just a terminal, res is just a scalar, but we
want a vector:
if length(res)<length(data.result)
   res=res*ones(length(data.result),1);
end


% different from regfitness.m
% -------------------------


% calculate fitness:
fitness=testclassfitnesssara(res,data.classes);

%resultind=res;
ind.result=res;


% same as regfitness.m
% -------------------

% now limit fitness precision, to eliminate rounding error problem:

ind.fitness=fixdec(fitness,params.precision);
```

A.2.4 Regression Fitness function

This fitness function is similar to that used in backpropagation neural network training rule.

```
function ind=regfitness(ind,params,data,terminals,varsvals)
%REGFITNESS    Measures the fitness of a GPLAB individual.
%   REGFITNESS(INDIVIDUAL,PARAMS,DATA,TERMINALS,VARSVALS) returns
%   the fitness of INDIVIDUAL, measured as the sum of differences
%   between the obtained and expected results, on DATA dataset, and
%   also returns the result obtained in each fitness case.
%
%   Input arguments:
%       INDIVIDUAL - the individual whose fitness is to measure (struct)
%       PARAMS - the current running parameters (struct)
%       DATA - the dataset on which to measure the fitness (struct)
%        TERMINALS - the variables to set with the input dataset (cell
array)
```

```matlab
%         VARSVALS - the string of the variables of the fitness cases
(string)
%   Output arguments:
%       INDIVIDUAL - the individual whose fitness was measured (struct)
%
%   See also CALCFITNESS, ANTFITNESS
%
%   Copyright (C) 2003-2007 Sara Silva (sara@dei.uc.pt)
%    Acknowledgements: Marco Medori (marco.medori@poste.it) and Bruno
Morelli
%   This file is part of the GPLAB Toolbox

X=data.example;
outstr=ind.str;
for i=params.numvars:-1:1

outstr=strrep(outstr,strcat('X',num2str(i)),strcat('X(:,',num2str(i),')
'));
end

try
    res=eval(outstr);
catch
    % because of the "nesting 32" error of matlab
    res=str2num(evaluate_tree(ind.tree,X));
end

%for t=1:params.numvars
    %for all variables (which are first in input list), ie, X1,X2,X3,...
%   var=terminals{t,1};
%   val=varsvals{t}; % varsvals was previously prepared to be assigned
(in genpop)
%   eval([var '=' val ';']);
    % (this eval does assignments like X1=2,X2=4.5,...)
%end

% evaluate the individual and measure difference between obtained and
expected results:
%res=eval(ind);

% if the individual is just a terminal, res is just a scalar, but we
want a vector:
if length(res)<length(data.result)
    res=res*ones(length(data.result),1);
end
sumdif=sum(abs(res-data.result));
ind.result=res;

% raw fitness:
ind.fitness=sumdif; %lower fitness means better individual
% now limit fitness precision, to eliminate rounding error problem:
ind.fitness=fixdec(ind.fitness,params.precision);
```

A.2.5 Genetic Algorithm test fitness for fuzzy clustering

```matlab
function [f] = test_programGA(x);

global last_fitness;
% changed default fitness from 2000000
defaultlast_fitness = 1000000;

% initialise variables
c = 0;
d = 0;
f = 0;

catString2 = 'C:\MATLAB701\work\cluster\catvars_info.txt';


    for i = 1:size(x,1)
        c = x(i,1);

        d = x(i,2);


        x_vals = [c; d];
        catString22   =   'C:\MATLAB701\work\cluster\catxvars_info.txt';
%string location for cluster parameters
        fid=fopen(catString22, 'a');
        fprintf(fid, '%4.0f  %2.0f\n',  x_vals);         %print  cluster
parameters to try
        st1 = fclose(fid)

        [centre,   UU,   f_functionx,   f_functions,   cv,   dv]   =
cluster_runGA(c,d);  % run cluster GA program with new

%cluster parameters


%%%%%%%%%%%%%%%%%%%%%%%%%%%%%%%%%%%%%%%%%%%%%%%%%%%%%%%%%%%%%%%%%%%%%%%%%%
%%%%%%%%%%%%%%%%%%%%%


        if i > 1

            data = load(catString2);
            filesize = length(data);
            disp(filesize);
            last_fit = data(filesize - 1);
            last_fitness = last_fit;

        elseif i == 1
```

```matlab
                last_fitness = defaultlast_fitness;
        end
        if last_fitness > f_functions
            % return this value back to the GA
            %msgbox();
            f(i) = f_functions;
            save bestfitVal f c d;
        elseif f_functions > last_fitness
            %msgbox('last_fitness');
            f(i) = last_fitness;
            save bestfitVal f iteration1 clusters;
        elseif last_fitness == null;    %null or zero
            %msgbox('f_functions initial');
            f(i) = default_fitness;
        end

    end
        %last_fitness = min(b);
        save opticlust centre UU f c d x i f_functionx;
        set(0,'userdata',{centre,UU,f,c,d,x,i, f_functionx});
        %save fitnessout zz;
        data=get(0,'userdata');
```

A.2.6 Fuzzy-c clustering evaluating GA individuals

```matlab
function [center, UU, f_functionx, f_function, iteration1, clusters] =
cluster_runGA(c,d)

%run fuzzy c cluster program and evlauate GA(x) individual

load phenom;          %load data set (training and test concatenated
together)


    if c > 0
        iteration = round(c)+ 2;
        iteration1 = iteration * 200;
    elseif c == 0
        iteration1 = c + 400;
    else c < 0
        iteration = c * -2;
        iteration1 = iteration * 200;
    end

    if d > 0
        clusters = round(d) + 2;
    elseif d == 0
        clusters = d + 2;
    else d < 0
        clusters = d * -2;
    end
    % check clusters and iterations are within limits
```

[A9]

```matlab
    if iteration1 > 100
        iteration1 = iteration1;
    else iteration1 < 100
        iteraction1 = 2000;
    end

    if iteration1 < 4000
        iteration1 = iteration1;
    else iteration1 > 4000
        iteraction1 = 4000;
    end

    if clusters > 3
        clusters = clusters;
    else clusters < 2
        clusters = 2;
    end

    if clusters < 10
        clusters = clusters;
    else clusters > 10
        clusters = 10;
    end

    %Fuzzy c clustering parameter defaults
    %=====================================
        %OPTIONS(1): exponent for the matrix U           (default:
2.0)
        %OPTIONS(2): maximum number of iterations         (default:
100)
        %OPTIONS(3): minimum amount of improvement        (default:
1e-5)
        %OPTIONS(4): info display during iteration        (default: 1)
    %The clustering process stops when the maximum number of iterations
    %is reached, or when the objective function improvement between two
    %consecutive  iterations  is  less  than  the  minimum  amount  of
improvement
    %specified. Use NaN to select the default value.

    options = [6.0, iteration1, 1e-8,1];
    %[f_functionx] = fcm(phenom', clusters, options);
    [center, UU, f_functionx] = fcm(phenom', clusters, options);

    s = length(f_functionx);
    f_function = f_functionx(s);

    save fitfunVal f_function iteration1 clusters;    % save fuzzy c
clustering output to file


    fitfunvals_cat = [f_function; iteration1; clusters];

catString1 = 'C:\MATLAB701\work\cluster\catvars_info.txt';
```

[A10]

```
        fid=fopen(catString1, 'a');
        fprintf(fid,  '%12.8f  %4.0f  %2.0f\n',  fitfunvals_cat);  %
output tested parameters and fuzzy c output to file
        st1 = fclose(fid)
```

A2.6.1   GA Toolbox parameters for Fuzzy-c/GA clustering:

Fitness function: @testGAfitness_display
Number of variables: 2
Best Fitness plot: select
Creation function: Uniform
Initial Population: default []
Initial Scores: default []
Initial Range: [1 : 6]
Scaling Function: Rank
Selection Function: Roulette or Tournament (size = 4)
Stopping Criteria:
      Generations: 100
      Time Limit: inf
      Fitness Limit: -inf
      Stall Generations: 100
      Stall Time Limit: 50 (increase to accommodate program)

Note always delete the GA text file "catxvars_info11.txt" you search file and delete – do every time before using Fuzzy-c/GA clustering technique

A.2.7 Neural Networks

Neural Network classifier program calling training and test data matrix variables.

```
%help bckpropagation
clf reset;
nntwarn off;
pausetime = 0.1;

% PROBLEM DEFINITION
%==================

% Example traininfg set.


%--------------------------------------------------------------------
--------------------------------------------------------
```

```matlab
%P =[50      100      200      300      400      100      100      100      100
200      100      50;
%    100      20       50       50       50       60       40       100      90
100      50       40;
%    10       10       50       50       50       60       40       100      90
100      40       50;
%    50       11       50       20       60       3        20       100      50
100      20       10;
%    100      50       50       100      100      400      200      100      200
100      50       100;
%    200      10       200      50       200      200      100      100      80
90       40       50;
%    30       11       50       20       60       50       50       100      100
90       30       40;
%    40       11       50       30       3        60       10       100      100
50       10       20];


% T = [-1      1        1        1        1        -1       -1       1
-1       1        1        -1];

% PLOT TRAINING VECTORS
%=======================

plot(P_train,T_train,'+');    % training signals and test output values
for plotting
title('Training Vectors');
xlabel('Input Vector P');
ylabel('Target Vector T');
pause


% INITIALIZE NETWORK ARCHITECTURE
%================================

% Set input vector size R, layer sizes S1, S2, & S3 batch size Q.

% Initialize weights and biases.



[R,Q] = size(P_train); S1 = 205; S2 = 308; [S3,Q] = size(T_train);



% Here a two-layer feed-forward network is created. The first layer has
205 tansig
% neurons, the second layer has 308 tansig neurons. The trainrp network
training function is to be used.

net    =    newff(minmax(P_train),[S1    S2    S3],{'tansig'    'tansig'
'purelin'},'TRAINRP','learngdm','mse');
net = init(net)                         % initialise NN with defined
parameters
```

[A12]

```matlab
net.trainParam.epochs = 4000;              % maximum epoch stop condition
%net.trainParam.mem_reduc = 2;             % if NN very difficult to train
due
                                           % to complexity this function
ensures quicker training with approximations
net.trainParam.show = 50;                  % display NN output for every
50 iterations
net.trainParam.mc = 0.9;                   % Momentium set 0.9 - 1 being
least random to ensure bounce from local minima
net.trainParam.lr = 0.000000001;          % NN learning rate - lower more
accurate steps
net.trainParam.goal = 1e-35;              % SSE goal
net.trainParam.min_grad = 1e-18;          % mimimum gradient during
learning

net = train(net,P_train,T_train);         % test NN with training data


[a,b]=size(P_train);
X = [1:b];
Y = sim(net,P_train);
Y1 = Y;
figure
plot(X,T_train,X,Y,'o')


[a,b]=size(P_test);                       % test NN with test data
X = [1:b];
Y = sim(net,P_test);
figure
plot(X,T_test,X,Y,'o')
```

[A13]

Appendix B

The following code displays the main digital signal processing techniques used within this thesis.

B.1 N-Reduction Techniques

B.1.1 Statistical N-Reduction Techniques

The n-dimensional technique used in some of WPT for horizontal scratch tests and GP burn and chatter phenomenon classification is listed below. This code is based on supplying the mean, standard deviation, kurtosis, skewness, max and min values:

```matlab
PPP = ones(96,120);                   % initialise matrix to store reduced
                                      % dataset 96 rows (variables) by 120
                                      % cases (columns)
for jk=1:1:120                        % for loop to go through 120 cases

P = training_datafull_time_force;  % data consists of AE and force
L1 = P(:,jk);


one_eight_windows = 75;               % setup data window length for
reduction
mean_amp_8array = zeros(1,16);     % setup individual matrices for stat
std_amp_8array = zeros(1,16);      % reduction
kurtosis_amp_8array = zeros(1,16);
skewness_amp_8array = zeros(1,16);
max_amp_8array = zeros(1,16);
min_amp_8array = zeros(1,16);


k = 0;
j = 0;

for j=1:16                  % for loop for 16 windows across signals

    if j == 1
        k = 1;
    else if j == 2
            k = 75;
        else if j == 3
                k = 75 * 2;
            else if j == 4
                    k = 75 * 3;
                else if j == 5
                        k = 75 * 4;
                    else if j == 6
```

[A14]

```matlab
                                  k = 75 * 5;
                                    else if j == 7
                                      k = 75 * 6;
                                        else if j == 8
                                          k = 75 * 7;
                                            if j == 9
                                            k = 75 * 8;
                                                else if j == 10
                                                  k = 75 * 9;
                                                    else if j == 11
                                                      k = 75 * 10;
                                                        else if j == 12
                                                          k = 75 * 11;
                                                            else if j == 13
                                                              k = 75 *
12;
                                                                else if
j == 14
                                                                        k =
75 * 13;

else if j == 15

k = 75 * 14;

else if j == 16

k = 75 * 15;
                    % store in 16 arrays with 6 factors each signal pass
                                    mean_amp_8array(:,j) =
mean(L1(1*k:(one_eight_windows * j), :));
                                    std_amp_8array(:,j) =
std(L1(1*k:(one_eight_windows * j), :));
                                    kurtosis_amp_8array(:,j) =
kurtosis(L1(1*k:(one_eight_windows * j), :));
                                    skewness_amp_8array(:,j) =
skewness(L1(1*k:(one_eight_windows * j), :));
                                    max_amp_8array(:,j) =
skewness(L1(1*k:(one_eight_windows * j), :));
                                    min_amp_8array(:,j) =
skewness(L1(1*k:(one_eight_windows * j), :));
                        end
                                    mean_amp_8array(:,j) =
mean(L1(1*k:(one_eight_windows * j), :));
                                    std_amp_8array(:,j) =
std(L1(1*k:(one_eight_windows * j), :));
                                    kurtosis_amp_8array(:,j) =
kurtosis(L1(1*k:(one_eight_windows * j), :));
                                    skewness_amp_8array(:,j) =
skewness(L1(1*k:(one_eight_windows * j), :));
                                    max_amp_8array(:,j) =
skewness(L1(1*k:(one_eight_windows * j), :));
                                    min_amp_8array(:,j) =
skewness(L1(1*k:(one_eight_windows * j), :));
                      end
                                    mean_amp_8array(:,j) =
mean(L1(1*k:(one_eight_windows * j), :));
```

[A15]

```
                                                  std_amp_8array(:,j) =
std(L1(1*k:(one_eight_windows * j), :));
                                                  kurtosis_amp_8array(:,j) =
kurtosis(L1(1*k:(one_eight_windows * j), :));
                                                  skewness_amp_8array(:,j) =
skewness(L1(1*k:(one_eight_windows * j), :));
                                                  max_amp_8array(:,j) =
skewness(L1(1*k:(one_eight_windows * j), :));
                                                  min_amp_8array(:,j) =
skewness(L1(1*k:(one_eight_windows * j), :));
                          end
                                                  mean_amp_8array(:,j) =
mean(L1(1*k:(one_eight_windows * j), :));
                                                  std_amp_8array(:,j) =
std(L1(1*k:(one_eight_windows * j), :));
                                                  kurtosis_amp_8array(:,j) =
kurtosis(L1(1*k:(one_eight_windows * j), :));
                                                  skewness_amp_8array(:,j) =
skewness(L1(1*k:(one_eight_windows * j), :));
                                                  max_amp_8array(:,j) =
skewness(L1(1*k:(one_eight_windows * j), :));
                                                  min_amp_8array(:,j) =
skewness(L1(1*k:(one_eight_windows * j), :));
                          end
                                                  mean_amp_8array(:,j) =
mean(L1(1*k:(one_eight_windows * j), :));
                                                  std_amp_8array(:,j) =
std(L1(1*k:(one_eight_windows * j), :));
                                                  kurtosis_amp_8array(:,j) =
kurtosis(L1(1*k:(one_eight_windows * j), :));
                                                  skewness_amp_8array(:,j) =
skewness(L1(1*k:(one_eight_windows * j), :));
                                                  max_amp_8array(:,j) =
skewness(L1(1*k:(one_eight_windows * j), :));
                                                  min_amp_8array(:,j) =
skewness(L1(1*k:(one_eight_windows * j), :));
                          end
                                                  mean_amp_8array(:,j) =
mean(L1(1*k:(one_eight_windows * j), :));
                                                  std_amp_8array(:,j) =
std(L1(1*k:(one_eight_windows * j), :));
                                                  kurtosis_amp_8array(:,j) =
kurtosis(L1(1*k:(one_eight_windows * j), :));
                                                  skewness_amp_8array(:,j) =
skewness(L1(1*k:(one_eight_windows * j), :));
                                                  max_amp_8array(:,j) =
skewness(L1(1*k:(one_eight_windows * j), :));
                                                  min_amp_8array(:,j) =
skewness(L1(1*k:(one_eight_windows * j), :));
                        end
                                                  mean_amp_8array(:,j) =
mean(L1(1*k:(one_eight_windows * j), :));
                                                  std_amp_8array(:,j) =
std(L1(1*k:(one_eight_windows * j), :));
                                                  kurtosis_amp_8array(:,j) =
kurtosis(L1(1*k:(one_eight_windows * j), :));
```

[A16]

```
                                            skewness_amp_8array(:,j) =
skewness(L1(1*k:(one_eight_windows * j), :));
                                            max_amp_8array(:,j) =
skewness(L1(1*k:(one_eight_windows * j), :));
                                            min_amp_8array(:,j) =
skewness(L1(1*k:(one_eight_windows * j), :));
                end
                                            mean_amp_8array(:,j) =
mean(L1(1*k:(one_eight_windows * j), :));
                                            std_amp_8array(:,j) =
std(L1(1*k:(one_eight_windows * j), :));
                                            kurtosis_amp_8array(:,j) =
kurtosis(L1(1*k:(one_eight_windows * j), :));
                                            skewness_amp_8array(:,j) =
skewness(L1(1*k:(one_eight_windows * j), :));
                                            max_amp_8array(:,j) =
skewness(L1(1*k:(one_eight_windows * j), :));
                                            min_amp_8array(:,j) =
skewness(L1(1*k:(one_eight_windows * j), :));
            end

                                            mean_amp_8array(:,j) =
mean(L1(1*k:(one_eight_windows * j), :));
                                            std_amp_8array(:,j) =
std(L1(1*k:(one_eight_windows * j), :));
                                            kurtosis_amp_8array(:,j) =
kurtosis(L1(1*k:(one_eight_windows * j), :));
                                            skewness_amp_8array(:,j) =
skewness(L1(1*k:(one_eight_windows * j), :));
                                            max_amp_8array(:,j) =
skewness(L1(1*k:(one_eight_windows * j), :));
                                            min_amp_8array(:,j) =
skewness(L1(1*k:(one_eight_windows * j), :));
            end
                                            mean_amp_8array(:,j) =
mean(L1(1*k:(one_eight_windows * j), :));
                                            std_amp_8array(:,j) =
std(L1(1*k:(one_eight_windows * j), :));
                                            kurtosis_amp_8array(:,j) =
kurtosis(L1(1*k:(one_eight_windows * j), :));
                                            skewness_amp_8array(:,j) =
skewness(L1(1*k:(one_eight_windows * j), :));
                                            max_amp_8array(:,j) =
skewness(L1(1*k:(one_eight_windows * j), :));
                                            min_amp_8array(:,j) =
skewness(L1(1*k:(one_eight_windows * j), :));
        end
                                            mean_amp_8array(:,j) =
mean(L1(1*k:(one_eight_windows * j), :));
                                            std_amp_8array(:,j) =
std(L1(1*k:(one_eight_windows * j), :));
                                            kurtosis_amp_8array(:,j) =
kurtosis(L1(1*k:(one_eight_windows * j), :));
                                            skewness_amp_8array(:,j) =
skewness(L1(1*k:(one_eight_windows * j), :));
                                            max_amp_8array(:,j) =
skewness(L1(1*k:(one_eight_windows * j), :));
```

[A17]

```
                                        min_amp_8array(:,j) =
skewness(L1(1*k:(one_eight_windows * j), :));
        end
                                        mean_amp_8array(:,j) =
mean(L1(1*k:(one_eight_windows * j), :));
                                        std_amp_8array(:,j) =
std(L1(1*k:(one_eight_windows * j), :));
                                        kurtosis_amp_8array(:,j) =
kurtosis(L1(1*k:(one_eight_windows * j), :));
                                        skewness_amp_8array(:,j) =
skewness(L1(1*k:(one_eight_windows * j), :));
                                        max_amp_8array(:,j) =
skewness(L1(1*k:(one_eight_windows * j), :));
                                        min_amp_8array(:,j) =
skewness(L1(1*k:(one_eight_windows * j), :));
        end
                                        mean_amp_8array(:,j) =
mean(L1(1*k:(one_eight_windows * j), :));
                                        std_amp_8array(:,j) =
std(L1(1*k:(one_eight_windows * j), :));
                                        kurtosis_amp_8array(:,j) =
kurtosis(L1(1*k:(one_eight_windows * j), :));
                                        skewness_amp_8array(:,j) =
skewness(L1(1*k:(one_eight_windows * j), :));
                                        max_amp_8array(:,j) =
skewness(L1(1*k:(one_eight_windows * j), :));
                                        min_amp_8array(:,j) =
skewness(L1(1*k:(one_eight_windows * j), :));
       end
                                        mean_amp_8array(:,j) =
mean(L1(1*k:(one_eight_windows * j), :));
                                        std_amp_8array(:,j) =
std(L1(1*k:(one_eight_windows * j), :));
                                        kurtosis_amp_8array(:,j) =
kurtosis(L1(1*k:(one_eight_windows * j), :));
                                        skewness_amp_8array(:,j) =
skewness(L1(1*k:(one_eight_windows * j), :));
                                        max_amp_8array(:,j) =
skewness(L1(1*k:(one_eight_windows * j), :));
                                        min_amp_8array(:,j) =
skewness(L1(1*k:(one_eight_windows * j), :));
      end
                                        mean_amp_8array(:,j) =
mean(L1(1*k:(one_eight_windows * j), :));
                                        std_amp_8array(:,j) =
std(L1(1*k:(one_eight_windows * j), :));
                                        kurtosis_amp_8array(:,j) =
kurtosis(L1(1*k:(one_eight_windows * j), :));
                                        skewness_amp_8array(:,j) =
skewness(L1(1*k:(one_eight_windows * j), :));
                                        max_amp_8array(:,j) =
skewness(L1(1*k:(one_eight_windows * j), :));
                                        min_amp_8array(:,j) =
skewness(L1(1*k:(one_eight_windows * j), :));
     end
                                        mean_amp_8array(:,j) =
mean(L1(1*k:(one_eight_windows * j), :));
```

[A18]

```
                                    std_amp_8array(:,j) =
std(L1(1*k:(one_eight_windows * j), :));
                                    kurtosis_amp_8array(:,j) =
kurtosis(L1(1*k:(one_eight_windows * j), :));
                                    skewness_amp_8array(:,j) =
skewness(L1(1*k:(one_eight_windows * j), :));
                                    max_amp_8array(:,j) =
skewness(L1(1*k:(one_eight_windows * j), :));
                                    min_amp_8array(:,j) =
skewness(L1(1*k:(one_eight_windows * j), :));
  end




end

% store in PPP matrix with concatenation

PPP(:,jk) = cat(1, mean_amp_8array(:,1), std_amp_8array(:,1),
kurtosis_amp_8array(:,1), skewness_amp_8array(:,1),
max_amp_8array(:,1), min_amp_8array(:,1), mean_amp_8array(:,2),
std_amp_8array(:,2), kurtosis_amp_8array(:,2),
skewness_amp_8array(:,2), max_amp_8array(:,2), min_amp_8array(:,2),
mean_amp_8array(:,3), std_amp_8array(:,3), kurtosis_amp_8array(:,3),
skewness_amp_8array(:,3), max_amp_8array(:,3), min_amp_8array(:,3),
mean_amp_8array(:,4), std_amp_8array(:,4), kurtosis_amp_8array(:,4),
skewness_amp_8array(:,4), max_amp_8array(:,4), min_amp_8array(:,4),
mean_amp_8array(:,5), std_amp_8array(:,5), kurtosis_amp_8array(:,5),
skewness_amp_8array(:,5), max_amp_8array(:,5), min_amp_8array(:,5),
mean_amp_8array(:,6), std_amp_8array(:,6), kurtosis_amp_8array(:,6),
skewness_amp_8array(:,6), max_amp_8array(:,6), min_amp_8array(:,6),
mean_amp_8array(:,7), std_amp_8array(:,7), kurtosis_amp_8array(:,7),
skewness_amp_8array(:,7), max_amp_8array(:,7), min_amp_8array(:,7),
mean_amp_8array(:,8), std_amp_8array(:,8), kurtosis_amp_8array(:,8),
skewness_amp_8array(:,8), max_amp_8array(:,8), min_amp_8array(:,8),
mean_amp_8array(:,9), std_amp_8array(:,9), kurtosis_amp_8array(:,9),
skewness_amp_8array(:,9), max_amp_8array(:,9), min_amp_8array(:,9),
mean_amp_8array(:,10), std_amp_8array(:,10), kurtosis_amp_8array(:,10),
skewness_amp_8array(:,10), max_amp_8array(:,10), min_amp_8array(:,10),
mean_amp_8array(:,11), std_amp_8array(:,11), kurtosis_amp_8array(:,11),
skewness_amp_8array(:,11), max_amp_8array(:,11), min_amp_8array(:,11),
mean_amp_8array(:,12), std_amp_8array(:,12), kurtosis_amp_8array(:,12),
skewness_amp_8array(:,12), max_amp_8array(:,12), min_amp_8array(:,12),
mean_amp_8array(:,13), std_amp_8array(:,13), kurtosis_amp_8array(:,13),
skewness_amp_8array(:,13), max_amp_8array(:,13), min_amp_8array(:,13),
mean_amp_8array(:,14), std_amp_8array(:,14), kurtosis_amp_8array(:,14),
skewness_amp_8array(:,14), max_amp_8array(:,14), min_amp_8array(:,14),
mean_amp_8array(:,15), std_amp_8array(:,15), kurtosis_amp_8array(:,15),
skewness_amp_8array(:,15), max_amp_8array(:,15), min_amp_8array(:,15),
mean_amp_8array(:,16), std_amp_8array(:,16), kurtosis_amp_8array(:,16),
skewness_amp_8array(:,16), max_amp_8array(:,16), min_amp_8array(:,16));

end
```

[A19]

B.1.2 Wavelet slit up

```matlab
%slice up wavelet matrix

namefile = noisebeforehit6_T74_filt2;

% split to 3 and split to 6 equal parts

sizeofnamefile = size(namefile);

sizeofnamefile_singlearray = sizeofnamefile(:,1);

thirds = round(sizeofnamefile_singlearray/3);

slice1_thirds_noisebeforehit6_T74 =  namefile(1:thirds);
slice2_thirds_noisebeforehit6_T74 =  namefile(thirds + 1 :(thirds *
2));
slice3_thirds_noisebeforehit6_T74 =  namefile((thirds*2) + 1 : (thirds
* 3));


sixths = round(sizeofnamefile_singlearray/6);

slice1_sixths_noisebeforehit6_T74 =  namefile(1:sixths);
slice2_sixths_noisebeforehit6_T74 =  namefile(sixths + 1 :(sixths *
2));
slice3_sixths_noisebeforehit6_T74 =  namefile((sixths*2) + 1 : (sixths
* 3));
slice4_sixths_noisebeforehit6_T74 =  namefile((sixths*3) + 1 : (sixths
* 4));
slice5_sixths_noisebeforehit6_T74 =  namefile((sixths*4) + 1 :(sixths *
5));
slice6_sixths_noisebeforehit6_T74 =  namefile((sixths*5) + 1 : ((sixths
* 6)- 3));
```

B.1.3 WPT to FFT split up

```matlab
phenom_val1 = 31;             %select STFT vector as FFT at point in time


cwpt1 = abs(d1_array_1stslice_STFT(:,phenom_val1));

cwpt2 = abs(d1_array_2ndslice_STFT(:,phenom_val1));

cwpt3 = abs(d1_array_3rdslice_STFT(:,phenom_val1));

cwpt4 = abs(d1_array_4thslice_STFT(:,phenom_val1));

cwpt5 = abs(d1_array_5thslice_STFT(:,phenom_val1));
```

[A20]

```
cwpt6 = abs(d1_array_6thslice_STFT(:,phenom_val1));

cwpt7 = abs(d1_array_7thslice_STFT(:,phenom_val1));

cwpt8 = abs(d1_array_8thslice_STFT(:,phenom_val1));

c5_c1_wpt_concatenate_slice = cat(1, cwpt8, cwpt7, cwpt6, cwpt5, cwpt4,
cwpt3, cwpt2, cwpt1);

% display each packet of information
subplot(3,3,1); plot(cwpt1); title('Atom 1 0.625 MHz');
subplot(3,3,2); plot(cwpt2); title('Atom 2 1.25 MHz');
subplot(3,3,3); plot(cwpt3); title('Atom 3 1.875 MHz');
subplot(3,3,4); plot(cwpt4); title('Atom 4 2.5 MHz');
subplot(3,3,5); plot(cwpt5); title('Atom 5 3.125 MHz');
subplot(3,3,6); plot(cwpt6); title('Atom 6 3.75 MHz');
subplot(3,3,7); plot(cwpt7); title('Atom 7 4.375 MHz');
subplot(3,3,8); plot(cwpt8); title('Atom 8 5 MHz');
```

B.1.4 STFT of WPT detailed signal

```
%STFT of WPT signal -  Filters are used to ensure just the packet
%information is looked at and no noise

filename = d1_array_1stslice;           %WPT filename with detailed
signal
text_title = '  d1_array_1stsliceT74 '; %Title of detailed signal
d1_array_1stslice_STFT = specgram(filename,128,625000,Kaiser(64,1),50);
specgram(filename,128,625000,Kaiser(64,1),50);  %1-625KHz
title(text_title);
pause;


filename = d1_array_2ndslice;
text_title = '  d1_array_2ndsliceT74 ';
d1_array_2ndslice_STFT =
specgram(filename,128,1250000,Kaiser(64,1),50);
specgram(filename,128,125000,Kaiser(64,1),50); %1-1.25MHz
title(text_title);
pause;

filename = d1_array_3rdslice;
text_title = ' d1_array_3rdsliceT74 ';
d1_array_3rdslice_STFT =
specgram(filename,128,1875000,Kaiser(64,1),50);
specgram(filename,128,1875000,Kaiser(64,1),50);   % 1- 1.875MHz
title(text_title);
pause;

filename = d1_array_4thslice;
```

```
text_title = '  d1_array_4thsliceT74 ';
d1_array_4thslice_STFT =
specgram(filename,128,2500000,Kaiser(64,1),50);
specgram(filename,128,2500000,Kaiser(64,1),50);  %1-2.5MHz
title(text_title);
pause;

filename = d1_array_5thslice;
text_title = '  d1_array_5thsliceT74 ';
d1_array_5thslice_STFT =
specgram(filename,128,3125000,Kaiser(64,1),50);
specgram(filename,128,3125000,Kaiser(64,1),50); %1-3.125Mhz
title(text_title);
pause;

filename = d1_array_6thslice;
text_title = '  d1_array_6thsliceT74 ';
d1_array_6thslice_STFT =
specgram(filename,128,3750000,Kaiser(64,1),50);
specgram(filename,128,3750000,Kaiser(64,1),50);  %1-3.75Mhz
title(text_title);
pause;

filename = d1_array_7thslice;
text_title = '  d1_array_7thsliceT74 ';
d1_array_7thslice_STFT =
specgram(filename,128,4375000,Kaiser(64,1),50);
specgram(filename,128,4375000,Kaiser(64,1),50);  %1-4.375MHz
title(text_title);
pause;

filename = d1_array_8thslice;
text_title = '  d1_array_8thslice ';
d1_array_8thslice_STFT =
specgram(filename,128,5000000,Kaiser(64,1),50);
specgram(filename,128,5000000,Kaiser(64,1),50);   %1-5Mhz
title(text_title);
pause;
```

B.1.5 Convert CWT signal into STFT Frequency bands

```
%convert CWT into STFT
filename = hit13_T35;

c_hit1 = cwt(filename,1:5,'db5','plot');   % 1 - 5 levels each level /2
from sampling rate


c_hit1_level1 = c_hit1(1,:);     %high frequency level 1
c_hit1_level2 = c_hit1(2,:);
c_hit1_level3 = c_hit1(3,:);
c_hit1_level4 = c_hit1(4,:);
```

```
c_hit1_level5 = c_hit1(5,:);     %low frequency level 5

filename = c_hit1_level1;    % high frequency
text_title = '  c_hit1_level1  ';
c_hit1_level1_STFT = specgram(filename,1024,5000000,Kaiser(512,1),375);
specgram(filename,1024,5000000,Kaiser(512,1),375);    % 1-5Mhz
title(text_title);
pause;


filename = c_hit1_level2;
text_title = '  c_hit1_level2  ';
c_hit1_level2_STFT = specgram(filename,1024,2500000,Kaiser(512,1),375);
specgram(filename,1024,2500000,Kaiser(512,1),375);    %1-2.5MHz
title(text_title);
pause;


filename = c_hit1_level3;
text_title = '  c_hit1_level3  ';
c_hit1_level3_STFT = specgram(filename,1024,1250000,Kaiser(512,1),375);
specgram(filename,1024,1250000,Kaiser(512,1),375);    %1-1.25Mhz
title(text_title);
pause;


filename = c_hit1_level4;
text_title = '  c_hit1_level4  ';
c_hit1_level4_STFT = specgram(filename,1024,625000,Kaiser(512,1),375);
specgram(filename,1024,625000,Kaiser(512,1),375);     %1-625KHz
title(text_title);
pause;


filename = c_hit1_level5;
text_title = '  c_hit1_level5  ';
c_hit1_level5_STFT = specgram(filename,1024,312500,Kaiser(512,1),375);
specgram(filename,1024,312500,Kaiser(512,1),375);      %1-312KHz
title(text_title);
pause;
```

B.1.6 FFT vector for STFT CWT signal

```
%Look at individual vector of STFT CWT signal

phenom_val1 = 24;    %vector number



c1 = abs(c_hit1_level1_STFT(:,phenom_val1));

c2 = abs(c_hit1_level2_STFT(:,phenom_val1));

c3 = abs(c_hit1_level3_STFT(:,phenom_val1));
```

```matlab
c4 = abs(c_hit1_level4_STFT(:,phenom_val1));

c5 = abs(c_hit1_level5_STFT(:,phenom_val1));


%low frequencies first in the concatenation

c5_c1_concatenate_slice = cat(1, c5, c4, c3, c2, c1);

subplot(3,2,1); plot(c1); title('Level 1 HF 2.5 MHz');
subplot(3,2,2); plot(c2); title('Level 2 HF 1.25 MHz');
subplot(3,2,3); plot(c3); title('Level 3 HF 625 KHz ');
subplot(3,2,4); plot(c4); title('Level 4 LF 312.5 KHz');
subplot(3,2,5); plot(c5); title('Level 5 LF 156.25 KHz');
subplot(3,2,6); plot(c5_c1_concatenate_slice); title('Concatenated Low
to High frequencies');
```

B.1.7 STFT of raw extracted time signal

```matlab
filename = T47_forcephenom;
text_title = ' T47_forcephenom ';


T47_forcephenom = specgram(filename,512,5000,Kaiser(512,10),375);
specgram(filename,512,5000,Kaiser(512,10),375);    %matrix,block size,
                                                   %sampling frequency
                                        5KHz,
                                                   %(window and window
                                                   %overlap) and NFFT
title(text_title);
```

B.1.8 Min Max of a raw extracted time signal

```matlab
%Looking for the time constant of the 4 max values within time signal
%opposite was used to find the 4 min values

x = 0;

fs = 2000000;
L = T53output;
q = 32742;
window = 1023;
M = L(q:q+window,1);
length_m = 0;

time_const_array = ones(1,4);
time_0_to_peak_to_0_array = ones(1,4);
max_amplitude_array = ones(1,4);
array_time_check = ones(1,4);
variables_array_max = ones(1,15);
```

[A24]

```matlab
false_length = 0;
ret_max_index = 0;
MM_256 = 0;
MM_206 = 0;


for x=1:4              %Look for 4 max values

    maxL = 0;
    maxL256 = 0;
    time_const_count_check = 0;
    time_const = 0;
    ret_max_index = 0;
    jjj = 256 * x;
    MM_256 = M((jjj - 255):(jjj),:)
    % window 0 - 20 length + 30
    MM_206 = M((jjj - 226):(jjj - 30),:)
    length_m = length(MM_256)-1;
    maxL = max(MM_206);
    ret_max_index = find(MM_206 == maxL);


    % Test for more than one ret_max_index values
    if length(ret_max_index) > 1
        ret_max_index = ret_max_index(1,1);
    else
        ret_max_index = ret_max_index;
    end

    count = 0;
    i = ret_max_index + 29;

    while MM_256(i) >= 0 && false_length == 0
        i = i - 1;
    end

    while MM_256(i) <= 0 && false_length == 0
        if i >= length_m
            false_length = 1;
        elseif length_m > i
            false_length = 0;
        end
    i = i + 1;
    count = count + 1;
    end



    while MM_256(i) >= 0 && false_length == 0
        if i < length_m
            false_length = 0;
        elseif i > length_m
            false_length = 1;
```

[A25]

```matlab
        end
        i = i + 1;
        count = count + 1;
    end



    while MM_256(i) <= 0 && false_length == 0
        if i < length_m
            false_length = 0;
        elseif i > length_m
            false_length = 1;
        end
    i = i + 1;
    count = count + 1;
    end

% calculate the time constant for min max values
i = 0;
time_const_count_check = ((ret_max_index + count) - ret_max_index);
time_const = ((time_const_count_check)/fs);
time_const_array(:,x) = time_const;
array_time_check(:,x) = ret_max_index;

count1 = 0;
count2 = 0;
count1_time = 0;
count2_time = 0;
count1_2_total_time = 0;
k1 = ret_max_index + 29;
k2 = ret_max_index + 29;
max_amplitude_array(:,x) = maxL;

while (MM_256(k1) >= 0)
    k1 = k1 - 1;
    count1 = count1 + 1;
end
count1_time = (count1/fs);

while (MM_256(k2) >= 0)
    k2 = k2 + 1;
    count2 = count2 + 1;
end

count2_time = (count2/fs);

count1_2_total_time = count1_time + count2_time;

time_0_to_peak_to_0_array(:,x) = count1_2_total_time;


end

%check spread of time constants from max components
```

[A26]

```
z = 0;
spread = 0;
spread_calc = 0;


spread_points = std(array_time_check);
spread_points_values = std(time_const_array);
spread_total = std(M);

variables_array_max = cat(1, max_amplitude_array(1,1),
time_const_array(1,1), time_0_to_peak_to_0_array(1,1),
max_amplitude_array(1,2), time_const_array(1,2),
time_0_to_peak_to_0_array(1,2), max_amplitude_array(1,3),
time_const_array(1,3),  time_0_to_peak_to_0_array(1,3),
max_amplitude_array(1,4), time_const_array(1,4),
time_0_to_peak_to_0_array(1,4),
spread_points,spread_points_values,spread_total);
```

Appendix C - Examples of Extracted Signals

C.1.1 Horizontal Scratch Single Grit Time Extracted AE signal Hit T212

The example below is the raw extracted Acoustic Emission of hit 2 (scratch 2) T212 which has been de-sampled by a factor of 4 and halved to ensure the example would give users an idea of the source information albeit not too large to extend the thesis content significantly. Each part concatenates together to make one AE time extracted signal.

Hit 2 T212								
Part 1	Part 2	Part 3	Part 4	Part 5	Part 6	Part 7	Part 8	Part 9
0.0019	0.0111	0.0048	0.0096	0.0003	-0.0122	0.0048	0.01	0.0061
0	-0.004	-0.0071	0.0112	-0.0036	-0.0133	0.0107	0.0073	-0.0007
-0.0014	-0.0149	-0.0085	-0.0075	-0.0019	-0.0134	0.0091	0.0008	0.0054
-0.0032	-0.011	-0.0155	-0.0197	0.0009	-0.0024	0.0101	0.0015	-0.0013
-0.0024	-0.0011	-0.0111	-0.0178	0.0022	0.0096	0.0083	0.001	0.0005
-0.0035	0.0058	-0.0096	-0.0098	0.004	0.0202	0.0026	0.0025	0.0009
-0.0017	0.0037	-0.0034	0.0024	0.0024	0.0155	-0.0025	-0.0015	-0.0058
0.0004	0.0036	0.0043	0.0086	-0.0084	0.0072	-0.0125	-0.0029	-0.0014
0.0001	0.0055	0.013	0.006	-0.0092	-0.0014	-0.0094	-0.0083	-0.0058
0.0044	0.0123	0.0196	0.0119	-0.0096	-0.0069	-0.0048	-0.0078	-0.003
0.0041	0.0069	0.0146	0.004	-0.0035	-0.0052	-0.0003	-0.0048	0.002
0.003	-0.0038	0.0032	-0.0013	0.0069	-0.0042	0.0111	-0.0042	-0.0031
0.0004	-0.0186	-0.0096	-0.0032	0.0075	0.0018	0.0051	0.008	0.0003
-0.0012	-0.0175	-0.017	-0.0018	0.0134	0.0046	0.0084	0.0068	0.0032
-0.0032	-0.013	-0.0179	0.0021	0.0067	0.0065	0.0013	0.006	0.0025
-0.0034	0.0003	-0.0105	0.003	0.0025	0.0066	-0.0049	-0.0023	0.0027
-0.0012	0.0113	-0.0042	-0.0017	-0.0031	0.0024	-0.0099	-0.0063	0.0031
-0.0016	0.0086	0.001	-0.0024	-0.0129	-0.0056	-0.0172	-0.0024	-0.0001
0.0002	0.0081	0.0122	-0.0006	-0.0102	-0.0034	-0.0126	0.0005	0.0026
0.001	0.0067	0.0132	0.0038	-0.0075	-0.0065	-0.0027	0.0077	-0.0011
0.0028	0.0044	0.0134	0.0067	-0.0012	-0.0086	0.0069	0.0073	-0.0047
0.002	-0.0039	0.008	0.0015	0.0047	-0.003	0.0136	0.0046	-0.0003
0.0024	-0.0083	0.0035	-0.0039	0.0067	-0.0031	0.0142	0.0024	0.0005
0.0014	-0.0114	-0.0027	-0.0137	0.0031	0.0017	0.0098	-0.0017	0.0036
-0.0001	-0.0052	-0.0087	-0.0142	0.0049	0.0042	0.0016	-0.0041	-0.0001
-0.001	0.001	-0.0119	-0.0106	0.0073	0.0025	0.0001	-0.0011	-0.0033

-0.0046	0.0097	-0.0052	0.0015	0.0053	0.0059	-0.0037	-0.0058	-0.0025
-0.0028	0.0161	0.0029	0.0064	0.0042	-0.0057	-0.0079	-0.0058	-0.0017
-0.0022	0.0112	0.0052	0.0094	0	-0.0069	-0.0063	-0.007	0.0002
-0.0012	0.0032	0.0086	0.0054	-0.0055	-0.0045	-0.0042	-0.0086	0.0015
0.0016	-0.0091	0.0014	0.0071	-0.0072	-0.0044	0.007	0.0035	-0.0015
0.003	-0.0116	-0.0057	0.01	-0.0094	0.0116	0.0106	0.0048	0.0023
0.0023	-0.0125	-0.0144	0.0125	-0.0076	0.013	0.0068	0.0085	0.0002
0.0027	-0.0023	-0.0131	0.0053	-0.0026	0.0129	-0.002	0.0029	-0.0026
-0.0001	-0.0001	-0.0071	-0.0038	0.002	0.0158	-0.0113	-0.0013	-0.0011
-0.001	0.0037	-0.0024	-0.0125	0.0119	0.0006	-0.0105	0.0004	-0.0014
-0.001	0.0014	-0.0011	-0.012	0.0065	-0.0037	-0.0067	-0.0023	0.0016
-0.0017	-0.002	0.0086	-0.005	0.003	-0.0118	-0.0044	-0.002	0.0063
0.0009	-0.0007	0.015	0.0017	-0.007	-0.0188	-0.0021	0.001	0.0078
-0.0001	-0.003	0.0248	0.0076	-0.0097	-0.0075	-0.0026	0.0051	0.0028
0.0026	-0.0044	0.0212	0.0019	-0.0063	-0.0078	0.0014	0.01	0.0008
0.002	-0.0053	0.0023	0.0013	0	-0.0045	0.0136	0.004	-0.0078
0.0004	-0.0034	-0.0057	-0.01	0.0028	0.0006	0.0135	-0.0034	-0.0083
-0.0015	0.0054	-0.017	-0.0131	0.0034	0.0019	0.0151	-0.007	-0.0037
-0.004	0.0154	-0.0093	-0.0057	0.0104	0.0114	0.0048	-0.0029	-0.0037
-0.0057	0.0129	-0.0046	-0.0004	0.0076	0.0102	-0.0077	-0.0026	0.0002
-0.004	0.0123	-0.0072	0.0045	0.0138	0.0045	-0.0071	-0.0006	0.0014
0.0006	0.0033	0.0014	0.0048	0.006	-0.0009	-0.0085	-0.0039	0.0023
0.0034	0.0011	-0.0024	0.0063	-0.0066	-0.0107	-0.0039	-0.0085	0.0031
0.0062	0.0023	0.0033	0.0117	-0.017	-0.0046	-0.0031	-0.0013	0.0065
0.0069	-0.0025	-0.0077	0.0058	-0.0218	0.0008	-0.0017	0.0036	0.0015
0.003	-0.0066	-0.0151	-0.0012	-0.0159	0.0064	-0.0008	0.0101	-0.0012
0.0009	-0.0158	-0.0037	-0.0072	0.0013	0.0117	0.0039	0.012	-0.0054
-0.0048	-0.0142	0.0017	-0.0039	0.0059	0.0081	0.0084	0.0036	-0.0038
-0.0056	-0.0137	0.0141	0.0008	0.0188	0.0028	0	-0.005	-0.0007
-0.0067	-0.0076	0.011	0.0004	0.0157	-0.0042	0	-0.01	0.0006
-0.0023	-0.0019	0.005	-0.0013	0.0131	-0.0109	-0.0057	-0.0085	0.0035
0.0061	0.0035	0.0002	-0.0062	0.0064	-0.0099	-0.0057	-0.0025	0.0048
0.0057	0.011	0.0039	0.0058	-0.0056	-0.0116	-0.0062	0.0072	0.0059
0.0097	0.0148	0.006	0.0136	-0.0105	-0.0089	-0.0037	0.0076	0.0073
0.0012	0.0147	0.0068	0.0095	-0.0171	-0.0046	0.0037	0.0039	0.003
-0.0048	0.006	0.0031	-0.003	-0.0141	0.0009	0.0055	0.003	-0.0027
-0.01	-0.0025	0.0015	-0.0158	-0.0035	0.0099	0.0115	0	-0.0044
-0.0143	-0.0088	-0.0058	-0.0133	0.0011	0.0138	0.0059	-0.0004	-0.0088
-0.0091	-0.0082	-0.0134	-0.0062	0.0038	0.0143	0.0046	-0.0042	-0.0072
-0.0031	-0.0026	-0.0142	0.0056	0.013	0.0137	0.0009	-0.0065	-0.0036
0.0033	0.0016	-0.0072	0.0056	0.006	0.0006	-0.0035	-0.0043	-0.0023
0.015	0.002	0.0016	0.0067	0.0056	-0.006	-0.0064	-0.003	-0.0021
0.0161	0.0064	0.0061	-0.0012	-0.0049	-0.0119	-0.0087	-0.002	0.0018

[A29]

0.0146	0.0091	0.0061	-0.0053	-0.0092	-0.0122	-0.0088	0.0019	0.0017
0.0056	0.009	0.002	-0.0055	-0.0068	-0.0053	-0.0056	0.0026	0.0059
-0.0048	0.0039	-0.0055	-0.0038	0.0005	0.003	0.001	0.008	0.0054
-0.0091	-0.0159	-0.0059	0.004	0.0093	0.0081	0.0072	0.0058	0.0027
-0.0126	-0.0235	-0.0065	0.0031	0.0145	0.0095	0.011	0.001	-0.0018
-0.0076	-0.0264	0.0024	0.0039	0.0125	0.0047	0.0083	-0.0042	-0.0027
-0.0097	-0.0061	0.0084	0.0043	0.007	-0.0059	0.0017	-0.0074	-0.001
-0.0091	0.0092	0.0115	0.0025	0.0007	-0.0063	-0.009	-0.0072	0.0017
0	0.0253	0.0013	0.0029	-0.0055	-0.0151	-0.0108	0.0018	0.0033
0.0128	0.0224	-0.001	0.0024	-0.0086	-0.0092	-0.0064	0.0018	0.0008
0.0202	0.0136	0.004	-0.004	-0.015	-0.0031	0.0038	0.0044	0.0009

C.1.2 AE example of chatter phenomenon

An example of chatter phenomenon from an extracted AE signal:

Chatter Signal 1st Trial

Part 1	Part 2	Part 3	Part 4	Part 5	Part 6	Part 7	Part 8	Part 9
0.0321	0.5594	-0.389	0.0839	-0.268	-0.7509	0.8067	-0.8494	0.6103
0.2508	0.3419	-0.7319	0.0906	-0.3424	-0.657	0.9508	-0.4548	0.3681
0.248	0.1504	-1.1257	0.2793	-0.3363	-0.4941	0.7603	-0.0104	0.1039
0.0892	0.1974	-1.2806	0.7312	-0.6686	-0.1717	0.4607	0.0096	0.4476
0.1056	0.1652	-1.3046	1.0864	-1.2397	-0.0356	0.4829	-0.2371	0.8383
0.3353	-0.0736	-1.2192	0.965	-1.2659	-0.4025	0.4863	-0.204	0.6109
0.4329	-0.2872	-0.8886	0.5165	-0.8232	-0.6417	-0.0539	0.2005	0.2319
0.2634	-0.2798	-0.6282	0.2917	-0.6554	-0.1656	-0.6114	0.5994	0.4144
0.0702	-0.0648	-0.5467	0.3716	-0.8089	0.3051	-0.6046	0.7302	0.6974
0.0631	-0.1469	-0.3635	0.3194	-1.0149	0.1765	-0.4895	0.8474	0.3253
0.217	-0.6329	0.1415	-0.1123	-0.9056	-0.2308	-0.6478	0.9272	-0.3762
0.3787	-0.791	0.704	-0.5735	-0.2874	-0.3707	-0.9722	0.709	-0.6128
0.3424	-0.4	0.8949	-0.7017	0.334	0.0326	-1.2798	0.4861	-0.2551
0.3082	0.0374	0.845	-0.7338	0.5368	0.489	-1.2384	0.5153	-0.1103
0.5759	0.1226	0.9773	-0.9112	0.549	0.4956	-0.7918	0.4687	-0.5589
0.5266	-0.0878	1.3496	-0.9493	0.7711	0.2971	-0.4244	0.0175	-0.8414
-0.0432	-0.2243	1.4074	-0.691	1.2335	0.3145	-0.5801	-0.5173	-0.5361
-0.2546	-0.024	0.9286	-0.6043	1.6422	0.5394	-0.9683	-0.6857	-0.0711
-0.0531	0.3506	0.511	-0.5837	1.591	0.7009	-0.8268	-0.4905	-0.0247
0.0025	0.4392	0.427	-0.0795	1.1134	0.813	-0.057	-0.3582	-0.3719
-0.2835	0.2943	0.2926	0.4872	1.0151	0.9496	0.5487	-0.681	-0.4449
-0.7233	0.2654	-0.1377	0.5721	1.3982	0.7014	0.414	-1.0259	-0.0604

-0.816	0.2916	-0.5704	0.3661	1.3273	-0.2417	0.1087	-0.8889	0.1766
-0.6318	0.2978	-0.6668	0.4901	0.6511	-0.758	0.4184	-0.4974	-0.0826
-0.6256	0.2922	-0.6034	1.024	0.0222	-0.2038	1.0065	-0.2834	-0.3114
-0.872	0.3661	-0.8765	1.16	-0.2996	0.0166	1.0983	-0.4003	-0.1685
-0.9226	0.3719	-1.3866	0.6474	-0.4216	-0.0028	0.577	-0.4845	0.0267
-0.4532	-0.0843	-1.3614	0.0119	-0.6439	0.3804	0.3071	-0.2143	0.1502
-0.1616	-0.6043	-0.7521	-0.1591	-1.2075	0.4843	0.9277	0.2755	0.1731
-0.4548	-0.5661	-0.3486	0.0723	-1.5872	0.6559	1.3548	0.5966	0.1755
-0.7733	-0.2045	-0.5506	0.0258	-1.2716	0.497	0.8377	0.558	0.3726
-0.6035	-0.2604	-0.7083	-0.2751	-0.9435	-0.0347	0.2448	0.5211	0.6463
0.0199	-0.7221	-0.1832	-0.5467	-1.3198	0.2229	0.2349	0.6653	0.7627
0.3725	-0.721	0.3878	-0.7748	-1.7614	0.4657	0.6629	0.8165	0.6523
0.1079	-0.2482	0.4817	-0.8503	-1.3379	0.384	0.6614	0.7572	0.6155
-0.2207	0.0982	0.4259	-0.7645	-0.4837	0.1869	-0.0557	0.4301	0.8998
0.0813	0.1289	0.5901	-0.4712	-0.3584	-0.1149	-0.5137	0.3265	1.1075
0.8506	0.0606	0.9948	-0.2936	-0.8574	0.1265	-0.4113	0.5339	0.8507
1.0477	0.4208	1.0264	-0.5495	-0.7353	0.0239	-0.3117	0.5172	0.4464
0.6683	0.8737	0.566	-0.6559	0.1134	-0.606	-0.7262	0.2082	0.3238
0.5401	0.7441	0.3782	-0.1485	0.7028	-0.815	-1.1949	-0.0217	0.1576
0.8289	0.361	0.8267	0.4944	0.8806	-0.5867	-0.8514	0.0127	-0.3573
1.1958	0.3614	1.2605	0.6025	0.9658	-0.3217	-0.4399	-0.0768	-0.8007
1.1128	0.8297	0.8089	0.3835	1.1103	-0.7602	-0.7524	-0.4637	-0.9548
0.6221	0.9494	-0.0643	0.5707	1.3094	-1.3456	-1.2868	-0.7293	-1.0493
0.3007	0.3247	-0.2025	1.0932	1.2424	-1.1755	-1.273	-0.7692	-1.2189
0.3681	-0.1579	0.3859	1.0962	1.0027	-0.6534	-0.5668	-0.6077	-1.4034
0.4464	-0.0298	0.5149	0.3875	0.9215	-0.4298	-0.1809	-0.4607	-1.4429
-0.0498	0.1449	-0.2974	0.1113	0.9344	-0.7635	-0.3913	-0.6097	-1.2216
-0.7122	-0.1687	-0.8534	0.7489	0.805	-0.934	-0.3702	-0.6156	-0.9158
-0.6807	-0.6572	-0.5496	1.0232	0.5126	-0.5308	0.1358	-0.295	-0.7756
-0.3756	-0.67	-0.3097	0.3723	0.3067	0.0011	0.8185	-0.0327	-0.6084
-0.6269	-0.3771	-0.5886	-0.2282	0.1805	0.1393	1.0654	-0.0822	-0.2621
-1.1357	-0.4624	-0.968	-0.2519	0.0595	-0.1375	0.9006	-0.258	0.0839
-1.1354	-0.909	-1.1079	-0.2156	-0.1349	-0.0563	0.8358	0.0137	0.3835
-0.6123	-1.0022	-0.9181	-0.5884	-0.4652	0.3804	0.966	0.4733	0.6854
-0.1962	-0.6178	-0.7198	-1.0042	-0.6116	0.6482	1.2385	0.5251	1.0285
-0.1983	-0.317	-1.0208	-1.0009	-0.6155	0.5839	1.0833	0.3565	1.268
-0.2269	-0.3988	-1.3472	-0.8749	-0.6582	0.4266	0.3806	0.2975	1.2827
-0.0195	-0.6311	-0.9553	-0.9085	-0.6544	0.7257	0.0905	0.546	1.3071
0.1987	-0.5469	-0.3288	-0.8729	-0.7415	1.1567	0.4256	0.7671	1.3234
0.2784	-0.237	-0.1724	-0.6188	-0.8484	1.103	0.5251	0.6308	1.0508
0.2933	0.033	-0.2859	-0.2155	-0.6778	0.6272	0.0457	0.4335	0.6833
0.4343	0.3312	-0.0276	0.1199	-0.3297	0.2942	-0.3567	0.2675	0.6672
0.5525	0.4112	0.8188	0.1321	-0.3324	0.3928	-0.3493	0.1522	0.7261

0.4817	0.3652	1.64	0.122	-0.6658	0.5192	-0.264	0.0372	0.2688
0.5155	0.6071	1.7069	0.5906	-0.5974	0.4032	-0.4505	-0.1068	-0.3973
0.5276	0.9687	1.2926	1.0878	-0.0756	0.0885	-0.9282	-0.0451	-0.71
0.3009	1.137	1.1787	0.9449	0.2306	-0.0209	-1.0314	0.0302	-0.7028
0.0524	0.997	1.4858	0.5288	-0.0065	0.0925	-0.4913	-0.2004	-0.7265
0.0137	0.8451	1.7445	0.4693	-0.2036	-0.0497	0.016	-0.698	-0.9395
0.1532	0.8246	1.3529	0.7612	0.1615	-0.3014	-0.0516	-1.0183	-1.0086
-0.0371	0.6518	0.5618	0.8695	0.5108	-0.4751	-0.5219	-0.7674	-0.7769
-0.3927	0.4838	0.201	0.4152	0.4642	-0.4874	-0.5899	-0.3337	-0.5021
-0.323	0.3877	0.1032	-0.154	0.373	-0.4171	-0.0573	-0.3495	-0.3685
-0.1622	0.1654	-0.2083	-0.3399	0.4582	-0.5637	0.2847	-0.8246	-0.3354
-0.2377	-0.1956	-0.6632	-0.2966	0.4791	-0.6952	0.127	-0.9221	-0.148
-0.3191	-0.6404	-1.0597	-0.2884	0.2381	-0.5316	-0.1146	-0.1881	0.1913
-0.1022	-0.9401	-1.3364	-0.482	0.1074	-0.1193	-0.1572	0.5285	0.3654
0.1745	-1.0554	-1.432	-0.8217	0.1141	0.2074	-0.014	0.5597	0.2516
0.1034	-1.0324	-1.1856	-0.8687	0.1453	0.1637	0.1742	0.3433	0.1728
-0.0335	-0.9999	-0.8835	-0.5174	0.3315	-0.0526	0.2346	0.5346	0.4705
-0.1114	-1.1679	-0.8111	-0.3145	0.2049	-0.1062	0.2329	0.9707	0.687
-0.1556	-1.1623	-0.7682	-0.4837	-0.1938	0.183	0.3166	0.9439	0.3266
-0.0185	-0.841	-0.5102	-0.5758	-0.1308	0.4679	0.3608	0.4622	-0.1028
0.0546	-0.5767	-0.0352	-0.3052	0.3081	0.2594	0.2564	0.235	0.0087
-0.1277	-0.4577	0.2929	0.102	0.5695	-0.2055	0.1248	0.4913	0.2833
-0.3817	-0.2668	0.3414	0.2522	0.4246	-0.2562	0.1362	0.6773	-0.0368
-0.4504	0.2333	0.2892	0.1656	0.0752	0.1223	0.2643	0.3298	-0.7079
-0.2693	0.7315	0.3238	0.3359	-0.032	0.1836	0.2981	-0.2674	-0.875
0.0787	0.8455	0.4459	0.748	0.1404	-0.1946	0.1622	-0.4258	-0.5377
0.237	0.8025	0.3449	0.7907	0.2625	-0.3872	0.1243	-0.2505	-0.4626
-0.2197	0.946	0.0876	0.5226	0.3081	-0.1435	0.283	-0.5585	-0.837
-0.6708	1.305	-0.0461	0.5755	0.2035	0.1305	0.2152	-1.1243	-0.9068
-0.2413	1.476	0.0171	0.8379	-0.1958	0.0056	-0.1224	-1.0714	-0.3655
0.5478	1.1896	0.028	0.7559	-0.3866	-0.1962	-0.3572	-0.5084	0.0529
0.6235	0.7231	-0.2513	0.4008	-0.1709	-0.04	-0.3886	-0.2008	-0.123
0.1007	0.4422	-0.3497	0.1624	-0.2254	0.2997	-0.3509	-0.3789	-0.2181
-0.0207	0.2753	-0.1265	0.0804	-0.6516	0.5345	-0.5383	-0.3864	0.4366
0.3733	-0.0499	0.0356	-0.0589	-0.8463	0.6402	-0.8495	0.1762	1.1847

C.1.3 AE example of burn phenomenon

An example of burn phenomenon from an extracted AE signal:

T55 Burn Test 1mm DOC

Part 1	Part 2	Part 3	Part 4	Part 5	Part 6	Part 7	Part 8	Part 9
0.4365	0.1624	0.914	-0.3025	0.015	-0.2316	0.1369	0.1313	0.8664
-0.3686	0.8254	-1.1279	0.4312	-1.3616	-0.5063	0.1814	0.4489	-0.4449
-0.7059	0.2342	-1.12	0.3266	-1.0072	-0.6911	-0.09	0.1775	-0.8492
-0.4148	-0.1692	0.6931	-0.3329	0.3714	0.5648	-0.1132	-0.34	0.429
0.4593	0.4477	1.2311	-1.0175	0.36	1.1224	0.4424	0.1648	0.907
0.3682	0.6944	-0.3414	-0.4751	0.0334	-0.0368	1.2678	0.326	-0.5773
-0.7677	0.2418	-1.4513	0.5154	-0.2141	-0.0754	0.6902	-0.2083	-1.8384
-0.7623	0.1828	-0.2196	-0.2121	-0.3119	1.1599	-0.7618	-0.0758	-1.3009
0.204	0.4417	1.1477	-1.3993	0.6183	1.2856	0.088	-0.1662	0.2616
0.3746	0.5231	0.3279	-1.2066	0.998	0.5074	1.7653	-0.2679	0.5804
-0.2581	0.4863	-0.8489	0.1059	0.5392	0.5425	0.4672	0.24	-1.7276
-0.7386	0.0056	-0.5993	0.5589	0.5065	1.1193	-1.1599	-0.4366	-3.1031
-0.5299	-0.2549	0.0409	-0.3993	0.9645	0.8555	-0.1723	-0.5873	-0.5668
0.2739	0.1367	0.018	-1.025	1.0489	-0.287	0.8163	0.83	1.0713
0.6101	-0.1295	-0.5672	-0.4869	0.4358	-0.7321	0.4002	0.0113	-1.0718
-0.1784	-0.3642	-0.7894	0.7748	0.8613	0.1435	-0.6813	-1.0084	-1.7658
-0.6189	0.1949	-0.3928	0.8823	0.9168	0.531	-1.5487	-0.0106	-0.0154
0.3213	-0.2878	0.1592	-0.086	-0.0463	-0.6676	-0.6336	0.7115	0.3609
1.0321	-1.0031	0.2445	-0.0313	0.4121	-1.8324	0.6733	0.518	0.124
0.3221	0.1009	-0.4089	0.5495	0.4209	-1.5586	-0.5024	-0.9347	0.8248
-0.5086	0.6139	-0.3809	1.0109	-0.519	-0.5677	-1.8251	-1.048	1.1593
0.0011	-0.6495	0.3659	0.7246	-0.0804	-0.3138	-0.1747	0.6368	0.1721
0.6568	-0.8071	0.5465	0.2076	-0.0968	-0.5983	1.5326	0.8531	-0.4053
0.3443	0.432	0.4448	0.8451	-0.8669	-0.9044	0.1299	-0.8431	0.997
-0.1054	0.6159	0.4575	0.9841	-0.3401	-1.0547	-1.5064	-2.1625	1.8012
-0.6011	-0.5301	0.5262	0.3832	-0.7228	0.225	-0.1148	0.0708	0.1706
-0.1676	-0.5263	0.2188	-0.0989	-1.3155	1.106	1.2394	1.8788	-0.4927
0.6708	0.2028	0.132	-0.2875	-0.2519	-0.0477	0.2177	-0.3443	1.0177
-0.2494	0.0407	0.9086	0.341	-0.1988	-0.2791	-0.4866	-1.8605	1.3699
-0.7626	0.205	0.6851	0.4907	-0.8568	0.7547	-0.0283	-0.7985	0.1466
0.2281	-0.1926	-0.4423	-0.2308	-1.1966	0.9944	0.4693	1.2557	-0.3041
0.1864	-0.6485	-0.1353	-0.6221	-0.6624	0.6856	0.4185	1.5165	1.0026

-0.8535	0.3459	0.784	-0.5419	0.4992	0.9309	-0.0521	-0.5967	1.3535
-0.7167	0.5331	0.1582	-0.2692	0.32	1.0468	-0.3691	-0.6394	-0.5877
0.362	-0.3781	-0.8392	-0.2768	-0.2686	0.3612	-0.4041	1.5752	-1.0388
0.1912	-0.6893	-0.3961	-0.8188	-0.408	0.3908	0.2007	2.1833	-0.0229
-0.7357	0.3296	-0.0599	-0.9617	0.4906	0.6139	0.3855	0.7913	-0.0248
-0.4719	0.7386	-0.3735	-0.4475	1.2059	-0.0136	-0.4994	-0.0878	-0.4563
0.6946	-0.3149	-0.2627	-0.5027	-0.2427	-0.2375	-0.6791	0.5993	-0.4171
1.2036	0.0381	-0.5565	-0.8937	-0.5531	-0.3817	0.1748	1.5056	0.0375
0.1033	0.5027	-0.7181	-0.45	0.977	-0.665	0.9585	1.0445	-0.3323
-0.9214	0.0119	-0.0331	0.0522	0.7741	-0.1596	0.8012	-0.9716	-0.7478
0.2019	0.6295	-0.0236	-0.3316	-0.1635	-0.2185	0.2794	-1.616	-0.4117
1.8015	0.7849	-0.3565	-0.668	0.2623	-1.275	0.5791	0.3861	-0.361
0.9286	-0.3946	0.0293	-0.1483	0.6187	-0.9149	0.9534	1.0209	-0.0713
-1.3121	-0.541	0.0391	0.6526	0.5694	0.6174	0.7169	-1.0031	-0.1593
-0.7431	0.8286	-0.3217	0.8914	0.7932	0.8255	0.2932	-2.4773	-0.7918
1.57	0.6602	0.1172	0.2308	0.0532	-0.3751	0.3917	-1.7447	-0.4591
0.9896	-0.9031	0.3781	-0.2719	-0.5537	-0.9924	0.5476	-0.3141	0.3042
-0.987	-0.4572	-0.1363	0.5294	0.8129	0.1143	-0.5441	-0.262	0.2721
-0.9407	0.364	-0.0388	1.3482	1.3194	1.1371	-1.3477	-1.0829	-0.5848
0.0828	0.2454	0.4192	0.9675	-0.2272	0.4322	-0.2364	-1.4823	-0.7064
0.5833	0.1751	0.1266	0.3172	-0.9509	-0.7726	0.5459	-1.0626	0.4603
0.1338	-0.8478	0.0071	0.1154	-0.2164	-0.4343	-0.4569	0.336	0.7076
-1.2304	-1.2195	0.4758	0.3987	0.5263	0.9205	-1.7724	1.1625	-0.3555
-1.2235	0.3629	0.4009	1.0503	0.0937	0.5643	-2.3771	0.0016	-0.5136
0.5407	0.7982	0.0131	0.9959	-1.2415	-0.5126	-1.0695	-0.6899	0.2968
0.8963	-0.9749	0.2546	-0.111	-1.273	-0.5202	0.6293	0.6051	0.6022
-0.8539	-1.5897	0.3489	-0.6718	0.0898	-0.2982	-0.2553	1.576	0.3928
-1.4388	0.1499	0.0256	0.1406	0.095	0.2306	-1.7013	1.1451	-0.023
0.79	1.0589	0.4087	1.0439	-1.2402	0.0232	-1.4431	0.2266	-0.3045
1.5617	-0.0594	0.341	0.3681	-1.4693	-0.8658	0.8061	0.4447	0.0954
-0.4959	-0.8573	-0.3464	-0.9912	-0.1067	-0.8578	1.852	0.9965	0.7491
-1.1659	-0.0701	0.23	-1.1238	0.8845	-0.2029	-0.1868	0.5774	0.544
0.0041	0.96	0.6299	-0.366	0.1725	0.578	-0.271	0.7712	-0.3516
1.2859	0.5974	-0.3109	0.2094	-0.6814	0.345	1.3712	0.5619	-0.3113
0.9327	-0.4865	-0.8987	-0.5898	-0.6876	-0.0588	1.7991	-0.1914	0.5684
-0.648	-0.176	0.0485	-1.715	0.3419	0.0564	1.1493	0.4105	0.641
-0.6209	1.1935	0.7581	-1.0398	1.5223	-0.0278	-0.1202	0.886	-0.1602
0.3352	1.1956	-0.6993	-0.2403	0.2636	1.038	0.3549	0.13	-0.5085
0.8204	-0.0197	-1.4275	-0.4654	-1.0961	1.5612	1.3269	-1.0607	0.1792
0.3777	-0.1765	-0.012	-0.5975	0.7676	0.0341	1.215	-0.9163	0.5723
-0.8441	0.7574	0.6714	-0.7689	1.8671	-0.5275	0.2676	0.5462	-0.0607
-0.8158	0.7629	-0.3902	-0.6487	-0.1563	0.714	-0.8831	0.7257	-0.4502
0.3833	-0.3043	-1.5869	0.2769	-0.8601	1.3147	0.0891	-0.5131	-0.0657

0.6426	-0.6722	-0.7821	0.4344	0.611	-0.0114	0.6572	-1.2112	0.3334
-0.2815	-0.1669	0.9412	-0.3306	1.0439	-1.1063	-0.4062	-0.4264	0.1029
-0.5476	0.0531	0.3054	0.0675	-0.4424	-0.4759	-0.5528	0.1787	-0.3469
0.0734	-0.1935	-1.1209	1.1197	-1.3682	0.257	-0.5408	-0.3672	-0.1853
0.2388	-0.756	-0.1316	0.9543	-0.0028	-0.1435	-0.3698	-0.4657	0.1563
0.2319	-1.1097	0.8978	0.3792	0.5968	-1.1776	-0.0066	-0.8561	0.0164
-0.0572	-0.0647	0.1346	0.4465	0.1508	-0.9319	-0.8487	-1.5933	-0.1848
-0.3607	0.4935	-0.3388	0.5528	0.1868	0.1988	-1.2663	-0.4756	-0.0954
0.7085	-0.9263	0.0943	0.6391	-0.5618	-0.1832	-0.2147	0.5386	0.0928
1.2356	-1.1337	0.578	1.2358	-0.253	-0.8719	-0.0077	-0.828	0.2531
-0.3783	0.2214	0.5323	1.4683	1.2282	-0.1101	-0.618	-1.4849	0.1155
-1.0721	0.5708	0.3556	0.1101	0.6117	0.5764	-0.4769	0.2754	-0.3195
0.3887	-0.0184	-0.0762	-0.6476	-0.8241	-0.071	-0.2849	1.0104	-0.1187
0.8419	-0.6195	-0.3789	0.8318	-0.1847	-0.2415	-0.0066	-0.4658	0.4405
-0.4162	-0.1217	0.7519	1.3094	0.9369	1.1886	0.4706	-0.9924	0.0464
-0.7709	1.3966	1.0635	-0.1924	0.4406	1.2355	-0.2027	0.4374	-0.4384
0.0884	0.9908	-0.3117	-0.9249	-0.272	-0.8765	-0.7291	1.3677	-0.0741
0.1637	-0.9963	-0.4188	-0.7351	-0.2371	-0.9445	0.533	0.7079	0.2027
-0.6581	-0.5812	0.5022	-0.4032	-0.2354	0.9235	1.1514	0.4369	0.0558
-0.8952	1.3381	0.5234	0.0579	-0.1858	0.4771	-0.0033	1.3956	-0.1478
-0.4704	1.2458	0.1036	-0.5322	-0.1317	-0.8899	-0.4014	1.5948	-0.2454
-0.0092	-0.4752	-0.2043	-1.1957	-0.8474	-0.508	0.709	0.7949	0.0522
0.1114	-1.2879	0.0029	-1.1264	-1.1815	-0.0457	1.0538	0.3938	0.3122
-0.4205	0.0158	0.3762	-1.085	-0.4708	-0.257	0.1254	0.5256	-0.0973
-0.6878	1.655	-0.2375	-0.1388	-0.2147	-0.2256	-0.2054	1.0226	-0.4874

C.1.3 AE example of grinding phenomenon

An example of grinding (no chatter or burn phenomenon) from an extracted AE signal:

No Burn/ Chatter (Grinding) T47 0.5mm DOC

Part 1	Part 2	Part 3	Part 4	Part 5	Part 6	Part 7	Part 8	Part 9
0.0774	-0.0164	0.0348	-0.0077	-0.0967	-0.1101	0.1622	-0.1142	-0.0288
0.006	0.0783	0.094	-0.0598	-0.1905	-0.1239	0.2371	-0.4052	-0.0718
-0.0505	0.0639	0.0828	-0.0568	-0.2853	-0.0697	0.5469	-0.1496	0.1288
0.0105	0.0131	0.0373	-0.1463	-0.221	-0.0949	0.4483	0.1567	0.2522
0.0852	-0.0115	0.0143	-0.2911	-0.1331	-0.0984	0.0806	0.1037	0.2171
0.0678	0.0225	0.0436	-0.3107	-0.2402	-0.1238	0.0818	-0.2221	0.2587
0.0209	0.0383	0.0788	-0.2814	-0.2462	-0.1987	0.1916	-0.2953	0.3348
0.1618	-0.01	-0.0148	-0.356	-0.0509	-0.0704	0.03	0.0276	0.2862

0.3219	0.0051	-0.1159	-0.4492	-0.0115	0.2433	-0.1124	0.1514	0.0389
0.245	-0.017	-0.1023	-0.43	-0.0797	0.3104	-0.0724	-0.1189	0.1718
0.1425	-0.0239	-0.0834	-0.3275	-0.1091	0.0774	-0.0205	-0.3567	0.2245
0.2359	0.0532	-0.0902	-0.2574	0.015	0.0678	-0.0217	-0.2779	-0.0198
0.3236	0.0455	-0.106	-0.2052	0.2619	0.2482	-0.1293	-0.0043	0.1096
0.2449	0.0481	-0.141	-0.0672	0.1727	0.1253	-0.2659	0.052	-0.0291
0.114	0.0253	-0.1054	0.0723	0.0135	0.0083	-0.2489	-0.1703	-0.3135
-0.0057	-0.0173	-0.0367	0.1664	0.2152	0.0764	-0.2796	-0.2842	-0.2899
0.0007	0.0505	-0.0161	0.2925	0.3218	0.0752	-0.3975	-0.1486	-0.309
0.1168	0.0387	0.0315	0.438	0.1733	0.1071	-0.413	-0.0575	-0.1558
0.0233	-0.0663	0.0639	0.517	0.1384	0.0901	-0.4599	-0.1547	-0.0052
-0.2051	-0.081	0.0366	0.4719	0.1965	-0.0452	-0.3831	-0.2282	-0.1177
-0.275	-0.0237	0.044	0.481	0.1661	-0.1379	-0.2098	-0.2341	-0.158
-0.1661	-0.0377	0.114	0.5292	0.1309	-0.0928	-0.2721	-0.0646	0.0223
-0.1035	-0.0779	0.15	0.4001	0.1017	-0.0403	-0.3416	0.1971	0.2075
-0.2543	-0.0094	0.0891	0.2907	0.0246	-0.1754	-0.1187	0.1063	0.221
-0.2792	0.0354	0.0432	0.2902	-0.0526	-0.2275	0.2046	-0.0326	0.1635
-0.1085	0.0169	0.0944	0.165	-0.1421	-0.0988	0.0339	0.1081	0.1332
-0.0628	0.0366	0.0749	-0.0804	-0.1918	-0.0671	-0.1941	0.2829	0.1404
-0.1163	0.042	-0.0557	-0.2903	-0.1385	-0.0168	0.1894	0.4633	0.2052
-0.1734	0.0321	-0.0955	-0.383	-0.1189	0.1513	0.4065	0.4861	0.2152
-0.1536	0.0318	-0.0662	-0.3571	-0.1741	0.2058	0.3065	0.2875	0.1186
-0.042	0.0202	-0.0135	-0.3699	-0.2165	0.1961	0.3671	0.2926	0.183
0.0781	-0.0059	0.0244	-0.4788	-0.1794	0.2381	0.4492	0.395	0.2754
0.1098	0.0056	-0.0334	-0.5627	-0.1003	0.1717	0.5832	0.2489	-0.09
0.022	0.088	-0.0409	-0.5529	-0.1126	0.034	0.632	0.1501	-0.4629
0.0506	0.0682	-0.0042	-0.3784	-0.0996	-0.0191	0.3893	0.1134	-0.1523
0.1382	-0.068	0.0055	-0.2036	0.0188	-0.0281	0.2798	-0.1133	0.2439
0.0872	-0.1013	-0.0375	-0.1709	0.081	-0.0123	0.3719	-0.2372	0.0363
0.009	-0.013	-0.0928	-0.1109	0.066	-0.0483	0.1984	-0.1795	-0.4405
-0.0497	0.0236	0.0389	0.0461	0.072	-0.1896	-0.0693	-0.2605	-0.6644
0.0044	-0.074	0.138	0.2894	0.13	-0.1895	-0.1065	-0.4621	-0.3291
0.0814	-0.1212	0.0084	0.424	0.1858	-0.0824	-0.0968	-0.6349	0.2387
-0.0062	-0.0914	-0.0717	0.3155	0.1329	-0.0855	-0.1669	-0.4744	0.2086
-0.0739	-0.0715	0.0193	0.2768	0.0362	-0.1133	-0.3347	-0.1364	-0.2664
-0.0207	0.0592	0.113	0.3993	0.0293	-0.1168	-0.4968	-0.2656	-0.3395
0.0251	0.1301	0.0154	0.4186	0.0139	-0.0663	-0.3882	-0.3195	-0.0509
-0.0507	0.0355	-0.1884	0.3453	0.0422	-0.0703	-0.2238	0.0191	0.1864
-0.1023	-0.0008	-0.1799	0.2237	0.052	-0.0977	-0.3837	0.1984	0.1766
-0.0582	0.0648	-0.0238	0.0797	-0.0847	0.0327	-0.5134	0.2281	-0.0805
-0.0986	0.1405	-0.045	0.0825	-0.0824	0.1371	-0.2736	0.1507	-0.1919
-0.0625	0.084	-0.1116	0.0274	0.0014	0.2008	-0.0419	0.1522	-0.0228
0.0507	-0.0534	-0.04	-0.1299	0.0365	0.1818	-0.0647	0.276	0.2146

[A36]

0.037	-0.0469	0.0356	-0.1528	-0.0078	0.0417	0.0261	0.3065	0.2711
0.035	0.0743	0.0411	-0.1571	-0.1889	0.0702	0.1951	0.1802	0.0134
0.0502	0.1415	0.0259	-0.227	-0.1276	0.1816	0.0773	-0.0342	-0.0009
0.0516	0.0877	0.0738	-0.3054	0.1127	0.133	0.0691	0.1242	0.4323
0.1471	-0.0088	0.1036	-0.2549	0.1051	-0.0986	0.2659	0.2981	0.3051
0.2391	-0.0062	0.0795	-0.1323	0.0418	-0.2028	0.1613	-0.0229	-0.2107
0.185	0.0525	0.0814	-0.1043	0.09	-0.0501	-0.0891	-0.1475	-0.0597
0.0672	-0.043	0.0115	-0.0295	0.1332	-0.0546	-0.1096	0.0632	0.1346
0.0537	-0.2386	-0.0661	0.026	0.2374	-0.1787	0.0357	0.0342	0.0007
0.1152	-0.23	-0.0266	-0.0223	0.1864	-0.2714	0.106	-0.1176	0.0665
0.0688	-0.0791	0.0142	-0.0252	-0.0403	-0.1992	-0.0291	-0.0064	0.0797
-0.0578	-0.0947	0.0066	0.023	-0.0408	0.0896	-0.116	0.049	-0.2209
-0.0513	-0.2038	0.0246	0.0992	0.0126	0.064	0.0464	-0.1884	-0.2913
0.006	-0.1478	0.0523	0.1352	-0.054	-0.1412	0.1156	-0.1107	0.1993
-0.1039	0.0746	-0.0192	0.0536	-0.1751	-0.1624	0.0091	0.2009	0.1934
-0.221	0.2037	-0.0868	0.0091	-0.2481	-0.0451	0.1027	0.0343	-0.3906
-0.1763	0.1081	0.0185	0.1189	-0.1526	0.1249	0.2685	-0.2678	-0.3614
-0.1353	0.0122	0.117	0.2339	-0.09	0.0883	0.2221	-0.1312	0.1748
-0.1596	0.0497	0.037	0.1795	-0.0893	0.0558	0.1441	0.0958	0.6072
-0.1704	0.1132	-0.0686	-0.0366	-0.1789	0.1488	0.108	-0.0687	0.1543
-0.1181	0.0958	0.0057	-0.132	-0.3098	0.2637	0.1597	-0.3011	-0.672
0.0122	0.0447	0.149	0.0252	-0.2045	0.4522	0.2893	-0.2864	-0.0943
0.1003	0.0574	0.1221	0.0383	-0.0384	0.3844	0.1635	-0.1452	0.8016
0.0896	0.0658	0.022	-0.1967	0.0037	0.1832	0.0184	0.1479	0.2198
0.0442	0.086	-0.073	-0.2865	-0.0221	0.29	0.1363	0.0734	-0.4558
0.0473	0.1083	-0.1472	-0.1764	0.0389	0.2099	0.152	-0.2996	-0.084
0.1344	0.0036	-0.1205	-0.1716	0.2107	-0.1368	-0.1539	-0.0305	0.2863
0.2006	-0.0764	-0.0917	-0.2042	0.235	-0.0361	-0.4556	0.3689	0.1269
0.1823	-0.0399	-0.0647	-0.0343	0.2446	0.1196	-0.3118	0.2062	-0.2423
0.1576	-0.0869	-0.1118	0.0016	0.3201	0.0016	-0.2115	-0.0254	-0.3703
0.153	-0.2076	-0.1672	-0.118	0.2815	-0.0831	-0.5335	0.0967	-0.0483
0.1505	-0.1959	-0.038	0.0429	0.1537	-0.2337	-0.6721	0.3038	0.0467
0.1209	-0.0716	0.0338	0.1914	0.0136	-0.3233	-0.417	0.2486	-0.2788
0.0129	0.0009	-0.0291	0.0825	0.0528	-0.3666	-0.0787	0.204	-0.324
-0.0257	-0.0126	-0.1458	0.0645	0.092	-0.3828	-0.1091	0.238	-0.091
-0.0446	-0.0841	-0.1588	0.0734	-0.0332	-0.3861	-0.3494	0.2633	-0.0303
-0.164	-0.1191	0.0881	0.0677	-0.0676	-0.4615	-0.146	0.321	-0.0694
-0.135	-0.0134	0.1949	0.2917	-0.0397	-0.2935	0.2463	0.1592	-0.1485
-0.0767	0.0899	0.0386	0.3801	0.0332	-0.1773	0.3825	-0.0173	-0.1846
-0.1771	0.0229	-0.0042	0.2452	0.0515	-0.261	0.3117	-0.0785	0.0877
-0.1745	-0.1061	0.1387	0.1786	-0.0811	-0.1302	0.1279	-0.1907	0.3383
-0.098	-0.0969	0.2691	0.1143	-0.1136	0.0764	0.1514	-0.3312	0.1675
-0.0969	0.0664	0.2418	0.1333	-0.0878	0.1616	0.494	-0.4945	0.032

-0.0327	0.1601	0.1482	0.1055	-0.1146	0.1491	0.6156	-0.3702	0.2308
0.0118	0.0645	0.1867	-0.0395	-0.0806	0.1071	0.3151	-0.2657	0.2844
-0.0314	-0.0079	0.2821	-0.1188	-0.0876	0.1558	-0.0253	-0.3654	0.1111
0.0106	0.0916	0.2366	-0.1655	-0.1231	0.2757	-0.0159	-0.2479	0.1083
0.0165	0.165	0.1348	-0.1207	-0.0012	0.3721	0.3684	-0.2021	0.1691
-0.0631	0.075	0.0753	-0.0624	0.0334	0.3317	0.4131	-0.1273	0.0909

D.1   3D Material Measurements for Horizontal SG Scratch tests

D.1.1 3D images of example SG scratches recorded by Fogalemap Interferometer
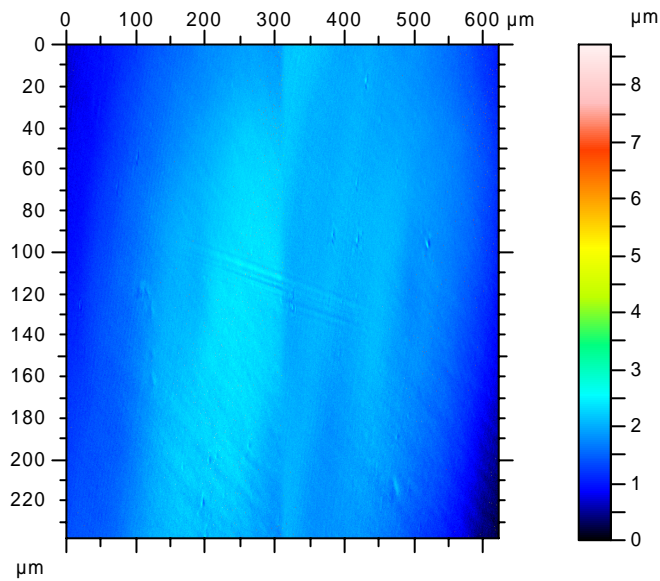
Figure D.1 T212 Hit 1
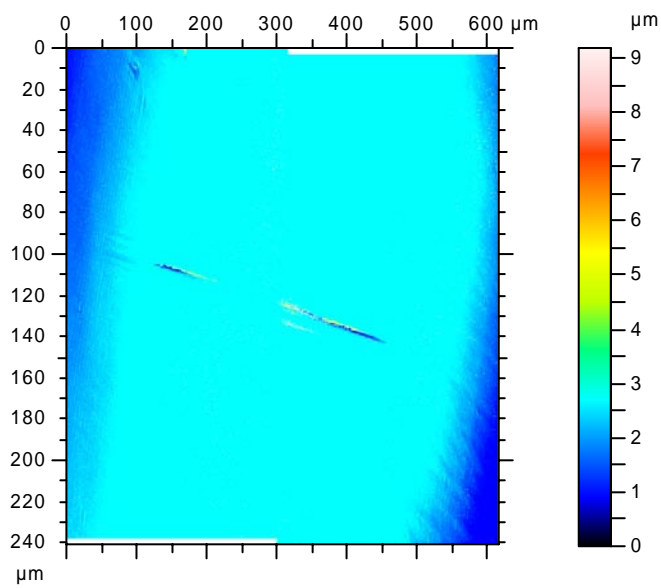
Figure D.2 T212 Hit 2
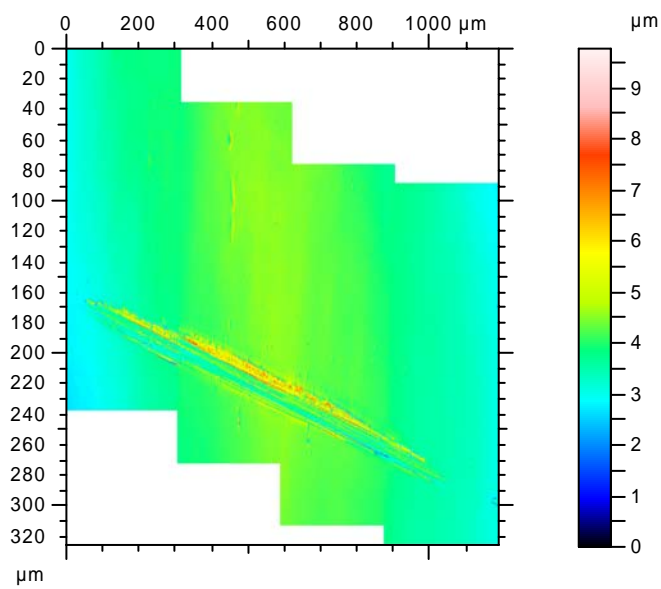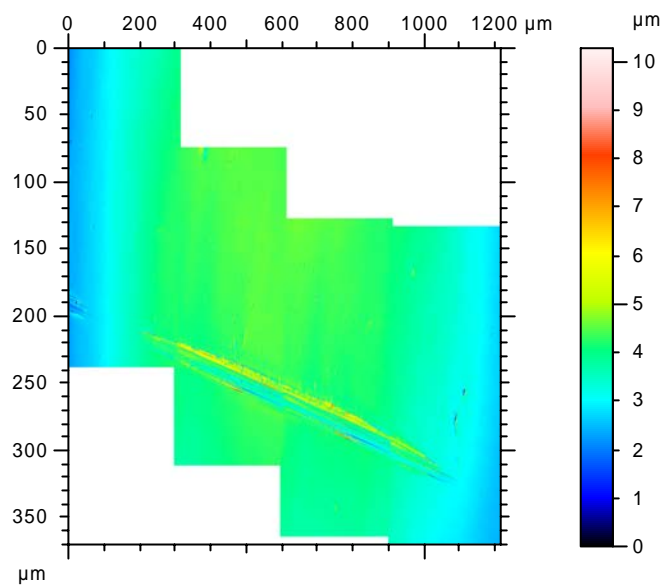

Figure D.3 T212 Hit 6
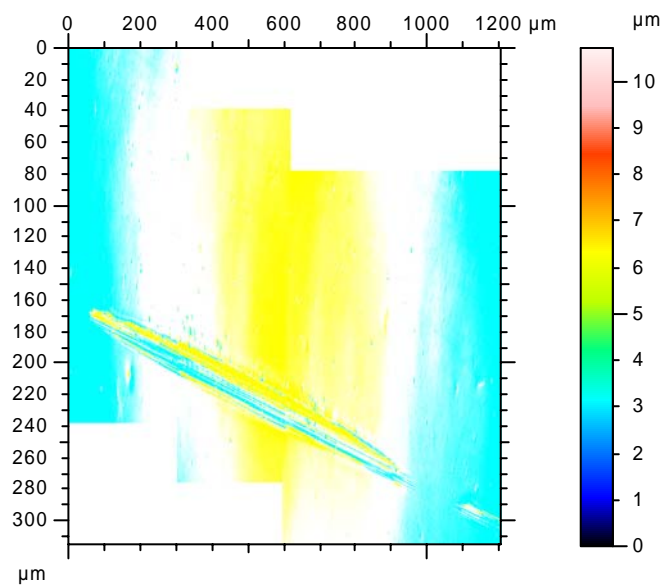
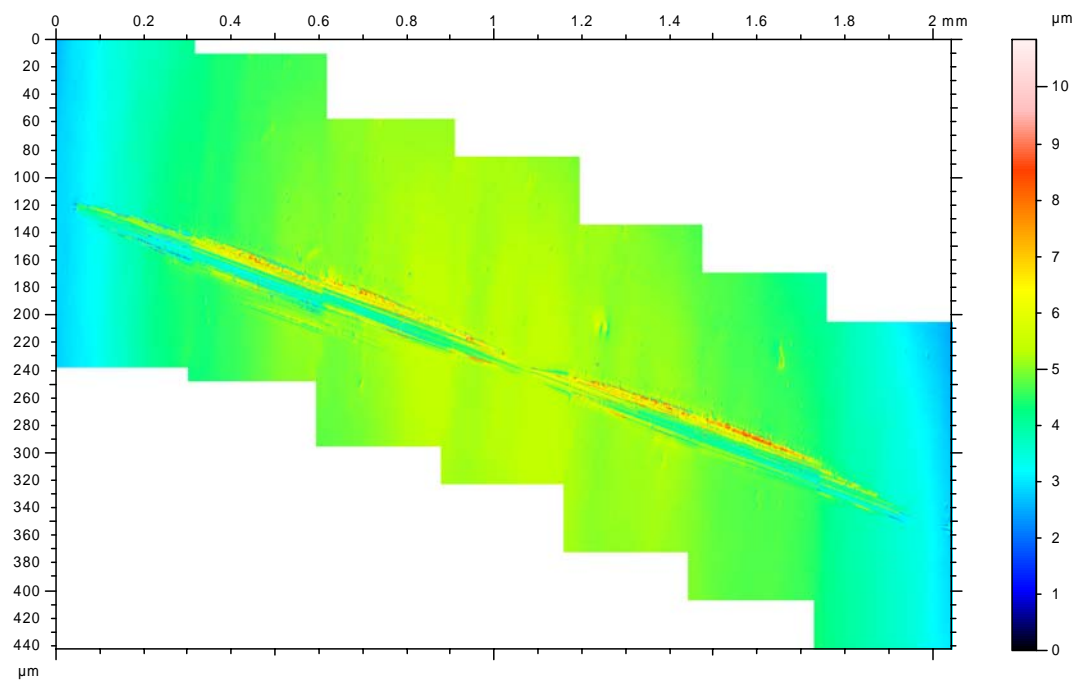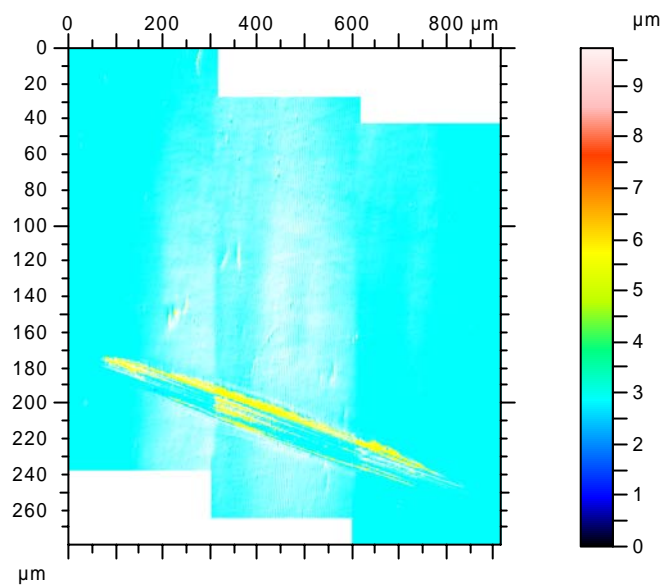Figure D.4 T212 Hit 7

Figure D.5 T212 Hit 8

Figure D.6 T212 Hit 10 and Hit 11
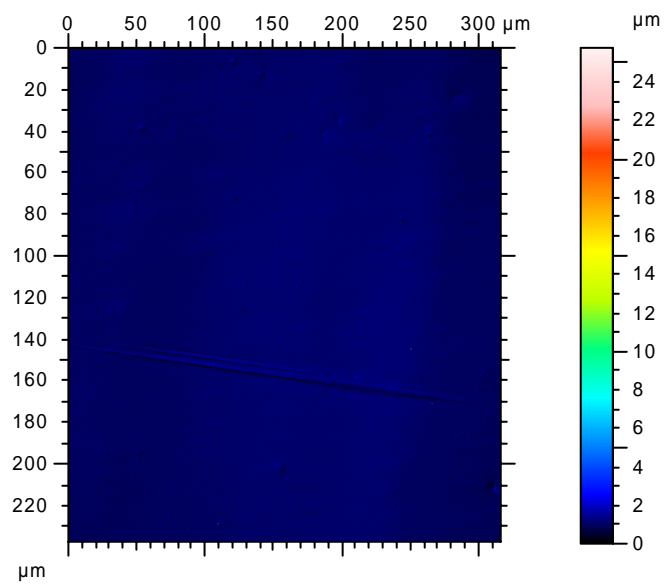

Figure D.7 T212 Hit 17

Figure D.8 T212 Hit 22